DOCTOR OF PHILOSOPHY

Identification and characterisation of FAM83 proteins as key regulators of CK1 protein kinases in cells
FAM83D recruits CK1 to the mitotic spindle for proper spindle positioning

Fulcher, Luke James

Award date:
2019

University of Dundee

Identification and characterisation of FAM83 proteins as key regulators of CK1 protein kinases in cells: FAM83D recruits CK1α to the mitotic spindle for proper spindle positioning

Luke James Fulcher

August 2019

A thesis submitted for the degree of Doctor of Philosophy

MRC Protein Phosphorylation and Ubiquitylation Unit,

University of Dundee

Contents:

List of Figures:

List of Tables:

Declarations:

I declare that the following thesis is based on the results of investigations conducted by myself, and that this thesis is of my own composition. Work other than my own is clearly indicated in the text by reference to the relevant researchers, or to their publications. This dissertation has not in whole, or in part, been previously submitted for a higher degree.

Luke J. Fulcher

I certify that Luke J. Fulcher has spent the equivalent of at least nine terms in research work in the Medical Research Council Protein Phosphorylation and Ubiquitylation Unit (MRC PPU), School of Life Sciences, University of Dundee, and that he has fulfilled the conditions of the Ordinance General No. 14 of the University of Dundee and is qualified to submit the accompanying thesis in application for the degree of Doctor of Philosophy.

Gopal P. Sapkota

Acknowledgements:

First and foremost, I would like to thank my supervisor Gopal for his continued support and advice throughout my doctoral studies, and for providing me with the opportunity to work on such exciting and motivating projects. It really has been a pleasure to work in his lab, and learn and develop as a scientist under his guidance. The GS lab is a fantastic environment to work in, and key to this positive atmosphere are the lovely bunch of scientists who I have been lucky to share the lab with over the years I've been here. When I first joined the lab, it was home to Tim, Polina, and Luke H, and all three of them made me feel extremely welcome. I'll forever miss Tim's BBQ skills (that duck was exceptional!), and watching Game of Thrones with Polina, accompanied by her amazing Greek culinary skills (her moussaka is to die for! And her friendship has kept me sane during the difficult times). Sampling the delights of the Dundee craft beer scene with Luke H (a.k.a. Hutchy lad), and getting to know him in the process, has also been an honour! Since then the lab has expanded rapidly, and is now home to many new awesome people: my Pokémon go buddies Kevin and Sascha (we must have totalled 1000 miles between us!), Karen (who always has the best experimental advice!), Luke S (a.k.a. Simpsy, who has been a constant source of banter throughout his time here!), Theresa (who keeps the lab a fun environment and always makes me smile as we pass in the corridor!), and Bill (the gem of the emerald isle who's always game for a pint of Guinness after a hard day at the bench!). To the exceptionally-talented students I have supervised, Craig and Selina, I thank you for all of your hard work and making my job as a supervisor so easy! It was a joy to teach you and watch you grow.

Of course, I am also extremely grateful to the many amazing people who I have encountered whilst working in the MRC PPU, for helping me keep a fun work-life balance. Michael, Connor, Sven and Florian (a.k.a. the yeah bois!) have been the best

bunch of Friday night pub-goers I could ask for! The many events and holidays over the years wouldn't have been the same without you! My Ganley and Alessi lab buddies Maria, Lambert, Marianna, Thanos, Alice, Francois, Anna, Michael, Catherine, Toby and Christina – it's been an absolute pleasure getting to know you all over the past few years! Attending parties with you all (more often than not hosted and catered by the exceptionally talented chef Thanos!) has been a source of joy during my PhD. Special thanks to Maria, Lambert and Marianna (team 31!) for being such amazing, supportive friends. I'm also extremely grateful to Ian Ganley for training me up during my first rotation project at the start of my PhD. It was great working in his lab, and I still use the techniques he taught me to this day. I was part of a baby boom year in the PPU when I joined, and every single person in the class of 2019 has been an amazing colleague to work and party alongside. To Tovell, Andy S, Andy W, Katie, Kristin, Dominika, and Anna - thank you for making my time here so enjoyable! Special shout-out to the JBC4 labs (Cohen and Virdee) who keep our secluded corridor a great place to be and work!

I would like to give my undying gratitude to the amazing support staff who I have been fortunate to work alongside during my studies. To Tom and Nikki who have undertaken the vast majority of the cloning work related to my studies – the progress of this project would not have been possible without your highly-appreciated help and advice, and I'll never forget the accidental shot of Tia Maria in the art bar with Tom! Special thanks go to Alan and Graeme for their amazing help and advice with the microscopy studies, and to Rosie, Arlene and Adam for their much-appreciated cell sorting and FACS support. To Laura, Edwin, Janis and Alison – thank you for all of your tissue culture help over the years, especially to Janis and Alison for the many laughs in TC! A huge thank you to David, Joby, Bob, Houjiang and Renata for all of their help and support with mass spectrometry and proteomics, and to the hard-working staff of the

MRC PPU reagents and services (formally the DSTT), DNA sequencing services, and central technical services, for keeping the research going and providing such fantastic resources to study with. A big thank you also goes to the hard-working people within MRC tech and MRC admin – thank you for all of your help throughout my time here. An enormous thank you goes to our collaborators in Canada, Chris, Leo and Lucy, for generating such amazing data and helping us untangle the role of FAM83D in cell division. Without your help and advice, it would not have been possible. Special thanks to our collaborators in the Smith and Bullock labs for their highly-appreciated advice and experimental inputs during the course of characterising the FAM83 proteins.

When I left my small village of Denholm to embark on my scientific journey, it would have been next to impossible if I didn't have the undying support of my family and friends. To my mum and dad, thank you for all of your love and guidance during my career-shaping, decision-making, and for always providing me with an energising Sunday lunch when I come home! To my aunt Sheila and Uncle Dave, thank you for stopping me getting too homesick and always inviting me for tea and to family get togethers, and most-recently, for taking me in and giving me a home for the final part of my PhD. To my sister Steph and brother Paul, thank you for helping to make many happy memories in the holiday seasons, and letting me feel revitalised for returning to the lab. To my dearest friends Andrew, Calum, Gari, Callum, Stacey, Jonny, Mel, Hannah, Kellie, Danni, Jen, Skye, Phil, Liam, Mike, and Greg – all of you have kept me sane and been a constant source of support and joy during my studies, and without you I wouldn't have managed to get through the PhD with no grey hairs in sight!

Thesis Summary:

The FAM83 family of proteins are classified based on the presence of a conserved domain of unknown function 1669 (DUF1669) within their N-termini. Although structural and bioinformatic studies suggest that the DUF1669 domain adopts a phospholipase D-like motif, no phospholipase D activity has yet been demonstrated for FAM83 members experimentally. Thus, the role and function of FAM83 proteins remains elusive. This study provides evidence that FAM83 proteins bind to different isoforms of the casein kinase 1 (CK1) family of Ser/Thr protein kinases and direct them to the distinct cellular sites in which the FAM83 proteins reside. FAM83 members mediate CK1 binding through their conserved DUF1669. In this capacity, FAM83 proteins may act as the A Kinase Anchoring proteins (AKAPs) of the CK1 world, and act analogously to the way AKAPs serve to regulate protein kinase A.

Regarded as constitutively-active, promiscuous protein kinases, the regulation of CK1 isoforms is critically important, yet poorly understood. This is particularly crucial when considering the reported participation of CK1 kinases in many, diverse signalling processes, from Wnt signalling to the regulation of Circadian rhythm. Mechanisms regulating CK1 isoforms, through controlling their cellular localisation and therefore substrate accessibility, are thus attractive regulatory targets to facilitate the study into specific CK1 functions, which rely on the recruitment of CK1 isoforms to the relevant cellular sites. As FAM83 proteins have the potential to act in such a manner, investigation was focussed on specific FAM83-CK1 interactions in order to further define this emerging regulatory role of FAM83 members.

FAM83D is unique amongst the FAM83 proteins, in that it is the only FAM83 member known to localise to the mitotic spindle. RNA interference approaches targeting FAM83D have been reported to impact chromosome alignment and cause a

delay in the timings of cell division. Whilst all FAM83 proteins appear to associate robustly with the CK1 alpha isoforms (CK1α), interestingly, the interaction between FAM83D and CK1α in asynchronous cell extracts was weak. Armed with the knowledge that FAM83D localises to the spindle apparatus in mitosis, a hypothesis that the FAM83D-CK1α interaction might only occur during cell division was developed. This study provides evidence that FAM83D binds and recruits CK1α to the mitotic spindle, and that the FAM83D-CK1α interaction is critical for correct and efficient spindle positioning. Cells devoid of *FAM83D*, or those harbouring a FAM83D CK1-binding-deficient knockin point mutation, fail to localise CK1α to mitotic spindles, and present with spindle orientation defects, and a concurrent delay in the metaphase-to-anaphase transition. As the spindle position determines the axis of cell division, correctly-orientated spindle positioning is critically important in both development and in the maintenance of healthy adult tissues.

When one thinks of mitotic kinases regulating spindle positioning, prominent players such as cyclin-dependent kinases, aurora kinases, and polo-like kinases tend to dominate the cell division limelight. However, these kinase families alone cannot account for the extent of protein phosphorylation reported over a cell division cycle, implying roles for other protein kinases in this process. Thus, implicating CK1α as a mitotic kinase provides further mechanistic insights into the regulation of mitosis, and the phosphorylation-mediated control of cell division.

As FAM83 proteins are an emerging family of proteins, tools to study them are scarce, yet warranted. In this vein, part of this study was devoted to developing unique approaches and technologies to aid in the investigation of FAM83 biology, and beyond. In this context, two nanobody-based strategies to either promote the phosphorylation of the target protein, or mark it for proteasomal degradation are described. These novel

tools have been employed here to explore the role of the FAM83D-CK1α interaction in cells, and I provide evidence that they are applicable for research into diverse biological processes and questions.

Abbreviations:

β-TRCP	Beta-transducin repeat containing protein
ACN	Acetonitrile
AdPROM	Affinity-directed PROtein Missile
aGFP	anti-green fluorescent protein nanobody
aGFP.16	anti-green fluorescent protein nanobody 16
AID	IAA17 degron sequence
AKAP	A-kinase anchoring protein
AME	Asymmetric membrane elongation
AML	Acute myeloid leukemia
APC	Adenomatous polyposis coli
APC/C	Anaphase-promoting complex/cyclosome
APS	Ammonium persulphate
Arg-DHFR	Arginine-tagged dihydrofolate reductase
ARNT	Aryl hydrocarbon receptor nuclear translocator
AS	Asynchronous
ASC	Apoptosis-associated speck-like protein containing a CARD
ATP	Adenosine triphosphate
AURK	Aurora kinase
AURKA	Aurora kinase A
AURKB	Aurora kinase B
AURKC	Aurora kinase C
AUX	Auxin
BCA	Bicinchoninic acid assay
Bim	Blocked in mitosis

BMAL	Brain and muscle ARNT-like 1
BMP	Bone morphogenetic protein
BSA	Bovine serum albumin
BUB	Budding uninhibited by benzimidazoles
BUBR	Budding uninhibited by benzimidazoles-related
CARD	Caspase recruitment domain
Cas9	CRISPR-associated protein 9
CCNB1	Cyclin B1
CD	Cluster of differentiation
CD2AP	Cluster of differentiation 2-associated protein
Cdc	Cell division cycle gene
Cdh1	Cdc20-homologue 1
CDK	Cyclin-dependent kinase
CDKL	Cyclin-dependent kinase-like
CG-NAP	Centrosomal and Golgi N-kinase anchoring protein
CK1	Casein Kinase 1
CK2	Casein Kinase 2
CMGC	CDK, MAPK, GSK, CDKL kinase superfamily
CML	Chronic myelogenous leukemia
CPC	Chromosome passenger complex
CRISPR	Clustered regularly interspaced short palindromic repeats
CRL	Cullin RING E3 Ligase
CRY	Cryptochrome
CUL	Cullin
D Box	Destruction box

DAPI	4’,6-diamidino-2-phenylindole
DDX3	DEAD-box RNA Helicase 3
DISC	Death-inducing-signalling-complex
DMEM	Dulbecco’s modified Eagle medium
DMP	Dimethyl pimelimidate dihydrochloride
DMSO	Dimethyl sulfoxide
DNA	Deoxyribonucleic acid
Dox	Doxycycline
DSP	Dithiobis Succinimidyl Propionate
DTT	Dithiothreitol
DUF1669	Domain of unknown function 1669
Dvl	Dishevelled
DYNLL1	Dynein light chain 1
DYRK	Dual-specificity tyrosine-regulated kinases
E1	E1 Ubiquitin-activating enzyme
E2	E2 Ubiquitin-conjugation enzyme
E3	E3 Ubiquitin Ligase
ECL	Electrochemiluminescence
EDTA	Ethylenediaminetetraacetic acid
EGF	Epidermal growth factor
EGFR	Epidermal growth factor receptor
EGTA	Ethylene glycol-bis(β-aminoethyl ether)-N,N,N’,N’-tetraacetic acid
Elo B/C	Elongin B/C
ERK 1/2	Extracellular signal-regulated kinase 1/2

FAM83	Family of sequence similarity 83
FBS	Foetal Bovine Serum
FPLC	Fast protein liquid chromatography
G1	Gap 1 phase
G2	Gap 2 phase
Gα	G protein alpha
GAP	GTPase-activating protein
GAPDH	Glyceraldehyde 3-phosphate dehydrogenase
GEF	Guanine nucleotide exchange factor
GFP	Green Fluorescent Protein
GLI	Glioma-associated oncogene
GRK2	G protein-coupled receptor kinase 2
gRNA	guide RNA
GPR	GoLoCo domain-containing protein
GSK3	Glycogen synthase kinase 3
GST	Glutathione S-transferase
HA	Hemagglutinin
HCl	Hydrochloric acid
HEK 293	Human embryonic kidney 293
HEPES	4-(2-Hydroxyethyl)piperazine-1-ethanesulfonic acid
Hh	Hedgehog
HIF1α	Hypoxia-inducible factor 1α
HKD	HXKXXXXD phospholipase D catalytic motif
HME1	Immortalised human mammary epithelial 1 cells
HMMR	Hyaluronan mediated motility receptor

HPLC	High performance liquid chromatography
HRP	Horseradish peroxidase
IAA	Indole-3 acetic acid
IgG	Immunoglobulin G
INCENP	Inner centromere protein
IP	Immunoprecipitate
IRES	Internal ribosome entry site
KD	Kinase-dead
KI	Knockin
KO	Knockout
LATS	Large tumour suppressor
LB	Luria Bertani broth
LDS	Lithium dodecyl sulphate
LIN5	Abnormal cell lineage 5
M	Mitotic phase
MAD	Mitotic arrest-deficient
MAPK	Mitogen-activated protein kinase
MBP	Maltose-binding protein
MCC	Mitotic checkpoint complex
MDM	Mouse double minute homologue
MDS	Myelodysplastic syndrome
MEM	Minimal essential medium
MEF	Mouse embryonic fibroblast
MPF	M-phase promoting factor
Mps1	Monopolar spindle 1

MS/MS	Tandem mass spectrometry
MST	Mammalian STE20-like protein kinase
mTOR	Mammalian target of rapamycin
mTORC1	Mammalian target of rapamycin complex 1
Nb	Nanobody
NEDD8	Neural precursor cell expressed, developmentally down-regulated 8
NEK	NIMA-related kinase
NFAT	Nuclear factor of activated T-cells
Nim	Never in mitosis
NIMA	Never in mitosis gene A
NP40	Nonidet P-40 substitute
NuMa	Nuclear mitotic apparatus
PAI1	Plasminogen activator inhibitor 1
PER	Period
PBD	Polo-box domain
PBS	Phosphate-buffered saline
PDB	Protein data bank
PEI	Polyethylenimine
PI3K	phosphatidylinositol 3-kinase
PKA	Protein Kinase A
PKC	Protein Kinase C
PLD	Phospholipase D
PLK	Polo-like kinase
PROTAC	PROteolysis-TArgeting Chimera

PTCH	Protein patch homologue
PTPN11	Protein tyrosine phosphatase non-receptor type 11
RBX	RING-box E3 ligase
RHAMM	Receptor for hyaluronan-mediated motility
RNA	Ribonucleic acid
RNAi	RNA interference
RING	Really interesting new gene
RFP	Red Fluorescent Protein
RPMI	Roswell Park Memorial Institute
S	Synthesis phase
SAC	Spindle assembly checkpoint
SCF	SKP1-Cul1-F-Box
SDS	Sodium dodecyl sulphate
SH2	Src homology 2 domain
Shh	Sonic Hedgehog
SHP2	Src homology phosphatase 2
siRNA	Small interfering RNA
SMAD1	Mothers against decapentaplegic homologue 1
SMO	Smoothened homologue precursor
STE20	Sterile 20 protein
STLC	S-Trityl L-Cysteine
TAE	Tris, acetic acid, EDTA
TBS	Tris-buffered saline
TBS-T	Tris-buffered saline tween
TEMED	Tetramethylethylenediamine

Tet	Tetracycline
TFA	Trifluoroacetic acid
TIR1	Transport inhibitor response 1
TNF	Tumour necrosis factor
TNFR1	Tumour necrosis factor receptor 1
TPX2	Targeting protein for Xklp2
TRAIL	TNF-related apoptosis-inducing ligand
Ub	Ubiquitin
UPS	Ubiquitin Proteasome System
VHL	Von Hippel-Lindau protein
VHH	Variable domain of a heavy chain only antibody
VPS34	Vacuolar protein sorting-associated protein 34
Wnt	Wingless/int-1
WT	Wild-type

Amino Acid Code:

Amino Acid	Three letter code	One letter symbol
Alanine	Ala	A
Arginine	Arg	R
Asparagine	Asn	N
Aspartic Acid	Asp	D
Cysteine	Cys	C
Glutamic Acid	Glu	E
Glutamine	Gln	Q
Glycine	Gly	G
Histidine	His	H
Isoleucine	Ile	I
Leucine	Leu	L
Lysine	Lys	K
Methionine	Met	M
Phenylalanine	Phe	F
Proline	Pro	P
Serine	Ser	S
Threonine	Thr	T
Tryptophan	Trp	W
Tyrosine	Tyr	Y
Valine	Val	V
Any amino acid	Xaa	X

List of Publications:

Fulcher LJ, He Z, Mei L, Macartney TJ, Wood NT, Prescott AR, Whigham AJ, Varghese J, Gourlay R, Ball G, Clarke R, Campbell DG, Maxwell CA, Sapkota GP. FAM83D directs protein kinase CK1α to the mitotic spindle for proper spindle positioning. EMBO Reports. 2019; 20: e47495.

Röth S, **Fulcher LJ**, Sapkota GP. Advances in targeted degradation of endogenous proteins. Cell Mol Life Sci. 2019.

Fulcher LJ, Bozatzi P, Tachie-Menson T, Wu KZL, Cummins TD, Bufton JC, Pinkas DM, Dunbar K, Shrestha S, Wood NT, Weidlich S, Macartney TJ, Varghese J, Gourlay R, Campbell DG, Dingwell KS, Smith JC, Bullock AN, Sapkota GP. The DUF1669 domain of FAM83 family proteins anchor casein kinase 1 isoforms. Sci Signal. 2018;11(531).

Macartney TJ, Sapkota GP, **Fulcher LJ**. An Affinity-directed Protein Missile (AdPROM) System for Targeted Destruction of Endogenous Proteins. *Bio-protocol* 2017;7(22): e2614.

Fulcher LJ, Hutchinson LD, Macartney TJ, Turnbull C, Sapkota GP. Targeting endogenous proteins for degradation through the affinity-directed protein missile system. Open Biol. 2017;7(5).

Fulcher LJ, Macartney T, Bozatzi P, Hornberger A, Rojas-Fernandez A, Sapkota GP. An affinity-directed protein missile system for targeted proteolysis. Open Biol. 2016;6(10).

1. Introduction:

1.1: Casein kinase 1:

CK1 kinases are a major focus of this thesis. Thus, an appreciation for the roles and regulation of CK1 kinases is required to aid the understanding of this thesis. The current knowledge on CK1 will be discussed in the following sections.

1.1.1: Overview of CK1 isoforms:

Protein kinases, which are enzymes that catalyse the phosphorylation of primarily Ser, Thr, and Tyr residues on protein substrates (Cohen, 2002a, Pawson & Scott, 2005), not only play central roles in controlling many diverse signal transduction pathways, but also represent important therapeutic targets (Cohen, 1999, Cohen, 2002b, Cohen, 2009). By phosphorylating their protein substrates, kinases are able to impart critical regulation on virtually every conceivable aspect of that substrate's function, such as its activity, stability, altering its binding to other effectors, or promoting a change in subcellular distribution (Pawson & Scott, 2005). Thus, protein kinases play essential roles within biological systems.

The human genome encodes over 500 protein kinases, which are classified into several families based on the sequence similarities of their kinase domains (Manning, Whyte et al., 2002). A dendrogram encapsulating all human protein kinases is commonly referred to as the kinome tree, where each specific branch represents a family of similar kinases (Manning et al., 2002). The serine/threonine (Ser/Thr) protein kinase CK1 family forms its own distinct branch of the kinome tree (Manning et al., 2002) (Figure 1-1), and constitute one of the first Ser/Thr protein kinase families to be discovered (Kumar & Tao, 1975). The CK1 branch includes the CK1 isoforms, and the closely-related vaccinia-

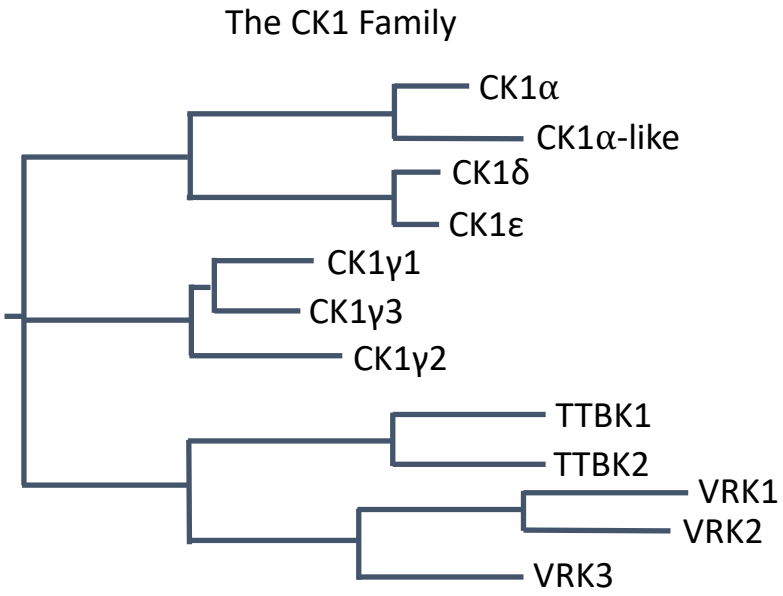

Figure 1-1: Phylogenetic schematic of the CK1 family of protein kinases: Phylogenetic tree depicting the human CK1 family members, adapted from Manning et al, 2002.

related kinases (VRKs), and tau tubulin kinase 1 (TTBK1) members (Ikezu & Ikezu, 2014, Manning et al., 2002) (Figure 1-1). Originally named casein kinases for their ability to phosphorylate casein *in vitro*, it should be noted that CK1 kinases are not the physiological casein kinases (Ishikawa, Xu et al., 2012, Venerando, Ruzzene et al., 2014). The bona fide casein kinase was recently identified as FAM20C, a Golgi-localised protein kinase that is capable of phosphorylating many secreted proteins, including casein (Ishikawa et al., 2012).

To date, six mammalian CK1 isoforms and their associated splice variants have been reported. These include the α, γ1, γ2, γ3, δ and ε CK1 isoforms, which have been grouped together based on their high degree of homology within their kinase domains located at their N-termini (Gross & Anderson, 1998, Knippschild, Gocht et al., 2005a, Schittek & Sinnberg, 2014) (Figure 1-2). Although another isoform, CK1β, has also been

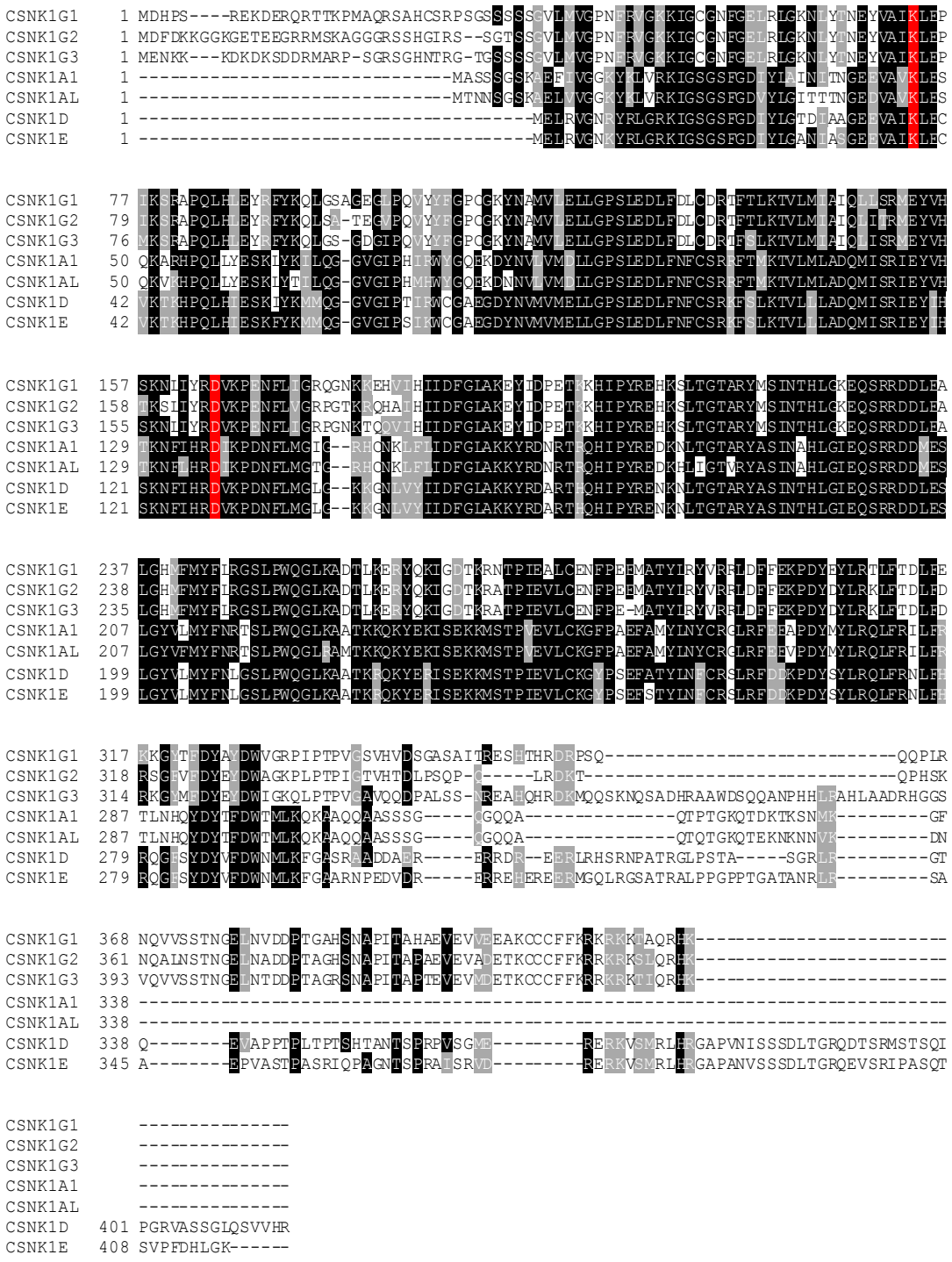

Figure 1-2: Multiple sequence alignment of the human CK1 proteins: The alignment was performed using Clustal Omega and visualised in boxshade. Shading indicates the % sequence similarity (black = identical, grey = similar; in more than 50% of sequences). The positions of two residues critical for catalytic activity are highlighted in red.

identified in cows, conclusive evidence for its existence and function in cows or other mammalian species remains elusive.

All CK1 isoforms have been reported to act as monomeric, constitutively-active enzymes (Gross & Anderson, 1998, Knippschild et al., 2005a, Schittek & Sinnberg, 2014). As ubiquitously-expressed and constitutively-active Ser/Thr protein kinases, CK1 isoforms have been reported to be involved in numerous, varied signalling pathways, and many proteins have been reported to be phosphorylated by CK1 isoforms (Cheong & Virshup, 2011, Gross & Anderson, 1998, Knippschild et al., 2005a, Schittek & Sinnberg, 2014). The CK1 family of kinases are conserved throughout evolution, and several CK1 orthologues have been identified in yeast (Hoekstra, DeMaggio et al., 1991, Wang, Vancura et al., 1992). Outside of the kinase domains, the non-catalytic C-termini of CK1 isoforms vary significantly and are not conserved between isoforms (Figure 1-2). However, the C-termini have been shown to play crucial roles in regulating substrate recognition, and in the modulation of kinase activity for some CK1 isoforms (Carmel, Leichus et al., 1994, Cegielska, Gietzen et al., 1998). That said, it should be noted that the C-termini are very small compared to other kinases, thereby suggesting that CK1 kinases may require functional interacting partners, or regulatory subunits, for their regulation.

1.1.2: Mode of CK1 action:

CK1 family members catalyse the transfer of phosphate on to Ser/Thr residues of their substrate proteins by utilising ATP exclusively as the source of the phosphate donor (Flotow, Graves et al., 1990, Tuazon & Traugh, 1991). Early attempts aimed at elucidating the substrate specificity of CK1 identified the requirement for a priming phosphorylation event in the -3 position, within the consensus sequence pS/pT-X-X-

S*/T*, where X is any amino acid and S*/T* denote CK1-phosphorylation residues (Flotow et al., 1990, Meggio, Perich et al., 1992, Meggio, Perich et al., 1991). This sequence is often referred to as the canonical CK1 consensus motif. Given this requirement for a priming phosphorylation event, CK1 isoforms were thought to act downstream of other kinases, and as such, this restricted their contribution within signalling cascades to one of a hierarchical manner. However, since the discovery of the canonical consensus motif, it has come to light that a cluster of acidic residues N-terminal to the target Ser/Thr phosphorylation sites, with an acidic amino acid at the n-3 position, can effectively substitute for the priming phosphorylation event (Agostinis, Pinna et al., 1989, Flotow & Roach, 1991, Graves, Haas et al., 1993, Marin, Meggio et al., 1994, Pulgar, Marin et al., 1999). Furthermore, a non-canonical S-L-S motif with a concurrent cluster of C-terminal acidic residues has also been shown to be phosphorylated by CK1 isoforms, albeit less efficiently than the canonical phospho-primed sequence (Knippschild et al., 2005a, Marin, Bustos et al., 2003). Such phosphorylation of S-L-S motifs are best showcased in two of the most robustly established CK1 substrates – nuclear factor of activated T-cells (NFAT) and β-catenin (Knippschild et al., 2005a, Marin et al., 2003).

1.1.3: Regulation of CK1 in cells:

Absence of selective CK1 inhibitors has led to confusion regarding exactly which CK1 isoform is the physiological kinase for each of the identified substrates. The kinase domains (sequence-wise and structurally) are very similar between CK1 isoforms (Figure 1-2), and all CK1 isoforms are constitutively active *in vitro*, and can phosphorylate substrate residues with identical motifs (Gross & Anderson, 1998, Knippschild et al., 2005a, Schittek & Sinnberg, 2014). Due to most cellular proteins harbouring at least one

CK1 consensus motif, it is not surprising that hundreds of CK1 substrates have been reported thus far. Added complexity arises when considering the cellular environment. Indeed, the substrate specificity of CK1 isoforms *in vitro* is thought to be largely different from that observed *in vivo*, and different isoforms are known to impact distinct biological processes, suggesting tight regulation of distinct isoforms in cells (Gross & Anderson, 1998, Knippschild et al., 2005a, Schittek & Sinnberg, 2014). This difference in the *in vitro* versus *in vivo* substrate specificity is attributed to intracellular regulatory mechanisms involved in modulating CK1 isoforms, such as functional binding partners and post-translational modifications. Furthermore, as the kinase domain of CK1 isoforms constitutes the vast majority of the protein sequence, regulatory domains that are prevalent in many other kinases are very small, if not completely absent in CK1 isoforms, adding further merit to the existence of regulatory CK1-binding partners in cells. These attributes have prompted researchers to ascertain the precise molecular mechanisms by which the activities of specific CK1 isoforms towards their cellular substrates are governed.

One such mode of regulation known to modulate CK1 function in cells involves the use of scaffold proteins, that act to direct and/or coordinate the correct positioning of protein complexes. Scaffolds can also act as signalosome assembly platforms, that act to bring functional enzymes, such as kinases, in close proximity to their substrate proteins, thereby increasing reaction efficiency through spatial control (Good, Zalatan et al., 2011). In some cases, scaffold/anchoring proteins have also been shown to allosterically activate their catalytic binding partners (Bayliss, Sardon et al., 2003, Good et al., 2011). In regard to the CK1 family of kinases, such scaffolds could be envisaged to regulate the constitutively-active CK1 members through multiple avenues. For example, scaffolds could bind and sequester CK1 isoforms at discreet cellular locations, either to

take CK1 isoforms towards or away from their substrates, or act as a physical bridge between CK1 isoforms and their substrates. Furthermore, CK1 scaffolds may act to promote optimal CK1 activation through direct allosteric activation. Indeed, several protein scaffolds have been found to exert regulation towards some of the CK1 family members. For example, the centrosomal and Golgi N-kinase anchoring protein (CG-NAP, aka AKAP450) was shown to interact with CK1δ and ε and recruit them to centrosomes (Sillibourne, Milne et al., 2002). Furthermore, the DEAD-box RNA helicase DDX3 has been shown to directly interact with CK1ε in a Wnt-dependent manner, to promote the phosphorylation of the Wnt receptor-associated protein Dishevelled (Dvl) (Cruciat, Dolde et al., 2013). Interestingly, in the case of some CK1 substrates such as NFAT and the circadian clock protein period 1 (PER1), a F-X-X-X-F motif on the substrate was found to mediate the interaction with CK1 (Okamura, Garcia-Rodriguez et al., 2004). Whether this interaction mechanism is universally applicable to every CK1-binding partner remains to be determined.

Additionally, post-translational modifications are known to be involved in the regulation of CK1 activity. These are largely thought to occur through reversible phosphorylation, either by CK1 itself through autophosphorylation, or by other kinases (Carmel et al., 1994, DeMaggio, Lindberg et al., 1992, Fish, Cegielska et al., 1995). In both cases, phosphorylation of CK1 was shown to be inhibitory towards intrinsic catalytic activity. How then the CK1 family kinases retain their constitutive activity remains unclear, although phosphatase involvement has been inferred (Gietzen & Virshup, 1999). Interestingly, NEDDylation of CK1α was also shown to occur (Huart, MacLaine et al., 2012), although the exact relevance of this NEDDylation event remains to be defined.

1.1.4: The roles of CK1 in biology:

Given the reported phosphorylation of numerous substrates by CK1 family isoforms, it is perhaps unsurprising that CK1 kinases have been implicated in many, diverse biological processes (Gross & Anderson, 1998, Knippschild et al., 2005a, Schittek & Sinnberg, 2014). The most evident of these processes will each be briefly summarised in the following sections:

1.1.4.1: Wnt signalling:

To date, the canonical Wnt signalling pathway is perhaps the best characterised CK1-regulated process. In short, stimulation of the cognate Wnt receptors with Wnt ligands lead to the nuclear translocation of the transcription factor β-Catenin, ultimately resulting in transcription of Wnt-dependent target genes (MacDonald, Tamai et al., 2009) (Figure 1-3). In the absence of Wnt ligands, β-Catenin is maintained within the so-called β-Catenin destruction complex, which is comprised of the scaffold proteins Axin and adenomatous polyposis coli (APC), the SKP1-Cul1-F-Box protein E3 ubiquitin ligase (SCF) substrate receptor β-TRCP, and the kinases glycogen synthase kinase 3 (GSK3) and CK1 (MacDonald et al., 2009, Stamos & Weis, 2013) (Figure 1-3). Within this destruction complex, the current model proposes that β-Catenin is first phosphorylated by CK1 on Ser45, thereby priming β-Catenin for subsequent, sequential phosphorylation on Thr41, Ser37, and Ser33 by GSK3 (Amit, Hatzubai et al., 2002, Gao, Seeling et al., 2002, Liu, Li et al., 2002, Marin et al., 2003, Yost, Torres et al., 1996). Next, this phosphorylated β-Catenin species is ubiquitinated by the β-TRCP-SCF complex, priming it for degradation via the proteasome (Cruciat, 2014). In the presence of Wnt ligands, however, Axin is expelled from the destruction complex through as yet unidentified mechanisms, and phosphorylated β-Catenin is thought to accumulate and saturate the destruction

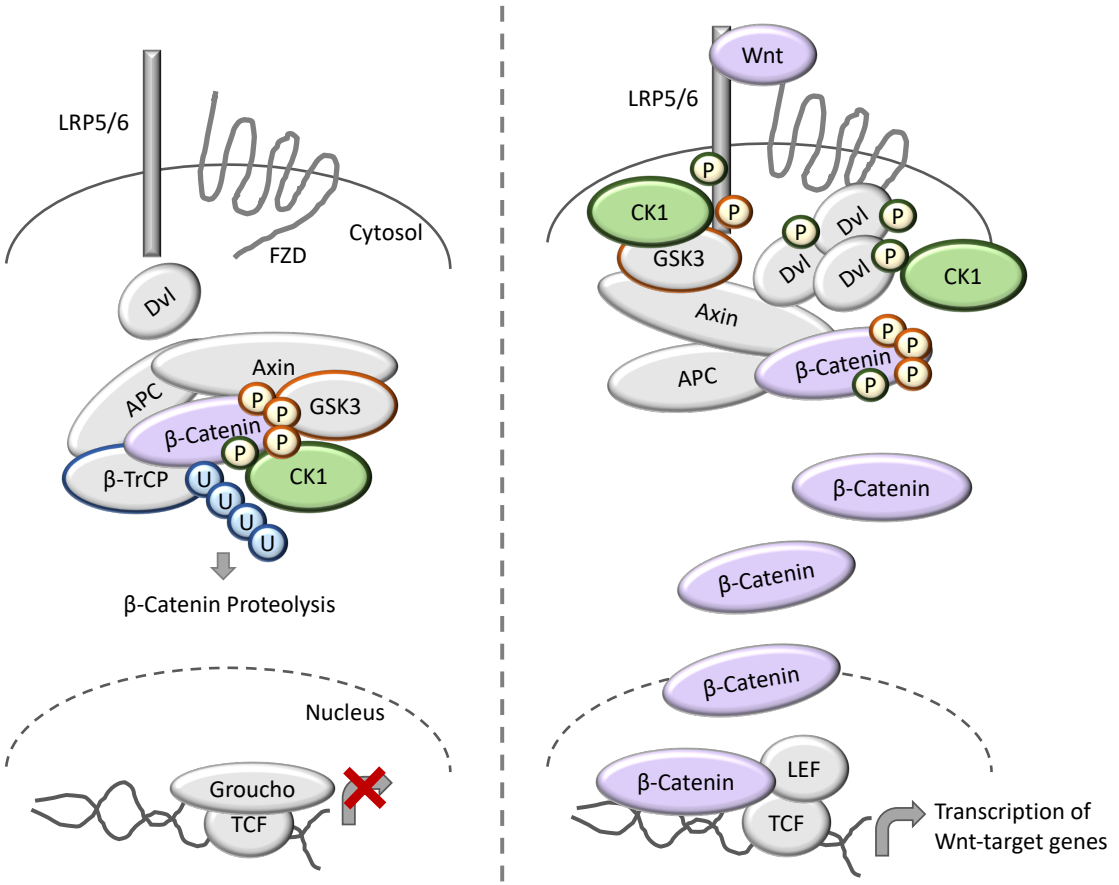

Figure 1-3: Schematic representation detailing the involvement of CK1 in Wnt signalling: In the absence of Wnt ligands, β-catenin is held by the so-called destruction complex composed of Axin, APC, the SCF E3 ubiquitin ligase substrate receptor β-TRCP, and the kinases CK1 and GSK3. Sequential phosphorylation of β-Catenin by CK1 and GSK3 triggers β-catenin ubiquitination by the β-TRCP-complex, and its subsequent proteasomal degradation. In the nucleus, Groucho binds TCF to block the transcription of Wnt target genes. Following binding of Wnt ligands to the receptors, LRP5/6 becomes phosphorylated, and triggers the formation of the Wnt signalosome, largely composed of Axin and Dvl. This recruits the destruction complex to the membrane. β-catenin is stabilised in the cytosol and is free to enter the nucleus where it displaces Groucho from TCF, and together with LEF activates transcription of Wnt target genes. CK1 has been reported to phosphorylate LRP5/6 and Dvl in the presence of Wnt ligands.

complex (Cruciat, 2014, Stamos & Weis, 2013, Teo & Kahn, 2010) (Figure 1-3). Subsequently, the newly translated β-Catenin is free to translocate to the nucleus and initiate transcription of Wnt target genes (Cruciat, 2014, Stamos & Weis, 2013, Teo & Kahn, 2010) (Figure 1-3).

Despite this seemingly conclusive model, the exact CK1 isoform that mediates phosphorylation of β-Catenin on Ser45 has not been irrefutably identified. This is largely due to the non-selective nature of CK1 inhibitors, and the fact that CK1 isoforms are largely essential for cell viability, thereby making genetic ablation experiments very challenging, if not impossible. Indeed, virtually all CK1 isoforms have been implicated in Wnt signalling (Cruciat, 2014, Del Valle-Perez, Arques et al., 2011, Gao & Chen, 2010), thereby making it extremely difficult to decipher the function of individual CK1 members within the Wnt pathway. Further complexity to the regulation of Wnt signalling by CK1 stems from the reported phosphorylation of the Wnt receptor-associated protein Dvl by CK1ε, which is thought to increase the affinity between Dvl and the Wnt receptor complex (Bryja, Schulte et al., 2007, Cheong & Virshup, 2011, Del Valle-Perez et al., 2011). Thus, in this context, CK1-mediated phosphorylation acts to promote Wnt signalling, in stark contrast to its inhibitory role within the destruction complex. Thus, exactly how CK1 isoforms can act to both positively and negatively regulate the same signalling pathway presents an intriguing paradox, yet adds further credence to the influence that CK1 regulating proteins and modifications are likely to have in coordinating these constitutively-active protein kinases.

1.1.4.2: p53 signalling:

The tumour suppressor protein p53 functions as a key regulator of many aspects of biology, including the cell cycle, apoptosis and DNA damage responses (Bieging, Mello et al., 2014). Both p53 and its inhibitory interacting proteins mouse double minute homologue 2 and 4 (MDM2 and MDM4) are substrates of CK1 isoforms (Dumaz, Milne et al., 1999, Knippschild, Milne et al., 1997, Winter, Milne et al., 2004). MDM2 and MDM4 are E3 ubiquitin ligases responsible for regulating p53 stability. CK1α, δ and ε

have all been shown to be capable of phosphorylating p53 at Ser9 *in vitro*, with phosphorylation by CK1α only occurring at high CK1α concentrations (Milne, Palmer et al., 1992). Additionally, CK1δ and ε were shown to phosphorylate p53 in cultured cells (Knippschild et al., 1997). CK1δ-mediated phosphorylation of MDM2 was shown to result in reduced affinity between p53 and MDM2, thereby resulting in stabilisation and subsequent activation of p53 (Dumaz et al., 1999, Knippschild et al., 1997, Winter et al., 2004). Thus, the data would suggest that CK1 activity is important in p53 activation.

However, and as seen in Wnt signalling, different CK1 isoforms can have contrasting effects on p53 signalling, depending on the experimental conditions used and the cell type being investigated. Indeed, knockdown of CK1α has been shown to activate p53 (Elyada, Pribluda et al., 2011, Jaras, Miller et al., 2014, Sarasqueta, Forte et al., 2013). In agreement, one study showed that CK1α associates with MDM2 to inactivate p53, through increasing MDM2-p53 binding affinity (Wu, Chen et al., 2012). This was further cemented through independent observations where CK1α knockdown led to a reduction in the MDM2-p53 interaction, thereby increasing p53 activity (Huart, MacLaine et al., 2009). Interestingly, in agreement with CK1α regulating p53 stability, a recent publication reported that ablation of CK1α in keratinocytes induced p53-dependent, sunburn-protective skin hyperpigmentation (Chang, Kuo et al., 2017). In addition, p53 activity leads to upregulation of CK1δ, but not CK1ε, thereby suggesting an autoregulatory feedback mechanism between CK1δ and p53 (Knippschild et al., 1997). Indeed, CK1δ kinase activity is reduced in p53-deficient primary lymphocytes, compared to wild-type controls (Maritzen, Lohler et al., 2003). Thus, at least in the case of p53 signalling, the role of CK1 phosphorylation appears more complex than a mere kinase-substrate relationship.

1.1.4.3: Hippo signalling:

During development, Hippo signalling contributes to correct organ maturation, through the regulation of cell proliferation and apoptosis (Zhao, Li et al., 2010). As such, dysfunctional Hippo signalling can lead to tumorigenesis and cancer. In mammals, the Hippo pathway begins through stimulation by growth-suppressive signals, such as cellular stresses and contact inhibition (Figure 1-4). Within the Hippo pathway, the upstream kinases mammalian STE20-like protein kinase 1/2 (MST1/2) act to phosphorylate the large tumour suppressor 1 and 2 (LATS1/2), and LATS1/2 subsequently phosphorylate the transcriptional co-activator yes-associated protein (YAP) and its paralog transcriptional co-activator with PDZ-binding domain (TAZ) (Zhao et al., 2010) (Figure 1-4). Phosphorylation of YAP/TAZ leads to their inhibition through phosphodegron-mediated proteolysis, in addition to promoting their separation from their cognate nuclear-localised transcription factor targets, such as SMAD (Zhao et al., 2010) (Figure 1-4). Effectively, YAP/TAZ phosphorylation leads to Hippo pathway inhibition.

CK1 isoforms have been suggested to regulate Hippo signalling. Indeed, CK1δ or ε have been proposed to phosphorylate YAP after priming phosphorylation from LATS1/2 (Zhao et al., 2010). This phosphorylation event was proposed to act as a phosphodegron signal, and mediate recruitment of the SCF E3 ubiquitin ligase complex containing β-TrCP (Zhao et al., 2010). Similarly, CK1ε has been reported to phosphorylate TAZ to promote TAZ degradation through a phosphodegron signal, again following priming phosphorylation from LATS1/2 (Liu, Zha et al., 2010). Interestingly, cross-talk between the Wnt and Hippo pathways has been suggested to be mediated through CK1ε (Xu, Wang et al., 2014). Following MST1 binding to CK1ε, CK1ε is sequestered and unable to phosphorylate Dvl, thereby leading to inhibition of the Wnt

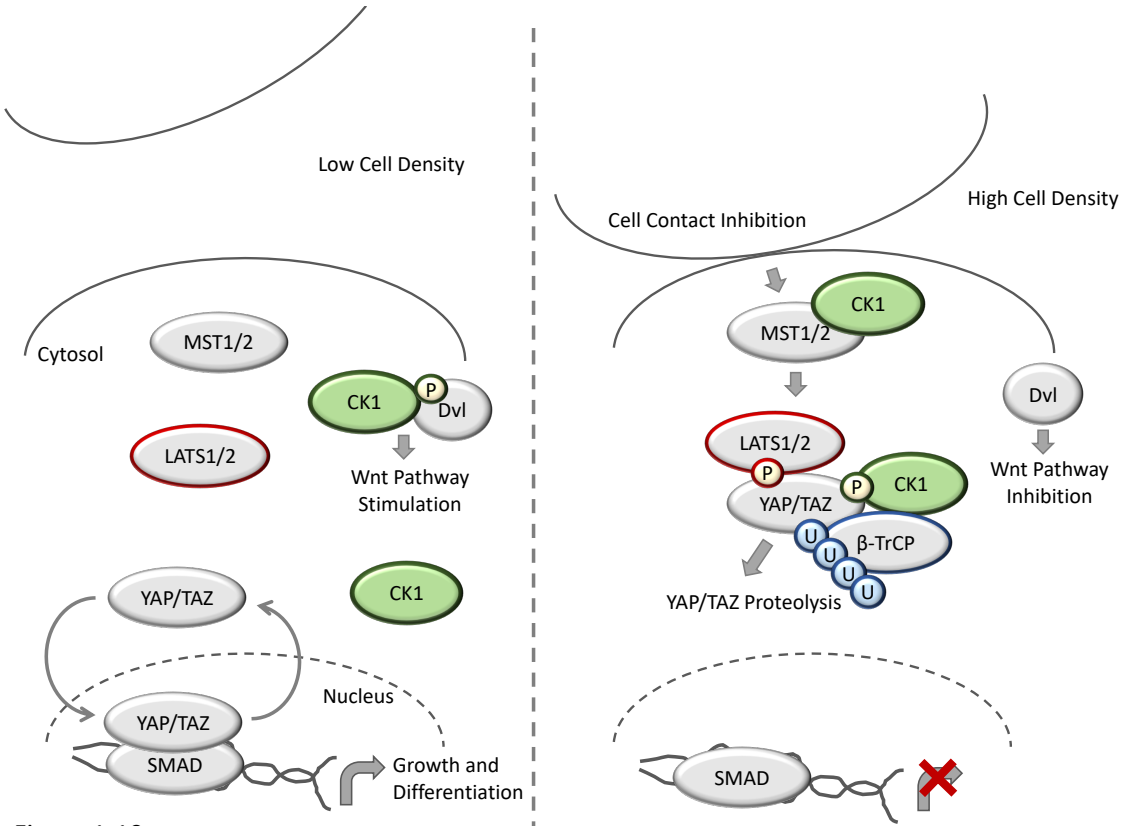

Figure 1-4: Schematic representation detailing the involvement of CK1 in Hippo signalling: Under conditions of low cell density, the YAP/TAZ transcriptional coactivator complex cycles between the cytosol and nucleus, and in the nucleus YAP/TAZ bind to their cognate transcription factor targets such as SMAD to trigger transcription of Hippo target genes to promote cell growth and differentiation. CK1 phosphorylates Dvl to promote Wnt signalling under these conditions. Under conditions of cell stress, such as contact inhibition, the kinase MST1/2 becomes activated and phosphorylates LATS1/2, which promotes LATS1/2-mediated phosphorylation of YAP/TAZ. YAP/TAZ phosphorylation acts as phosphodegron signal to promote YAP/TAZ ubiquitination by β-TrCP, and subsequent YAP/TAZ proteolysis. As YAP/TAZ cannot enter the nucleus, Hippo target gene transcription is suppressed and cells cease to grow. CK1 has been reported to phosphorylate YAP/TAZ after priming phosphorylation from LATS1/2, and following CK1 binding to MST1/2, CK1 phosphorylation of Dvl is restricted, leading to inhibition of Wnt signalling.

signalling pathway (Xu et al., 2014). Thus, in this context, MST1 can act as key regulator of CK1ε, by promoting a change in its subcellular localisation and restricting access between CK1ε and its substrates.

1.1.4.4: Cell division:

The cell cycle in eukaryotes is divided into two main phases: interphase, in which the cell replicates its DNA and duplicates its organelles in preparation for division; and M phase, in which cell division takes places, creating two genetically identical daughter cells in the process (Nigg, 2001). Throughout the cell division cycle, checkpoint mechanisms are in place to ensure the correct and efficient replication and distribution of both the DNA, and the cytoplasm (Macurek, Lindqvist et al., 2008, Nigg, 2001). The yeast orthologue of CK1 was among the first kinases identified to have a role in the regulation of cell cycle progression (Hoekstra, Liskay et al., 1991). In mammals, however, where there are multiple CK1 isoforms present, the precise contribution of each isoform to the regulation of the cell division cycle is not well understood. CK1δ has been found to localise to centrosomes, and displays high affinity towards microtubules in response to DNA damage, suggesting a checkpoint role for CK1δ in cell division (Behrend, Milne et al., 2000, Stoter, Bamberger et al., 2005). Furthermore, inhibition of CK1δ/ε using IC261 is accompanied with cell cycle arrest (Behrend et al., 2000).

In addition to CK1δ, CK1α has long been suggested to have a role in mitosis. Early immunostaining efforts identified CK1α on mitotic spindles (Brockman, Gross et al., 1992), and CK1α morpholinos triggered mitotic arrest and chromosomal alignment defects in mouse oocytes (Wang, Lu et al., 2013).

1.1.4.5: Circadian rhythm:

Circadian rhythms are biological processes that oscillate in a predictable, entrainable manner, that are regulated by an endogenous time keeper, or circadian clock (Takahashi, 2017). CK1 was the first kinase found to regulate the circadian clock. In *Drosophila,* the CK1 orthologue doubletime (dbt) phosphorylates the transcription

factor PERIOD (PER), which acts to modulate the oscillatory circadian cycle (Kloss, Price et al., 1998). In mammals, in the brain and periphery, oscillatory transcriptional feedback encompasses the positive regulatory CLOCK-BMAL (Brain and muscle ARNT-like 1) complex, which acts to activate transcription of the mammalian PER orthologues PER1-3, as well as cryptochrome proteins termed CRY1-2 (King & Takahashi, 2000, Reppert & Weaver, 2002) (Figure 1-5). Following their transcription, the newly-synthesised PER and CRY proteins dimerise and translocate to the nucleus where they bind and inhibit the CLOCK-BMAL complex, thereby preventing their own transcription (King & Takahashi, 2000, Reppert & Weaver, 2002) (Figure 1-5). In doing so, one circadian cycle is thus completed. Subsequently, CK1-dependent phosphorylation of PER proteins induces PER degradation by the proteasome, thereby initiating a new circadian cycle, and the process repeats (Akashi, Tsuchiya et al., 2002, Takano, Uchiyama et al., 2004, Vielhaber, Eide et al., 2000) (Figure 1-5). CK1ε has also been shown to phosphorylate BMAL and CRY proteins (Eide, Vielhaber et al., 2002), although the relevance of these phosphorylation events are yet to be determined.

The exact physiological CK1 isoform(s) responsible for PER1/2 phosphorylation is a subject of debate, but CK1δ and ε have both been implicated, and the vast majority of data support roles for both isoforms in the regulation of circadian rhythm. Perhaps the most striking evidence for the involvement of CK1 in the regulation of circadian rhythm stems from evidence gathered in *CSNK1E*-deficient mice (Etchegaray, Machida et al., 2009). In these mice, which lack expression of CK1ε, the length of circadian rhythms were significantly longer compared to wild-type littermates (Etchegaray et al., 2009). Similarly, mice heterozygous for *CSNK1D* deletion present with longer circadian rhythms, whereas homozygous *CSNK1D* knockout mice died in the perinatal period (Etchegaray et al., 2009). Furthermore, a mutation in the Syrian hamster *CSNK1E1* gene

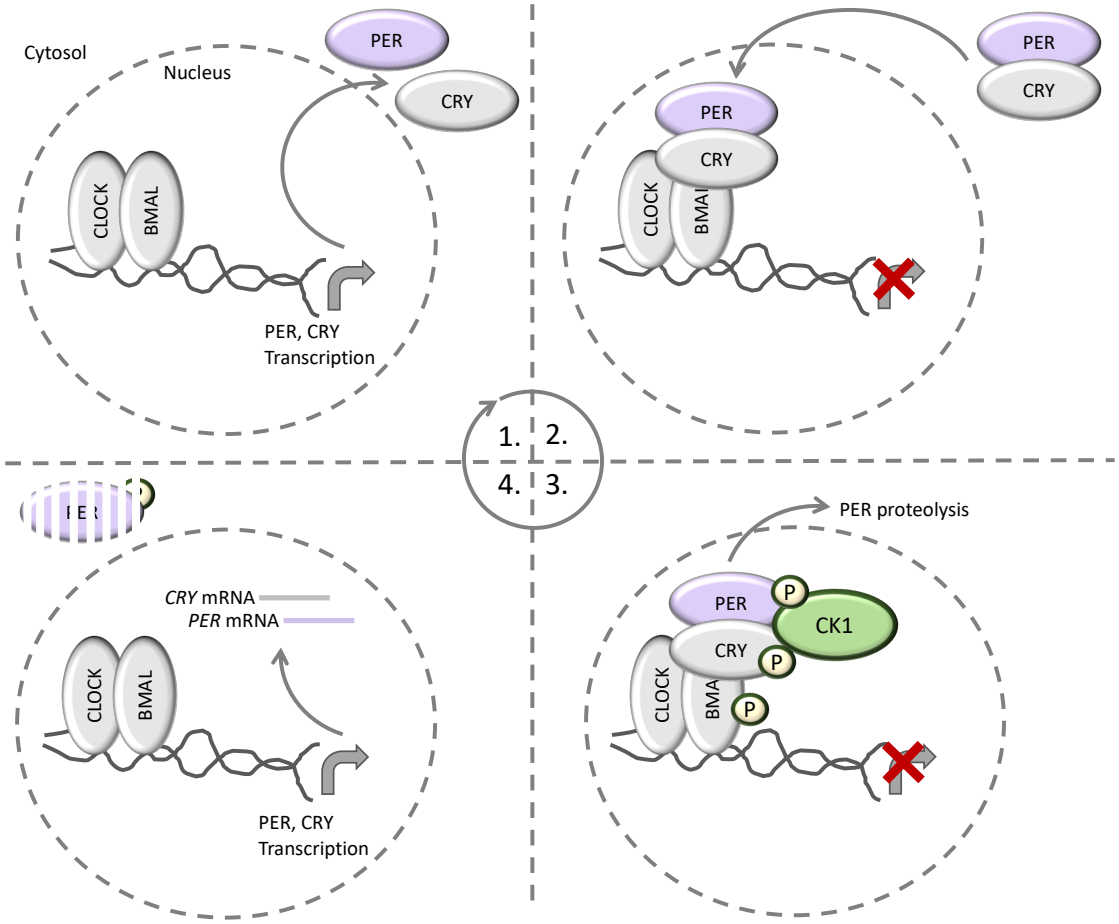

Figure 1-5: Schematic representation detailing the involvement of CK1 in the regulation of circadian rhythm: The circadian cycle begins with the CLOCK-BMAL complex, which acts to activate the transcription of PER and CRY. Following their translation, PER and CRY proteins heterodimerise and translocate to the nucleus where they act to inhibit CLOCK-BMAL, thereby preventing their own transcription. Subsequently, CK1 phosphorylates PER to trigger PER proteolysis and relieve CLOCK-BMAL inhibition. The cycle then begins again. CK1 has also been reported to phosphorylate CRY and BMAL, but the relevance of these phosphorylation events remains to be elucidated.

(T178C) increases catalytic activity towards PER proteins, resulting in reduced PER stability and shorter circadian rhythms (Meng, Logunova et al., 2008). Collectively, there is strong evidence supporting roles for both CK1δ and ε in circadian rhythm regulation, suggesting that there may be redundancy between these two enzymes.

As CK1δ and ε are very closely related proteins (Figure 1-2), it is feasible that they may act redundantly in some contexts. The fact that *CSNK1E*-deficient mice are surprisingly viable, whereas *CSNK1D*-deficient mice are not (Etchegaray et al., 2009), perhaps suggests that the non-circadian rhythm functions of CK1δ are indispensable for viability, whereas those of CK1ε are not. Thus, there seems to be a limit to CK1δ and ε redundancy, likely dependent on the biological process in question.

1.1.4.6: Hedgehog signalling:

Hedgehog (Hh) signalling is critical for both correct development and maintenance of healthy adult cells, although the activity of the Hh signalling pathway is vastly reduced in adulthood (Ingham & McMahon, 2001). Hh signalling contributes to the maintenance of epithelia and tissue regeneration, thus, unsurprisingly, dysfunctional Hh signalling can lead to tumorigenesis and cancer (Beachy, Karhadkar et al., 2004, Wicking, Smyth et al., 1999). Within the mammalian Hh pathway, ligands such as sonic hedgehog (Shh) bind to the negative regulator of the pathway, the transmembrane receptor protein patch homologue (PTCH), which is in complex with the positive Hh regulator smoothened homologue precursor (SMO) (Varjosalo & Taipale, 2008) (Figure 1-6). Upon PTCH stimulation, SMO is released from PTCH, and is free to mediate activation and release of GLI transcription factors from a cilia-localised, GLI-inhibitory multiprotein complex containing the kinases CK1, GSK3 and protein kinase A (PKA) (Varjosalo & Taipale, 2008) (Figure 1-6). Once free, the GLI transcription factors are free to translocate to the nucleus and induce transcription of Hh-dependent target genes (Figure 1-6). Conversely, in the absence of PTCH stimulation by Hh ligands, SMO remains bound to PTCH, and the GLI transcription factors are phosphorylated by CK1,

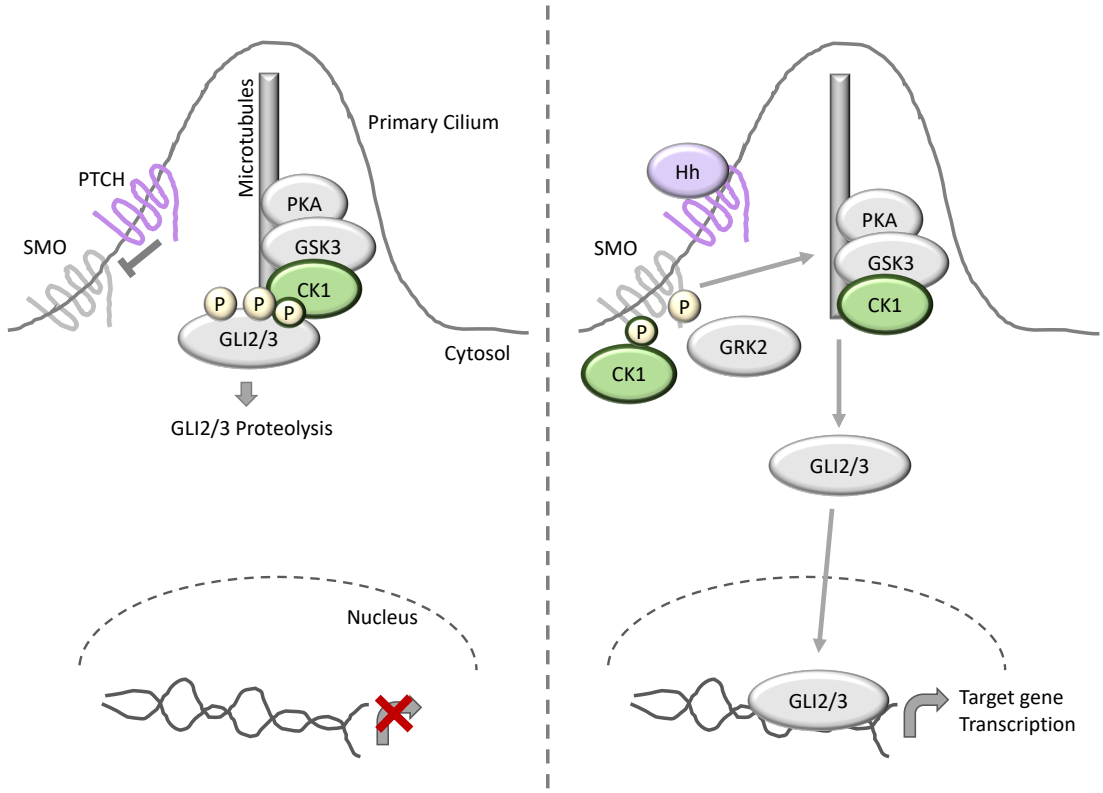

Figure 1-6: Schematic representation detailing the involvement of CK1 in hedgehog signalling: In the absence of hedgehog (Hh) ligands, the Hh receptor PTCH associates with SMO to inhibit SMO function. The GLI2/3 transcription factors are held in complex by a primary cilium-localised inhibitory complex consisting of the kinases CK1, GSK3 and PKA. Following GLI2/3 phosphorylation by CK1, GSK3 and PKA, GLI2/3 is marked for proteasomal degradation. In the presence of Hh ligands, SMO is released from PTCH and is free to mediate the release of GLI2/3 from the inhibitory kinase complex. GLI2/3 can now translocate to the nucleus and induce Hh target gene transcription. CK1 and GRK2 have been reported to phosphorylate SMO to promote full SMO activation and maximal release of GLI2/3 from the inhibitory complex.

GSK3 and PKA to trigger their proteasomal degradation (Denef, Neubuser et al., 2000, Taipale, Cooper et al., 2002, Varjosalo & Taipale, 2008) (Figure 1-6).

In addition to the role of CK1 in promoting GLI transcription factor proteolysis, CK1 was also shown to have a positive regulatory role within the Hh pathway. Mammalian SMO was shown to be phosphorylated by CK1α and G protein-coupled receptor kinase 2 (GRK2), to promote full SMO activation and release of GLI transcription

factors from the inhibitory multiprotein complex (Chen, Sasai et al., 2011). Thus, as seen with the other signalling pathways reviewed above, CK1 isoforms appear to have both a positive and negative regulatory influence on the Hh signalling pathway.

1.1.4.7: Apoptosis:

Programmed cell death, or apoptosis, is an evolutionary conserved mechanism whereby cells act to terminate themselves in an effort to limit the proliferation of faulty and disease-prone cell populations (Elmore, 2007). In short, proteins called death receptors such as Fas, and tumour necrosis factor receptor 1 (TNFR1), act to transduce extrinsic apoptotic cues, ultimately leading to the formation of the intracellular death-inducing-signalling-complex (DISC) (Elmore, 2007). DISC proteins go on to recruit caspases in order to propagate the apoptotic signal (Elmore, 2007). The involvement of CK1 in apoptosis has been well documented, and CK1 has been implicated in various programmed cell death molecular pathways. CK1 isoforms can phosphorylate the TNF receptor p75, thereby negatively regulating p75-mediated apoptosis (Beyaert, Vanhaesebroeck et al., 1995). Furthermore, inhibition of CK1 isoforms, or RNAi-mediated silencing of *CSNK1A1,* sensitises tumour cells to TNF-related apoptosis-inducing ligand (TRAIL)-induced apoptosis (Izeradjene, Douglas et al., 2004). Recently, IC261-mediated inhibition of CK1δ/ε was shown to result in decreased expression of anti-apoptotic proteins, with a concurrent heightened sensitivity to apoptosis, in pancreatic cancer cells (Brockschmidt, Hirner et al., 2008).

Again, the exact contribution of each CK1 isoform in apoptosis is not well established, and more selective tools are required in order to ascertain which CK1 kinase acts where in the various apoptotic pathways.

1.1.5: CK1 in disease:

Given the involvement of CK1 isoforms in many, key signalling pathways involved in regulating proliferation, cell growth and viability, it is unsurprising that dysfunctional CK1 activity has been linked to disease. Of note, neurodegeneration and cancer are particularly prominent diseases that CK1 isoforms have been implicated in (Knippschild et al., 2005a, Knippschild, Kruger et al., 2014, Knippschild, Wolff et al., 2005b). In addition to the obvious effects dysfunctional CK1 activity would have on p53-dependent genomic stability (see section 1.2.4.2), CK1ε mutations in breast cancer were found to cause loss-of-function in the canonical Wnt signalling pathway (Foldynova-Trantirkova, Sekyrova et al., 2010). CK1ε expression was also found to be elevated in a variety of adenoid cystic carcinomas, including those derived from ovarian, renal and prostatic cancers (Rodriguez, Yang et al., 2012, Yang & Stockwell, 2008). Additionally, CK1α was found to be essential for acute myeloid leukemia (AML) viability, and treatment with D4476 resulted in selective killing of the AML cells (Jaras et al., 2014). However, a common theme that has emerged whilst investigating the functions of CK1 isoforms, is that they can act in both a positive and negative manner within the same signalling pathways. As such, it is very difficult to call an individual CK1 isoform a tumour suppressor or an oncogene.

The role of CK1 isoforms in neurodegenerative diseases is perhaps best showcased in Alzheimer's disease (AD). CK1δ transcripts are up-regulated 30-fold in the hippocampus of AD brains (Ghoshal, Smiley et al., 1999), and it is thought that CK1δ phosphorylates the AD-related protein tau, leading to the formation of neurofibrillary tangles (Li, Yin et al., 2004). CK1ε has been proposed to regulate the processing of amyloid precursor protein (APP), and thus dysfunctional CK1ε activity has been linked to the formation of amyloid plaques (Flajolet, He et al., 2007).

Given such pleiotropy in the cellular roles of CK1 kinases, they have long been deemed undruggable kinases. Thus, methods to selectively inhibit CK1-specific functions, in a temporally and spatially controlled manner, are highly warranted, yet extremely challenging to generate. That said, recent years have seen increasing interest in CK1 isoforms as drug targets (Knippschild et al., 2014). However, due to high homology between their kinase domains (Figure 1-2), isoform-specific CK1 inhibitors have been next to impossible to develop. However, several small molecule CK1 inhibitors have been generated and many have been used to aid research into CK1 function (Table 1-1) (Knippschild et al., 2014). However, due to their non-isoform-selective nature, data should be interpreted with caution, especially when assigning CK1-substrate relationships.

As alternative approaches to kinase inhibition, the thalidomide-related drug lenalidomide was recently found to induce the degradation of CK1α through recruiting CK1α to the cereblon-containing Cullin 4 ubiquitin E3 ligase complex, for its subsequent ubiquitination and proteolytic degradation (Stahl & Zeidan, 2017). Such treatment with lenalidomide was shown to be effective in the treatment of pre-leukemic human myelodysplastic syndrome (MDS) (Stahl & Zeidan, 2017). As an alternative strategy, CK1α-derived peptides were successfully employed to block binding between CK1α and MDM2 (Huart et al., 2012). These blocked the CK1α-MDM2 interaction without inhibiting CK1α kinase activity, and led to a reduction in p53 proteolysis with concurrent heightened p53 stability (Huart et al., 2012). Such approaches are attractive as they provide a means to inhibit selective CK1-dependent processes, whilst rendering other, unrelated CK1-associated processes intact. Although, one can imagine that such peptides would impact the binding to other CK1-interacting proteins, and lenalidomide-induced proteolysis is known to target many proteins other than CK1α for proteasomal

Inhibitor	CK1 Isoform targeted	In vitro IC50 (μM)	Known off-targets	References
CKI-7	α/δ/ε	6.00	ERK8/SGK1/MNK1/AMPK/PIM1/PIM3	Chijiwa et al, 1989, Bain et al, 2007
IC261	δ/ε	2.50	CK1α/PIM1/PIM3	Mashhoon et al, 2000, Bain et al, 2007
D4476	δ	0.30	CK1α/ALK5/p38	Rena et al, 2004
DAA	δ	0.30	CK2	Cozza et al, 2008
R-DRF053	δ/ε	0.01	CDKs	Oumata et al, 2008
PF-670462	δ/ε	0.013/0.08	PKA/PKC/p38/GSK3	Walton et al, 2009
PF-4800567	δ/ε	0.032/0.70	EGFR	Walton et al, 2009
CR8	δ/ε	Not reported	CDKs/GSK3	Bettayeb et al, 2008, Delehouze et al, 2014
Hua-1h	γ	0.02	CK1α/δ	Hua et al, 2012
Bischof-5	δ/ε	0.04/0.199	CK1α	Bischof et al, 2012
SR-653234	δ/ε	0.16/0.54	FLT3/CDKs	Bibian et al, 2013
SR-1277	δ/ε	0.049/0.26	FLT3/CDKs	Bibian et al, 2013
SR-3029	δ/ε	0.044/0.26	FLT3/CDKs	Bibian et al, 2013
Richter-1	δ/ε	0.02/0.21	CK1α/CK1αL/FLT3	Richter et al, 2014
Richter-2	δ/ε	0.14/0.52	CK1αL/CK1γ/FLT3/CLK/DYRK1/DYRK2/MLCK	Richter et al, 2014
Halekotte 11-b	δ	0.04	CK1ε/CK1α/p38/JNK/RIPK/LCK	Halekotte et al, 2017

Table 1-1: Summary of CK1-inhibitory agents: Known CK1 inhibitors are listed, along with the respective CK1 isoform(s) that they target. Their *in vitro* IC50 values and known off-targets are provided, along with the appropriate reference(s).

degradation (An, Ponthier et al., 2017). Interestingly, CK1-activating compounds, such as pyrvinium pamoate, have also been described (Kucherenko, Zelenak et al., 2012), although their mechanism of action remain contentious (Venerando, Girardi et al., 2013). However, these are thought to be very non-selective drugs, and as such, their potential value in both basic research and in therapeutics, remain to be determined.

1.2: Post-translational control of cell division:

As mentioned in the previous subchapter, CK1 kinases are known to participate in the regulation of cell division. In this thesis, I present evidence supporting a role for CK1α in mitotic spindle positioning. Thus, an appreciation for the post-translational mechanisms regulating cell division, and in particular mitotic spindle positioning, is required to aid the understanding of this thesis, and will be discussed in the following sections.

Accurate execution of the cell division cycle results in the precisely coordinated replication and subsequent separation of DNA and cytoplasm into two newly-formed daughter cells (Figure 1-7). The cell cycle is divided into two main phases: interphase and mitosis. Interphase is further divided into the Gap 1 phase (G1), where the cell synthesises mRNA and proteins in preparation for the subsequent stages of the cell cycle, Synthesis phase (S), where DNA replication occurs, and Gap 2 phase (G2), a period of rapid cell growth and protein synthesis where the cell prepares for mitosis. Multiple regulatory checkpoints exist in cells to ensure that the cell cycle occurs with precision and accuracy, and errors at any point can be detrimental to the cell and organism as a whole (Dephoure, Zhou et al., 2008, King, Deshaies et al., 1996, Kronja & Orr-Weaver, 2011). Many disease states, most notably cancer, have been linked to aberrant cell cycle control (Dephoure et al., 2008, Massague, 2004, Williams & Stoeber, 2012). Deciphering the regulatory modes of the cell cycle is thus a topic of wide research interest, from both a basic science and therapeutic standpoint. Whilst many regulatory mechanisms exist in the G1, S and G2 phases, this sub-chapter will focus on the regulatory mechanisms coordinating M phase of the eukaryotic cell cycle, particularly those pertaining to phosphorylation- and ubiquitination-mediated regulation.

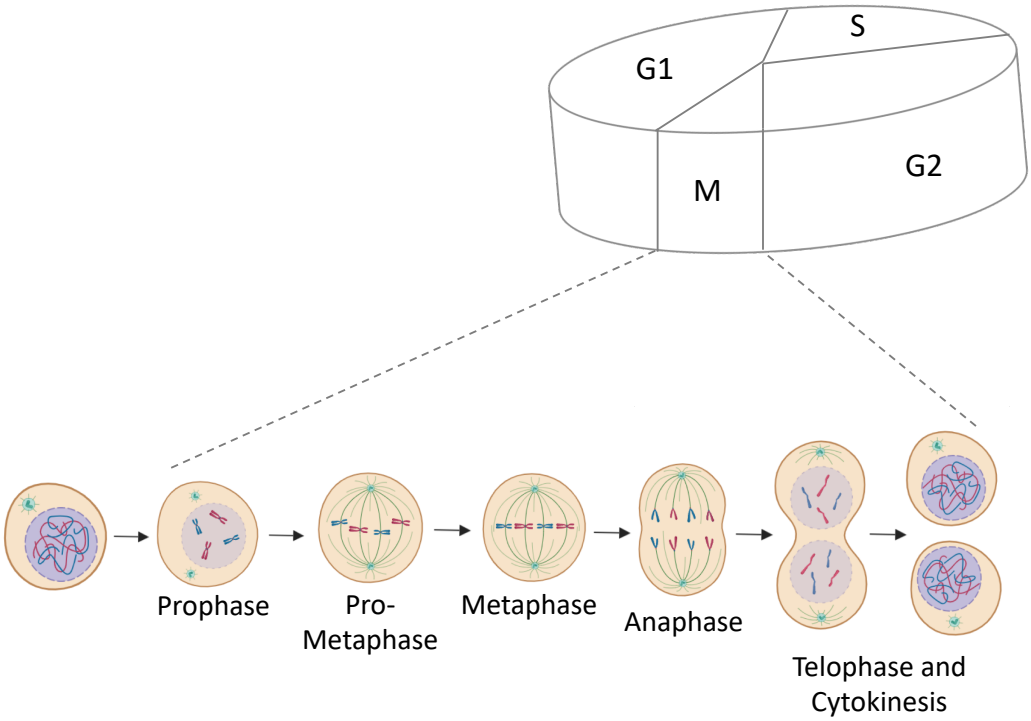

Figure 1-7: Overview of the cell division cycle: The eukaryotic cell cycle is divided into 4 main stages – G1, S, G2 and M. M phase is the shortest phase and can be further subdivided into prophase (where the chromatin condenses), prometaphase (where the mitotic spindle begins to be established and spindle microtubules start to capture the chromosomes), metaphase (where the chromosomes are lined up along the cell equator), anaphase (where sister chromatids separate and the cell begins to divide), telophase (where the sister chromatids reach opposite poles and the nuclear envelope starts to reform), and cytokinesis (the division of the cytoplasm). *Created with BioRender.*

1.2.1: Overview of mitotic kinases:

The entry into mitosis is accompanied by a profound increase in the level of protein phosphorylation throughout the cell (Dephoure et al., 2008, Ly, Whigham et al., 2017, Nousiainen, Sillje et al., 2006). Many studies have determined the critical roles protein phosphorylation plays in key mitotic processes, such as chromosome condensation and mitotic spindle assembly (Nigg, 2001). Historically, the observation that protein phosphorylation was dramatically increased following entry into mitosis

was a key cornerstone in the identification of M-phase promoting factor (MPF) (Masui & Markert, 1971, Rao & Johnson, 1970). MPF consists of a protein kinase termed cell division cycle 2 [Cdc2, aka cyclin-dependent kinase 1 (CDK1)], and its associated regulatory subunit called Cyclin B (Lohka, Hayes et al., 1988). Since then, several other protein kinases have been identified as having instrumental roles in eukaryotic cell division, and enormous effort has been devoted to understanding the roles of these protein kinases in mitosis, and to the identification of their physiological substrates.

The most-studied of these protein kinases will be individually explored in the subsequent sections.

1.2.1.1: Cyclin-dependent kinases:

Cyclin-dependent kinases (CDKs) are Ser/Thr protein kinases, whose activity is dependent on a regulatory subunit termed cyclin. CDKs belong to the CMGC branch of the human kinome tree, along with the MAPKs, GSK3, CDK-like kinases, and members of the dual-specificity tyrosine-regulated kinases (DYRKs) (Manning et al., 2002). To date, 20 members of the CDK family have been identified, and these have been designated CDK1-CDK20 (Malumbres, Harlow et al., 2009). Like the other CMGC kinases, CDKs are proline-directed Ser/Thr kinases with a preference for the S/T-P-X-K/R consensus motif (Echalier, Endicott et al., 2010).

CDKs were first identified through genetic and biochemical studies in model organisms such as yeast and *Xenopus* (Malumbres & Barbacid, 2005). These experiments established CDKs as critical regulators of the cell cycle. The founding member, CDK1, was identified in genetic screens searching for yeast mutants with defects in cell division (Hartwell, 1974, Hartwell, Mortimer et al., 1973). CDK1, designated Cdc2 in *Schizosaccharomyces pombe,* and Cdc28 in *Saccharomyces cerevisiae*, was found to be

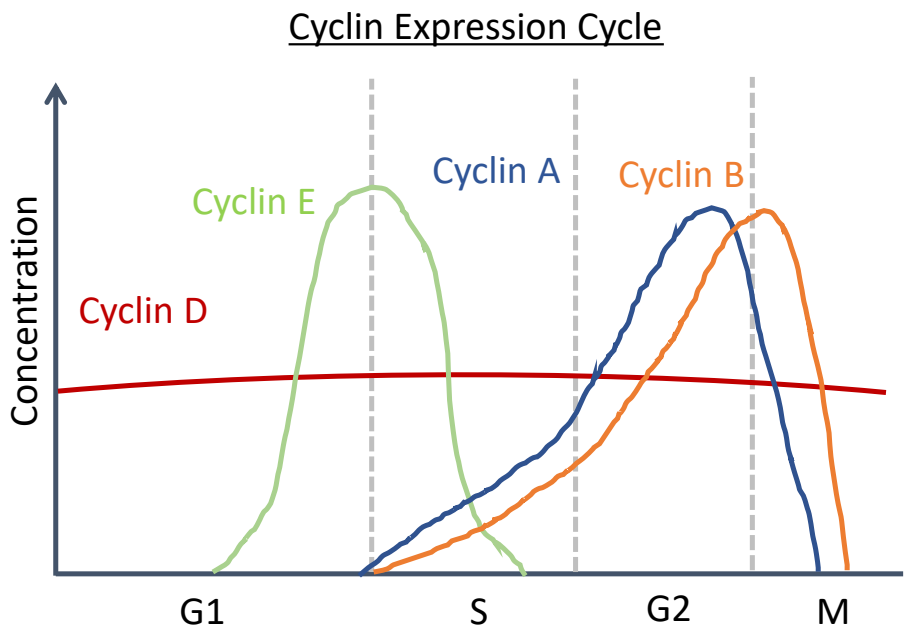

Figure 1-8: Overview of cyclin expression during a mammalian cell cycle: Cyclin D levels remain constant during the cell cycle. Cyclin E levels rise dramatically at the G1/S transition. Cyclin A and Cyclin B levels rise in G2 and decline during M phase.

essential for cell-cycle progression (Russell & Nurse, 1986), and soon after its discovery, a Cdc2 homologue was identified in human cells (Lee & Nurse, 1987). With the advent of cDNA libraries and polymerase chain reaction (PCR) technology, many other CDK family members were identified, and their role as crucial regulators of eukaryotic cell division began to be appreciated (Elledge & Spottswood, 1991, Matsushime, Ewen et al., 1992, Meyerson, Enders et al., 1992, Xiong, Zhang et al., 1992).

Independent studies in sea urchin oocytes led to the identification of some proteins that were synthesised and degraded at each cleavage division (Evans, Rosenthal et al., 1983). Due to this cyclical nature in their expression, these proteins were termed cyclins (Figure 1-8). Subsequently, cyclins were cloned from fertilised sea urchin and clam embryos, and their expression was demonstrated to promote meiosis in *Xenopus* embryos (Swenson, Farrell et al., 1986). In agreement with their reported evolutionary conservation, related proteins termed cdc13, Cln and Cyclin B were

identified in *S. pombe, S. cerevisiae* and humans, respectively. The biochemical connection between CDKs and cyclins came in 1989 when researchers determined that CDK1 associates with Cyclin A and B in starfish, clam and *Xenopus* oocytes (Nurse, 1990). In mammals, subsequent studies identified the additional cyclins, Cyclin C, D and E. CDK1-Cyclin binding is required for CDK1 catalytic activity, and isolated CDKs present with minimal enzymatic output (Xiong & Beach, 1991).

Following completion of DNA synthesis, A-type cyclins bind CDK1 and CDK2 and these CDK-Cyclin A complexes act to resolve S phase and promote entry into the G2 phase (Malumbres & Barbacid, 2005). During G2, A-type cyclins are degraded through ubiquitin-mediated proteolysis, and the B-type cyclins are actively synthesised. Consequently, CDK1 associates with the newly-formed Cyclin B and this active complex is thought to regulate several key steps during the G2/M transition (Malumbres & Barbacid, 2005, Nigg, 2001). Of note, CDK1-Cyclin B complexes have been shown to localise to centrosomes during prophase to phosphorylate the motor protein Eg5, in order to promote centrosome separation (Nigg, 2001). Many substrates have been reported for CDK1-Cyclin B during this transition. These include histones, whose phosphorylation by CDK1 promote chromosome condensation, and lamins, whose phosphorylation trigger nuclear envelope breakdown. CDK1 activity has also been shown to activate several other mitotic protein kinases (Malumbres & Barbacid, 2005, Nigg, 2001).

The inactivation of CDK1-Cyclin B complexes is required for proper mitotic exit. This inactivation is achieved through the proteasomal degradation of Cyclin B following ubiquitination by the anaphase-promoting complex E3 ligase (see section 1.3.2) (Chang, Xu et al., 2003, King et al., 1996). Although many CDK1-Cyclin B substrates have been identified (Enserink & Kolodner, 2010, Ly et al., 2017, Malumbres & Barbacid, 2005),

direct kinase-substrate relationships are challenging to demonstrate as inhibition of CDK1 leads to G2 arrest, and cells already in mitosis rapidly exit the cell cycle following CDK1 inhibition (Vassilev, 2006). Thus, many of the reported substrates may be indirectly dephosphorylated following mitotic exit.

1.2.1.2: Polo-like kinases:

The discovery of CDKs prompted investigation into other protein kinase that may cooperate with CDKs in the regulation of cell division. One such kinase family identified in this vein was the polo-like kinase (PLK) family. PLKs are Ser/Thr protein kinases that were first described in lower eukaryotes (Llamazares, Moreira et al., 1991, Sunkel & Glover, 1988). In *Drosophila melanogaster,* a mutant of the protein polo was found to present with defects in mitosis (Sunkel & Glover, 1988), and subsequently, PLK homologues were identified in mammals (Barr, Sillje et al., 2004).

All PLKs have a similar architecture. PLKs present with an N-terminal kinase domain, and a C-terminal regulatory domain containing two signature motifs, termed polo boxes (Barr et al., 2004). Humans have 5 PLK enzymes, termed PLK1-5, however the exact role and contribution of each PLK isoform is not well understood (Barr et al., 2004). As PLK1 is thought to mediate most of the functions attributed to the *D. melanogaster* polo, the focus will be on PLK1 in the subsequent sections.

Similar to many other protein kinases, human PLK1 is activated through phosphorylation within its T-loop (at Thr210), by an upstream protein kinase (Jang, Ma et al., 2002, Lee & Erikson, 1997, Qian, Erikson et al., 1999). Whilst still a topic of debate, Aurora kinase A has been reported to be the upstream PLK1 kinase in cells (Macurek et al., 2008), although other kinases have also been implicated (Ji, Hwang et al., 2010). Emerging as a key regulatory feature of PLK1 in cells, the polo boxes have been shown

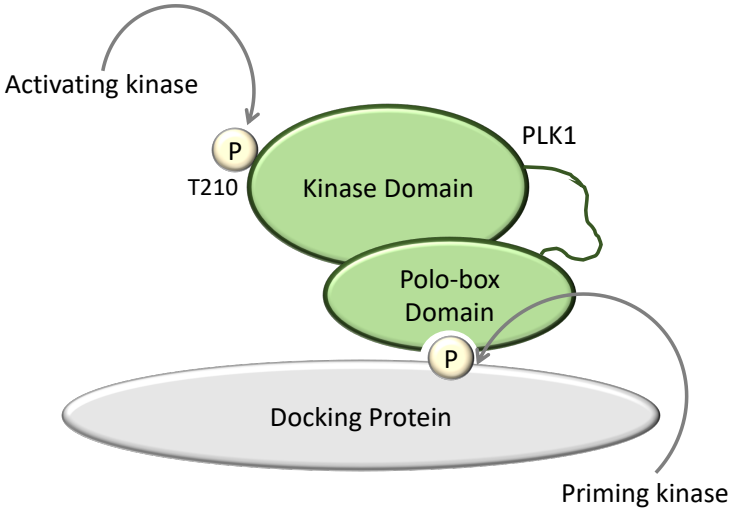

Figure 1-9: Overview of PLK1 regulation: PLK1 is activated by phosphorylation at T210 in its kinase domain by an upstream kinase (largely thought to be AURKA). Following phosphorylation of docking proteins, the newly-formed phosphoepitope acts as a receptor for the polo-box domain of PLK1 to bind, thereby facilitating PLK1 localisation to distinct cellular sites.

to be instrumental in mediating PLK localisation (Jang, Lin et al., 2002, Lee, Grenfell et al., 1998, Reynolds & Ohkura, 2003, Song, Grenfell et al., 2000) (Figure 1-9). The polo-box domain (PBD) of PLK1 acts as a phosphopeptide-binding motif, and in this capacity, the PBD facilitates the recruitment of PLK1 to phosphorylated docking proteins, following priming phosphorylation of the docking protein by a distinct kinase (Cheng, Lowe et al., 2003, Elia, Cantley et al., 2003, Elia, Rellos et al., 2003, Neef, Preisinger et al., 2003). In cases where the phosphorylated docking proteins are localised to cellular structures, such as kinetochores and centrosomes (where PLK1 is known to reside), PBD-mediated targeting also imparts spatial control towards PLK1 (Arnaud, Pines et al., 1998, Golsteyn, Mundt et al., 1995, Lee, Yuan et al., 1995, Seong, Kamijo et al., 2002); and many PBD-binding proteins have been identified (Park, Soung et al., 2010). In the absence of a phosphopeptide ligand, the PBD is thought to associate with the kinase

domain of PLK1, thereby impeding kinase activation and substrate binding (Marshall, 1994). However, upon PBD-phosphopeptide association, the kinase domain is thought to be released from the PBD, and together with T-loop phosphorylation, acts to activate PLK1 (Marshall, 1994).

In both interphase and mitosis, PLK1 localises to centrosomes, and centrosome-localised PLK1 in mitosis has been reported to be critical for spindle pole formation, and positioning of the mitotic spindle (see section 1.3.3) (Connell, Chen et al., 2017, Kiyomitsu & Cheeseman, 2012). Interestingly, following inhibition of PLK1, monopolar spindles form due to defective centrosome separation, and cells arrest in mitosis (Connell et al., 2017, Kiyomitsu & Cheeseman, 2012). Whilst the exact PLK1-dependent substrate landscape is not fully elucidated, many proteins involved in centrosome function and microtubule dynamics have been reported (Park et al., 2010, Santamaria, Wang et al., 2011). Recent attempts at defining the optimal PLK1 substrate motif have been made, with (E/D/Q)-X-(S/T)-Ø, where Ø denotes a hydrophobic amino acid, emerging as the putative consensus motif (Barr et al., 2004).

In mitotic cells, PLK1 also associates with kinetochores, the centromere-associated protein complexes to which microtubules attach that are required for chromosome segregation, during the latter stages of cell division (Arnaud et al., 1998, Barr et al., 2004). Kinetochores can sense unattached chromosomes, and even one unattached chromosome can trigger a checkpoint mechanism known as the spindle assembly checkpoint (SAC) (Musacchio, 2015). The localisation of PLK1 to kinetochores thus suggests a role for PLK1 in kinetochore assembly, regulation of kinetochore-microtubule connections, and/or modulation of the SAC. CDK1 has been suggested as a priming kinase for PBD-mediated PLK1 recruitment (Barr et al., 2004), but whether this holds true for the kinetochore-localised PLK1 remains unclear, as CDK1/Cyclin B activity

would be reduced at this stage of mitosis. Thus, other kinases may act in this capacity, and thereby promote localised PLK1 activity in mitosis.

1.2.1.3: Aurora kinases:

The *aurora* gene was first identified in the late 1980s in a *Drosophila* screen aimed at identifying genes whose products control cell cycle progression (Glover, 1989, Glover, 1991, Glover, Leibowitz et al., 1995). Since the discovery of homologues in other species, the Aurora kinases (AURKs) have emerged as central players in cell division (Carmena, Ruchaud et al., 2009). AURKs are thus highly conserved, and present with similar domain architecture between homologues (Ke, Dou et al., 2003). AURKs possess an N-terminal domain, a Ser/Thr protein kinase domain, and a C-terminal domain (Bolanos-Garcia, 2005). The N- and C- terminal domains are thought to be important in regulating AURK stability, as well as in determining the interaction partners of distinct AURK members (Bolanos-Garcia, 2005).

In humans there are three AURKs, designated AURKA, B and C, and they have different localisation profiles (Nigg, 2001). AURKA localises to the duplicated centrosomes at the start of S phase, and shifts to bipolar spindle microtubules during mitosis (Bischoff & Plowman, 1999, Giet & Prigent, 1999). AURKB, on the other hand, localises to chromosomes in prophase, the centromere in prometaphase and metaphase, before shifting to the central spindle in anaphase and the mid-body in cytokinesis (Bischoff & Plowman, 1999, Giet & Prigent, 1999). The least-studied family member, AURKC, is localised to chromosomes during mitosis, and, unlike AURKA and B, is principally expressed in the male and female germline of mammals (Carmena et al., 2009, Wang, Jiang et al., 2014).

Interestingly, AURKs have distinct modes of regulation through binding different regulatory proteins. For example, following nuclear envelope breakdown, AURKA is recruited to spindle microtubules by binding the microtubule-associated protein targeting protein for Xklp2 (TPX2), where TPX2 serves the additional purpose of allosterically activating AURKA (Carmena et al., 2009, Chen, Mohan et al., 2014, Kufer, Sillje et al., 2002). At this time point, AURKA activity is required for spindle assembly and spindle microtubule dynamics. AURKB is a component of the chromosome passenger complex (CPC), which consists of three AURKB-regulatory proteins termed inner centromere protein (INCENP), borealin and survivin (Kelly, Sampath et al., 2007, Vader, Kauw et al., 2006a, Vader, Medema et al., 2006b). INCENP, borealin and survivin all act as both targeting and activating subunits of AURKB (Kelly et al., 2007, Vader et al., 2006a, Vader et al., 2006b). The CPC has been linked to correction of microtubule-chromosome attachment errors, and activation of the SAC (Vader et al., 2006b). Interestingly, a single amino acid change in human AURKA (G198N) renders the kinase AURKB-like, promoting localisation to chromosomes and interaction with INCENP and survivin. Curiously, this AURKA mutant was able to rescue mitotic defects resulting from AURKB knockdown (Fu, Bian et al., 2009, Hans, Skoufias et al., 2009).

Additionally, centrosomal AURKA was shown to be activated and localised by the protein Bora, a highly-conserved AURKA-interacting protein originally identified due to its phenotypic similarity to AURKA (Hutterer, Berdnik et al., 2006). Bora-depleted cells frequently present with multipolar mitotic spindles, an effect reminiscent of TPX2 knockdown. Thus, Bora is thought to be a key AURKA activator in cells (Hutterer et al., 2006). The AURKA-Bora complex was suggested to be the upstream PLK1-activating kinase, thereby illustrating some of the crosstalk evident in mitotic kinase regulation (Macurek et al., 2008).

1.2.1.4: Kinetochore kinases:

Given the name kinetochore by Lester Sharp in the 1930s, kinetochores are the power-generating business ends of chromosomes during mitosis (Sharp, 1934). In their capacity to bridge spindle microtubules to chromosomes, kinetochores are key focal points of phosphorylation-mediated regulation, for both the SAC and cell cycle progression (London & Biggins, 2014, Sacristan & Kops, 2015). The kinases CDK1, PLK1 and AURKB discussed above have all been implicated in the regulation of the SAC and subsequent attachment error-correction (Sacristan & Kops, 2015). However, two other kinases have critical roles in the SAC and their roles and regulation will be subsequently explored.

The transition to anaphase is triggered by the E3 ligase anaphase-promoting complex/cyclosome (APC/C), which acts to ubiquitinate inhibitors of mitotic exit (cyclin B) and of chromosome segregation (securin), thereby marking them for proteolysis (Chang et al., 2003, Pines, 2011). Thus, when an attachment error is created, the SAC acts to inhibit the APC/C, and in doing so, prevents the metaphase-to-anaphase transition. The kinetochore-localised multi-protein complex responsible for the inhibition of APC/C in response to attachment error is called the mitotic checkpoint complex (MCC) (Sacristan & Kops, 2015). The MCC assembles on unattached kinetochores, and following its assembly, is free to diffuse throughout the cell to inhibit the APC/C (Sacristan & Kops, 2015). MCC assembly is coordinated by the kinase monopolar spindle 1 (Mps1), and Mps1 activity drives the recruitment of SAC proteins such as the kinase budding uninhibited by benzimidazoles 1 (BUB1), the regulatory proteins BUB3, mitotic arrest-deficient 1 (Mad1), Mad2, the APC/C co-activator cdc20, and the pseudokinase BUB-related 1 (BUBR1) (Kemmler, Stach et al., 2009, Murray,

2011, Nijenhuis, von Castelmur et al., 2013, Vleugel, Hoogendoorn et al., 2012). Mps1 is thus the master regulator of the SAC.

Mps1 is activated by autophosphorylation upon its localisation to kinetochores, which is regulated by AURKB, again illustrating some of the cross-talk evident between mitotic kinases (Kang, Chen et al., 2007, Santaguida, Vernieri et al., 2011, Saurin, van der Waal et al., 2011). Mps1 is then in a position to efficiently recruit the MCC, including the BUB1 kinase. The importance of BUB1 is perhaps best showcased in yeast-centred experiments, where deletion of *BUB1* in *S. pombe* increases the rate of chromosome missegregation, and deletion of *BUB1* in *S. cerevisiae* causes slow growth and chromosome loss (Bernard, Hardwick et al., 1998, Warren, Brady et al., 2002). BUB1 is also required for the kinetochore localisation of MAD1, MAD2 and BUBR1, following its recruitment by Mps1 (Klebig, Korinth et al., 2009). BUB1 has been linked to the phosphorylation and subsequent inhibition of cdc20, thereby providing a mechanistic insight into how the SAC acts to inhibit the APC/C following chromosome attachment error (Reddy, Rape et al., 2007, Tang, Shu et al., 2004).

1.2.1.5: Underappreciated mitotic kinases:

Whilst research has primarily focussed on the roles and regulation of the conventional mitotic kinase families mentioned above, it is beginning to be appreciated that these kinase families alone, cannot account for the full extent of protein phosphorylation that is evident during mitosis (Ly et al., 2017, Malik, Lenobel et al., 2009, Malik, Nigg et al., 2008, Nousiainen et al., 2006). Interestingly, a recent proteomic study sought to identify and assign cell cycle-regulated phosphopeptides to known kinases, based on the optimal consensus motifs present within the phosphopeptides (Ly et al., 2017). In this manner, whilst CDKs and PLKs were identified within the top ten

kinase families, the vast majority of phosphopeptides conformed to the predicted motifs for CK1, CK2, PKA and GSK3 kinases (Ly et al., 2017). Indeed, mitotic roles for some of these kinases, and others such as protein kinase C (PKC) and NIMA-related kinases (NEKs), have also been reported (Fry, Bayliss et al., 2017, Martini, Soliman et al., 2018, O'Regan, Blot et al., 2007, Saurin, Durgan et al., 2008).

Like CK1 (see section 1.2.4.4), CK2 isoforms are highly conserved, and are thought to be constitutively-active Ser/Thr protein kinases (Litchfield & Luscher, 1993). CK2 has been implicated in the regulation of chromosome condensation through the phosphorylation of condensin 1 (Takemoto, Kimura et al., 2006). CK2-mediated condensin 1 phosphorylation is thought to inhibit the action of condensin 1 during interphase, until the G2/M transition (Takemoto et al., 2006). Additionally, ablation of CK2 in *S. cerevisiae* was shown to block cell cycle progression through inhibition of the G1/S and G2/M transitions (Glover, 1998, Lorenz, Pepperkok et al., 1993, Pepperkok, Lorenz et al., 1994, Pepperkok, Lorenz et al., 1991). Interestingly, a subset of CK2 was shown to localise to the mitotic spindle apparatus through association with the peptidyl-prolyl isomerase Pin1 (St-Denis, Bailey et al., 2011).

The mitotic role of GSK3 is beginning to be unravelled, particularly in the context of spindle microtubule regulation. GSK3 activity was shown to be required for the SAC, as GSK3 inhibition or its knockdown with RNAi reduced mitotic arrest in the presence of the SAC-inducing microtubule-stabilising agent taxol (Rashid, Mazur et al., 2018). GSK3 inhibition has also been linked to defects in chromosome alignment and spindle dynamics (Wakefield, Stephens et al., 2003).

The role of PKC in mitosis is well-documented. PKCε was shown to regulate the process of cytokinesis, and inhibition of PKCε blocked cells in the final stages of separation (Saurin et al., 2008). At the molecular level, PKCε is phosphorylated by p38

MAPK, GSK3, and PKCε itself, and these phosphorylation events were shown to promote the association between PKCε and 14-3-3 binding proteins (Saurin et al., 2008). The interaction between PKCε and 14-3-3 was determined to be important in regulating this cytokinetic function of PKCε. More recently, PKCε was reported to impact the earlier stages of mitosis, with PKCε activity being linked to the coordination of mitotic spindle assembly and centrosome migration, through modulating dynein motor protein function (Martini et al., 2018).

The NEKs are a curious group of mitotic kinases. The founding member of this family was identified in the filamentous fungus *Aspergillus nidulans*, as part of a screen aimed at identifying regulators of the cell cycle (Morris, 1975). This screen identified two types of mutant: those that became blocked in mitosis (bim), or those that became blocked in interphase, and were never in mitosis (nim) (Morris, 1975). The first of the latter class was found to encode a Ser/Thr protein kinase, and was called nimA (Oakley & Morris, 1983, Osmani, McGuire et al., 1991, Osmani, May et al., 1987). NIMA-related kinases have since been identified in higher eukaryotes, and different NEKs have been attributed to different functions within the cell cycle (Fry et al., 2017, O'Regan et al., 2007). For example, NEK2 localises to the centrosome and been linked to the regulation of centrosome separation, and a complex containing NEK6, 7 and 9 has been shown to coordinate spindle assembly (Fry et al., 2017, O'Regan et al., 2007). Thus, despite the name, NEKs do participate in mitosis, and are emerging as key regulators of cell division.

Thus, whilst CDKs, PLKs and Aurora kinases have been the main focus of research in terms of kinases coordinating cell division, the contribution of other kinase families to the phosphorylation-mediated control of mitosis cannot be ignored, and is beginning to be unravelled and appreciated.

1.2.2: Proteolytic control of mitosis:

Central to the progression of mitosis is the proteasomal-mediated degradation of cell cycle-regulated proteins. This is particularly evident in the metaphase-to-anaphase transition, where the targeted degradation of specific proteins is critical for the segregation of sister chromatids, and subsequent progression through the cell cycle (Chang et al., 2003, Pines, 2011). Two different ubiquitin E3 ligase complexes are thought to be the main players coordinating the proteolysis of cell cycle-regulated proteins: the Skp1/Cullin/F-box (SCF) E3 ligase complex, and the APC/C.

The SCF is functional throughout the cell cycle, but its activity is most profound at the G1/S and G2/M boundaries where SCF-mediated ubiquitylation and subsequent degradation of proteins triggers these cell cycle phase transitions (Pintard, Willems et al., 2004). The APC/C on the other hand is mainly required within M phase, and acts to regulate the progression through and exit from mitosis. The APC/C will now be explored in more detail in the next section.

1.2.2.1: The APC/C:

The APC/C is a large multi-protein complex, harbouring 14 subunits (Brown, VanderLinden et al., 2015, Chang, Zhang et al., 2014, Dube, Herzog et al., 2005). No clues about the biochemical functions of most of these subunits can be inferred from their sequence composition. However, two subunits termed Apc2 and Apc11 have homology with proteins involved in other ubiquitination systems. Apc2 resembles a cullin, and Apc11 shares homology with a really interesting new gene (RING)-H2 protein (Deshaies, 1999, Gmachl, Gieffers et al., 2000, Yu, Peters et al., 1998). Thus, the Apc2-11 complex is thought to comprise the catalytic core of the APC/C. Despite containing a cullin subunit, substrate recognition by the APC/C is mediated through a different mechanism

to other cullin RING E3 ligases (CRLs). Two distinct co-activating proteins, Cdc20 and Cdh1, act to coordinate APC/C activity and substrate recognition at different stages of the cell cycle (Fang, Yu et al., 1998, Kramer, Gieffers et al., 1998, Sigrist & Lehner, 1997, Visintin, Prinz et al., 1997).

Cdc20 was originally identified in *Drosophila* as *fizzy*, a gene required for normal metaphase-to-anaphase transition (Dawson, Roth et al., 1993). Subsequently, fizzy mutants were shown to block the mitotic degradation of cyclins A and B, thereby implicating fizzy as a key regulator of mitotic cyclin stability (Dawson, Roth et al., 1995). Subsequently, a distinct *Drosophila* protein was identified that shared significant homology to Fizzy, and was termed Fizzy-related. In contrast to Fizzy, Fizzy-related was required for cyclin removal during the G1 phase (Sigrist & Lehner, 1997). In higher eukaryotes, Fizzy-related is called Cdh1. Subsequent studies in yeast and humans determined that the Cdc20-associated APC/C complex was the principle driver of chromosome segregation in the metaphase-to-anaphase transition (Pines, 2011).

To avoid the catastrophic effects resulting from chromosome missegregation, APC/C-Cdc20 activity is tightly regulated. APC/C binds Cdc20 only in mitosis, once APC/C has been phosphorylated (Golan, Yudkovsky et al., 2002, Kraft, Herzog et al., 2003, Kramer, Scheuringer et al., 2000, Lahav-Baratz, Sudakin et al., 1995). Even then, as detailed above (see section 1.3.1.4), the SAC can inhibit APC/C-Cdc20 activity until all chromosomes are correctly bioriented (Musacchio, 2015). Following APC/C-Cdc20-mediated ubiquitination of B-type cyclins, which inhibits the kinase activity of CDK1, and of securin, an inhibitor of the protease separase, the subsequent proteolysis of securin activates separase and triggers sister chromatid separation through cleavage of cohesin (Figure 1-10) (Primorac & Musacchio, 2013). Cohesin is a component of the protein complex that mediates sister chromatid cohesion, thus its proteolysis promotes rapid

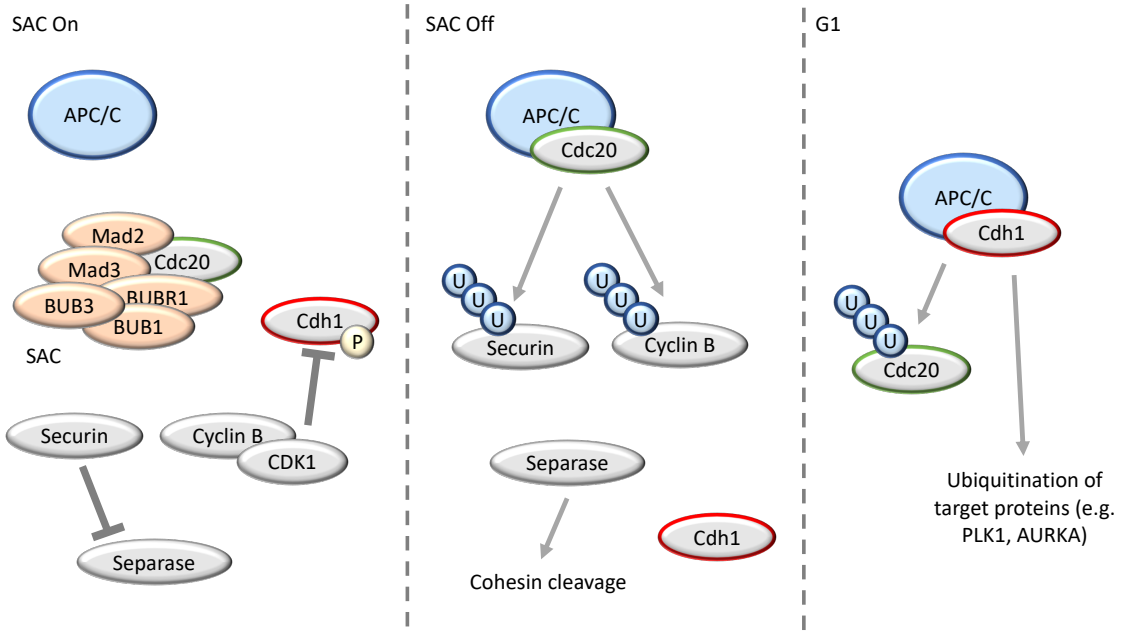

Figure 1-10: Modes of regulation of the anaphase-promoting complex/cyclosome (APC/C): When a kinetochore is unattached to a chromosome, the spindle assembly checkpoint (SAC), consisting of the proteins Mad2, Mad3, BUB1, BUB3 and BUBR1, is activated and sequesters the APC/C coactivator Cdc20. In the absence of Cdc20 binding, the APC/C substrates securin and cyclin B are stabilised, leading to inhibition of separase, and maintenance of CDK1-cyclin B activity respectively. CDK1-cyclin B phosphorylates the APC/C coactivator Cdh1 to inhibit it during this time. Once all kinetochores are engaged with the chromosomes, the SAC is turned off, and Cdc20 associates with APC/C leading to APC/C activation. APC/C-Cdc20 ubiquitinates securin and cyclin B, leading to cohesin cleavage by separase, and inhibition of CDK1/cyclin B activity respectively. Following mitotic exit, Cdh1 associates with APC/C, and APC/C-Cdh1 ubiquitinates Cdc20 and other target proteins such as PLK1 and AURKA.

chromosome segregation. In contrast, the APC/C-Cdh1 complex is active throughout G1 and in post-mitotic cells (Peters, 1998).

The E3 ligase activity of the APC/C is tightly coordinated to ensure that specific APC/C substrates are only degraded at the appropriate times during the cell cycle. The formation of both APC/C-Cdc20 and APC/C-Cdh1 complexes are subject to regulation by mitotic kinases (Golan et al., 2002, Kraft et al., 2003, Kramer et al., 2000, Lahav-Baratz et al., 1995). Phosphorylation of APC/C by CDK1 and PLK1 is thought to increase Cdc20

binding, and subsequently promote more APC/C E3 ligase activity (Golan et al., 2002, Kraft et al., 2003, Kramer et al., 2000, Lahav-Baratz et al., 1995). In contrast, CDK1-mediated phosphorylation of Cdh1 inhibits APC/C-Cdh1 binding, and thereby prevents Cdh1-induced activation of the APC/C in mitosis (Blanco, Sanchez-Diaz et al., 2000, Kramer et al., 2000, Zachariae, Schwab et al., 1998). Thus, during the metaphase-to-anaphase transition, where APC/C-Cdc20 activity results in the degradation of cyclin B and a concurrent reduction in CDK1 activity, CDK1-mediated Cdh1 phosphorylation is also reduced, allowing APC/C-Cdh1 complex formation following mitotic exit. Furthermore, a key APC/C-Cdh1 substrate during G1 is Cdc20, and Cdc20 proteolysis allows efficient APC/C-Cdh1 assembly, and prevents premature progression through the cell cycle (Robbins & Cross, 2010). The binding of Cdc20 or Cdh1 to APC/C, in addition to promoting activation of APC/C, is also thought to control substrate recognition (Pines, 2011). Once bound to APC/C, these coactivators act to recruit substrates through their WD40 propeller domains. The WD40 domains recognise degron sequences in target proteins, such as the destruction (D) and KEN boxes (Pines, 2011). Once recruited to the APC/C, the substrates are ubiquitinated, promoting their proteasomal degradation (Pines, 2011).

Thus, there is an important interplay between the processes of ubiquitination and phosphorylation in mitosis, and these processes are tightly controlled to ensure the error-free transition through the cell cycle.

1.2.3: Mechanisms of spindle positioning:

During mitosis, all animal cells establish a microtubule-based, diamond-shaped structure, known as the mitotic spindle (Figure 1-11). The central organiser of the spindle is the centrosome, from which microtubules are nucleated. Microtubules

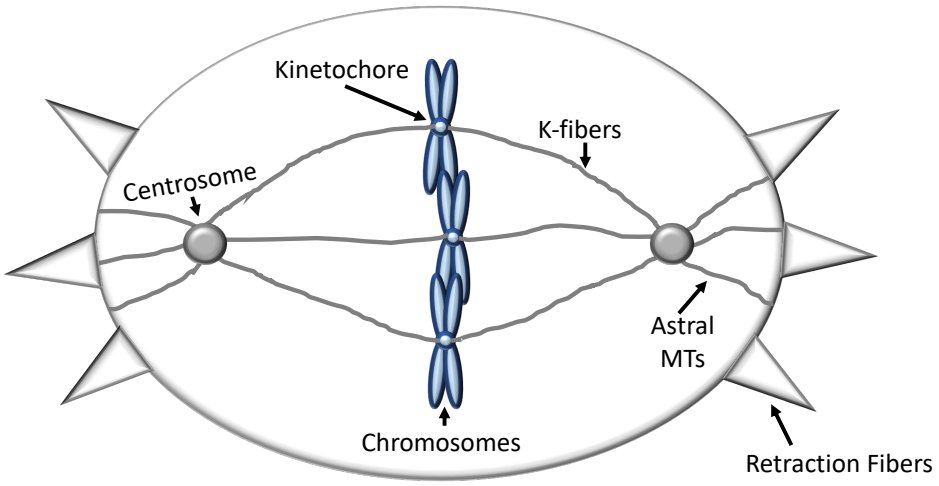

Figure 1-11: Schematic overview of the cell division machinery: Centrosomes are anchored to the cell cortex by astral microtubules (astral MTs), and to the chromosomes by kinetochore microtubules (K-fibers). Kinetochores are the chromosome-associated protein complex to which K-fibers bind. The cell adheres to the extracellular matrix through the action of retraction fibers.

emanating from the centrosome towards the chromosomes are called kinetochore microtubules, as they bind the kinetochores of sister chromatids (Figure 1-11). Microtubules emanating from the centrosome towards the cell cortex, an actin-rich cytoskeleton beneath the plasma membrane, are known as astral microtubules (Figure 1-11). Astral microtubules are important in propagating the force required to pull apart the sister chromatids during the metaphase-to-anaphase transition (Grill & Hyman, 2005, Siller & Doe, 2009).

As correct and efficient positioning of the mitotic spindle determines the axis of cell division, and is critically important in both development and in the maintenance of healthy adult tissues (Bergstralh, Dawney et al., 2017, Gonczy, 2008, Kiyomitsu & Cheeseman, 2012, Lu & Johnston, 2013), mechanisms regulating spindle orientation have been a strong focus of research during the last few decades (Figure 1-12). The most

established of these spindle positioning mechanisms will now be examined in the following sections.

1.2.3.1: Cortical pulling:

One of the major pathways contributing to spindle positioning in metazoans depends on forces generated at the cell cortex acting on astral microtubules, and thus centrosomes, which literally pull the spindle at both ends to establish correct spatial positioning. At the molecular level, seminal work in *Caenorhabditis elegans* identified that these pulling forces are primarily generated by a conserved protein complex composed of a large coiled-coil protein called LIN5 (abnormal cell lineage 5), two near-identical tetratricopeptide and GoLoCo domain-containing proteins (GPR1/2), and heterotrimeric G protein alpha subunits (Gα) (Gotta, Dong et al., 2003, Grill, Howard et al., 2003, Park & Rose, 2008). Gα is localised to the plasma membrane through the process of myristoylation, and as such, the whole LIN5-GPR1/2-Gα complex is recruited to the cell cortex beneath the plasma membrane (Park & Rose, 2008). In higher eukaryotes such as humans, LIN5 is known as nuclear mitotic apparatus (NuMa), and GPR1/2 is called LGN (thus named for its 10 Leu-Gly-Asn repeats). NuMa directly associates with the minus-end directed motor protein dynein to promote dynein recruitment to the cell cortex (Kotak, Busso et al., 2012, Nguyen-Ngoc, Afshar et al., 2007, Okumura, Natsume et al., 2018). This cortically-anchored dynein is then thought to generate pulling forces on the astral microtubules, to promote spindle positioning (Figure 1-12). In mammals, NuMa/dynein levels are drastically enriched at the cell cortex as the cell progresses from metaphase into anaphase (Kiyomitsu & Cheeseman, 2013, Kotak, Busso et al., 2013).

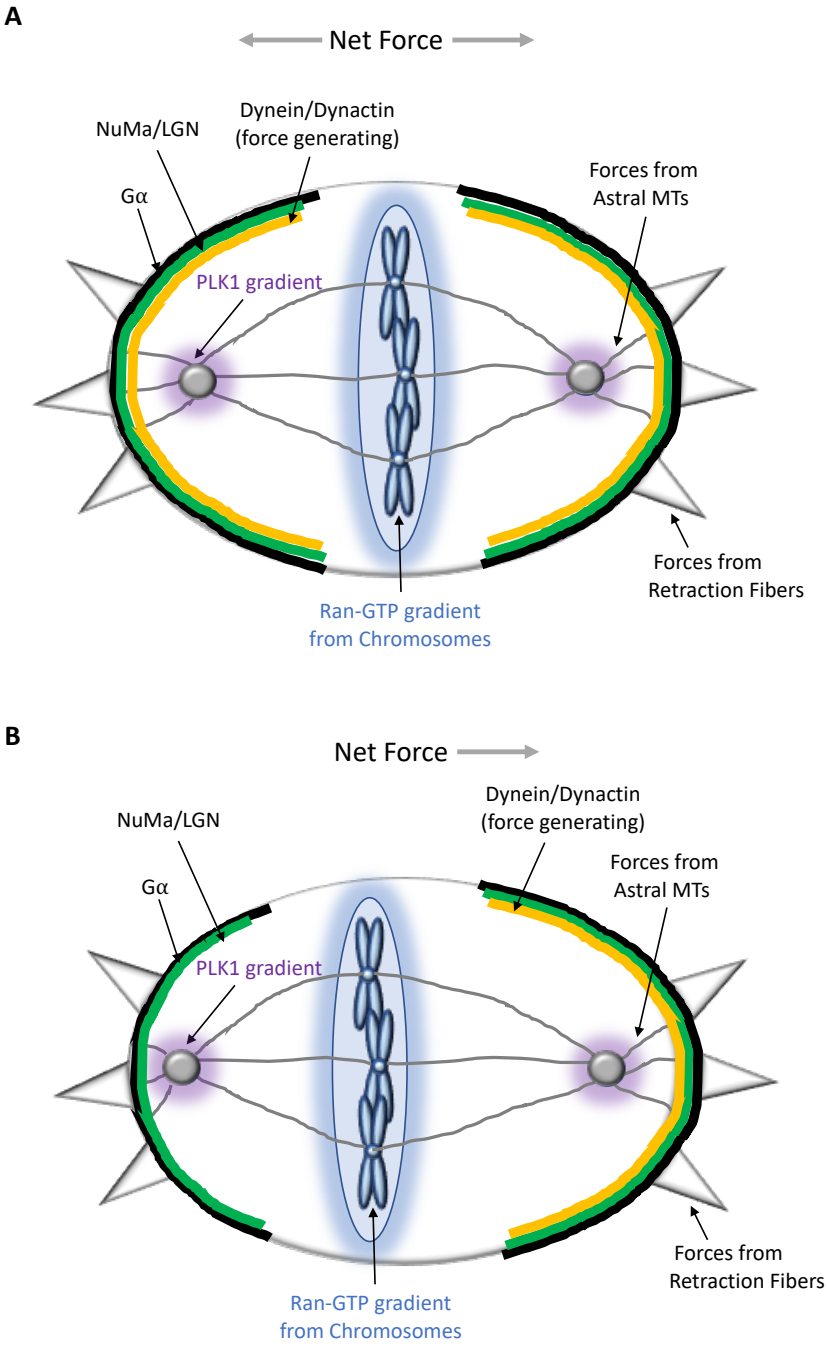

Figure 1-12: Mechanisms of spindle positioning in mammals: A: Spindle pole-localised PLK1 negatively regulates dynein/dynactin localisation at the cell cortex, downstream of dynein recruitment to the cortex by LGN/NuMa. Simultaneously, RAN-GTP gradient emanating from the chromatin negatively regulates NuMa/LGN localisation to midcortical regions, creating LGN/NuMa/Dynein asymmetry. Forces pulling on astral microtubules (MTs) generated by dynein motor complexes, and extrinsic forces from retraction fibers help position the mitotic spindle. **B:** If a spindle pole gets too close to the cortex on one side, PLK1 activity strips the dynein motor complexes from the adjacent cortex, resulting in greater net pulling forces on the opposite side of the cell, causing the spindle to be pulled close towards the opposite cortex. Following reestablishment of a centralised spindle, dynein complexes can reform at the adjacent cortex.

This intrinsic mechanism of spindle positioning is also subject to post-translational control. Of note and of relevance here, the spindle-pole localised kinase PLK1 has been strongly implicated in spindle orientation (Connell et al., 2017, Kiyomitsu & Cheeseman, 2012, Tame, Raaijmakers et al., 2016). The current model proposes that when the spindle pole gets too close to the cell cortex (too much pulling force in one direction), the spindle pole-localised PLK1 activity acts to strip cortical dynein, thereby reducing the pulling forces emanating from that near-cortex (Kiyomitsu & Cheeseman, 2012) (Figure 1-12). Pulling forces on the opposite spindle pole are therefore now greater, and the spindle is pulled closer towards the centre, before the dynein complexes are re-localised to the recently-depleted cortex (Kiyomitsu & Cheeseman, 2012) (Figure 1-12). This elegant mechanism thereby acts to keep the spindle in a constant dynamic equilibrium, and acts to ensure the axis of division is precisely defined.

1.2.3.2: Extrinsic mechanical forces:

Even though mammalian cells appear rounded as they enter mitosis, they still remain attached to the underlying substrate through the action of so-called retraction fibers, defined as membranous outgrowths containing dense actin filaments (McNally, 2013). Intriguingly, when HeLa cells were grown on different shapes of fibronectin-based micropatterns, cells adapted to these shapes, yet still divided along the long axis as determined by the interphase geometry of the micropattern (Thery, Racine et al., 2005). Thus, the external environment appears to critically influence the positioning of the mitotic spindle.

As there was a good correlation between the organisation of the retraction fibers, and the geometry of the micropattern, it was hypothesised that retraction fibers might be instrumental in this extrinsic control of spindle positioning (Thery, Jimenez-

Dalmaroni et al., 2007, Thery et al., 2005). Indeed, laser-induced severing of retraction fibers abolished the cells ability to effectively orientate their spindles, in a manner dependent on astral microtubules (Fink, Carpi et al., 2011). Thus, external forces controlled through the action of retraction fibers appear to rely on internal astral microtubules to coordinate spindle positioning, suggesting that the external information is being relayed intracellularly. Subcortical actin clouds have been proposed to mediate this relay function, but this is still a topic of active research (Fink et al., 2011).

Importantly, the NuMa-LGN-Gα complex is also required for spindle positioning when cells are grown on fibronectin-coated micropatterns (Kiyomitsu & Cheeseman, 2012, Kotak, Busso et al., 2014), and the localisation of the NuMa-LGN-Gα complex is linked to the organisation of retraction fibers during metaphase (Machicoane, de Frutos et al., 2014, Tame et al., 2016). Thus, mounting evidence suggests that the intrinsic cortical pulling machinery can also detect and integrate information from the extrinsic retraction fibre cues.

1.2.3.3: Chromosomal Ran-GTP gradient:

For the intrinsic and extrinsic spindle positioning mechanisms described above to function, the NuMa-LGN-Gα complex cannot be localised to the entire cell cortex. Indeed, the NuMa-LGN-Gα complex has been found primarily on cortical regions near the spindle poles, and excluded from midcortical regions near the spindle midzone, which is in proximity to the chromosomes (Kiyomitsu & Cheeseman, 2012). Thus, it was reasoned that a midzone- or chromosome-derived signal was responsible for excluding the NuMa-LGN-Gα complex from these cortical regions (Kiyomitsu & Cheeseman, 2012). Through a series of elegant experiments involving the manipulation of chromosome position during mitosis, it was found that a chromosome-derived signal is responsible

for removing NuMa-LGN-Gα complexes from the midzone cell cortex (Kiyomitsu & Cheeseman, 2012). Subsequent investigation found that the chromosome signal responsible for this NuMa-LGN-Gα exclusion, was the Ras-related GTPase Ran (Kiyomitsu & Cheeseman, 2012) (Figure 1-12).

The cycling of Ran between its GTP- and GDP-bound forms is coordinated, like most GTPases, by a guanine nucleotide exchange factor (GEF), and a GTPase-activating protein (GAP) (Kalab & Heald, 2008). In the case of Ran, the RanGAP is cytoplasmic, and the RanGEF is nuclear and localises to chromatin. The RanGEF is called regulator of chromatin condensation 1 (RCC1), and RCC1 promotes the Ran-GTP conformation (Klebe, Prinz et al., 1995). As RCC1 is on chromatin, the ratio of RanGTP/RanGDP is much higher on chromatin than in the cytoplasm. As a consequence of this, the RanGTP gradient emanates from the chromosomes, and diminishes as the signal diffuses away from the chromatin (Klebe et al., 1995). This RanGTP gradient was found to be instrumental in restricting the localisation of the NuMa-LGN-Gα complex to the cell cortex, and thus is a key determinant of correct and efficient spindle positioning (Kiyomitsu & Cheeseman, 2012). However, the molecular details surrounding how RanGTP can accomplish this function remain to be defined.

Collectively, there appears to be multiple mechanisms coordinating spindle positioning in mammals (Figure 1-12), and they likely act cooperatively to ensure proper spindle orientation in response to mechanical, environmental and spatio-temporal signals. Whilst the general framework of spindle positioning has been well established, the molecular details remain to be fully elucidated, and there is scope for many new players to have a role in this vital physiological process. In line with this, in this thesis, I report the involvement of the kinase CK1α and an associated regulatory protein termed FAM83D, in spindle positioning. Whilst CK1 has been extensively studied (see chapter

1.2), FAM83D remains relatively uncharacterised. FAM83D belongs to the FAM83 family of proteins, which will be discussed further in the following section.

1.3: FAM83 proteins:

1.3.1: Overview of the FAM83 family of proteins:

The FAMily of sequence similarity 83 (FAM83) group of proteins consists of eight members, designated FAM83A-H. Each FAM83 protein is encoded by a distinct gene and, interestingly, the genes encoding the FAM83 proteins are only found in vertebrates (Bartel, Parameswaran et al., 2016, Cipriano, Miskimen et al., 2014b). FAM83 proteins are classified based on the presence of a conserved, globular, domain of unknown function (termed DUF1669, aka Pfam PF07894) within their N-termini (Bozatzi & Sapkota, 2018, Cipriano et al., 2014b) (Figure 1-13). Outside of this domain, the C-termini are not conserved between FAM83 members, and differ in both their length (Figure 1-13) and sequence composition (Bozatzi & Sapkota, 2018, Cipriano et al., 2014b) (Figure 1-14). By definition, domains are functional and/or structural units of a protein (Ponting & Russell, 2002). Thus, grouping proteins together based on the presence of a conserved domain such as the DUF1669, can potentially provide clues into their functions and facilitate hypothesis-driven research into the role of those domain-containing proteins. With this notion in mind, deciphering the biochemical role of the DUF1669 will be a prerequisite in determining the cellular functions of FAM83 members.

Annotation databases such as UniProt suggest that, within the DUF1669, there is a single, short stretch of amino acids that resembles the catalytic motif of the phospholipase D (PLD) enzyme (Bartel et al., 2016, Bozatzi & Sapkota, 2018). The conventional PLD catalytic motif is composed of the amino acid sequence H/R-X-K-X-X-

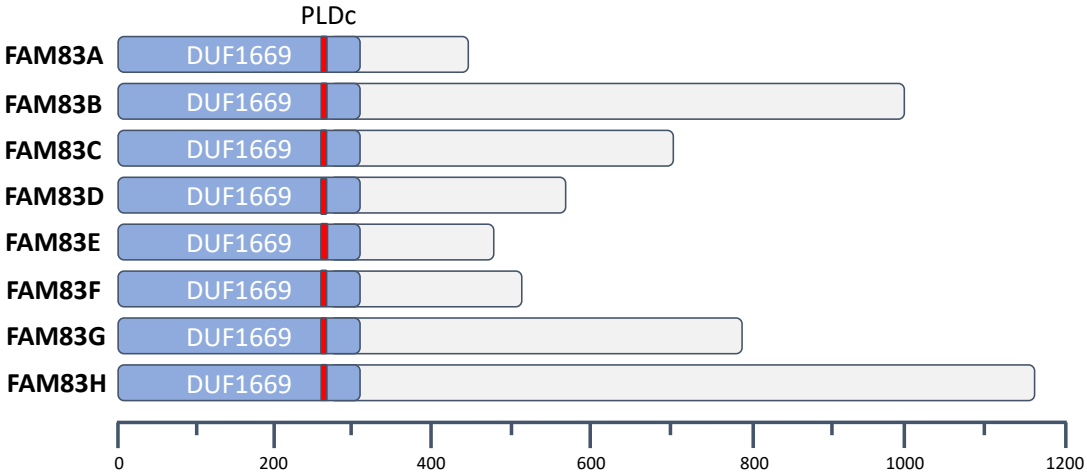

Figure 1-13: Schematic overview of the FAM83 family of proteins: The relative size and location of the conserved N-terminal domain of unknown function 1669 (DUF1669) for the human FAM83 proteins is highlighted in blue, and the non-conserved C-termini are in grey. The scale at the bottom refers to protein length in amino acids. The putative phospholipase D-like catalytic motif (PLDc) is highlighted in red.

X-X-D/E (hereafter referred to as HKD motif), where x is any amino acid (Selvy, Lavieri et al., 2011, Sung, Roper et al., 1997). With the exception of PLD6 which has only one HKD motif, PLD1-5 present with two HKD motifs within a single polypeptide (Figure 1-15), and both are crucial for maximal catalytic activity (Choi, Huang et al., 2006, Selvy et al., 2011). PLD6 is phylogenetically closer to the bacterial endonuclease Nuc, which interestingly also contains a single HKD motif (Choi et al., 2006) (Figure 1-15). The crystal structure of Nuc revealed that Nuc dimerises in order to form a functional complex (Stuckey & Dixon, 1999). Whilst dimerisation, either between the two HKD motifs of a single PLD enzyme or between HKD motifs of distinct PLD enzymes, has also been suggested to be a prerequisite for PLD activity (Kam & Exton, 2002), this has yet to be determined with structural studies.

PLDs act to hydrolyse the most abundant membrane lipid phosphatidylcholine, to yield phosphatidic acid and choline (Selvy et al., 2011). Phosphatidic acid is rapidly

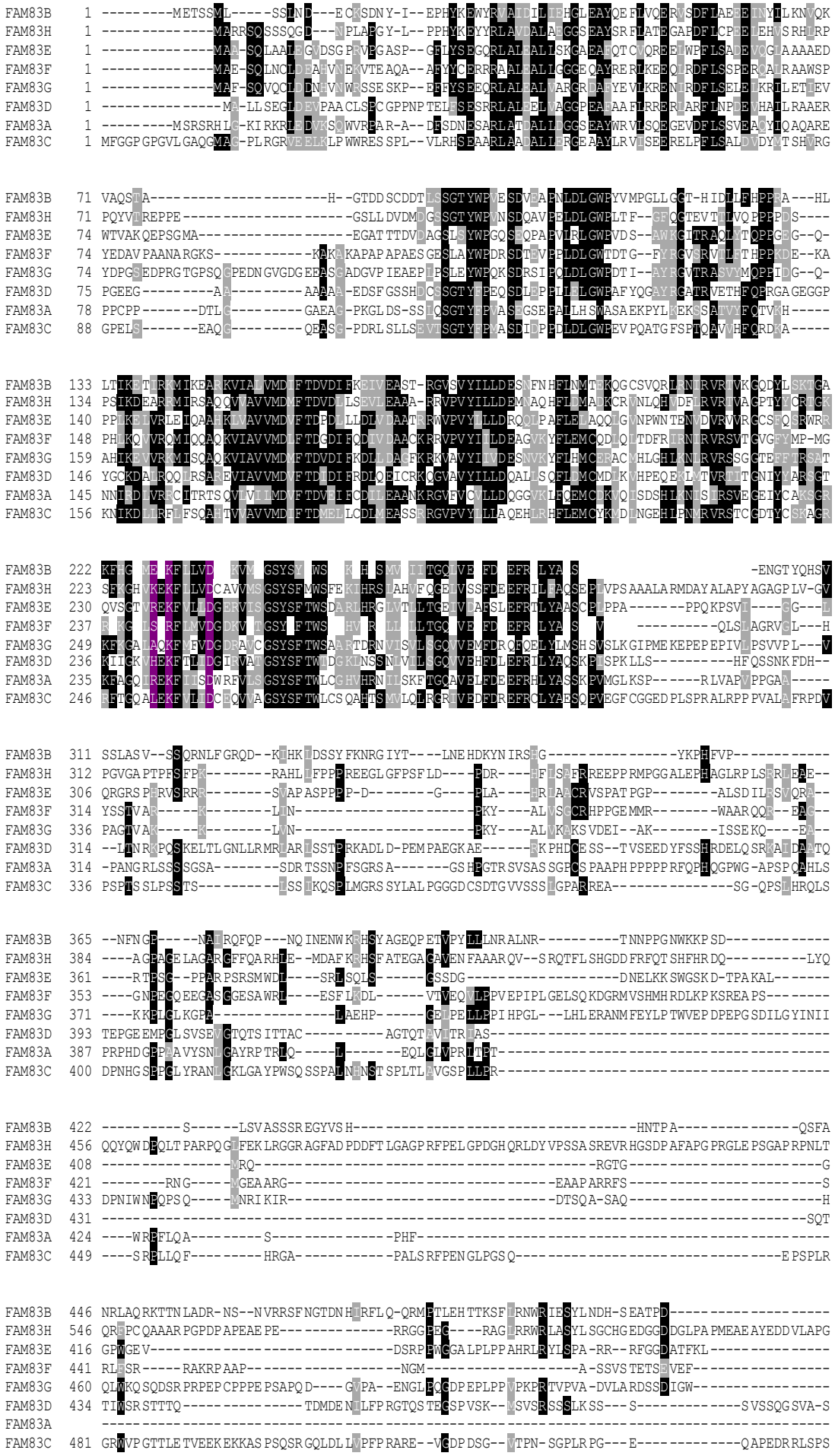

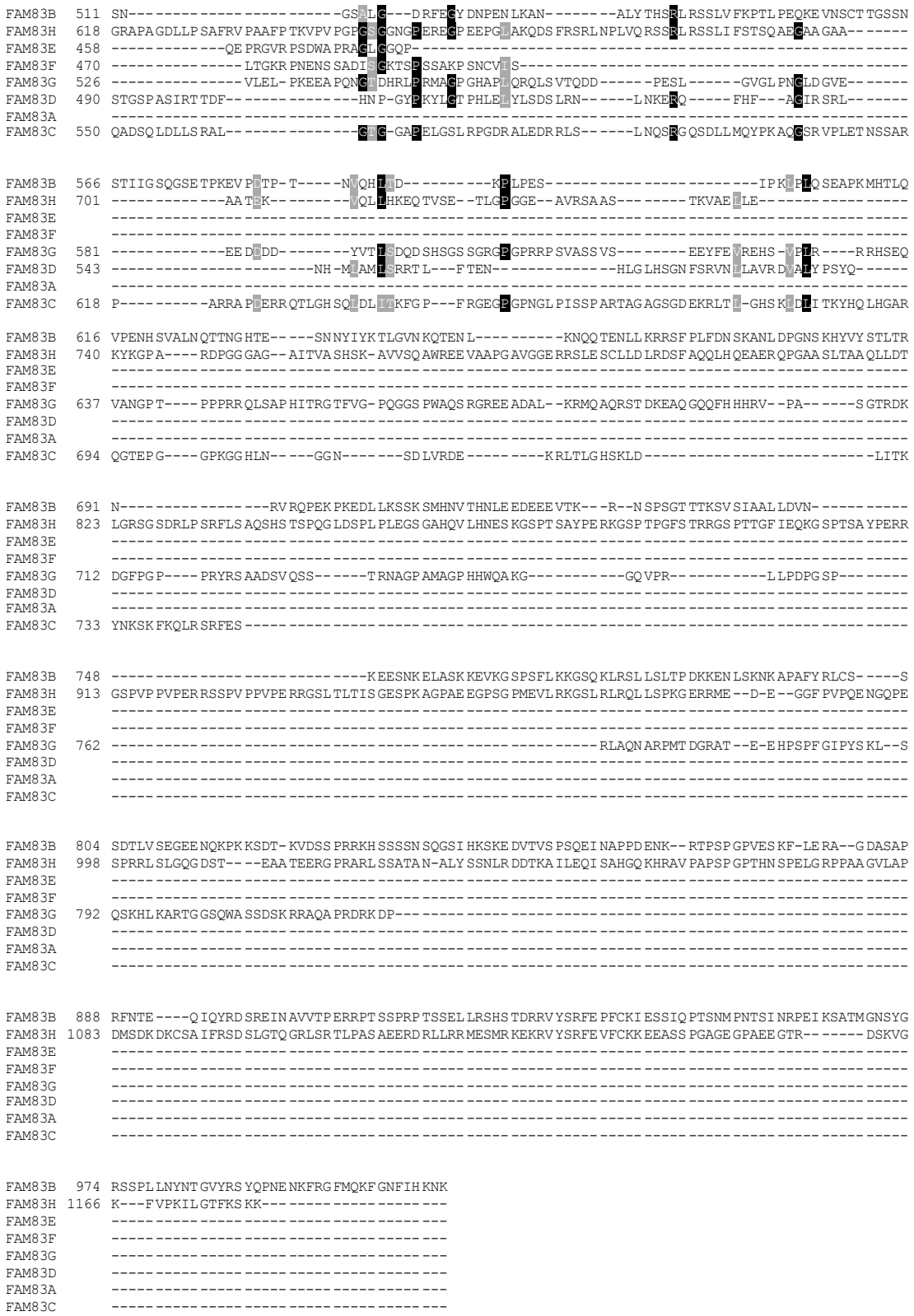

Figure 1-14: Multiple sequence alignment of the human FAM83 proteins: The alignment was performed using Clustal Omega and visualised in boxshade. Shading indicates the % sequence similarity (black = identical, grey = similar; in more than 50% of sequences). The positions of the putative phospholipase D-like catalytic motifs (HXKXXXXD) are highlighted in purple.

converted to diacylglycerol through the action of phosphatidic phosphatase, and the resulting diacylglycerol serves to activate isoforms of the protein kinase C (PKC) family of kinases (Roffey, Rosse et al., 2009, Selvy et al., 2011). PLDs are thus involved in the regulation of phospholipid metabolism, and intracellular signal transduction (Jenkins & Frohman, 2005). In humans there are six PLD isoforms termed PLD1-6. PLD1 and 2 are ubiquitously expressed, whereas PLD3 and 4 are transmembrane proteins localised to the endoplasmic reticulum (Nelson & Frohman, 2015). PLD5 does not contain a HKD motif, and is thus thought to be catalytically-inactive (Nelson & Frohman, 2015). Intriguingly, PLD6, which harbours only a single HKD motif, localises to the mitochondrial network (Nelson & Frohman, 2015).

The combination of biochemical and structural studies have led to a strong understanding of how PLD enzymes act to hydrolyse phosphatidylcholine (Selvy et al., 2011). The histidine of the HKD motif mediates nucleophilic attack of the phosphate within phosphatidylcholine, yielding a covalent intermediate. The subsequent completion of the hydrolysis reaction is mediated by a water molecule (Selvy et al., 2011). Alternatively, a primary alcohol can act on the covalent intermediate via a transphosphatidylation reaction (Selvy et al., 2011). Thus, due to this critical biochemical role, the histidine of the HKD motif is essential for enzymatic function, and is often mutated to an alanine in order to abolish PLD activity in functional studies of PLD enzymes.

In the case of FAM83 proteins, which contain this PLD-like catalytic motif within their DUF1669, the histidine of the HKD motif is absent in all members apart from FAM83D, and the lysine of the HKD is substituted by an arginine in FAM83F (Figure 1-12). Furthermore, there is only one HKD motif present in each FAM83 member, opposed to the two HKD motifs seen in most PLD isoforms, and outside this pseudo-PLD motif

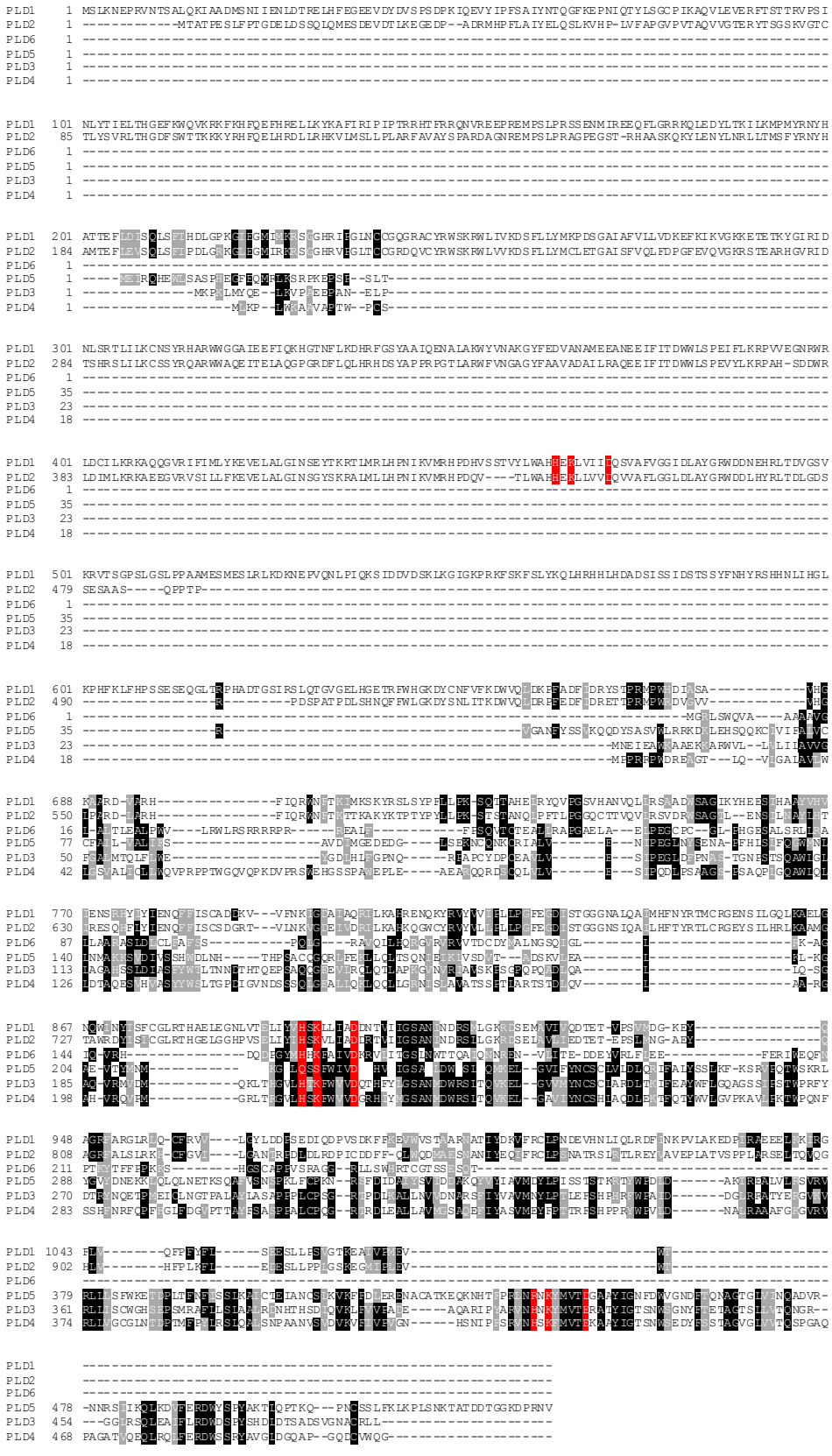

Figure 1-15: Multiple sequence alignment of the human phospholipase D (PLD) proteins: The alignment was performed using Clustal Omega and visualised in boxshade. Shading indicates the % sequence similarity (black = identical, grey = similar; in more than 50% of sequences). The positions of the catalytic motifs (HXKXXXXD) are highlighted in red.

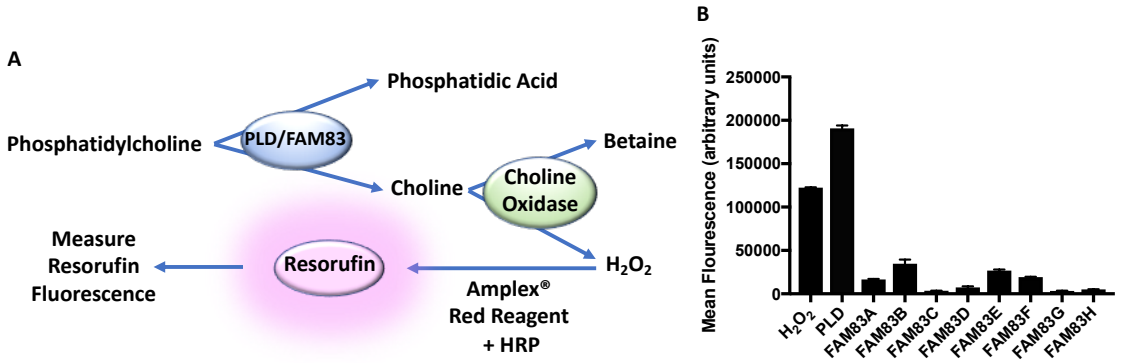

Figure 1-16: The FAM83 family of proteins do not appear to possess any PLD activity: **A:** Schematic representation of the assay used to measure phospholipase D (PLD) activity. PLD cleaves phosphatidylcholine into phosphatidic acid and choline. Choline is then turned into hydrogen peroxide (H_2O_2) and betaine through the action of choline oxidase. The Amplex red reagent, in combination with horseradish peroxidase (HRP) act on H_2O_2 to form a fluorescent species called resorufin. Resorufin fluorescence is subsequently measured as a read-out of PLD activity. **B:** Mean resorufin fluorescence recorded for *Staphylococcus aureus* PLD and FAM83A-H. H_2O_2 was included as a positive control (n=1).

there is very little homology between PLDs and the DUF1669. Collectively, these observations suggest that the PLD-like catalytic motif in the DUF1669 of FAM83 proteins is not active. Indeed, no PLD activity could be detected for any FAM83 member, including FAM83D which harbours an intact HKD motif, when evaluated for their ability to cleave phosphatidylcholine *in vitro* (Figure 1-16). However, preliminary structural studies on the DUF1669 of both FAM83A and B suggest that the features and positioning of the HKD motif closely mirrors that seen in PLD structures (Figure 1-17). Thus, taking all these data into account, FAM83 proteins are classified as pseudo-PLD enzymes.

Pseudoenzymes, defined as sequence-predicted enzymes without any detectable enzymatic activity, are thought to have evolved from gene duplication events that remove the selective pressure on the catalytic activity of the additional copies (Murphy, Farhan et al., 2017a). In the absence of this selective pressure, the now

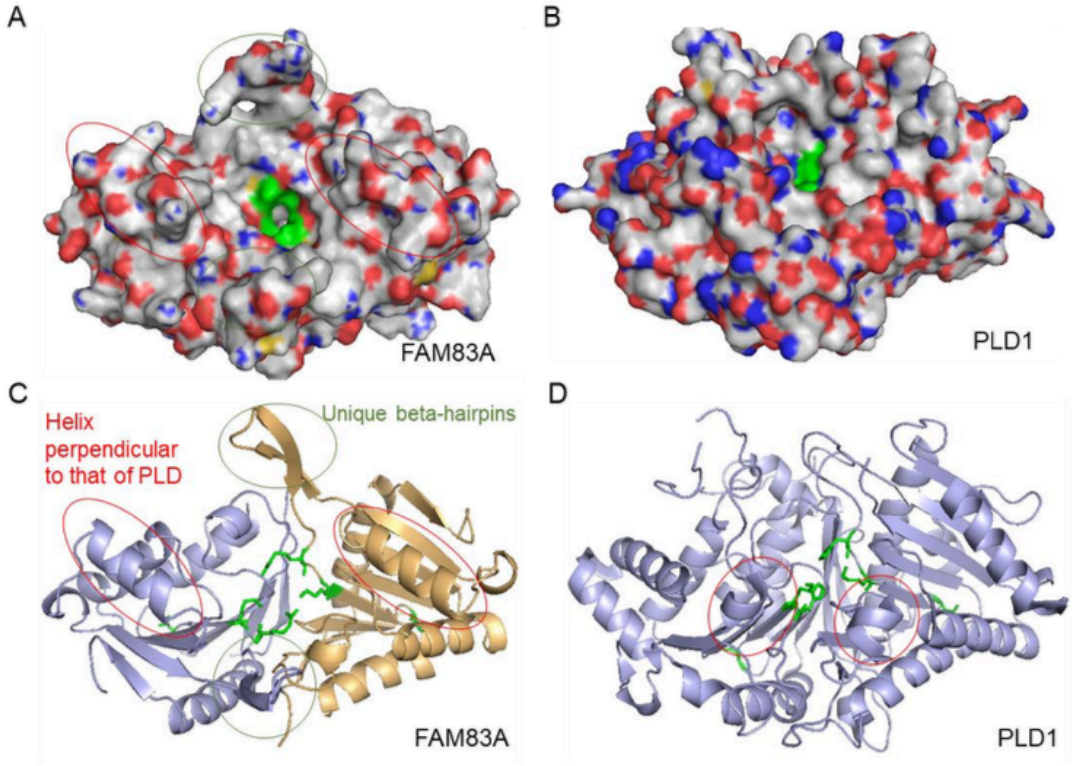

Figure 1-17: Crystal structure of the FAM83A DUF1669: A: Structure of the FAM83A DUF1669 domain, resolved in collaboration with the Bullock laboratory (Structural Genomics Consortium, Oxford). The structure reveals a unique dimer with a phospholipase D (PLD)-like fold, that brings the putative PLD catalytic motif together at the catalytic cleft (shown in green). **B:** The structure of PLD1 from PDB entry 1F01. **C:** Ribbon diagram depicting the folding of the FAM83A DUF1669 into a dimer, with two alpha helices perpendicular to that of PLD. The putative PLD-like catalytic cleft is shown in green. Unique beta-hairpins, which are absent from PLD1, are circled in grey. **D:** Ribbon diagram depicting the folding of PLD1, with the analogous alpha helices to panel C. circled in red (adapted from Leiros *et al*, 2000). *Figure taken from Polyxeni Bozatzi's doctoral thesis, 2018, University of Dundee.*

redundant additional copies are then able to mutate and adopt new functions. The full extent of the role of pseudoenzymes in cells is only beginning to be unravelled, but mounting evidence suggests that pseudoenzymes can regulate signalling pathways through multiple, diverse avenues (Eyers & Murphy, 2013, Murphy et al., 2017a, Murphy, Mace et al., 2017b). For example, pseudoenzymes can act on their ancestral catalytic counterparts to allosterically activate them, modulate signalling outputs, or act

as signalosome assembly platforms (Eyers & Murphy, 2013, Murphy et al., 2017b). Currently, the knowledge on FAM83 protein biology is limited, and as such, whether FAM83 members can act on their putative PLD ancestors to modulate PLD function is not known. That said, FAM83B overexpression in HME1 mammary epithelial cells was shown to increase PLD1 activity, although this was attributed to an indirect effect resulting from activation of the epidermal growth factor receptor (EGFR) following FAM83B overexpression (Cipriano, Bryson et al., 2014a).

Due to the amino acid compositions of FAM83 proteins not revealing any robust functional clues into FAM83 or DUF1669 function, research into the cellular roles of FAM83 proteins has often been serendipitous in nature. Often appearing in biochemical screens and interactome studies, the reported roles of FAM83 proteins highlight the diverse, often unrelated, pathways in which these FAM83 members appear to participate in. The findings of some of these studies will be summarised in the subsequent subsections.

1.3.2: FAM83A and B in chemoresistance and oncogenesis:

FAM83A was originally identified in a phenotypic screen searching for proteins that, when overexpressed, were capable of reversing the cytostatic effects of the EGFR inhibitor AG1478 in human breast cancer HMT3522 cells (Lee, Meier et al., 2012). FAM83A overexpression increased the proliferation and invasion rates of these cells, whilst its deletion rendered the cells sensitive to tyrosine kinase inhibitors (Lee et al., 2012). At the molecular level, FAM83A was proposed to mediate this chemoresistant function through binding and promoting the phosphorylation of c-Raf and the p85 subunit of phosphatidylinositol 3-kinase (PI3K), resulting in aberrant activation of the

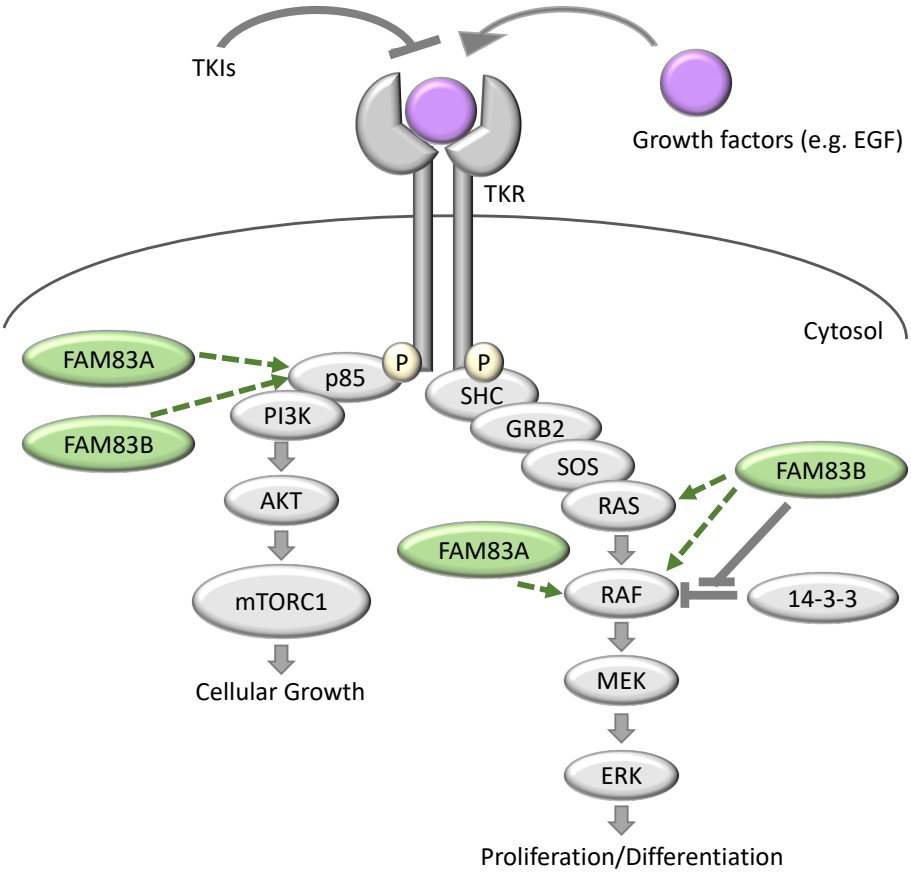

Figure 1-18: The proposed model by which FAM83A and FAM83B act to modulate receptor tyrosine kinase signalling: Growth factors such as epidermal growth factor (EGF) bind to their cognate cell surface tyrosine kinase receptors (TKRs) to trigger receptor dimerisation, autophosphorylation, and activation. The signal is then transduced through the RAS/RAF/MEK/ERK and PI3K-AKT-mTORC1 signalling pathways, resulting in cell growth and proliferation. Lee *et al,* 2012 suggested that FAM83A binds to the p85 subunit of PI3K and to RAF, to sustain the activation of the pathway. Subsequently, Cipriano *et al,* 2013 suggested that FAM83B associates with RAS and RAF, with the latter interaction proposed to prevent association of RAF with inhibitory 14-3-3 proteins. FAM83B was also shown to bind the p85 subunit of PI3K. As FAM83A and B act downstream of the receptors, they were proposed as candidates capable of bypassing inhibition of growth signalling caused by tyrosine kinase inhibitors (TKIs) in chemotherapy, thereby contributing to TKI resistance.

mitogen-activated protein kinase (MAPK) pathway, downstream of EGFR stimulation (Lee et al., 2012) (Figure 1-18).

In a similar vein, FAM83B was discovered through its ability to promote oncogenic transformation in a screen searching for proteins whose overexpression could act as a substitute for Ras-induced transformation of immortalised human mammary epithelial cells (Cipriano, Graham et al., 2012). Like FAM83A, FAM83B was also proposed to bind c-Raf, and also Ras, to trigger activation of MAPK signalling cascade (Cipriano et al., 2012) (Figure 1-18). FAM83B was suggested to mediate this function through blocking the association of c-Raf with 14-3-3, thereby increasing c-Raf membrane localisation and downstream signalling (Cipriano, Miskimen et al., 2013). In the same study, FAM83B overexpression was shown to activate the PI3K-Protein kinase B (PKB) signalling pathway (Figure 1-18), and promote resistance to inhibitors of the PI3K, PKB and mammalian target of rapamycin (mTOR) kinases (Cipriano et al., 2013). As mentioned in section 1.1.1, FAM83B-driven hyperactivation of the EGFR-MAPK pathway was shown

to activate PLD1, and this PLD1-activation effect was essential for transformation of these cells (Cipriano et al., 2014a).

However, whilst these overexpression-based studies are informative, no information on the endogenous functions of FAM83A or B have yet been described, and as such, this has limited the understanding into the physiological roles of these FAM83 members.

1.3.3: FAM83D in mitosis and proliferation:

FAM83D was uncovered in a proteomic screen of isolated human mitotic spindles from HeLa cells, designed to identify novel components of the spindle apparatus (Sauer, Korner et al., 2005). Subsequently, FAM83D (aka Chica) was shown to localise to the mitotic spindle, and knockdown of FAM83D by RNA interference

approaches was shown to trigger chromosome congression and alignment defects (Santamaria, Nagel et al., 2008). At the molecular level, FAM83D was shown to bind the microtubule-binding protein hyaluronan mediated motility receptor (HMMR, aka RHAMM, CD168), in order to localise to the spindle microtubules (Dunsch, Hammond et al., 2012). Other FAM83D-interacting proteins include the light chain of the motor protein dynein (DYNLL1) (Dunsch et al., 2012) and the chromokinesin Kid (Santamaria et al., 2008), and these interactions are reported to be important in regulating the function of FAM83D in coordinating chromosome alignment in mitosis.

At the transcript level, *FAM83D* mRNA expression is elevated in many types of cancer, with increased *FAM83D* expression predicting reduced survival rates (Huang, Ma et al., 2017, Perez-Pena, Alcaraz-Sanabria et al., 2017, Shi, Sun et al., 2016). As such, *FAM83D* transcript levels have been suggested to offer some prognostic value (Walian, Hang et al., 2016).

1.3.4: FAM83G in cell signalling and disease:

A proteomic screen aimed at identifying novel interacting proteins of the human mothers against decapentaplegic homologue 1 (SMAD1) transcription factor, which is a mediator of the bone morphogenetic protein (BMP) signalling pathway, identified FAM83G [thereafter also referred to as protein associated with SMAD1 (PAWS1)] as a SMAD1-interacting partner (Vogt, Dingwell et al., 2014). FAM83G was shown to be a substrate of the type I BMP receptor kinases, and to modulate non-canonical BMP signalling (Vogt et al., 2014). Subsequently, FAM83G was shown to regulate actin cytoskeletal dynamics through association with a cytoskeleton-regulating protein termed cluster of differentiation 2 (CD2)-associated protein (CD2AP) (Cummins, Wu et al., 2018). More recently, FAM83G was shown to promote hyperactive wingless/int1

(Wnt) signalling and subsequent body axis duplication, when overexpressed in *Xenopus* embryos (Bozatzi, Dingwell et al., 2018). Wnt signalling was diminished when *FAM83G* was knocked out in U2OS osteosarcoma cells, implying an essential role for FAM83G in the regulation of the Wnt signalling pathway (Bozatzi et al., 2018).

In terms of disease, a large proportion of knowledge into the role of FAM83G has arisen from non-human genetic studies. Mice presenting with a spontaneous woolly hair phenotype were determined to possess homozygous mutations in the *FAM83G* gene (Radden, Child et al., 2013), and an autosomal recessive *FAM83G* mutation in dogs (R52P) was shown to cause hereditary palmoplantar hyperkeratosis syndrome, a skin disorder characterised by thickening of the footpads, epidermal hyperplasia and hair morphology defects (Drogemuller, Jagannathan et al., 2014, Sayyab, Viluma et al., 2016). Recently, a *FAM83G* mutation (A34E) in humans was shown to cause analogous hyperkeratotic phenotypes to those reported to result from the R52P substitution in dogs (Maruthappu, McGinty et al., 2018). As Wnt signalling has been extensively linked to the development of skin and hair, these disease mutations may disrupt the Wnt-dependent FAM83G functions. Indeed, this tantalising hypothesis was recently tested, and expression of FAM83G(A34E) or FAM83G(R52P) mutant proteins could not rescue Wnt signalling in *FAM83G* knockout cells (Wu, Jones et al., 2019).

1.3.5: FAM83H in cytoskeletal regulation and disease:

FAM83H is perhaps unique amongst the FAM83 proteins in that it has a very well documented disease phenotype following its mutation. Autosomal dominant mutations in *FAM83H* have been reported in patients presenting with hereditary hypocalcified Amelogenesis Imperfecta (AI), a rare dental disease characterised by soft, hypocalcified enamel (Kim, Lee et al., 2008, Lee, Lee et al., 2011, Pourhashemi, Ghandehari Motlagh

et al., 2014, Urzua, Martinez et al., 2015). Many of the *FAM83H* mutations found in AI are predicted to encode truncated FAM83H protein fragments, but the precise molecular mechanism(s) by which FAM83H promotes AI are yet to be defined. However, as *FAM83H* knockout mice appear to have normal, functional enamel, the most likely explanation is that FAM83H acquires a novel function(s) when it is truncated in the disease state (Kuga, Kume et al., 2013, Lee et al., 2011, Wang, Hu et al., 2016).

FAM83H was found to regulate the keratin cytoskeleton through its ability to interact and co-localise with specific keratins and casein kinase 1 (CK1) isoforms (Kuga et al., 2013). Both the knockdown and overexpression of FAM83H resulted in disruption of the keratin cytoskeleton, and similar defects resulted from chemical inhibition of CK1 (Kuga et al., 2013). In ameloblasts, the disease-relevant cells, FAM83H and CK1α were found on keratin filaments, and also on desmosomes, implying a potential role in cell junction regulation (Kuga, Sasaki et al., 2016b). In these cells, the truncated, disease-associated forms of FAM83H triggered disruption of both desmosomes and the keratin cytoskeleton following their overexpression (Kuga et al., 2016b), in agreement with a possible newly-acquired role in the disease state. In colorectal cancer cells with a compromised keratin cytoskeleton, FAM83H and CK1 isoforms were found to bind and co-localise with the DNA binding protein SON in nuclear speckles, where they may act to regulate invasion of these cancer cells (Kuga, Kume et al., 2016a).

Despite these advances, molecular knowledge on the physiological role of FAM83H is lacking, and as such, has limited the understanding into how FAM83H function may go awry following its mutation in AI.

1.3.6: The cellular roles of FAM83C, E and F remain to be defined:

Other than clinical studies suggesting a pro-oncogenic role for FAM83C and E in certain cancers, no studies have yet explored the physiological functions of these proteins. FAM83F, on the other hand, has been the subject of some recent reports, implying a role for FAM83F in the p53 tumour suppressor pathway (Salama, Benitez-Riquelme et al., 2019). FAM83F was reported to bind p53 and promote p53 stabilisation, and knockdown of FAM83F was associated with a reduction in p53-dependent target gene transcription in response to DNA damage (Salama et al., 2019). FAM83F was also found to activate MAPK signalling in papillary thyroid cancer (Fuziwara, Saito et al., 2019), and three micro-RNAs were found to suppress oesophageal squamous cell carcinoma and non-small-cell lung carcinoma by targeting *FAM83F* transcripts (Gu, Zhan et al., 2018, Mao, Liu et al., 2016, Yang, Wei et al., 2017).

2. Materials and Methods:

2.1: Materials:

2.1.1: Chemicals and other reagents:

The chemicals and reagents used in this thesis are listed in Table 2-1.

Reagent	Source	Cat. Number
4-(2-Hydroxyethyl)piperazine-1-ethanesulfonic acid (HEPES)	Sigma-Aldrich	H3375
Acetic Acid	Sigma-Aldrich	71251
Acetone	Sigma-Aldrich	90872
Acetonitrile (HPLC grade)	Sigma-Aldrich	271004
Acrylamide [bis-acrylamide 40% (w/v)]	National Diagnostics	EC-852
Agarose	Thermo Fisher Scientific	16500
Agarose beads	Cell Signalling Technology	37478
Amersham Hyperfilm ECL	GE Healthcare	GE28-9068-36
Ammonium Bicarbonate	Sigma-Aldrich	09830
Ammonium Persulfate (APS)	Sigma-Aldrich	09913
Ampicillin	Formedium	AMP100
Amplex Red Phospholipase D Assay Kit	Thermo Fisher Scientific	A12219
β-mercaptoethanol (BME)	Sigma-Aldrich	M6250
BCA assay kit	Pierce	23225
Blasticidin	Thermo Fisher Scientific	R210-01
Bortezomib (proteasome inhibitor)	LC Laboratories	B-1408
Bovine Serum Albumin (BSA)	Sigma-Aldrich	A7906
Bromophenol Blue	Sigma-Aldrich	B0126
CellLight Actin-RFP	Thermo Fisher Scientific	C10502
CK1tide (optimised CK1 substrate peptide)	DSTT	EP5630
cOmplete, MINI, EDTA-free, protease inhibitor cocktail tablets	Roche	4693159001
Coomassie protein assay reagent (Bradford reagent)	Thermo Fisher Scientific	23200
D4476 (CK1 inhibitor)	Merck	218696
Dimethyl pimelimidate dihydrochloride (DMP)	Sigma-Aldrich	D8388
Dimethyl Sulphoxide (DMSO)	Sigma-Aldrich	D8418
Dithiobis Succinimidyl Propionate (DSP)	Thermo Fisher Scientific	22585
Dithiothreitol (DTT)	Sigma-Aldrich	D9779

DNA gel loading dye, purple (6x)	NEB	7025
DNeasy Blood and Tissue kit	Qiagen	69506
Doxycycline (hydrochloride)	Sigma-Aldrich	D3072
Dulbecco's modified Eagle medium (DMEM)	Thermo Fisher Scientific	11960-085
Dulbecco's phosphate buffered saline (PBS)	Thermo Fisher Scientific	14190
Enhanced electrochemiluminescence reagent (ECL)	GE Healthcare	RPN2109
Ethanol	Fisher Chemical	10000652
Ethylene glycol-bis(β-aminoethyl ether)-N,N,N',N'-tetraacetic acid (EGTA)	Sigma-Aldrich	E8145
Ethylenediaminetetraacetic acid (EDTA)	Formedium	EDTA250
Fibronectin	Sigma-Aldrich	F2006
FLAG M2 affinity agarose	Sigma-Aldrich	A2220
Foetal Bovine Serum (FBS)	Sigma-Aldrich	F7524
Formic acid	VWR	84865
Gelatin (from porcine skin)	Sigma-Aldrich	G1890
Geneticin (G418)	Thermo Fisher Scientific	10131027
GFP-TRAP agarose beads	ChromoTek	GTA
Glutathione	Sigma-Aldrich	G4251
Glycerol	VWR	24386
Glycine	VWR	10119
HA-magnetic beads	Pierce	88837
Hexadimethrine bromide (polybrene)	Sigma-Aldrich	H9268
Hoechst DNA stain	Thermo Fisher Scientific	H3569
HPLC-grade water	VWR	22934
Hydrochloric Acid (HCl)	Sigma-Aldrich	258148
Hygromycin-B	Thermo Fisher Scientific	10687010
Immobilon-P Polyvinylidene Fluoride (PVDF), 0.45 µM membrane	Merck	IPVH00010
InstantBlue Coomassie protein stain	Expedeon	SKU: ISB1L
Iodoacetamide	Sigma-Aldrich	I1149
iScript cDNA synthesis kit	Bio-Rad	1708891
Isopropanol	Sigma-Aldrich	I9516
Kanamycin	Sigma-Aldrich	60615
KOD hot start polymerase kit	Toyobo	71086-3
LDS sample buffer (4x)	Thermo Fisher Scientific	NP0007
L-Glutamine	Sigma-Aldrich	25030024
Lipofectamine RNAiMAX	Thermo Fisher Scientific	11668030
LoBind Eppendorf Tubes	Sigma-Aldrich	Z666505
L-shaped micropatterns	CYTOO	20-013-00

Luria Bertani broth (LB) and LB agar plates	Central Technical Services, University of Dundee	N/A
Lys-C protease	Alpha Laboratories	125-05061
Magnesium Acetate	Sigma-Aldrich	M5661
Manganese chloride	Sigma-Aldrich	244589
Methanol	Fisher Chemical	11976961
MG132 (proteasome inhibitor)	Sigma-Aldrich	C2211
MLN4924 (NEDDylation inhibitor)	Active Biochem	A-1139
MOPS gel running buffer	Formedium	MOPS-SDS-5000
Nocodazole (microtubule polymerisation inhibitor)	Sigma-Aldrich	487928
Nonidet P-40 substitute (NP40)	Sigma-Aldrich	74385
NuPAGE NOVEX 4-12% Bis-Tris polyacrylamide gels	Thermo Fisher Scientific	NP0322BOX
Opti-MEM	Thermo Fisher Scientific	31985062
Paraformaldehyde 16% (w/v)	Thermo Fisher Scientific	28908
Penicillin/Streptomycin	Thermo Fisher Scientific	15140122
Phosphatase assay buffer	New England Biolabs	P0753S
Phospholipase D from *Streptomyces chromofuscus*	Millipore	525200
PhosSTOP phosphatase inhibitor tablets	Roche	4906837001
Plasmid Maxi, Midi and Mini kits	Qiagen	27104
Polyethylenimine (PEI)	Polysciences	23966-1
Ponceau S	Sigma-Aldrich	P7170
Precision Plus Protein All Blue standards	Bio-Rad	1610373
Prolong Gold Antifade mounting reagent with DAPI	Thermo Fisher Scientific	P36931
Propidium Iodide solution	Sigma-Aldrich	P4864
ProTAME (APC/C inhibitor)	Boston Biochem	1-440
Protein G sepharose	GE Healthcare	17061801
Puromycin	Sigma-Aldrich	P9620
Quick-load 1 kb DNA ladder	NEB	N0552
RFP-TRAP agarose beads	ChromoTek	RTA
RNAse A	Thermo Fisher Scientific	EN0531
RNeasy kit	Qiagen	74104
RO-3306 (CDK1 inhibitor)	Sigma-Aldrich	SML0569
RPMI Medium	Thermo Fisher Scientific	31870
Sequencing grade modified Trypsin	Promega	V511
Skimmed milk powder	Marvel	N/A
Sodium Azide	Sigma-Aldrich	S2002
Sodium β-glycerophosphate	Sigma-Aldrich	G6501
Sodium borate	Sigma-Aldrich	B3545

Sodium Chloride	Sigma-Aldrich	S7653
Sodium Fluoride	Sigma-Aldrich	S7920
Sodium Orthovanadate	Sigma-Aldrich	S6508
Sodium Pyrophosphate	Sigma-Aldrich	221368
Spin-X Column	Corning	8161
SsoFast EvaGreen Supermix	Bio-Rad	172-5200
StrataClone Blunt PCR cloning kit	Agilent	240207
S-Trityl L-Cysteine (STLC) (Eg5 inhibitor)	Sigma-Aldrich	164739
Sucrose	VWR	A15583.36
Supersignal West Pico chemiluminescent substrate	Thermo Fisher Scientific	34580
SYBR Safe DNA stain	Thermo Fisher Scientific	S33102
Tetramethylethylenediamine (TEMED)	Sigma-Aldrich	T9281
Triethylammonium bicarbonate	Sigma-Aldrich	T7408
Trifluoroacetic acid (TFA)	Thermo Fisher Scientific	T6508
Tris (hydroxymethyl) aminomethane (Tris)	VWR	103157P
Triton X-100	Sigma-Aldrich	T8787
Trypsin protease	Pierce	13454189
Trypsin/EDTA	Thermo Fisher Scientific	59417C
Tween 20	Sigma-Aldrich	P1379
Universal nuclease	Pierce	88701
Urea	VWR	28876.367
X-gal (for blue-white colony screening)	Sigma-Aldrich	BG-3-G
X-ray films	Konica Minolta	A9KN
Zeocin	Thermo Fisher Scientific	R25001
γ^{32}P-ATP	PerkinElmer	N/A

Table 2-1: Chemicals and reagents used in this thesis.

2.1.2: Buffers and solutions:

Compositions of buffer and solutions used in this thesis are listed in Table 2-2.

Buffer/Solution	Composition
6-13% (w/v) acrylamide gels	375 mM Tris-HCl (pH 8.6), 0.1% (w/v) SDS, and 6-13% (w/v) acrylamide. 0.1% (w/v) APS and 0.1% (v/v) TEMED were used to polymerise the gels.
Blocking solution	5% (w/v) milk powder in TBS-T (1x)
BSA primary antibody solution	5% (w/v) BSA in TBS-T (1x), 0.02% sodium azide
Buffer A	50 mM Tris-HCl pH 7.5, 0.1 mM EGTA
Cell freezing medium	90% (v/v) FBS, 10% (v/v) DMSO
DNA staining buffer	50 µg/ml propidium iodide, 50 µg/ml RNAse A, in PBS + 1% (w/v) FBS

Immunofluorescence blocking solution	1% (w/v) BSA in PBS (1x)
Immunofluorescence quenching buffer	10 mM HEPES pH 7.4 in DMEM
Immunofluorescence permeabilisation buffer	0.2% (v/v) NP40 in PBS
Kinase assay buffer	50 mM Tris-HCl pH 7.5, 0.1 mM EGTA, 10 mM magnesium acetate, 2 mM DTT
LB plates	1% (w/v) tryptone peptone, 0.5% (w/v) yeast extract, 86 mM NaCl, 2% (w/v) bactoagar, 100 µg/ml ampicillin or 25 µg/ml kanamycin after autoclaving for 20 min
LB broth	1% (w/v) tryptone peptone, 0.5% (w/v) yeast extract, 86 mM NaCl, 100 µg/ml ampicillin or 25 µg/ml kanamycin after autoclaving for 20 min
Lysis buffer with DSP	40 mM HEPES pH 7.4, 120 mM NaCl, 1 mM EDTA pH 8.0, 1 mM sodium 2-glycerophosphate, 50 mM sodium fluoride, 1 mM activated sodium orthovanadate, 10 mM sodium pyrophosphate, 1% (v/v) Triton X-100, 1 tablet of cOmplete protease inhibitors per 25 ml lysis buffer. 2.5 mg/ml DSP (in DMSO) was added fresh before use.
Mammalian cell lysis buffer	50 mM Tris-HCl pH 7.5, 120 mM NaCl, 1 mM EGTA pH 8.0, 1 mM EDTA pH 8.0, 1 mM activated sodium orthovanadate, 1 mM sodium 2-glycerophosphate, 50 mM sodium fluoride, 10 mM sodium pyrophosphate, 270 mM sucrose, 0.5% (v/v) NP40, 1 tablet of cOmplete protease inhibitors per 25 ml lysis buffer.
Milk primary antibody solution	5% (w/v) milk powder in TBS-T (1x)
PEI	1 mg/ml PEI in 25 mM HEPES, pH 7.5
Phosphatase assay wash buffer	200 mM NaCl, 50 mM Tris-HCl pH 7.5, 1% (v/v) Triton X-100
Sample buffer (5x)	312.5 mM Tris-HCl pH 6.8, 50% (v/v) glycerol, 10% (w/v) SDS, 0.1% (w/v) bromophenol blue, 5% (v/v) BME.
SDS-PAGE running buffer (1x)	25 mM Tris-HCl (pH 8.3), 192 mM glycine, 0.1% (w/v) SDS
SDS lysis buffer	1% (w/v) SDS. 1 tablet of PhosSTOP and 1 tablet of cOmplete protease inhibitors were added fresh before use.
Stacking gel	125 mM Tris-HCl pH 6.8, 0.1 % (w/v) SDS, 4% (w/v) acrylamide. 0.075% (w/v) APS and 0.1% (v/v) TEMED were used to polymerise the gels.
TAE buffer (1x)	40 mM Tris-acetate pH 8.0, 1 mM EDTA
Tris buffered saline (TBS) buffer (1x)	50 mM Tris-HCl pH 7.5, 150 mM NaCl

TBS-T buffer (1x)	50 mM Tris-HCl pH 7.5, 150 mM NaCl, 0.1% (v/v) Tween 20
Transfer buffer (1x)	25 mM Tris-HCl pH 8.3, 192 mM glycine, 10% (v/v) methanol

Table 2-2: Buffers and solutions used in this thesis.

2.1.3: Antibodies:

The antibodies used in this thesis, in addition to their optimised incubation conditions, are listed in Table 2-3. All the non-commercially available antibodies were raised in sheep by the Division of Signal Transduction Therapy (DSTT), University of Dundee, and purified in-house on CH Sepharose that was covalently coupled to the antigen used to raise the antibody. Antibodies were eluted with 50 mM glycine pH 2.5, and then dialysed for 16 h in PBS at 4°C. Species-specific HRP-coupled secondary antibodies were obtained from either Thermo Fisher Scientific or Cell Signalling Technologies (CST).

Antibody	Company	Cat. Number	Ab dilution	Ab conditions
ASC	Adipogen	AL177	1:1000	5% BSA TBS-T
α-Tubulin	Thermo Fisher Scientific	MA1-80189	1:5000	5% BSA TBS-T
Aurora A	CST	12100	1:1000	5% milk TBS-T
CK1α	Bethyl Laboratories	A301-991A	1:1000	5% BSA TBS-T
CK1α	DSTT	SA527, Bleed 3	1:1000	5% milk TBS-T
CK1δ	CST	12417	1:1000	5% BSA TBS-T
CK1δ	DSTT	SA609, Bleed 3	1:1000	5% milk TBS-T
CK1ε	CST	12448	1:1000	5% BSA TBS-T
CK1ε	DSTT	SA610, Bleed 2	1:1000	5% milk TBS-T
Cullin2	Invitrogen	51-1800	1:1000	5% BSA TBS-T
Cyclin A2	CST	4656	1:1000	5% BSA TBS-T
Cyclin B1	CST	4138	1:1000	5% BSA TBS-T
DYNLL1	Abcam	EP1660Y	1:1000	5% BSA TBS-T
ERK 1/2	CST	4695	1:1000	5% BSA TBS-T
FAM83B	Abcam	143829	1:1000	5% BSA TBS-T
FAM83B	DSTT	SA270, Bleed 3	1:1000	5% milk TBS-T
FAM83D (C-term)	DSTT	SA102, Bleed 3 (depleted against N-term)	1:1000	5% milk TBS-T

FAM83D (N-term)	DSTT	SA102, Bleed 3	1:1000	5% milk TBS-T
FAM83G	DSTT	S876C, Bleed 3	1:1000	5% milk TBS-T
FAM83H	DSTT	SA273, Bleed 4	1:1000	5% milk TBS-T
FLAG-HRP	Sigma-Aldrich	A8592	1:2000	5% milk TBS-T
GAPDH	CST	2118	1:5000	5% BSA TBS-T
GFP	ChromoTek	3H9	1:2000	5% BSA TBS-T
GFP	DSTT	S268B, Bleed 2	1:2000	5% milk TBS-T
GFP	Roche	11814460001	1:500	5% BSA TBS-T
HIF1α	BD Transduction Laboratories	610959	1:1000	5% BSA TBS-T
HMMR (human)	Millipore	ABC323	1:1000	5% milk TBS-T
HMMR (mouse)	Abcam	124729	1:1000	5% milk TBS-T
phosphoHistone H3 (S10)	CST	9701	1:1000	5% BSA TBS-T
SHP2 (C-term)	CST	3397	1:1000	5% BSA TBS-T
SHP2 (N-term)	CST	3752	1:1000	5% BSA TBS-T
SMAD1	DSTT	S618C, Bleed 3	1:1000	5% milk TBS-T
Ubiquitin	Dako	106260	1:2000	5% milk TBS-T
UVRAG	MBL	M160-3	1:1000	5% BSA TBS-T
VHL	CST	68547	1:1000	5% BSA TBS-T
VPS34	DSTT	S672B	1:1000	5% milk TBS-T

Table 2-3: Antibodies used for immunoblotting in this thesis.

The antibodies used for immunofluorescence are listed as a separate table in Table 2-4. Alexa Fluor 488 donkey anti-sheep IgG (A11015), Alexa Fluor 594 goat anti-mouse IgG (A11005), Alexa Fluor 594 donkey anti goat IgG (A11058), and Alexa Fluor 594 goat anti-rabbit IgG (A11012) were used at 1:500 dilution for immunofluorescence experiments, and were obtained from Thermo Fisher Scientific.

Antibody	Company	Cat. Number	Ab dilution
CK1α	Bethyl Laboratories	A301-991A	1:500
CK1α	Santa Cruz	Sc6477	1:100
CK1α	DSTT	SA527, Bleed 3	1:500
CK1ε	Sigma Aldrich	HPA026288	1:500
FAM83D (C-term)	DSTT	SA102, Bleed 3 (depleted against N-term)	1:500
HMMR (human)	ABC323	1:1000	1:500
HMMR (mouse)	Abcam	124729	1:500

Table 2-4: Antibodies used for immunofluorescence in this thesis.

2.1.4: Primers:

Human qPCR primers (Table 2-5) were either designed using the National Centre for Biotechnology Information (NCBI) Primer-BLAST online software tool (Ye, Coulouris et al., 2012), and generated by Invitrogen, or obtained from peer-reviewed published literature. For genomic DNA sequence amplification, primers (Table 2-6) were designed to have a melting temperature of 60°C using SnapGene. All primers were resuspended in nuclease-free water to a final concentration of 100 mM, and stored at -20°C.

Target	Sequence (5'-3')
CK1α	F - AATGTTAAAGCAGAAAGCAGCAC
	R - TCCTCAATTCATGCTTAGAAACC
Cyclin B1	F - GCAGTGC-GGGGTTTAAATCT
	R - GCCATGTTGATCTTCGCCTT
FAM83D	F - ACGTTGATTGATGGCATCCG
	R - CCTTGGACTGTGGTTTTCGG
GAPDH	F - TGCACCACCAACTGCTTAGC
	R - GGCATGGACTGTGGTCATGAG
HMMR	F - CAAAAGAGAAACAAAGATGAGGGG
	R - CCACTTGATCTGAAGCACAAC

Table 2-5: qPCR primers used in this thesis.

Target	Application	Sequence (5'-3')
CSNK1A1	Genomic DNA amplification to confirm N-term *mCherry* knockin	F – AGTAACAGGTAACACCTGCTGAGC
		R - AGACATTAGCAAAACTCCAAGTCGCG
CSNK1E	Genomic DNA amplification to confirm N-term *mCherry* knockin	F – TGTGAGGTCTTGGTGTCATGACG
		R - CTCAGAAGTGGCACTGAAAGGC
FAM83D	Genomic DNA amplification to confirm knockout	F - GTTGCCTATAAAGCGGGACTGC
		R – TACTCCCAGCAGGCCTCAATTTCC
FAM83D	Genomic DNA amplification to confirm C-term *GFP* knockin	F – GGGAACACAAACCAGCATCACC
		R - AGGGGGGGAAAAAGTACAGAAGC
FAM83D	Genomic DNA amplification to confirm F283A mutation knockin	F – CCCTCTGAGGCTGAGCATTTAGTG
		R - GTGGTGATGCTGGTTTGTGTTCC
FAM83D		F - ATTGGAAGGAAAGCAGCCAATGG

	Genomic DNA amplification to confirm *FAM83D*cDNA-IRES-*GFP*-PolyA knockin (Exon 1)	
		R - TCGGGGTTCAGGAAACGAGC
FAM83D	Genomic DNA amplification to confirm *FAM83D*cDNA-IRES-*GFP*-PolyA knockin (3' Junction)	F – GCATCAAGGTGAACTTCAAGATCCG
		R -ACTCTCGTGTTTATCTGCTTTTTACAGC
GFP	Genomic amplification of GFP knockin genes from within the *GFP* sequence	F – GACCACTACCAGCAGAACACCC
		R - GCTGAACTTGTGGCCGTTTACG
HMMR	Genomic amplification to confirm knockout	F – CTGCCGCTACCTTGAGGATCTC
		R – TGGTTACTGTGCTGTGCATTGC
mCherry	Genomic amplification of mCherry knockin genes from within the *mCherry* sequence	F – GACTACACCATCGTGGAACAGTACG
		R - GTTGTGGGAGGTGATGTCCAAC

Table 2-6: PCR primers used to amplify the genomic DNA from the CRISPR-modified cell lines generated in this thesis, for DNA sequencing.

2.1.5: siRNA oligonucleotides:

All siRNA oligonucleotides used in this thesis were purchased from Dharmacon. The product references for siRNAs against human CK1α (*CSNK1A1*) are J-003957-13, J-003957-14, J-003957-15, and J-003957-16, and against human SHP2 (*PTPN11*) are L-003947-00-0005. The non-targeting control siRNA reference is D-001810-01-05.

2.1.6: cDNA plasmids:

All the plasmids encoding the mammalian expression constructs used in this thesis were generated by the DSTT (University of Dundee) cloning team, and each given a unique identifier (DU) number. All DNA constructs were sequence verified by the DNA Sequencing and Services facility, University of Dundee, using Applied Biosystems Big-Dye Ver 3.1 chemistry on an Applied Biosystems model 3730 automated capillary DNA sequencer. The details of all the plasmids used in this thesis are freely available to the research community worldwide, and can be found at

https://mrcppureagents.dundee.ac.uk. For the pRetroX Tet-On and pBABE retroviral systems, plasmids were commercially-sourced from Clontech.

cDNA constructs were cloned into pBABED-puro, pBABED-hygro, pcDNA5/FRT/TO, or pCMV5 vectors, with N- or C-terminal FLAG, HA, GFP or mCherry tags where indicated. pcDNA5-FRT-TO vectors were either transiently-expressed, or used to generate stable tetracycline-inducible Flp-In T-REx cell lines as per the manufacturers guidelines (Thermo Fisher Scientific). pBABED denotes a Dundee-modified version of the pBABE vector. pBABED plasmids were either transiently-expressed, or used to generate stable cell lines through retroviral infection.

All the plasmids used in this thesis are listed in Table 2-7.

Expressed	Vector	DU number / source
aGFP	pBABED P	54218
aGFP.16	pBABED P	54238
aGFP.16-CK1α	pBABED P	29403
aGFP.16-CK1α (K46D)	pBABED P	29555
aGFP.16-CK1α (D136N)	pBABED P	28707
aGFP.16-CK1ε	pBABED P	29613
aGFP.16-CK1ε (D128N)	pBABED P	29629
aGFP-VHL	pBABED P	54023
Empty vector	pRetroX-Tight	Clontech
FAM83A-GFP	pcDNA5 FRT/TO	42864
FAM83B-GFP	pcDNA5 FRT/TO	42833
FAM83C-GFP	pcDNA5 FRT/TO	42825
FAM83D-GFP	pcDNA5 FRT/TO	42835
FAM83E-GFP	pcDNA5 FRT/TO	42826
FAM83F-GFP	pcDNA5 FRT/TO	42832
FAM83G-GFP	pcDNA5 FRT/TO	42816
FAM83H-GFP	pcDNA5 FRT/TO	42865
FLAG-aASC	pBABED P	54821
FLAG-aCS3	pBABED P	60195
FLAG-aNSa1	pBABED P	54816
FLAG-VHL-aASC	pBABED P	54832
FLAG-VHL-aCS3	pBABED P	54844
FLAG-VHL-aCS3	pRetroX-Tight	57058
FLAG-VHL-aNSa1	pBABED P	54843
GAG/POL	pCMV	Clontech
GFP only	pcDNA5 FRT/TO	41455
GFP-FAM83A	pcDNA5 FRT/TO	44235

GFP-FAM83B	pcDNA5 FRT/TO	44236
GFP-FAM83C	pcDNA5 FRT/TO	42473
GFP-FAM83C (D259A)	pcDNA5 FRT/TO	28479
GFP-FAM83C (F293A)	pcDNA5 FRT/TO	28480
GFP-FAM83D	pcDNA5 FRT/TO	29092
GFP-FAM83D (D249A)	pcDNA5 FRT/TO	29110
GFP-FAM83D (F283A)	pcDNA5 FRT/TO	29109
GFP-FAM83E	pcDNA5 FRT/TO	44237
GFP-FAM83E (D243A)	pcDNA5 FRT/TO	28481
GFP-FAM83E (F277A)	pcDNA5 FRT/TO	28482
GFP-FAM83F	pcDNA5 FRT/TO	44238
GFP-FAM83F (D250A)	pcDNA5 FRT/TO	28268
GFP-FAM83F (F284A)	pcDNA5 FRT/TO	28488
GFP-FAM83G	pcDNA5 FRT/TO	33272
GFP-FAM83G (D262A)	pcDNA5 FRT/TO	28476
GFP-FAM83G (F296A)	pcDNA5 FRT/TO	28477
GFP-FAM83H	pcDNA5 FRT/TO	44239
GFP-FAM83H (D236A)	pcDNA5 FRT/TO	28428
GFP-FAM83H (F270A)	pcDNA5 FRT/TO	28487
GFP-FAM83H (M1-L284) – FAM83G (S311-P823)	pcDNA5 FRT/TO	28683
HA-CK1α	pCS2	28216
mCherry-CK1α	pcDNA5 FRT/TO	28407
mCherry-CK1α (N141A)	pcDNA5 FRT/TO	28839
mCherry-CK1ε	pcDNA5 FRT/TO	28406
Tet-On	pRetroX-Tet-On	Clontech
VHL	pBABED P	54217
VHL-aGFP	pBABED P	54024
VHL-aGFP.16	pBABED P	54294
VHL-aGFP.16	pRetroX-Tight	54388
VSV-G	pCMV	Clontech

Table 2-7: List of cDNA plasmids used in this thesis.

All plasmids relevant to CRISPR/Cas9 gene editing, including both the guide RNAs and donor constructs, are listed in Table 2-8.

Target	KO/KI?	gRNA / Donor?	DU number
CSNK1A1	N-term mCherry KI	Sense gRNA	57522
		Antisense gRNA	57527
		Donor	57578
CSNK1E	N-term mCherry KI	Sense gRNA	54377
		Antisense gRNA	54383
		Donor	57623
FAM83D	KO	Sense gRNA	52007
		Antisense gRNA	52023
FAM83D	C-term GFP KI	Sense gRNA	54048
		Antisense gRNA	54054

		Donor	54198
FAM83D	C-term GFP KI with F283A mutation	Sense gRNA	57831
		Antisense gRNA	57835
		Donor	57512
FAM83D	*FAM83D* cDNA-IRES-*GFP*-PolyA KI	Sense gRNA	60528
		Antisense gRNA	60530
		Donor	60707
HMMR	KO	Sense gRNA	60921
		Antisense gRNA	60934

Table 2-8: List of CRISPR/Cas9 plasmids used in this thesis.

2.1.7: Proteins:

Proteins tagged with GST at the N-terminus were expressed and affinity purified by the protein production team within the DSTT, University of Dundee, with the exception of GST-FAM83G-6xHis, which was purified by Dr. Polyxeni Bozatzi, a previous lab member. A complete list of proteins used in this these is provided in Table 2-9.

Protein	Tag	DU or cat. number	Source
CK1α	GST (N-term)	329	DSTT
FAM83A	GST (N-term)	24611	DSTT
FAM83B	MBP (N-term)	28495	DSTT
FAM83C	GST (N-term)	28269	DSTT
FAM83D	GST (N-term)	28270	DSTT
FAM83E	GST (N-term)	28271	DSTT
FAM83F	GST (N-term)	28272	DSTT
FAM83G	GST (N-term), 6xHis (C-term)	28293	Polyxeni Bozatzi (Bozatzi et al., 2018)
FAM83G (F296A/F300A)	GST (N-term)	28049	DSTT
FAM83H	GST (N-term)	28403	DSTT
PLD	N/A	525200	Millipore

Table 2-9: List of purified recombinant proteins used in this thesis.

2.2: Methods:

2.2.1: Mammalian cell culture:

2.2.1.1: Cell culture:

U2OS osteosarcoma, HeLa, A549 adenocarcinoma, HaCaT human keratinocytes, human embryonic kidney HEK 293, retroviral production HEK 293 FT, J774 mouse monocyte and mouse embryonic fibroblasts (MEFs) were grown in DMEM supplemented with 10% (v/v) FBS, 2 mM L-glutamine, and 100 U/ml pen/strep (hereafter referred to as full medium). Human MDA-MB-231 breast cancer, MDA-MB-468 mammary gland adenocarcinoma and K-562 erythroleukemia cells were grown in RPMI medium supplemented with 10% (v/v) FBS, 2 mM L-glutamine, and 100 U/ml pen/strep. Cells were maintained at 37°C in a humidified incubator set to 5% CO_2. All cell culture procedures were performed under aseptic conditions.

Cells were grown to 80-90% confluency in a 10 or 15 cm Nunclon-coated dish (Thermo Fisher Scientific). For passaging the cells, cell medium was aspirated from the dish, and the cells washed 1 x in PBS (or 2 x for HaCaTs). The PBS was then aspirated and washed cells were incubated with 1-2 ml trypsin/EDTA at 37°C until all cells were detached from the culture surface. Detached cells were resuspended in fresh full medium, and pipetted a few times to detach cell clumps. Cells were seeded into new culture plates at the desired dilutions/densities. For cell counting, a Countess automated cell counter (Thermo Fisher Scientific) was used.

The *HMMR*$^{-/-}$ knockout and wild-type MEFs from close littermates were a kind gift from Christopher Maxwell, University of British Columbia.

2.2.1.2: Freezing/thawing cells:

Confluent cells were trypsinised as described above, and resuspended in full medium. The cell suspension was briefly centrifuged (3 min, 500 x*g*) to pellet the cells. The medium was then aspirated and cells were resuspended in freezing medium (Table 2-2). Equal volumes of the cells:freezing medium mix were aliquoted into 1 ml cryovials and stored in a cell-freezing chamber (Mr. Frosty, Thermo Fisher Scientific), for 24 h at -80°C. For long-term storage, frozen cryovials were transferred to liquid nitrogen.

To thaw cells, frozen cryovials were placed in a 37°C water bath for 2 min. Thawed cells were resuspended in 5 ml of full medium, followed by a brief centrifugation (3 min, 500 x*g*) to pellet the cells. The freezing medium was aspirated, and cells were resuspended in fresh full medium before transferring to a new culture dish.

2.2.1.3: Transient transfection of cells:

Transient transfections of cDNA plasmids were performed on sub-confluent (60-70%) cells. For a 10 cm dish of cells, 2 µg cDNA, 20 µl PEI, and 1 ml Opti-MEM were vortexed for 20 s, incubated at room temperature for 20 min, and added dropwise to target cells. For an individual well of a 6-well dish, transfections were performed as for a 10 cm dish, except 500 ng cDNA, 4 µl PEI, and 250 ml Opti-MEM were used. Cells were incubated in the transfection mix for 24 h prior to lysis.

2.2.1.4: RNA interference (RNAi):

Cells were seeded at 1 x 10^5 cells per well in a 6-well culture dish. The cells were transfected with 10 nM of the relevant small interfering RNA (siRNA) oligonucleotides, using 4 µl of Lipofectamine RNAiMAX per well in 250 µl Opti-MEM, as recommended by

the manufacturer. 16 h post-transfection, the transfection medium was aspirated, and replaced with fresh full medium. Cells were lysed and processed 48 h post-transfection.

2.2.1.5: Retroviral infection:

Stable cell lines obtained through retroviral infections were generated in accordance with the relevant biological safety regulations. For generating the retroviral particles encoding the protein of interest (POI), 6 µg of the pBABED plasmid encoding the POI was incubated with 2.2 µg of vesicular stomatitis virus G (VSV-G) and 3.8 µg of GAG/POL expression plasmids, in 300 µl Opti-MEM in a 1.5 ml Eppendorf tube. In a separate tube, 24 µl of PEI was incubated with 300 µl Opti-MEM. Following 5 min, the two tubes were combined, and the resulting mix incubated at room temperature for 20 min. Following incubation, the mix was added dropwise to a 10 cm dish of 70% confluent HEK 293 FT cells. 16 h post-transfection, the transfection mix was safely disposed of, and fresh medium was added to the HEK 293 cells. 24 h later, the retroviral medium was collected and syringe filtered through 0.45 µM sterile filters. On occasion, fresh medium was applied to the HEK 293 cells, and a second batch of retrovirus was collected 24 h later. Target cells (60-70% confluent) were infected with the optimised titre of the retroviral medium, which was diluted in fresh medium and supplemented with 8 µg/ml polybrene to aid infection (Hesse, Ebbesen et al., 1978). 24h-post infection, the retroviral medium was safely disposed of, and replaced with fresh full medium containing the appropriate antibiotic to select cells that had successfully integrated the retroviral construct (2 µg/ml for puromycin, 50 µg/ml for hygromycin). Selected cells were used for subsequent experiments, and the successful expression of the POI was confirmed by Western blotting. Uninfected cells were selected with the relevant antibiotic as a selection control.

For the pRetroX-Tet-On retroviral system, stable cell lines were produced following the manufacturers' protocol (Clontech). In brief, cells were first infected with retroviruses encoding the Tet-On plasmid, and selected in G418. Following selection, Tet-On-positive cells were then infected with the pRetroX-tight retrovirus encoding the gene of interest. Following successful selection with puromycin, Tet-inducible expression was tested through titration with different doxycycline concentrations (0.02-2 μg/ml) and confirmed through Western blotting.

2.2.1.6: Generation of tetracycline-inducible Flp-In T-REx cells:

Flp-In T-REx U2OS and HEK 293 cells were maintained in full medium supplemented with 15 μg/ml blasticidin and 100 μg/ml zeocin, in order to maintain expression of the Tet-repressor and integrity of the Flp-recombination site respectively. For a 10 cm dish, subconfluent (60-70%) cells were transfected with 1 μg of the pcDNA5-FRT/TO vector encoding the POI, along with 9 μg of the pOG44 Flp recombinase plasmid. Plasmids were diluted in 1 ml Opti-MEM with 20 μl of 1 mg/ml PEI. The transfection mix was vortexed for 20 s, and left to incubate at room temperature for 20 min. Following incubation, the transfection mix was applied dropwise to cells. 24 h post-transfection, the medium was replaced with fresh full medium supplemented with 15 μg/ml blasticidin and 50 μg/ml hygromycin-B for 2-3 weeks. The selection medium was replenished every 2-3 days until positive clones were selected, verified and expanded. The addition of hygromycin B acts to ensure correct integration of the cDNA of interest. Tet-inducible protein expression was induced with 20 ng/ml doxycycline for 16 h prior to lysis, unless otherwise stated in the figure legends, and confirmed with immunoblotting and/or immunofluorescence.

2.2.1.7: Generation of fluorescent tag knockin cells using CRISPR/Cas9:

The CRISPR/Cas9 system (Cong, Ran et al., 2013) was employed to perform genome editing. The guide RNAs (gRNAs) and donor plasmids used in this thesis are listed in Table 2-8. Transfection of the CRISPR plasmids was performed on subconfluent (60-70%) cells. For a 10 cm culture dish, 1 ml Opti-MEM and 20 µl of PEI were combined with 1 µg each of the sense and antisense gRNA plasmids, along with 3 µg of the fluorescent tag donor plasmid flanked by 500 bp homology arms at the 5' and 3' ends. The antisense gRNA plasmid also carried the Cas9 D10A nickase sequence. Nickase cleaves one strand of the DNA that is complementary to the gRNA, therefore successful double strand breaks require target-specific *nicks* on both strands recognised by the sense and antisense gRNAs simultaneously. Thus, the potential off-target double strand breaks are vastly reduced compared to the wild-type Cas9 enzyme. The transfection mix was vortexed for 20 s, incubated at room temperature for 20 min, and added dropwise to cells. 24 h post-transfection, the transfection medium was replaced with fresh full medium supplemented with 2 µg/ml puromycin for selection of transfected cells. 24 h later, the puromycin-containing medium was replenished. 24 h later, the medium was replaced with normal full medium for a further 24 h, and the transfection process was repeated once more. GFP or mCherry positive cells were then sorted by fluorescence-activated cell sorting (FACS), and individual GFP or mCherry positive cells were plated on individual wells of a 96-well plate, which had been pre-coated with 1% (w/v) gelatin, and filled with 200 µl of conditioned medium supplemented with 20% (v/v) FBS. For FACS, the transfected cells were trypsinised, resuspended in full medium and pelleted, before being resuspended in 3 ml DMEM containing 1% (v/v) FBS. To minimise the chance of cells getting trapped in the meniscus, the 96-well plate was briefly centrifuged

(30 s, 500 x*g*). Viable clones were expanded and positive cells were analysed by immunoblotting, genomic PCR and DNA sequencing.

2.2.1.8: Generation of knockout cells using CRISPR/Cas9:

To generate knockout cells, cells were transfected and processed as for fluorescent tag knockin cells (section 2.2.1.7) except that no donor plasmid was used in combination with the gRNAs, and instead of FACS, single cell sorting was utilised to obtain single cell clones. The guide RNAs (gRNAs) and donor plasmids used in this thesis are listed in Table 2-8. Successful knockouts were confirmed by immunoblotting, genomic PCR and DNA sequencing.

2.2.1.9: Stimulation of cells with small molecule inhibitors:

The small molecule inhibitors used in this thesis are listed in Table 2-1. If not purchased from a commercial source, inhibitors were provided as 10 mM stocks dissolved in DMSO by the DSTT (University of Dundee), and stored in aliquots at -20°C. The commercially-sourced small molecule inhibitors were also dissolved in DMSO and stored in aliquots at -20°C, unless otherwise stated. Cells were treated with the inhibitors by adding the inhibitor straight to the culture medium, and incubating for the desired length of time at 37°C, as indicated in the figure legends. An equivalent volume of DMSO was used as a vector control.

2.2.1.10: Synchronisation of cells using small molecules:

For synchronisation, cells were arrested at prometaphase with nocodazole (100 ng/ml) for 12 h, before floating mitotic cells were isolated by mitotic shake-off. The presence of floating cells, and hence confirmation that the nocodazole treatment had

been successful, was monitored by brightfield microscopy. Collected mitotic cells were washed 3 x in PBS before re-plating in fresh full medium for 45 min prior to lysis, to allow them to re-establish their spindles and progress into mitosis. Brightfield microscopy was used to confirm cells had re-established their mitotic spindles and aligned their chromosomes, typically 45 min after release from nocodazole-containing medium. Alternatively, cells were synchronised in mitosis with 5 µM of the Eg5 inhibitor S-Trityl L-Cysteine (STLC) (Skoufias, DeBonis et al., 2006) for 16 h. Following STLC incubation, brightfield microscopy was used to confirm the presence of mitotic cells, and hence successful Eg5 inhibition. Floating, mitotic cells were isolated by shake-off and either lysed immediately, or washed 3 x in PBS and re-plated in fresh full medium. Where indicated, MG132 and ProTAME were used at 20 µM. For either G2 arrest or forced mitotic exit, cells were treated with 10 µM of the CDK1 inhibitor RO-3306 (Vassilev, 2006) for 24 h or 1 h respectively, prior to lysis.

2.2.1.11: Preparation of cells for flow cytometry:

U2OS cells treated with or without synchronisation agents as described in section 2.2.1.10 were collected and washed 2 x in PBS containing 1% (v/v) FBS. Cells were fixed in 90% (v/v) ice-cold methanol for 16 h overnight at -20°C.

2.2.1.12: Analysis of cell cycle stage by DNA distribution profiling:

Following methanol fixation, cells were adjusted to around 200,000 cells, washed 2 x in PBS containing 1% (v/v) FBS, and stained with 300 µl DNA staining buffer (Table 2-2). Following 20 min incubation at room temperature protected from light, samples were analysed and data acquired on a fluorescence-activated cell sorting (FACS) Canto [Becton Dickinson, (BD)] using BD FACSDIVA software. Data was visualised

using FlowJo software (Tree Star, BD). Pulse-width analysis was used to ensure the exclusion of doublets and clumps prior to evaluation of cell cycle distribution using the Watson-Pragmatic model.

2.2.1.13: Cell lysis:

Unless otherwise stated, cells destined for lysis were washed twice in ice-cold PBS and scraped on ice in lysis buffer supplemented with protease inhibitors (Table 2-2). Extracts were transferred to Eppendorf tubes and incubated on ice for 10 min, and then clarified at 13,000 x*g* for 20 min at 4°C. Samples were either processed immediately or snap-frozen in liquid nitrogen and stored at -80°C.

If chemical cross-linking with DSP was required, cells were lysed on ice in DSP lysis buffer containing fresh DSP (Table 2-2), after two washes in ice-cold PBS. Lysed extracts were incubated on ice for 30 min, before quenching the cross-linking reaction with 0.2 M Tris-HCl pH 7.5. During the quenching process, samples were incubated on ice for 30 min with regular vortexing performed every 5 min. Samples were then clarified at 13,000 x*g* for 20 min at 4°C, and either processed immediately, or snap-frozen in liquid nitrogen and stored at -80°C.

For DNA or mRNA isolation, cells were lysed and processed using a Qiagen DNeasy blood and tissue kit or RNeasy kit respectively, as per the manufacturer's instructions.

2.2.1.14 Quantification of spindle orientation:

U2OS cells were seeded at 3,000 cells per well in 96-well plates with L-shaped micropatterns (CYTOO) at a density of 15,000 cells/ml. Prior to seeding, plates were coated with 20 µg/ml fibronectin (Sigma-Aldrich) for 2 h at room temperature. Following

seeding, cells were imaged every 5 or 10 min for up to 24 h at 37°C in a 5% CO_2 environmental chamber using an ImageXpress Micro High Content Screening System (Molecular Devices Inc.).

To measure spindle orientation in subconfluent cultures, cells were seeded at 50% confluency, grown overnight and imaged as described above. Spindle angles were measured using a vector drawn through the division axis at anaphase bisecting a vector drawn through the cell's long axis determined prior to prophase.

2.2.2: General molecular biology:

2.2.2.1: Plasmid transformation, amplification and purification:

Competent *E. coli* DH5α cells were generated and maintained by the DSTT, University of Dundee, and stored at -80°C. For transformation of plasmids, one vial of DH5α cells were thawed on ice, and 1 µl of plasmid DNA (10-20 ng) was added. The cell:plasmid mix was incubated on ice for 20 min, and then heat-shocked at 42°C for 45 s to facilitate DNA uptake. Cells were then returned to ice for 2 min. Following incubation, 500 µl of LB medium was added to the cells, and they were incubated at 37°C with shaking for 30 min, to allow them to recover. Subsequently, 150 µl of the transformed cells in LB were transferred and spread onto a LB agar plate containing 100 µg/ml ampicillin or 50 µg/ml kanamycin as appropriate. Plates were then placed inside a 37°C incubator and left for 16 h overnight.

To amplify the plasmids, a single transformed bacterial colony was used to inoculate 4 ml (miniprep) or 100 ml (midiprep) LB medium containing 100 µg/ml ampicillin or 50 µg/ml kanamycin as appropriate. The bacteria:LB mix was placed inside a shaking incubator set to 37°C for 16 h overnight. Following incubation, cells were

pelleted by centrifugation (2000 x*g*, 10 min, 4°C), and the plasmid DNA was isolated and extracted following the manufacturer's instructions. Qiagen DNA mini or midi kits were used for this purpose.

2.2.2.2: Measurement of DNA and RNA concentration:

The concentration of extracted DNA and RNA in an aqueous solution (elution buffer) was measured on a NanoDrop spectrophotometer (Thermo Fisher Scientific) at a wavelength of 260 nm. The 260/280 and 260/230 ratios were calculated to assess the purity of the DNA. The NanoDrop was calibrated with the appropriate elution buffer prior to use. The elution buffers were provided in the Qiagen kits.

2.2.2.3: Agarose gel electrophoresis:

In order to analyse the size and purity of DNA products, they were assessed by electrophoresis on 1% (w/v) agarose gels. To visualise the DNA, each gel was stained with SYBR safe DNA stain at 1:10,000 dilution. The DNA to analyse (0.5 µg) was mixed with 1x DNA loading dye and loaded into the gel. A 1 kbp DNA ladder (NEB) was used in parallel for size reference. Gels were electrophoresed in 1x TAE running buffer (Table 2-2) at 100 V for 30 min. Stained DNA was visualised using a UV transilluminator.

2.2.2.4: Quantitative reverse transcription PCR (qRT-PCR):

The Qiagen RNeasy kit was used to isolate RNA from cells. cDNA was produced using 1 µg of isolated RNA using the SuperScript cDNA kit (Bio-Rad) as per the manufacturer's instructions.

qPCR reactions were performed in triplicate, in 10 µl final volumes for 384-well plates. Each reaction contained cDNA equivalent to 1 ng/µl RNA, 50% (v/v) SsoFast EvaGreen Supermix (Bio-Rad), and 0.5 µM each of appropriate forward and reverse

primers (Table 2-5). qPCR was performed within a CFX384 real-time qPCR machine (Bio-Rad). Data was normalised to the mean of the housekeeping gene GAPDH, and analysed using the $2^{-\Delta\Delta Ct}$ method for comparing relative gene expression (Livak & Schmittgen, 2001). Plots were generated, and statistical analyses performed, using GraphPad Prism software.

2.2.2.5: PCR:

The Qiagen DNeasy blood and tissue kit was used to isolate DNA from cells following the manufacturer's instructions. PCR was performed using the KOD hot start DNA polymerase kit (Toyobo) following the manufacturer's protocol, within a PCR thermal cycler (PT-200, MJ research). PCR reactions were performed in 50 µl final volumes, and each reaction contained 25 mM $MgSO_4$, dNTPs (2 mM each), 3 µl DMSO, 1x KOD hot start DNA polymerase buffer, 10 µM each of appropriate forward and reverse primers (Table 2-6), 200 ng template DNA, and 1 U KOD hot start DNA polymerase. PCR products were analysed by agarose gel electrophoresis as described in section 2.2.2.3.

2.2.2.6: Subcloning of PCR products:

PCR products were ligated into pSC-B vectors using the StrataClone Blunt PCR cloning kit (Agilent), in accordance with the manufacturer's instructions. Each ligation reaction contained 3 µl StrataClone cloning buffer, 1 µl StrataClone vector mix, and 2 µl of the PCR product. Reactions were incubated at room temperature for 5 min, and 5 µl of the reaction was subsequently transformed into a thawed vial of StrataClone SoloPack competent cells as per the manufacturer's instructions. Following transformation and recovery in LB medium, 50 µl of the cell:LB mix was plated onto LB

agar plates containing 2% (w/v) X-Gal in order to enable blue-white colony screening. Plates were inverted and incubated at 37°C for 16 h overnight. Following incubation, white colonies were chosen and used to inoculate 4 ml LB medium, which was subsequently grown for 16 h overnight at 37°C with shaking. Plasmid DNA was then isolated using the Qiagen miniprep kit as per the manufacturer's instructions.

2.2.2.7: DNA mutagenesis:

DNA mutagenesis for all plasmids (Table 2-7) was performed by the DSTT (University of Dundee) cloning team. The QuikChange site-directed mutagenesis approach (Stratagene) was used in combination with KOD polymerase (Novagen). All mutations were verified by DNA sequencing (see section 2.2.2.8).

2.2.2.8: DNA sequencing:

Sequencing of all plasmid DNA was performed by the DNA sequencing service (University of Dundee) using Applied Biosystems Big-Dye v3.1 chemistry, on an Applied Biosystems model 3730 automated capillary DNA sequencer, using the appropriate sequencing primers.

2.2.3: General biochemistry:

2.2.3.1: Measurement of protein concentration:

The Bradford method (Bradford, 1976) was used in order to determine protein concentration. For calibration, a standard curve was generated through plotting absorbance against a serial dilution of BSA standards (0.125 - 2 mg/ml). Samples to be measured were first diluted in water by a factor of 10, and then 5 µl aliquots were dispensed in triplicates into a 96-well plate, along with the standard curve, which was also in triplicate. A blank sample (water) was included to measure the background

absorbance. Just prior to measuring, 200 µl of the Coomassie-based Bradford reagent was added to each sample, and following a 5 min incubation at room temperature, absorbances at 595 nm were measured using a VersaMax microplate reader and SoftMax Pro v4.8 software (Molecular Devices). The protein concentration of each sample was subsequently calculated from the mean absorbance per triplicate, with reference to the standard curve.

2.2.3.2: Immunoprecipitation (IP):

Clarified cell extracts were first incubated with blank agarose or protein-G sepharose beads, in order to pre-clear extracts and remove non-specific bead-interacting proteins. This was performed for 1 h at 4°C on a rotating wheel. The pre-cleared extracts (0.3-1 mg/ml for Western blot applications, or 10 mg final protein concentration for proteomics) were subsequently incubated with the appropriate antibody-coupled beads for 4 h, or overnight, at 4°C on a rotating wheel. An Input aliquot was taken from the pre-cleared sample prior to adding the beads, in order to confirm the presence of the protein of interest in the whole cell lysate. Following incubation, beads were pelleted and the flow-through extract was retained to assess IP efficiency by immunoblotting. Beads were then washed once in lysis buffer supplemented with NaCl to a final concentration of 500 mM, and twice in normal lysis buffer (Table 2-2). Beads were then resuspended in 1x SDS sample buffer (typically 30 µl). Input, IP and flow-through samples were incubated at 95°C for 5 min to denature samples prior to SDS-PAGE.

2.2.3.3: Covalent-coupling of antibodies to protein G sepharose beads:

To covalently cross-link an antibody to protein G sepharose beads, 1 µl of the beads per µg of the antibody were first incubated for 1 h at 4°C on a rotating wheel. The antibody-bound beads were then washed 5 x with 10 volumes of 0.1 M sodium borate, pH 9.0. Washed beads were subsequently resuspended in 20 mM dimethyl pimelimidate dihydrochloride (DMP) in 0.1 M sodium borate, followed by gentle agitation for 30 min at room temperature. This incubation step was repeated once more with fresh DMP in sodium borate. Beads were then washed in 10 volumes of 50 mM glycine pH 2.5 in order to strip the beads of any antibodies that had not been covalently bound. Finally, beads were neutralised by washing 2 x in 0.2 M Tris-HCl pH 8.0, with the second wash taking place for 30 min at room temperature. For storage, beads were resuspended in PBS containing 0.01% (w/v) sodium azide and stored at 4°C.

For elution of proteins bound to covalently-coupled beads, no reducing agent was added to the SDS sample buffer, in order to keep the antibody bound to the beads.

2.2.3.4: Separation of proteins by SDS-PAGE:

SDS-PAGE was performed using either the commercially available NuPAGE bis-tris electrophoresis system (Thermo Fisher Scientific), or the ATTO vertical polyacrylamide slab gel electrophoresis system (ATTO Corp.). Protein-based samples were prepared for SDS-PAGE by first heating in 1x SDS sample buffer at 95°C for 5 min. For precast NuPAGE novex gels, electrophoresis was carried out in an XCell SureLock Mini-Cell filled with 1x MOPS running buffer, and performed at a constant voltage of 150 V for 80 min.

For the ATTO system it was necessary to prepare the gels prior to electrophoresis. The Slab minigels (90 mm x 80 mm x 1 mm) were poured between glass

plates. The separating gel was typically prepared at final acrylamide concentrations of 6-13% (w/v) (Table 2-9). Polymerisation was initiated by addition of 0.075% (w/v) APS and 0.1% (v/v) TEMED, and the gel mix was poured into the gel assembly unit. 100% (v/v) isopropanol was gently applied to the gel surface to remove any bubbles, and the separating gel was allowed to polymerise for 20 min at room temperature. Following polymerisation, the isopropanol was completely poured off and the stacking gel (Table 2-9) was prepared and poured directly on top of the separating gel. A Teflon comb was immediately inserted into the stacking gel, and the gel was allowed to polymerise for 20 min at room temperature. Gels were either used immediately, or stored at 4°C wrapped in a damp paper towel to prevent them from drying out. Gels were introduced into the ATTO electrophoresis chamber, and filled with 1x SDS-PAGE running buffer (Table 2-2). Electrophoresis was performed at a constant voltage of 150 V for around 80 min, until the dye front had reached the bottom of the gel.

For both the NuPAGE and ATTO systems, samples (typically 10-20 µg protein) were loaded on to the gel using a Gilson pipette equipped with gel-loading tips, and pre-stained protein standards were loaded in parallel for molecular weight reference.

2.2.3.5: Staining proteins with InstantBlue:

Following SDS-PAGE, gels were washed in deionised water and incubated in 20 ml InstantBlue (Expedeon) on a rocking platform for 20-60 min. Following incubation, the gel was de-stained by repeated washing in deionised water for 1-2 h.

	Stacking	Separating				
Percentage acrylamide	4	6	8	10	12	13
H_2O (ml)	7.6	11.6	10.6	9.6	8.6	8.1
1 M Tris-HCl pH 6.8 (ml)	1.25	N/A	N/A	N/A	N/A	N/A
1.5 M Tris-HCl pH 8.8 (ml)	N/A	5	5	5	5	5
10% (w/v) SDS (µl)	100	200	200	200	200	200
40 % (w/v) polyacrylamide (ml)	1	3	4	5	6	6.5
10% (w/v) APS (µl)	100	200	200	200	200	200
TEMED (µl)	10	16	16	16	16	16

Table 2-10: Recipes for stacking and separating gels used to make the Slab minigels used in combination with the ATTO electrophoresis system.

2.2.3.6: Immunoblotting (Western blotting):

Following the successful resolution of protein samples by SDS-PAGE, proteins were transferred onto PVDF membranes which had been pre-activated in 100% (v/v) methanol just prior to transfer assembly. Transfer was performed at 80 V for 80 min using the Bio-Rad transfer apparatus filled with transfer buffer (Table 2-2), and a cooling block to limit over-heating. When blotting for smaller molecular weight proteins, the length of transfer time was reduced to 50 min.

In order to visualise transfer efficiency in a reversible manner, PVDF membranes were briefly immersed in Ponceau S staining buffer for 1-2 min, before rinsing in 100% (v/v) methanol to visualise the stained protein bands. Where appropriate, membranes were cut into smaller strips with a scalpel, to enable proteins of different molecular weights to be probed at the same time. Membranes were washed in blocking buffer (Table 2-2) for 5 min to remove the ponceau stain, before continuing the block in fresh blocking buffer for 30 min at room temperature on a rocking platform. Blots were briefly

washed in 1x TBS-T to remove the blocking buffer, and incubated with the primary antibody solution (Table 2-2) for either 1 h at room temperature, or 16 h at 4°C. Following incubation, membranes were washed 3 x for 10 min in 1x TBS-T, before incubating with the HRP-conjugated secondary antibodies (typically 0.2 µg/ml) in blocking solution (Table 2-2) for 1 h at room temperature. Membranes were again washed for 3 x 10 min in 1x TBS-T, and incubated with enhanced chemiluminescence (ECL) reagent for 1 min. The excess ECL was drained off the membrane, and membranes were either developed using an X-ray cassette with films (Konica Minolta) in the dark room, or on the ChemiDoc imaging system (Bio-Rad). X-rays were developed using a Konica automatic developer.

2.2.3.7: Immunofluorescence microscopy:

Cells were seeded onto 22 x 22 mm sterile coverslips in 6-well culture plates. Coverslips were sterilised in 100% (v/v) ethanol and allowed to dry prior to plating cells. For imaging of mitotic cells, sterilised coverslips were coated in poly-L-lysine solution prior to seeding cells. Cells were washed 2 x in PBS and fixed in 4% (w/v) paraformaldehyde for 20 min at room temperature. Paraformaldehyde was diluted in PBS from a 16% (w/v) stock solution. Following incubation, the paraformaldehyde was removed, and the cross-linking reaction was quenched by washing 2 x in quenching buffer (Table 2-2), before incubating in quenching buffer for 10 min at room temperature. Coverslips were subsequently washed in PBS and permeabilised with 0.2% (v/v) NP40 in PBS for 3 min. Coverslips were then washed 2 x in IF blocking buffer (Table 2-2), followed by a 15 min incubation in blocking buffer to reduce non-specific epitope binding. Primary antibodies (Table 2-4) were prepared in blocking solution (Table 2-2) and added directly to the coverslip within a humidified chamber (typically 100 µl

antibody solution). Coverslips were incubated with the primary antibody for 1-1.5 h at 37°C. Following the incubation period, the coverslips were returned to the 6-well dish and washed for 3 x 10 min in blocking solution, and then incubated with the Alexa Fluor-conjugated secondary antibodies (Thermo Fisher Scientific) for 1 h at room temperature, protected from light. Next, coverslips were washed again for 3 x 10 min in blocking solution, and then processed for mounting. To mount, coverslips were briefly dipped into deionised water using tweezers, dried on a paper towel, and then mounted onto glass slides using ProLong Antifade reagent with DAPI. The mounted coverslips were left to dry overnight at room temperature, protected from light. Clear nail polish was used to seal the edges of the coverslip onto the glass slide once the mounting media had dried. For freeze-thaw permeabilisation with liquid nitrogen and PI3P staining, the Ganley method was used (Munson & Ganley, 2016). To image, cells were either visualised on a DeltaVision system (Applied Precision) with an immerse-oil 63X objective and processed with SoftWoRx (Applied Precision), or on a Zeiss LSM710 confocal microscope using a 63X Plan-Apochromat objective (NA 1.40). Alternatively, cells were imaged on a Nikon TiE inverted microscope (60x objective) and visualised with NIS Elements (Nikon). Where applicable for the DeltaVision system, Z-series were collected at 0.2 µM intervals, and deconvolved using SoftWoRx. Images were processed and figures assembled using Adobe Photoshop or OMERO software (Allan, Burel et al., 2012).

2.2.3.8: Quantification of CK1α spindle localisation:

For quantification of CK1α spindle localisation on STLC-induced monopolar spindles, the mean pixel intensities of CK1α staining on the spindle were calculated by measuring the mean pixel intensities of CK1α in the region of interest (roi) demarcated by the outer border of the DAPI ring (hereafter referred to as the spindle roi).

Subsequently, the ratio between the spindle roi and the background cytoplasmic CK1α staining was calculated, by measuring the mean cytoplasmic CK1α pixel intensities in the cytoplasmic roi, defined as the whole cell minus the spindle roi. The resulting ratios were plotted on a box plot with whiskers indicating the highest and lowest values. A ratio of >1 indicates CK1α is present on the spindle, and a ratio of ≤ 1 indicates CK1α is not present on the spindle. One might expect the theoretical ratio to be close to 1 in the *FAM83D*$^{-/-}$ cells. However, lower mean CK1α intensity in the DAPI-stained area relative to the cytoplasm implies exclusion of CK1α in DNA-rich regions. This results in a lower mean CK1α staining intensity in the overall spindle roi versus the cytoplasmic roi and therefore a ratio of less than 1. The ImageJ macro developed by Graeme Ball (Dundee Imaging Facility), used for this purpose is included in the appendix.

2.2.3.9: Live cell imaging:

For the mitotic assays, U2OS cells were grown in 96-well plates (Corning) and imaged for up to 24 h at 37°C in a 5% CO_2 environmental chamber using a 40X 0.75 NA dry objective with the MetaXpress v 5.0.2.0 software (Molecular Devices Inc.) on the ImageXpress Micro XL epifluorescence microscope (Molecular Devices Inc.). For the analysis of cell division kinetics, cells were first stained with Hoechst (1 µg/ml) to label DNA, and images were taken every 5 min. Movies were made in the MetaXpress v 5.0.2.0 software (Molecular Devices Inc.). For actin localisation experiments, U2OS cells were seeded at 20% confluency in 24-well plates, and 1 µl CellLight Actin-RFP (Thermo Fisher Scientific) was added per 5000 cells, and incubated at 37° C for 16 h. Following the incubation, U2OS cells were seeded on L-shaped micropatterns (CYTOO) at 30,000 per ml. For the analysis of actin localisation, images were taken every 2 min, and movies were made using MetaXpress v 5.0.2.0 software (Molecular Devices Inc.). Images of

actin localisation were projected from prophase to metaphase (Image J, z-projection standard deviation) for analysis. For the analysis of cortical asymmetric membrane elongation, images were taken every 1 min, and movies were made in the MetaXpress v 5.0.2.0 software (Molecular Devices Inc.).

2.2.4: *In vitro* assays:

2.2.4.1: *In vitro* kinase assays:

In order to assay kinase activity, 25 µl reactions were prepared encompassing 200 ng of the kinase and 2 µg of the protein substrate, within kinase assay buffer (Table 2-2) containing 0.1 mM $^{\gamma 32}$P-ATP (~500 cpm/pmol). Reactions were incubated at 30°C for 30 min with shaking, and terminated through addition of 9 µl 1x SDS sample buffer containing 5% (v/v) β-mercaptoethanol, and subsequent heating at 95°C for 5 min. Samples were then resolved by SDS-PAGE, and gels stained with InstantBlue in order to visualise the protein bands. Gels were then de-stained as described in section 2.2.3.5, and dried. Radioactivity within the gel was analysed by autoradiography by exposing the dried gel on Hyperfilm for different exposure times within a cassette. For long exposures, the cassette containing the Hyperfilm (typically 3 films on top of each other) was placed at -80°C to enhance the autoradiographic signal. Films were then developed using a Konica automatic developer.

Alternatively, for kinase assays against a substrate peptide instead of a protein substrate, reactions were set up as per the method described by Hastie et al (Hastie, McLauchlan et al., 2006). In short, 50 µl reactions were prepared containing the substrate peptide. An optimised CK1 substrate peptide (CK1tide, DSTT, EP5630) was used to assay CK1 kinase activity. Following incubation at 30°C for 30 min with shaking, 40 µl of the reaction was spotted onto p81 phosphocellulose (2 x 2 cm, Whatman) and

immediately immersed in 75 mM phosphoric acid, stirring continuously with a magnetic stirrer. The p81 papers were washed for 3 x 5 min with fresh 75 mM phosphoric acid each wash, until the $^{\gamma 32}$P-ATP that that not been incorporated into the peptide was washed off. Following the final wash, the p81 papers were briefly immersed in 100% (v/v) acetone and dried with a hair dryer within a fume hood. Dried p81 papers were transferred into 1.5 ml Eppendorf tubes, and radioactivity was measured using a scintillation counter (PerkinElmer). To measure the specific radioactivity (cpm/pmol) of the $^{\gamma 32}$P-ATP, 1 µl of the stock $^{\gamma 32}$P-ATP was diluted 1:100 and measured in parallel. This was performed in order to determine the stoichiometry of the reaction.

2.2.4.2: *In vitro* phosphatase assays:

In order to assay phosphatase activity, lysed extracts from asynchronous and mitotic *FAM83D*$^{GFP/GFP}$ knockin U2OS cells were subjected to immunoprecipitation with GFP TRAP beads (ChromoTek), and washed 3 x in wash buffer (Table 2-2). Beads were resuspended in 20 µl phosphatase-assay buffer (New England Biolabs) containing 1 mM $MnCl_2$, with or without λ-phosphatase (1 U, DSTT) for 30 min at 30°C with shaking. Following incubation, beads were washed 3 x in wash buffer and eluted at 95°C for 5 min in 1x SDS sample buffer. Input and immunoprecipitation samples were subjected to Western blotting as described in section 2.2.3.6.

2.2.4.3: *In vitro* phospholipase D assays:

In order to assay phospholipase D (PLD) activity, purified FAM83 proteins were subjected to the Amplex Red Phospholipase D assay kit (Thermo Fisher Scientific) as per the manufacturers' instructions. As a positive control, 1 U phospholipase D from *Streptomyces chromofuscus* was analysed in parallel. As FAM83 proteins are thought to

not possess any PLD-like activity, protein mass, rather than units of activity, was used to assay any putative PLD activity *in vitro*.

2.2.5: Mass spectrometry:

2.2.5.1: Preparation of samples for mass spectrometry:

For mass spectrometric analysis, cells were first lysed in lysis buffer (Table 2-2) as described in section 2.2.1.13. Next, clarified lysates were incubated with Protein A agarose beads for 1 h on a rotating wheel at 4°C, in order to pre-clear non-specific binding proteins. Pre-cleared extracts were then filtered through Spin-X columns (Corning) by centrifugation for 5 min at 13,000 x*g*, and filtered extracts (5 – 10 mg protein) were incubated with 10-20 µl packed beads for 16 h at 4°C on a rotating wheel. Following incubation, beads were washed once in lysis buffer supplemented to a final concentration of 500 mM NaCl, and twice with normal lysis buffer. Bead-bound proteins were denatured and eluted in 1x SDS sample buffer supplemented with 2% (v/v) β-mercaptoethanol for 5 min at 95°C. Samples were then filtered through Spin-X columns to remove the beads from the eluate. The filtered eluate was loaded onto a 4-12% bis-tris gradient gel, and proteins were separated by SDS-PAGE as described in section 2.2.3.4. Gels were stained with InstantBlue for 20 min, and de-stained in deionised water as described in section 2.2.3.5. A small portion of the eluate was retained for analysis by Western blotting.

2.2.5.2: In-gel digestion of proteins for mass spectrometry:

In an attempt to minimise potential protein contaminants, all steps from this point were performed under a laminar flow hood (model A3VB, Bassaire Ltd.). Disposable scalpels were used to cut protein bands of interest from the InstantBlue stained gels into 1-2 cm cubes, which were subsequently transferred into LoBind 1.5 ml

Eppendorf tubes. Gel pieces were washed once in HPLC grade water, and then shrank in 100% (v/v) acetonitrile for 5 min with gentle shaking. The acetonitrile was aspirated, and gel pieces were re-swollen with 50 mM Tris-HCl pH 8.0 for 5 min with shaking. The shrinking-swelling process was repeated once more, and the proteins within the gel pieces were reduced with 5 mM DTT in 50 mM Tris-HCl pH 8.0 for 20 min at 65°C. Next, the proteins within the gel pieces were alkylated with 20 mM iodoacetamide in 50 mM Tris-HCl for 20 min at room temperature. Gel pieces were subsequently shrank again in acetonitrile for 5 min, and re-swollen in 50 mM triethylammonium bicarbonate pH 8.0 containing 5 µg/ml trypsin for 16 h overnight at 37°C for digestion. The next day, an equivalent volume of acetonitrile was added to the digest for 15 min with shaking, and the supernatant was collected into a new LoBind 1.5 ml Eppendorf tube. Gel pieces were then re-swollen with 0.1% (v/v) TFA for 5 min with shaking, and peptides were extracted twice with acetonitrile for 5 min each with shaking. After each extraction, the supernatant was removed and combined with the previous supernatant. The supernatants were then dried using a SpeedVac, and dried peptides were submitted for analysis by the mass spectrometry team (MRC PPU, University of Dundee).

2.2.5.3: Peptide analysis by liquid chromatography-tandem mass spectrometry (LC-MS/MS):

Digested peptides were reconstituted in HPLC-grade 5% (v/v) acetonitrile containing 0.1% (v/v) formic acid, and injected into a U3000 RSLC HPLC chromatography system (Thermo Fisher Scientific) coupled to a linear ion trap-orbitrap hybrid mass spectrometer (Orbitrap-VelosPro, Thermo Fisher Scientific). Peptides were trapped on a nanoViper Trap column (2 cm x 100 µM, C18 5 µM, 100 *Å*, Thermo Fisher Scientific), and subsequently separated on a 15 cm EasySpray column (Thermo Fisher Scientific), equilibrated with a flow rate of 300 nl/min. Data was acquired in the data-dependent

mode, automatically switching between MS and MS-MS acquisition. Full scan spectra (m/z 400-1,600) were acquired in the orbitrap with resolution set to 60,000 at m/z 400. The 20 most intense ions, above a specified minimum signal threshold of 2,000, were fragmented by collision induced dissociation and recorded in the linear ion trap (full AGC target; 30,000. Msn AGC target; 5,000). Raw files were subsequently converted into a list of identified peptides, along with the precursor intensity of the identified peptides, and submitted to the in-house Mascot server (MRC PPU, University of Dundee). Data was searched against the SwissProt human database with variable modifications allowing for oxidation of Met, phosphorylation of Ser/Thr or Tyr residues, along with oxidation or dioxidation modifications. Carbamidomethylation of Cys was set as a fixed modification. Error tolerances were set to 10 ppm for MS1 and 0.6 Da for MS2. LC-MS-MS analysis was performed by Dr. David Campbell, Robert Gourlay and Joby Varghese (MRC PPU, University of Dundee). Data analysis was performed using Scaffold v 4.4.6 (Proteome Software).

2.2.6: Statistical analysis:

All experiments, with the exemption of protein interactome mass spectrometry-based experiments that were performed in a qualitative manner and subsequently verified by additional approaches, are representative of at least 3 biological replicates. qRT-PCR and *in vitro* assay experiments comprised 3-4 technical replicates per biological replicate, unless otherwise stated. Data are presented as the mean with error bars indicating the standard error of the mean. For box plots, the whiskers denote the minimum and maximum measured values. The middle line represents the median, and the box ranges depict the 25^{th}/75^{th} percentiles.

Statistical significance of any differences between experimental groups was assessed with either a student's *t*-test (two tailed, homoscedastic), or one-way ANOVA with post-hoc Tukey's test, using GraphPad Prism software with standard settings. Differences in means were considered significant if $P < 0.05$.

All immunoblots and immunofluorescence images are displayed as representative images from at least 3 fields of view, from at least 2 independent experiments.

3. The FAM83 family of proteins anchor Casein Kinase 1 isoforms in cells:

3.1: Background:

Following the discovery that FAM83G interacted with the transcription factor SMAD1 (Vogt et al., 2014), and the demonstration that this interaction promoted the transcription of non-canonical bone morphogenetic protein (BMP) target genes (Vogt et al., 2014), it was hypothesised that the other FAM83 proteins may act in a similar way. To test this in a non-biased manner, transgenic human embryonic kidney HEK 293 cell lines, each stably expressing a single copy of a *FAM83* gene under the control of the tetracycline (Tet)-inducible promoter, were generated. Each FAM83 protein was tagged with a green fluorescent protein (GFP) at the N-terminus. In these cell lines, expression of each GFP-FAM83 protein was induced in response to doxycycline in a time-dependent manner, with detectable amounts evident 30 min after doxycycline treatment (Figure 3-1A). In a similar vein, U2OS osteosarcoma cell lines, stably integrated with a single copy of each *FAM83* gene tagged at the C-terminus with GFP, also under the control of the Tet-inducible promoter, were generated. This time, all FAM83-GFP proteins displayed robust expression following 24 h treatment with doxycycline, except FAM83B, which did not express (Figure 3-1B). As a control, HEK 293 and U2OS cells expressing free GFP under the Tet-inducible promoter were also generated (Figure 3-1A&B).

Following successful induction with doxycycline, extracts from these HEK 293 and U2OS cell lines were subjected to anti-GFP immunoprecipitation, and the eluates were separated by SDS-PAGE. The gel sections corresponding to the entire lane for each sample were excised and digested with the protease trypsin. The resulting tryptic peptides were analysed by mass spectrometry, and assigned to human proteins within

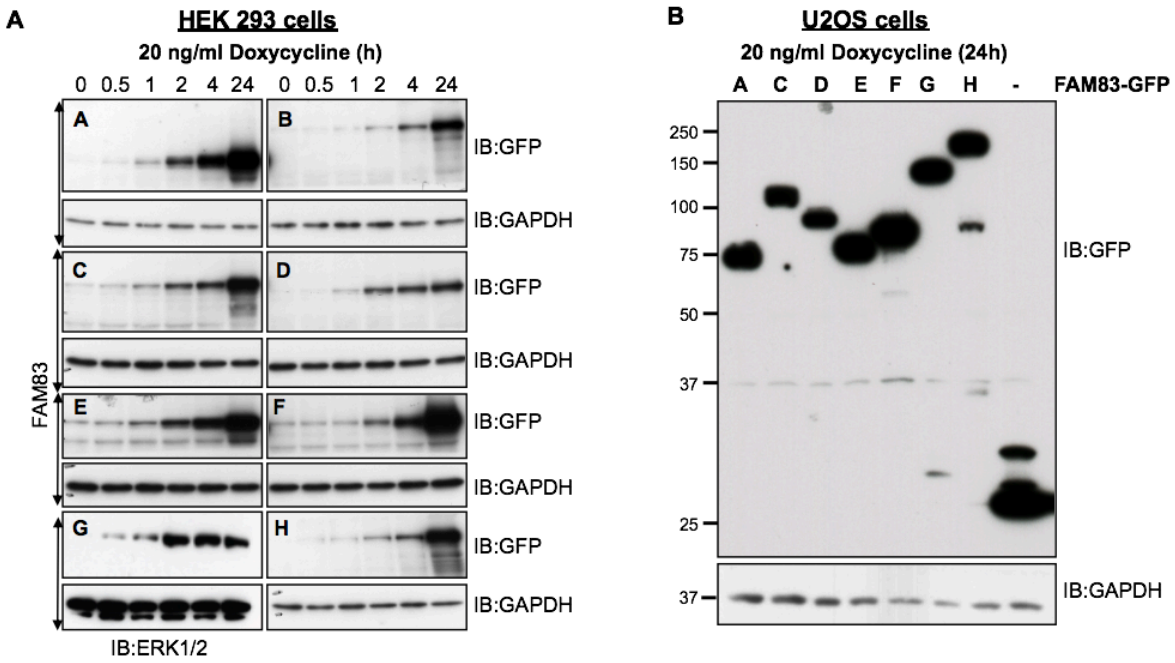

Figure 3-1: Generation of HEK 293 and U2OS cells for tetracycline-inducible expression of FAM83 proteins: A: A single copy of each *FAM83A-H* gene was tagged with GFP at the N-terminus, and stably inserted downstream of a tetracycline-inducible promoter in Flp-In T-REx HEK 293 cells. GFP-FAM83 expression was induced by treating cells with 20 ng/ml doxycycline, and cells were lysed at the indicated times after treatment. Extracts (10 μg protein) were resolved by SDS-PAGE and separated proteins were subjected to immunoblotting (IB) with the indicated antibodies (*credit: Sabin Shrestha*, n=2). **B:** As in A, except that Flp-In T-REx U2OS cells were used and the GFP tag was inserted at the C-terminus of the *FAM83* genes. FAM83B-GFP expression could not be detected in U2OS cells. Unconjugated GFP was used as a control (*credit: Tim Cummins,* n=2).

the UniProt database. Each FAM83 protein was correctly identified within each sample, and some known interactors were also found. These included SMAD isoforms in FAM83G immunoprecipitates (Vogt et al., 2014), and HMMR and DYNLL1 in FAM83D immunoprecipitates (Dunsch et al., 2012). Under these conditions, common FAM83 interacting proteins that did not depend on the cell line used or position of the GFP tag were screened. This approach resulted in the surprising identification of isoforms of the casein kinase 1 (CK1) family of Ser/Thr protein kinases as putative FAM83 interacting

CK1 isoforms identified by mass-spectrometry in FAM83 IPs

HEK 293 Top 3 precursor ion intensities (x 10^7)

GFP-FAM83	A	B	C	D	E	F	G	H	GFP
CK1α	185	828	211	99	662	283	1380	144	10
CK1α-like	143	787	176	76	501	232	1060	118	8
CK1δ	127	412	46	7	381	5	16	117	8
CK1ε	127	412	46	8	389	5	19	118	9

U2OS Top 3 precursor ion intensities (x 10^7)

FAM83-GFP	A	B	C	D	E	F	G	H	GFP
CK1α	101	N/A	36	84	709	902	905	234	1
CK1α-like	100	N/A	0	0	668	833	817	0	0
CK1δ	78	N/A	18	13	468	4	9	198	1
CK1ε	99	N/A	28	19	599	5	11	198	2

Table 3-1: Mass fingerprinting identifies CK1 isoforms as putative FAM83-interacting proteins: Mass fingerprinting of protein interactors of N-terminal (HEK 293 cells) or C-terminal (U2OS cells) GFP-tagged FAM83A-H proteins identified one or more CK1α, α-like, δ and ε isoforms. Included in the tables are values of the top 3 precursor ion intensities for the indicated CK1 isoforms identified in each GFP-FAM83A-H (HEK 293) and FAM83A-H-GFP (U2OS), and control GFP pull-down obtained using Scaffold Q/Q+S V4.4.6 (HEK 293 cells) and V4.3 (U2OS cells) analysis of the LC-MS-MS data. Note: FAM83B-GFP did not express in U2OS cells (*credit: Tim Cummins and Gopal Sapkota*, n=1).

partners. Analysis of the top three precursor ion intensities of the individual identified CK1 isoforms found within the HEK 293 samples revealed that, whilst all GFP-FAM83 proteins interacted with CK1α and α-like isoforms, GFP-FAM83A, B, E, and H also interacted with CK1δ and ε (Table 3-1). Similar patterns in spectral intensities were observed for CK1α, δ and ε isoforms, bound to FAM83-GFP proteins within the U2OS cell extracts, however CK1α-like was not detected in FAM83C, D or H immunoprecipitations (Table 3-1). Thus, these data suggested that FAM83 proteins may interact with CK1 isoforms in cells, and that there may be some selectivity with regard to which CK1 isoforms can bind each FAM83 member.

Regarded as promiscuous, constitutively-active protein kinases (Knippschild et al., 2005a, Schittek & Sinnberg, 2014, Venerando et al., 2014), the regulation of CK1 isoforms in cells is critically important, yet poorly understood. Interacting proteins that are capable of regulating CK1 isoforms, in terms of modulating their localisation within the cell, their access to substrates, their stability and/or catalytic activity, remain elusive. That said, two scaffold proteins, the centrosomal and Golgi N-kinase anchoring protein (CG-NAP) (Sillibourne et al., 2002), and the DEAD-box RNA helicase DDX3 (Cruciat et al., 2013), have been reported to regulate the centrosomal localisation of CK1δ, and the phosphorylation of Dvl by CK1ε, respectively. The potential existence of regulatory CK1-interacting proteins is supported by the analogous role of the A-kinase anchoring proteins (AKAPs). AKAPs are well-established protein scaffolds that act to control the activity, localisation, and substrate specificity of protein kinase A (PKA), through direct association (Hoshi, Langeberg et al., 2005). Thus, I postulated that FAM83 proteins, if they do indeed interact with CK1 isoforms in cells, may act to regulate the constitutively-active CK1 kinases through one or more of these potential mechanisms.

3.2: Results

3.2.1: FAM83 members interact with CK1 isoforms:

To verify the putative interactions between FAM83 proteins and CK1 isoforms, GFP-FAM83A-H and control free GFP immunoprecipitates from HEK 293 extracts were probed for co-immunoprecipitation of endogenous CK1α, δ and ε isoforms. In agreement with the proteomic data described above (Table 3-1), CK1α was found in the eluates of all GFP-FAM83 precipitations but, critically, was not found in the eluate of the

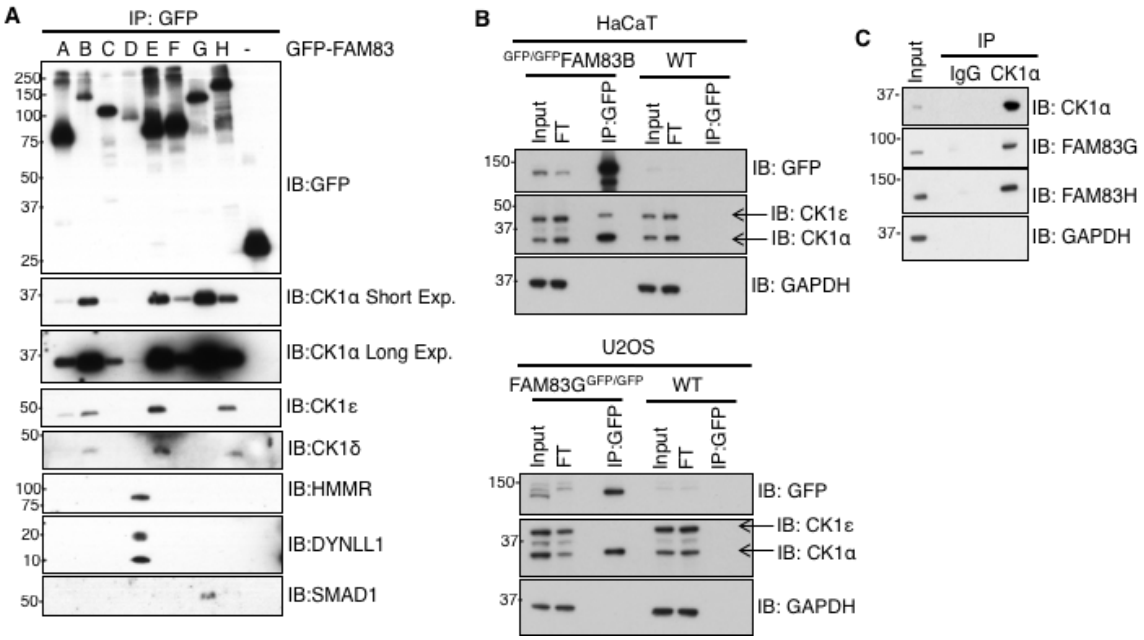

Figure 3-2: FAM83 proteins interact with CK1 isoforms: A: Anti-GFP immunoprecipitations (IP) of GFP control or GFP-FAM83A-H proteins expressed in Flp-In T-REx HEK 293 cells, resolved by SDS-PAGE, were subjected to immunoblotting (IB) with antibodies against the indicated CK1 isoforms and other interacting proteins (n=3). **B: Top panel:** Wild-type (WT) HaCaT or GFP-FAM83B knockin (*GFP/GFPFAM83B*) HaCaT cells were lysed and extracts (5 mg protein) were subjected to IP with anti-GFP beads. IPs, Input extracts (20 μg), and post-IP flow through (FT) extracts (20 μg), were resolved by SDS-PAGE, before being subjected to IB with the indicated antibodies (n=3). **Lower panel:** As in Top panel, except that wild type (WT) U2OS and FAM83G-GFP knockin (*FAM83GGFP/GFP*) U2OS cells were employed (n=3). **C:** WT U2OS extracts (1 mg protein) were subjected to IPs using either pre-immune IgG or an anti-CK1α antibody coupled to Protein-G sepharose beads. Input extracts (20 μg) and IPs were resolved by SDS-PAGE, and subjected to IB with the indicated antibodies (*credit: Polyxeni Bozatzi,* n=3).

GFP control (Figure 3-2A). The interaction of GFP-FAM83B, E, G and H with CK1α appeared stronger than that of GFP-FAM83A, C, D and F (Figure 3-2A). CK1δ and ε were more selective in their choice of GFP-FAM83 binding partner, with endogenous CK1δ and ε found only in GFP-FAM83A, B, E and H immunoprecipitates (Figure 3-2A), consistent with the proteomic data (Table 3-1). Concomitantly, endogenous SMAD1 was

only found in GFP-FAM83G eluates, whereas HMMR and DYNLL1 co-precipitated exclusively with GFP-FAM83D (Figure 3-2A).

Next, I sought to verify the FAM83-CK1 interactions at more endogenous levels. In the absence of robust immunoprecipitating antibodies recognising FAM83 proteins, I turned to CRISPR/Cas9-engineered cell lines, previously generated within the lab. These were human HaCaT keratinocytes in which a GFP knockin tag was introduced at the N-terminus of *FAM83B* (generated by Gopal Sapkota), and U2OS cells in which the GFP was knocked into the C-terminus of *FAM83G* (generated by Polyxeni Bozatzi). Lysates from these cells were subjected to anti-GFP immunoprecipitations. Whereas endogenous CK1α was found in the eluates of both GFP-FAM83B and FAM83G-GFP, CK1ε was only evident in the precipitates of GFP-FAM83B (Figure 3-2B), consistent with the over-expression data (Figure 3-2A). In agreement, in the reciprocal experiment in which endogenous CK1α was immunoprecipitated from U2OS cell extracts, FAM83G and H could be detected in the eluate (Figure 3-2C). Importantly, no FAM83G or H were found in the pre-immune IgG control precipitate (Figure 3-2C).

Given that all eight FAM83 members contain the DUF1669 domain within their N-termini, and that the C-termini are not conserved between FAM83 proteins (Figure 1-12), it seemed reasonable that the apparently common interaction between FAM83 proteins and CK1 isoforms might take place via the conserved DUF1669 region of FAM83 proteins. In order to map the minimal domain within FAM83 proteins that can bind CK1 isoforms, Myc-tagged FAM83G fragments were co-expressed with hemagglutinin (HA)-tagged CK1α in *FAM83G* knockout U2OS cells, and coimmunoprecipitation experiments were performed (Figure 3-3A). HA-CK1α immunoprecipitates harboured only those Myc-FAM83G fragments that contained residues 165-307 within the DUF1669 domain (Figure 3-3A). Next, to test if the DUF1669-CK1 interaction was direct, an *in vitro* binding

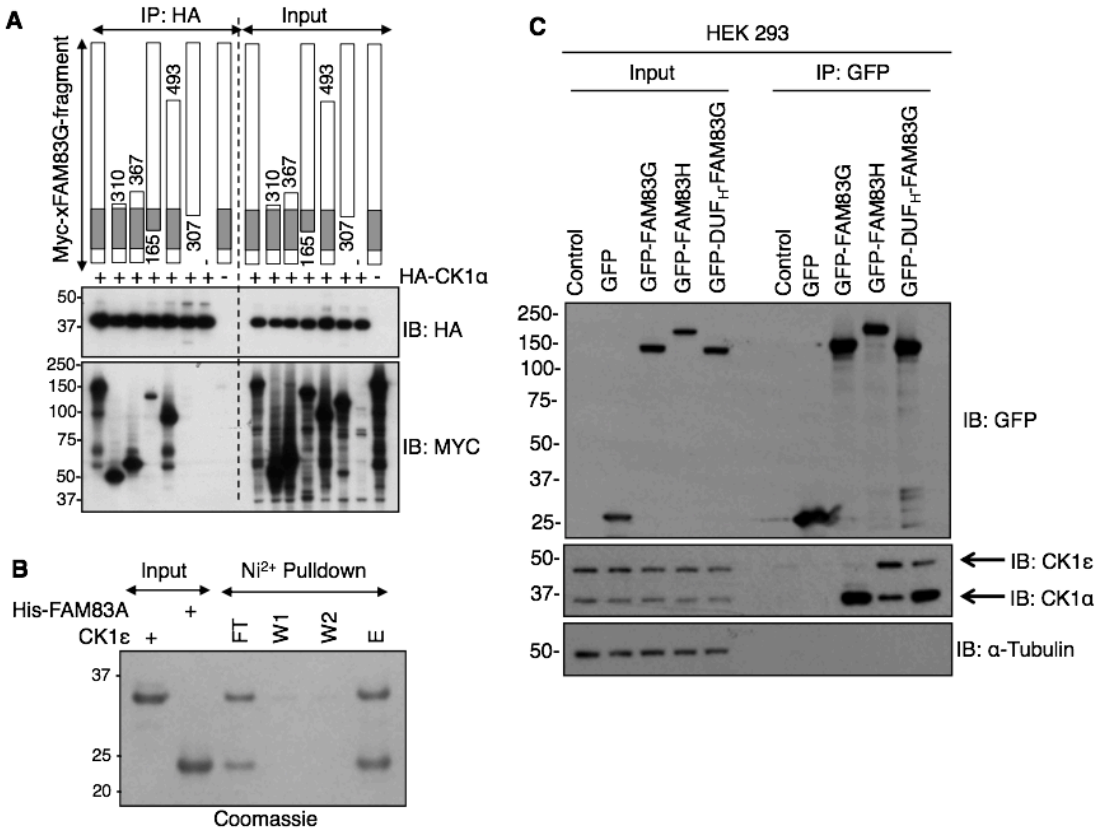

Figure 3-3: The DUF1669 of FAM83 members is sufficient in mediating the interaction with CK1 isoforms: A: The indicated fragments of Myc-tagged *Xenopus* FAM83G (xFAM83G) were co-expressed with HA-CK1α in *FAM83G* knockout U2OS cells for 48 h. Anti-HA immunoprecipitates (IP) or whole-cell extracts (Input) were subjected to immunoblotting (IB) with anti-myc and anti-HA antibodies as indicated (*credit: Polyxeni Bozatzi,* n=3). **B:** Ni-sepharose agarose resin was loaded with 6xHis-FAM83A(122-304) fragments and used to pull down the CK1ε kinase domain (a.a. 1-294). Resin was washed twice with buffer containing 5 mM imidazole before elution with 250 mM imidazole. The Input, flow through (FT), washes (W1 and W2) and eluate (E) were analysed by SDS-PAGE, and staining the gel with Coomassie blue (*credit: Daniel Pinkas, Joshua Bufton, and Alex Bullock,* n=3). **C:** The GFP-FAM83G DUF1669 domain, which interacts with CK1α only, was switched with the DUF1669 domain of GFP-FAM83H, which interacts with both CK1α and CK1ε. U2OS cells were transfected with this chimera (GFP-DUF$_H$-FAM83G) or wild type GFP-tagged FAM83 constructs. Input extracts and GFP-IPs were resolved by SDS-PAGE, and subjected to IB with the indicated antibodies (n=3).

assay between the kinase domain of CK1ε and a purified recombinant His-tagged FAM83A fragment incorporating residues 124-304 was performed. Following nickel-

purification of His-FAM83A(124-304) and its subsequent elution with imidazole, both the FAM83A fragment and the CK1ε kinase domain were evident in the eluate, suggesting a direct association (Figure 3-3B).

To probe the isoform-specific nature of the FAM83-CK1 interaction, the DUF1669 domain of FAM83G, a CK1α-specific interactor, was switched with the DUF1669 domain of FAM83H, which interacts with both CK1α and ε. This chimeric protein (GFP-DUF1669$_{FAM83H}$-FAM83G) was expressed in HEK 293 cells, and subjected to anti-GFP immunoprecipitation. Strikingly, the GFP-DUF1669$_{FAM83H}$-FAM83G chimera interacted with both CK1α and ε, much like the wild-type GFP-FAM83H protein (Figure 3-3C). Collectively, these results suggest that the DUF1669 domain of FAM83 proteins is sufficient to confer selectivity towards specific CK1 isoforms.

A CK1 docking motif, comprised of the amino acid sequence F-X-X-X-F, was identified in some CK1 interacting proteins, namely nuclear factor of activated T cells 1 (NFAT1), Period 1 (PER1) and PER2 (Okamura et al., 2004). Mutation of either phenylalanine residue within the F-X-X-X-F motif abolished the interaction between CK1 and these proteins (Okamura et al., 2004). One such F-X-X-X-F motif is also present within the DUF1669 domain of every FAM83 protein, and is evolutionarily conserved. Interestingly, whereas FAM83A-G have just one F-X-X-X-F motif, FAM83H harbours four such motifs. Thus, whether mutations within the F-X-X-X-F motif of FAM83 proteins would be sufficient to disrupt their interaction with CK1 isoforms was tested. FLAG-tagged wild-type and various mutant forms of FAM83G [FAM83G(F296A), FAM83G(F300A), FAM83G(F296A, F300A)] were co-expressed with HA-CK1α, and screened for their ability to bind immunoprecipitated HA-CK1α. Whereas wild-type FLAG-FAM83G interacted robustly with HA-CK1α, the FLAG-FAM83G(F296A) and FLAG-

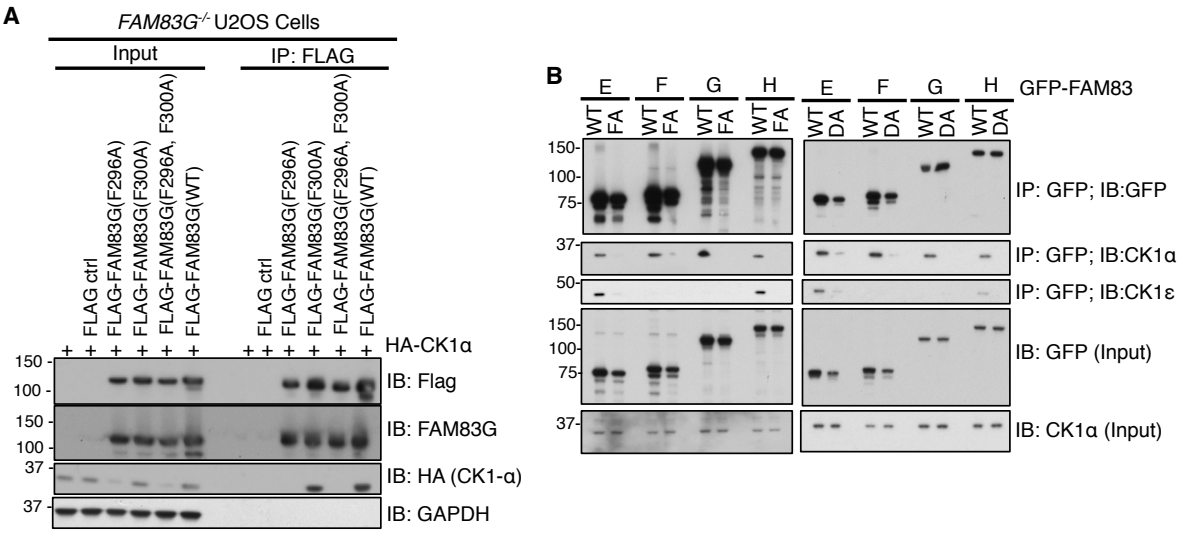

Figure 3-4: Two conserved residues within the DUF1669 mediates CK1 binding: A: Control Flag empty vector or the indicated FLAG-tagged FAM83G mutants were overexpressed in *FAM83G*$^{-/-}$ U2OS cells**.** Anti-FLAG immunoprecipitates (IP) or whole-cell extracts (Input) were subjected to immunoblotting (IB) with anti-FLAG and anti-CK1α antibodies as indicated (*credit: Polyxeni Bozatzi,* n=3). **B.** Wild-type (WT), FA and DA mutants of GFP-FAM83E-H were transiently expressed in U2OS cells. Input extracts and GFP-trap IPs were resolved by SDS-PAGE, and subjected to IB using the indicated antibodies (n=3).

FAM83G(F296A,F300A) mutants did not (Figure 3-4A). Somewhat surprisingly, the FLAG-FAM83G(F300A) mutant still interacted robustly with HA-CK1α (Figure 3-4A), suggesting that the mode in which FAM83 members interact with CK1 isoforms might be different to that of the NFAT1, PER1 and PER2, which required both phenylalanine residues to be intact. Consistent with this idea, mutational scanning of conserved residues within the 165-307 amino acid region of FAM83G uncovered another mutation, D262A, that also disrupted the interaction between FAM83G and CK1α (Figure 3-4A).

Armed with the knowledge that the FAM83G D262A and F296A mutations both abolish the FAM83G-CK1α interaction, it was speculated that mutation of the equivalent residues within other FAM83 members might also disrupt their association with CK1α. The analogous residues to FAM83G D262 and F296 were mutated in FAM83E (D243 and F277), FAM83F (D250 and F284), and FAM83H (D236 and F270) to alanine, and these

constructs were expressed in U2OS cells with an N-terminal GFP tag, in parallel with the respective wild-type GFP-FAM83 member as a control. Hereafter, these aspartate and phenylalanine mutants are referred to as DA and FA respectively. Extracts from wild-type, DA and FA GFP-FAM83E-H were subjected to anti-GFP immunoprecipitations, and probed for their ability to bind endogenous CK1α or ε isoforms. In comparison to wild-type GFP-FAM83E-H, both the DA and FA mutations attenuated the interactions between FAM83E-H and CK1α and ε (Figure 3-4B). Consistent with previous observations, although GFP-FAM83E and H bound to both CK1α and ε, GFP-FAM83F and G only bound to CK1α (Figure 3-4B).

Collectively, these observations suggest that the interaction between CK1 isoforms and the DUF1669 domain of FAM83 proteins may be mediated through a conserved structural motif surrounding the residues equivalent to D262 and F296 in FAM83G.

3.2.2: FAM83 proteins co-localise with CK1α in cells:

Given the observed interactions between all of the FAM83 members and CK1α in cell extracts, I sought to explore whether FAM83 proteins also interact with CK1α in cells. For this purpose, mCherry-CK1α was co-expressed with each GFP-FAM83 member in U2OS cells, with the expression of GFP-FAM83A-H under the control of the Tet-inducible promoter. Upon induction of GFP-FAM83 expression, overlapping co-localisation between every GFP-FAM83 member and mCherry-CK1α was observed (Figure 3-5A). Interestingly, each GFP-FAM83 protein exhibited a distinct, largely unique, pattern of subcellular localisation. Both GFP-FAM83A and B exhibited pan-cellular staining, with additional perinuclear staining evident for GFP-FAM83A, and plasma

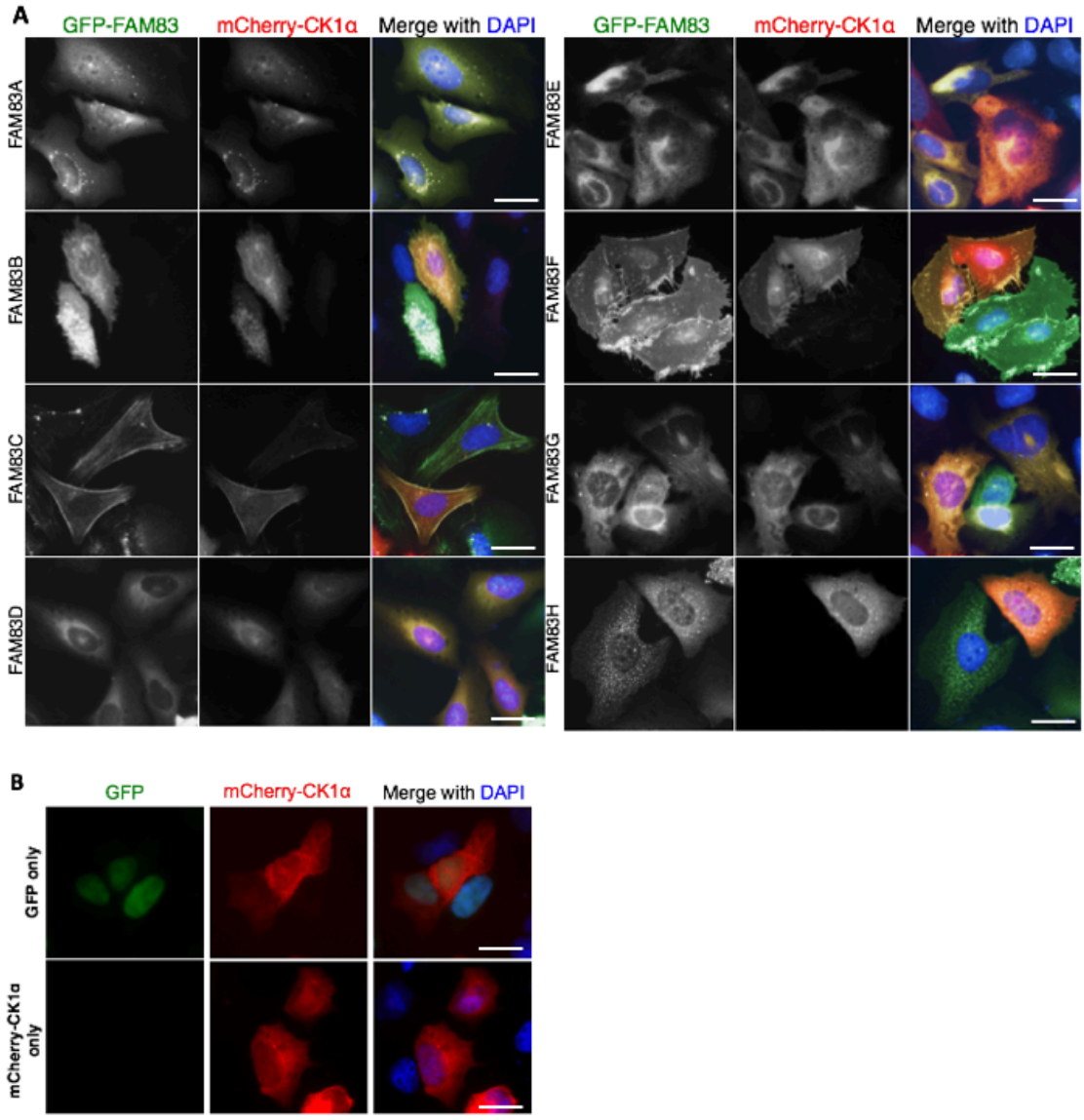

Figure 3-5: FAM83 proteins and mCherry-CK1α co-localise in cells. A: U2OS cells stably integrated with Tet-inducible expression of GFP-FAM83A-H were transfected with mCherry-CK1α. GFP-FAM83A-H expression was induced with doxycycline for 24 h, prior to fixing cells for fluorescence microscopy. Images were taken using a Nikon TiS inverted microscope. Images were processed using NIS Elements (Nikon) and Adobe Photoshop using identical parameters across all the images. The number of cells across 3 independent experiments which displayed identical staining patterns as the representative image were documented for each experiment: GFP-FAM83A (n=50); GFP-FAM83B (n=31); GFP-FAM83C (n=37); GFP-FAM83D (n=32); GFP-FAM83E (n=55); GFP-FAM83F (n=44); GFP-FAM83G (n=43); GFP-FAM83H (n=32).Scale bars; 20 µM. **B:** As in A. except that U2OS cells stably integrated with Tet-inducible expression of unconjugated GFP, or wild-type U2OS cells, both transfected with mCherry-CK1α, were imaged. Scale bars; 20 µM.

membrane staining for GFP-FAM83B (Figure 3-5A). GFP-FAM83C displayed distinct fibrous patterns of fluorescence, reminiscent of actin cytoskeletal staining (Figure 3-5A). GFP-FAM83D displayed some cytoplasmic staining, with some punctate staining in the nucleus (Figure 3-5A). FAM83D has previously been reported to localise to the spindle apparatus during mitosis (Dunsch et al., 2012, Santamaria et al., 2008) and a detailed investigation into FAM83D is presented later (see chapter 4). GFP-FAM83E was found in the cytoplasm and in the perinuclear region, whereas GFP-FAM83F was most prominently located on the plasma membrane, with some additional staining evident in the cytoplasm and nucleus (Figure 3-5A). In line with previous reports, GFP-FAM83G was diffusely localised within the cytoplasm and nucleus (Figure 3-5A) (Bozatzi et al., 2018, Cummins et al., 2018, Vogt et al., 2014). GFP-FAM83H was found primarily in cytoplasmic punctate structures, although analogous structures were also observed in the nucleus (Figure 3-5A). This GFP-FAM83H localisation pattern is consistent with that reported for FLAG-FAM83H overexpressed in HCT116 cells (Kuga et al., 2016a, Kuga et al., 2013). As a control, free, unfused GFP was co-expressed with mCherry-CK1α in U2OS cells. Under these conditions, the GFP signal was predominantly nuclear, and did not overlap with the mCherry-CK1 α signal, which was present throughout the cell (Figure 3-5B). When expressed on its own, mCherry-CK1α was also found throughout the cells (Figure 3-5B).

Given the potential caveats of exploring co-localisation between two over-expressed proteins, I next sought to confirm whether endogenous CK1α also displayed similar overlapping subcellular distributions with certain GFP-FAM83 members. For this purpose, I chose GFP-FAM83B, F and H, due to their distinct and pronounced localisation patterns (Figure 3-5A). Overlapping plasma membrane and perinuclear staining was observed between GFP-FAM83B and CK1α (Figure 3-6). Likewise, GFP-FAM8F and CK1α

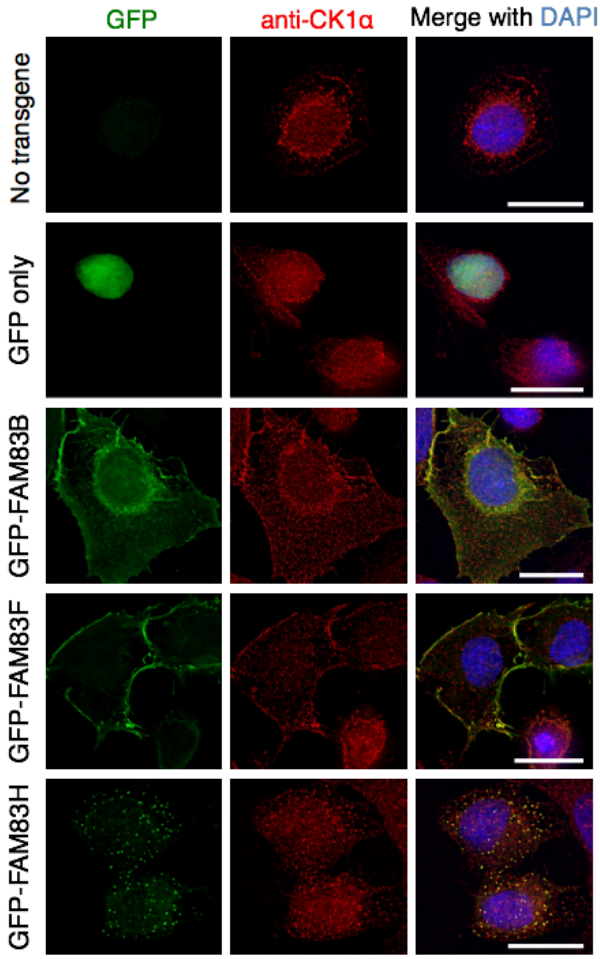

Figure 3-6: FAM83 proteins and endogenous CK1α co-localise in cells: U2OS cells stably integrated with Tet-inducible expression of unconjugated GFP (negative control) or GFP-FAM83B, F or H were treated with doxycycline for 16 h, prior to fixing cells for fluorescence microscopy. Following fixation, cells were stained with an anti-CK1α antibody to enable visualisation of endogenous CK1α. Images were taken using a DeltaVision widefield fluorescence microscope and deconvolved using SoftWoRx. The number of cells across 3 independent experiments which displayed identical staining patterns as the representative image were documented for each experiment: GFP-FAM83B (n=56); GFP-FAM83F (n=60); GFP-FAM83H (n=48); GFP only (n=38); CK1α only (n=82). Scale bars; 20 µm (*credit: Kevin Wu*).

exhibited overlapping fluorescence at the plasma membrane, and GFP-FAM83H co-localised with CK1α on the cytoplasmic and nuclear puncta (Figure 3-6). No overlapping

fluorescence was detected between endogenous CK1α and free GFP, which was employed as a negative control (Figure 3-6).

As a whole, these observations suggest that upon overexpression, each FAM83 protein is capable of promoting a change in the localisation of endogenous CK1α, so that CK1α is relocated to the distinct subcellular compartments in which the FAM83 member in question resides.

3.2.3: The association between FAM83 proteins and specific CK1 isoforms is selective in cells:

The above data demonstrates co-localisation between GFP-FAM83 proteins and CK1α. However, FAM83A, B, E and H also interact with CK1δ and ε isoforms in cell extracts (Figure 3-2A). Thus, I sought to test whether this selectivity in the interactions between certain FAM83 members and CK1 isoforms persists in cells. I compared the subcellular distributions of mCherry-CK1α and mCherry-CK1ε with GFP-FAM83F, a selective CK1α-interacting protein, and GFP-FAM83H, which interacts with both CK1α and ε, in U2OS cells. As observed earlier, overlapping fluorescence was detected between both GFP-FAM83F and H, and mCherry-CK1α, at the plasma membrane and cytoplasmic puncta, respectively (Figure 3-7A). In contrast, GFP-FAM83H, but not GFP-FAM83F, appeared to co-localise with mCherry-CK1ε, at these cellular sites (Figure 3-7A).

To verify if this binding specificity of GFP-FAM83F and H extended to endogenous CK1α and ε, the experiment was repeated with endogenous CK1α and ε staining. In wild-type U2OS cells, endogenous CK1α and ε both exhibited pan-cellular staining (Figure 3-7B). Consistent with the mCherry-CK1α and ε overexpression data above (Figure 3-7A), endogenous CK1α co-localised with GFP-FAM83F on the plasma membrane, whereas

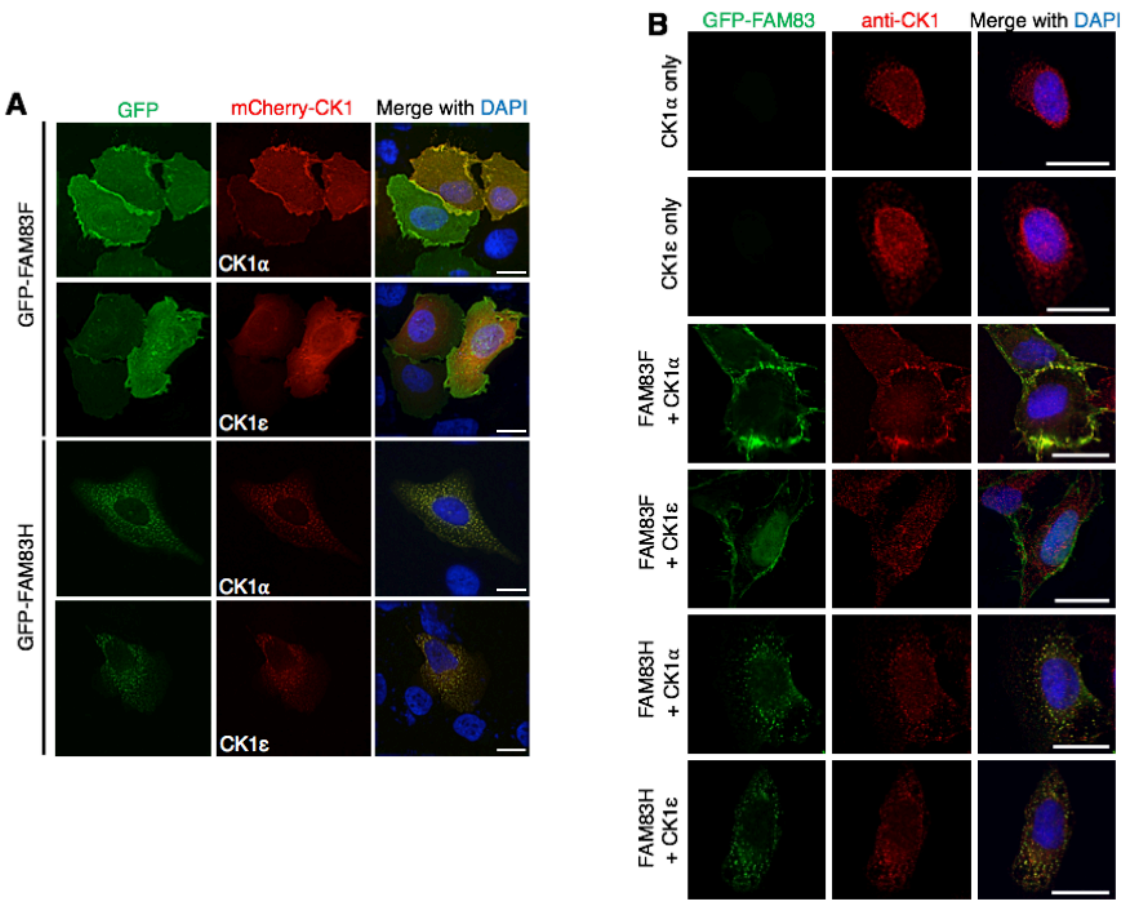

Figure 3-7: The association between FAM83 proteins and specific CK1 isoforms is selective in cells: A: U2OS cells stably integrated with Tet-inducible expression of GFP-FAM83F or GFP-FAM83H were transfected with either mCherry-CK1α or mCherry-CK1ε. GFP-FAM83F and GFP-FAM83H expression was induced with doxycycline for 24 h, prior to fixing cells for fluorescence microscopy. Images were taken using a DeltaVision widefield fluorescence microscope and deconvolved using SoftWoRx. The number of cells across 3 independent experiments which displayed identical staining patterns to the representative image were documented for each experiment: GFP-FAM83F + mCherry-CK1α (n=44); GFP-FAM83F + mCherry-CK1ε (n=40); GFP-FAM83H + mcherry-CK1α (n=32); GFP-FAM83H + mCherry-CK1ε (n=40). Scale bars; 20 µm (*credit: Kevin Wu*). **B.** U2OS cells stably integrated with Tet-inducible expression of GFP-FAM83F or H were induced with doxycycline for 16 h, prior to fixing cells for fluorescence microscopy. Cells were stained with anti-CK1α or CK1ε to visualise endogenous CK1α and CK1ε respectively. Untransfected cells stained with anti-CK1α or CK1ε were used as negative controls. Images were taken using a DeltaVision widefield fluorescence microscope and deconvolved using SoftWoRx. The number of cells across 3 independent experiments that displayed identical staining patterns to the representative image were documented for each experiment: GFP-FAM83F+CK1α (n=60); GFP-FAM83F+CK1ε (n=43); GFP-FAM83H+CK1α (n=48); GFP-FAM83H+CK1ε (n=35); CK1α only (n=82); CK1ε only (n=27). Scale bars; 20 µm (*credit: Kevin Wu*).

endogenous CK1ε did not (Figure 3-7B). In contrast, both endogenous CK1α and ε co-localised with GFP-FAM83H on the cytoplasmic punctate structures (Figure 3-7B).

Collectively, these data recapitulate the distinct sets of interactions between FAM83 members and CK1 isoforms detected in extracts, within the cellular environment.

3.2.4: Association with CK1 determines the subcellular localisation of FAM83 proteins:

Next, I asked whether the interaction between CK1 and FAM83 proteins was important for their subcellular localisations. To this end, I chose GFP-FAM83C because of its distinct localisation on the actin-like fibers (Figure 3-5A). Having confirmed that only wild-type GFP-FAM83C coimmunoprecipitated HA-CK1α, and that GFP-FAM83C(D259A), GFP-FAM83C(F293A), and free GFP did not (Figure 3-8A), U2OS cells expressing these FAM83C constructs were subjected to fluorescence microscopy, with co-expressed mCherry-CK1α. Whereas GFP-FAM83C and mCherry-CK1α co-localised along the actin-like filaments, both GFP-FAM83C(D259A) and GFP-FAM83C(F293A)were predominantly found within the cytoplasm, in slightly distorted fibrous patterns, that did not overlap with mCherry-CK1α fluorescence (Figure 3-8B). These observations suggest that the interaction between FAM83C and CK1α is important in determining the subcellular localisation of both proteins. However, these experiments suffer from the possibility that the endogenous FAM83C protein, which is still present in the cells, may be influencing the association between the overexpressed GFP-FAM83C proteins and CK1α. Thus, I sought to examine the role of FAM83-CK1 interactions in determining subcellular localisation of each protein, in a more refined model.

Having shown that FAM83H localises to distinct cytoplasmic punctate structures when over-expressed in U2OS cells (Figure 3-5A), *FAM83H* knockout U2OS cells were generated by Tim Cummins using CRISPR/Cas9, and either wild-type, FA or DA GFP-

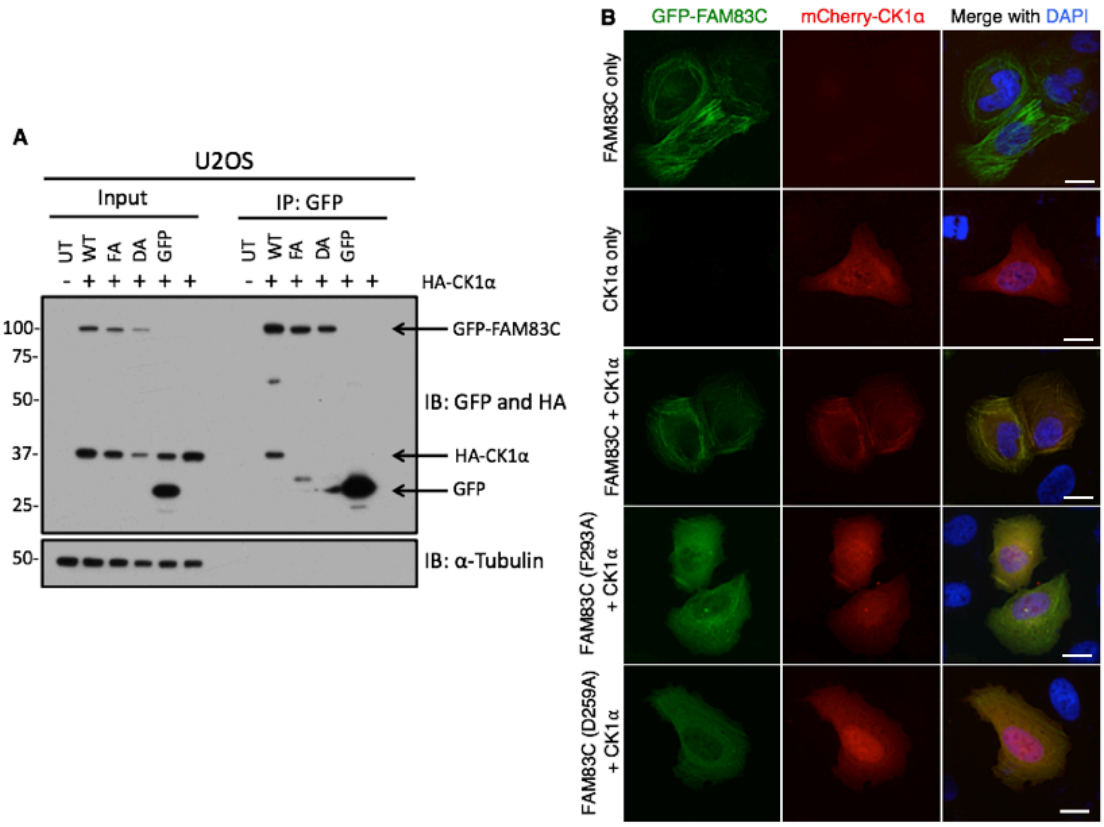

Figure 3-8: The subcellular localisation of FAM83C is determined by its association with CK1α: A: U2OS cells were co-transfected with plasmids encoding either unconjugated GFP, wild-type GFP-FAM83C (WT), GFP-FAM83C-F293A (FA) or GFP-FAM83C-D259A (DA), and HA-CK1α as indicated. Untransfected and HA-CK1α only transfected cells were included as controls. Input extracts and anti-GFP immunoprecipitates (IP) were resolved by SDS-PAGE, and subjected to immunoblotting (IB) with the indicated antibodies (n=3). **B:** U2OS cells were transfected with plasmids encoding either wild-type GFP-FAM83C, GFP-FAM83C-F293A or GFP-FAM83C-D259A together with mCherry-CK1α as indicated. Representative images from cells expressing GFP-FAM83C or mCherry-CK1α alone are also included. 24 h-post transfection, cells were fixed and processed for fluorescence microscopy. Images were taken using a DeltaVision widefield fluorescence microscope and deconvolved using SoftWoRx. The number of cells across 3 independent experiments that displayed identical staining patterns to the representative image were documented for each experiment: GFP-FAM83C only (n=46); GFP-FAM83C + mCherry-CK1α (n=44); GFP-FAM83C(F293A) + mCherry-CK1α (n=41); GFP-FAM83C(D259A) + mCherry-CK1α (n=43); mCherry-CK1α only (n=45). Scale bars; 20 µm (*credit: Kevin Wu*).

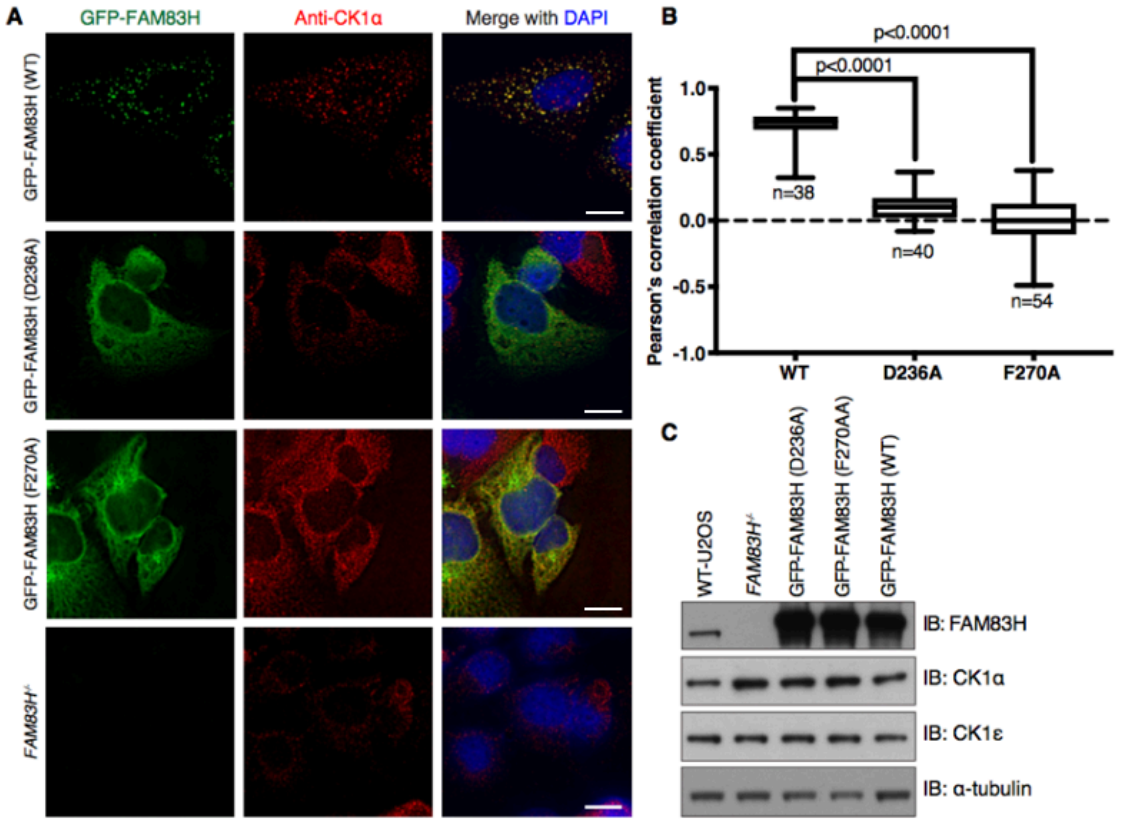

Figure 3-9: FAM83H co-localises with, and in part determines the subcellular localisation of, endogenous CK1α: A: *FAM83H*$^{-/-}$ U2OS cells were transfected with rescue vectors encoding GFP-FAM83H, GFP-FAM83H(D236A), GFP-FAM83H(F270A) or left Untransfected. Cells were fixed in methanol and stained with anti-CK1α. DNA was stained with DAPI. Representative images from one field of view, representative of 3 independent experiments are included. Scale bars; 10 µm. (*credit: Theresa Tachie-Menson and Graeme Ball*). **B:** The boxplot shows the range, mean, lower and upper quartile of the Pearson's correlation coefficients of GFP-FAM83H and endogenous CK1α within above-background pixels in the cytoplasm. n=3. (*credit: Theresa Tachie-Menson and Graeme Ball*). **C:** Analysis of protein expression of rescue constructs transfected in *FAM83H*$^{-/-}$ U2OS cells, in comparison to wild-type (WT) cells, as indicated by immunoblotting (IB) (*credit: Theresa Tachie-Menson,* n=3).

FAM83H mutants were restored through transient transfections. In *FAM83H* knockout cells, CK1α was primarily cytoplasmic with few perinuclear puncta (Figure 3-9A). When GFP-FAM83H was expressed in the *FAM83H* knockout background, both GFP-FAM83H and endogenous CK1α adopted a pan-cellular punctate pattern with the majority of GFP-FAM83H puncta overlapping with endogenous CK1α staining, suggesting robust co-

localisation (Figure 3-9A). When the CK1-interaction deficient GFP-FAM83H DA and FA mutants were expressed in *FAM83H* knockout cells, they displayed cytoplasmic, non-punctate fluorescence that did not overlap with endogenous CK1α (Figure 3-9A). The intensity of CK1α punctate staining both in *FAM83H* knockout cells, and in *FAM83H* knockout cells expressing the CK1-binding–deficient mutant forms of FAM83H, was lower compared to that seen in cells expressing wild-type GFP-FAM83H (Figure 3-9A), suggesting that the interaction with FAM83H determines the localisation of CK1α to the punctate structures.

Next, the co-localisation correlation between CK1α and wild-type GFP-FAM83H, or the DA and FA GFP-FAM83H mutants was quantified. The localisation of CK1α positively correlated with that of wild-type GFP-FAM83H (Pearson correlation coefficient 0.7523), whereas it did not correlate with the GFP-FAM83H DA (0.001504) or GFP-FAM83H FA (0.001504) mutants (Figure 3-9B). Rescue of *FAM83H* knockout U2OS cells with wild-type or mutant GFP-FAM83H constructs was confirmed by immunoblotting, which suggested that the abundance of FAM83H in these cells was substantially higher than the amount of endogenous FAM83H in wild-type U2OS cells (Figure 3-9C). Consistently, in the FAM83H knockout U2OS cells, endogenous CK1ε displayed similar immunostaining patterns to CK1α and exhibited significant co-localisation correlation with wild-type GFP-FAM83H, but not with the CK1-binding deficient GFP-FAM83H DA or FA mutants (Figure 3-10A&B).

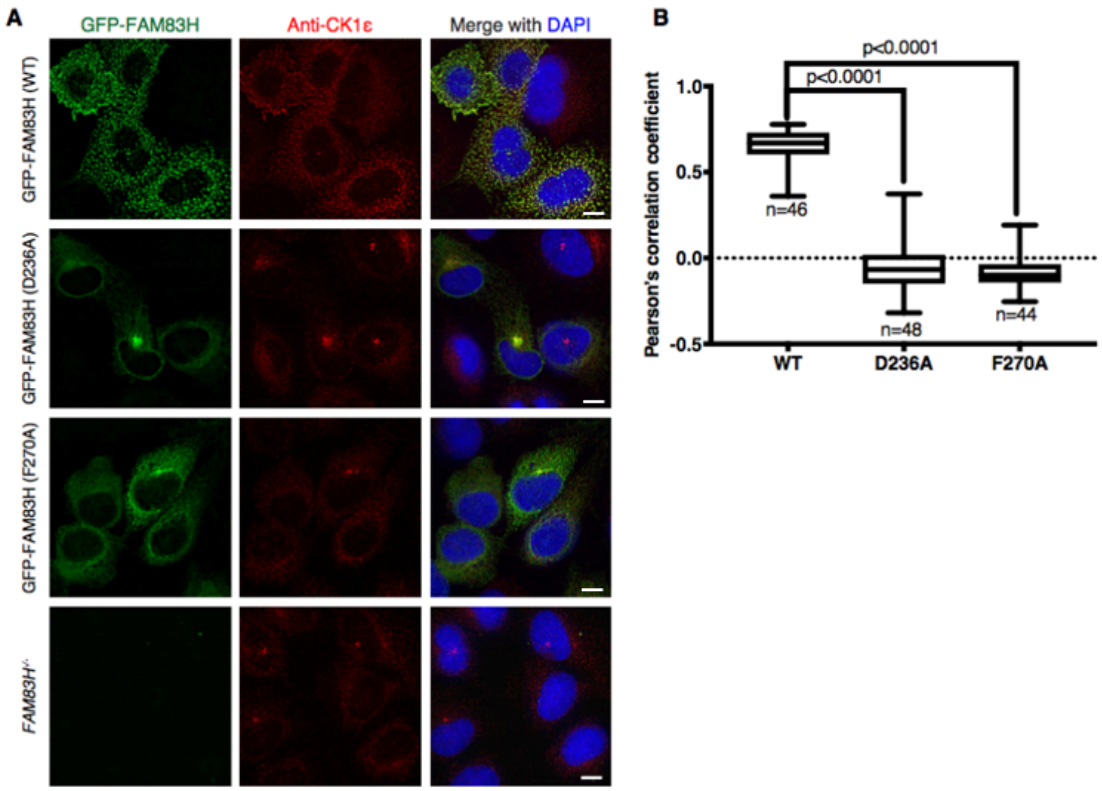

Figure 3-10: FAM83H co-localises with, and in part determines the subcellular localisation of, endogenous CK1ε: A: *FAM83H*$^{-/-}$ U2OS cells were transfected with rescue vectors encoding GFP-FAM83H, GFP-FAM83H-D236A, GFP-FAM83H-F270A, or left Untransfected. Cells were fixed in methanol and stained with anti-CK1ε. DNA was stained with DAPI. Representative images from one field of view, representative of 3 independent experiments are included. Scale bars; 10 µm (*credit: Theresa Tachie-Menson and Graeme Ball*). **B:** The boxplot shows the range, mean, lower and upper quartile of the Pearson's correlation coefficients of GFP-FAM83H and endogenous CK1ε. The boxplot shows the range, mean, lower and upper quartile of the Pearson's correlation coefficients. Data were obtained from three independent experiments (*credit: Theresa Tachie-Menson and Graeme Ball*).

3.2.5: The intrinsic catalytic activity of CK1 is not required for the association of CK1 with FAM83 proteins:

In their capacity as CK1-interacting proteins, it is possible that FAM83 members may by substrates of CK1 isoforms, or act to regulate the intrinsic catalytic activity of

these CK1 kinases. Next, whether CK1α could phosphorylate FAM83 proteins *in vitro* was tested, using purified recombinant FAM83 proteins. Whereas FAM83B, C and G appeared to be robustly phosphorylated by CK1α, the other FAM83 members exhibited poorer phosphorylation (Figure 3-11A). The precise CK1α-dependent phosphorylation sites on most FAM83 proteins have not been mapped, and whether these phosphorylation events occur in cells, and the functional consequences of these phosphorylation events, if any, remain to be investigated. The low activity of CK1α towards some of the FAM83 substrates in this *in vitro* assay may be due to the poor purity of some of these recombinant proteins (Figure 3-11A). Alternatively, lack of detectable phosphorylation might simply reflect lack of a priming phosphorylation event, as the priming kinase is not present in the assay conditions. The optimal CK1 consensus phosphorylation motif is pS/T-X-X-S/T (Knippschild et al., 2005a, Schittek & Sinnberg, 2014), thus lack of this priming phospho-Ser/Thr may render some of the FAM83 members unphosphorylatable by CK1. Previous work in the lab mapped the CK1α-dependent phosphorylation site on FAM83G to be S614 *in vitro*, but this phosphorylation event did not impact FAM83G function in Wnt signalling, which requires its association with CK1α (Bozatzi et al., 2018). Thus, the exact role and relevance of CK1-dependent FAM83 phosphorylation remains to be further defined.

Next, in order to examine whether the intrinsic catalytic activity of CK1α was affected by its association with FAM83 proteins, an *in vitro* CK1α kinase assay with increasing concentrations of an optimised CK1 peptide substrate (CK1tide) was performed, and whether addition of equimolar amounts of either wild-type FAM83G, or

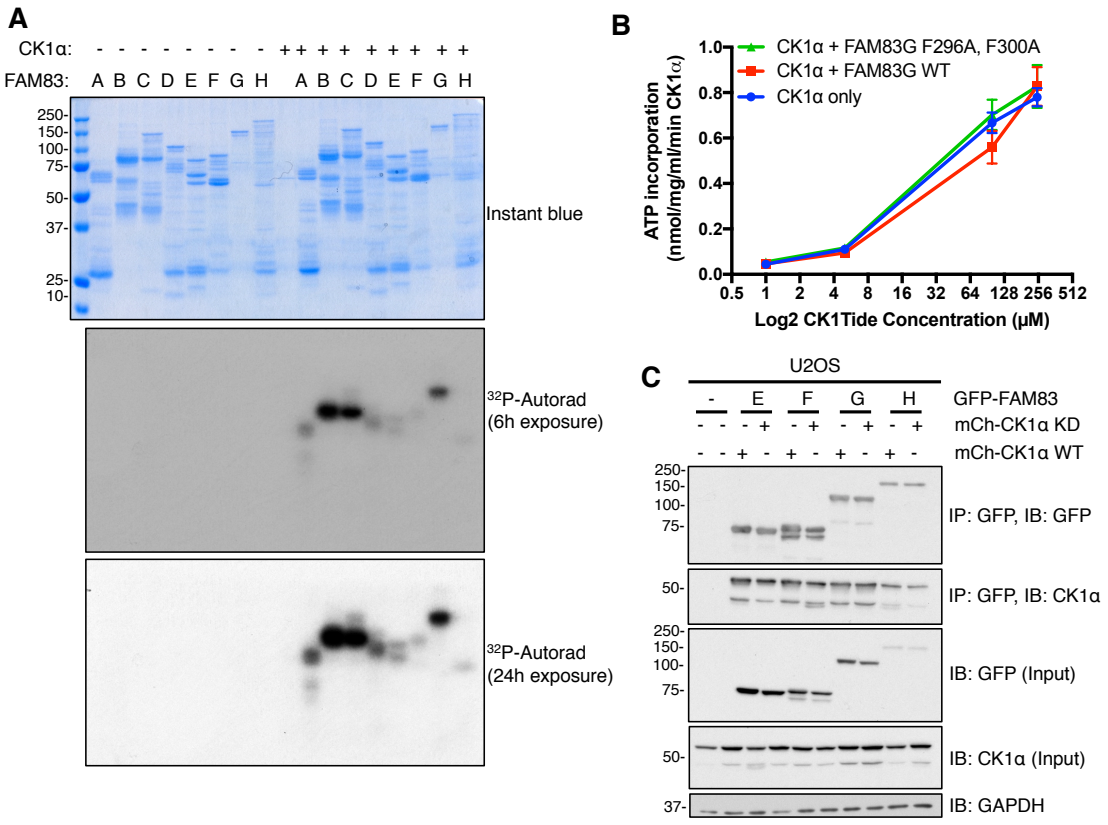

Figure 3-11: Dissecting the links between intrinsic CK1 catalytic activity and the FAM83-CK1 interaction: A: An *in vitro* kinase assay was set up using 200 ng of GST-CK1α, 2 µg of substrate (GST-FAM83A, C, D, E, F, or H, MBP-FAM83B, or GST-FAM83G-6XHis) and [$^{\gamma 32}$P]-ATP (~500 cpm/pmol). After reactions were stopped, samples were resolved by SDS-PAGE and the gel was stained with InstantBlue, dried and subjected to ^{32}P autoradiography for the indicated times (*credit: Polyxeni Bozatzi and Karen Dunbar,* n=3). **B:** An *in vitro* kinase assay was set up with 50 ng of GST-CK1α and increasing amounts of CK1tide as indicated. The effects adding of equimolar amounts of wild-type (WT) GST-FAM83G-6xHis or the CK1 interaction-deficient GST-FAM83G(F296A,F300A) mutant on intrinsic CK1α activity were evaluated. Data points represent the average from 3 independent experiments, each containing 3 technical replicates. Error bars represent SEM. **C:** U2OS cells were transiently co-transfected with GFP-FAM83E-H and either mCherry-tagged WT CK1α or a catalytically inactive [kinase dead (KD)] mutant [CK1α(N141A)]. Following transfection, cells were lysed and extracts subjected to anti-GFP immunoprecipitation (IP). Input and IP samples were resolved by SDS-PAGE, and subjected to immunoblotting (IB) with the indicated antibodies (n=3).

CK1-interaction-deficient FAM83G(F296A, F300A), altered the rate of CK1α catalysis or its Michaelis constant (Km) towards the CK1tide substrate was tested. Under these conditions, the addition of either wild-type FAM83G or mutant FAM83G(F296A, F300A) did not appear to significantly affect the intrinsic kinase kinetics of CK1α, at all CK1tide concentrations tested (Figure 3-11B).

Finally, I assessed whether the kinase activity of CK1α was required for its interaction with FAM83 proteins. For this purpose, GFP-FAM83E, F, G or H were transiently co-expressed with either mCherry-tagged wild-type CK1α, or an mCherry-tagged CK1α catalytic inactive mutant CK1α(N141A) in U2OS cells, and coimmunoprecipitation experiments were performed. Equal amounts of both the wild-type and kinase-dead CK1α mutant were detected in the immunoprecipitates of GFP-FAM83E-H, suggesting that CK1α kinase activity is dispensable for the interaction with FAM83 proteins (Figure 3-11C).

3.3: Conclusions:

CK1 isoforms are known to regulate a myriad of cellular processes (Del Valle-Perez et al., 2011, Knippschild et al., 2005a, Venerando et al., 2014), yet how they are capable of achieving such a feat remains poorly defined. The identification of FAM83 proteins as CK1-anchoring proteins may present one avenue of regulating the constitutively-active CK1 kinases in mammalian cells. These findings suggest that the DUF1669 of FAM83 proteins anchor CK1α, δ and ε isoforms to distinct cellular compartments, and in doing so, FAM83 members place themselves in an ideal position to regulate CK1 isoforms by a number of potential routes. One possibility is that, through sheer control of CK1 localisation, CK1 is physically unable to phosphorylate certain

substrates as they are not available within that cellular compartment. Alternatively, other proteins bound to FAM83 members might be optimally presented to CK1 as substrates, and in that capacity FAM83 proteins can act as signalosome assembly platforms. At least for FAM83G, it seems unlikely that direct binding of FAM83G to CK1α acts to allosterically activate or inhibit the intrinsic CK1α catalytic activity, although this will have to be assessed on a case-by-case basis for each FAM83 member.

The way in which FAM83 proteins can bind and direct CK1 isoforms to specific cellular sites is reminiscent of the AKAPs that serve to regulate PKA (Hoshi et al., 2005). Unlike AKAPs, which bind to the regulatory domain of PKA, the DUF1669 of FAM83 proteins appears to interact directly with the kinase domain of CK1 isoforms. There are many other examples of the crucial roles that scaffolding and anchoring proteins play in organising and streamlining signal transduction in cells. Of note, targeting protein for Xklp2 (TPX2) is a scaffold protein that recruits Aurora kinase A to the mitotic spindle, and also serves as an allosteric activator of the kinase (Bayliss et al., 2003, Chen et al., 2014).

Precisely how FAM83 members affect the diverse functions of CK1 isoforms in cells is largely unclear. However, some of the influences FAM83 members have on regulating CK1 functions are beginning to be uncovered. Previous work in the lab has established that FAM83G is a critical regulator of Wnt signalling in both human cells and *Xenopus* embryos, and its over-expression in *Xenopus* embryos leads to hyperactivation of Wnt signalling, and the subsequent formation of a secondary body axis (Bozatzi et al., 2018). Whereas wild-type FAM83G over-expression drives Wnt signalling, two FAM83G mutants incapable of binding CK1α are unable to activate Wnt signalling, or induce axis duplication in *Xenopus* embryos, thus highlighting the key role the FAM83G-CK1α plays in correct development (Bozatzi et al., 2018). Future efforts aimed at establishing the

roles that other FAM83-CK1 interactions have in biology, both at the process and molecular levels, will shed light on how and where these FAM83-CK1 complexes act.

Given the involvement of CK1 isoforms in such a wide range of cellular processes, it is perhaps unsurprising that the mis-regulation of CK1 kinases have been linked to diseases such as cancer and neurodegeneration (Knippschild et al., 2005a, Schittek & Sinnberg, 2014). The pleiotropic nature of CK1 within various signalling pathways, combined with poor understanding on how these kinases are regulated, have limited the exploration of CK1 isoforms as potential therapeutic targets. That said, several inhibitors of CK1 have been developed, including CKI-7, IC261, D4476, PF-670462, and PF-4800567 (Table 1-1). However, these compounds lack selectivity towards specific, individual CK1 isoforms, and as such, their use has often prevented the unequivocal identification of individual CK1 isoform-substrate relationships (Badura, Swanson et al., 2007, Behrend et al., 2000, Chijiwa, Hagiwara et al., 1989, Rena, Bain et al., 2004, Walton, Fisher et al., 2009). Even if it were possible to target individual CK1 isoforms, given their involvement in many physiological processes, coupled with their conflicting roles within the same signalling pathways at different stages of signal amplification (Del Valle-Perez et al., 2011, Knippschild et al., 2005a, Schittek & Sinnberg, 2014), pan-cellular inhibition of a CK1 isoform will likely not be beneficial. Thus, targeting distinct CK1-containing complexes, such as those of FAM83 proteins, may present an alternative, more specific means of shutting down selective CK1-dependent processes, without impacting non-related CK1 cellular functions.

4. FAM83D directs CK1α to mitotic spindles for proper spindle positioning:

4.1: Background:

Having identified FAM83 proteins as putative CK1-anchoring proteins in cells, I next sought to test this hypothesis in a focussed way, by exploring the roles of individual FAM83-CK1 interactions in more physiological settings. Whilst the function of the FAM83G-CK1α complex was characterised in Wnt signalling in parallel (Bozatzi et al., 2018), and some evidence points to FAM83H-CK1 complexes having a role in cytoskeletal dynamics (Kuga et al., 2016a, Kuga et al., 2013), the biology of the other FAM83-CK1 interactions have not been investigated. With this in mind, I set off to characterise the function of FAM83D, and explore the role of its interaction with CK1.

FAM83D (also known as c20orf129 and Chica) was originally identified in a proteomic screen of isolated human mitotic spindles (Sauer et al., 2005). Subsequently, FAM83D was shown to localise to the mitotic spindle apparatus, and knocking down *FAM83D* with RNA interference approaches was shown to result in both chromosomal alignment and congression defects, with a concurrent delay in the length of mitosis (Dunsch et al., 2012, Santamaria et al., 2008). Collectively, these observations pointed to a role for FAM83D in the cell division cycle. The current model proposes that FAM83D is recruited to the spindle through binding the microtubule-associated protein hyaluronan mediated motility receptor (HMMR, also known as RHAMM or CD168) at its C-terminus (Dunsch et al., 2012). In support of this model, FAM83D fragments lacking the C-terminal 394-615 amino acids fail to bind HMMR, and do not localise to the spindle apparatus in mitosis (Dunsch et al., 2012). Thus, it seems likely that FAM83D and HMMR exist in a stable complex. Recent reports have highlighted the critical role HMMR plays

in cell division, as mice or cells lacking *HMMR* take longer to progress through mitosis, and fail to resolve spindle positioning defects due to defective clearance of cortical dynein force-generating complexes (Chen, Connell et al., 2018, Connell et al., 2017). Few other FAM83D interacting proteins have been reported, however the interaction between FAM83D and dynein light chain 1 (DYNLL1) has been linked to correct and efficient spindle orientation dynamics (Dunsch et al., 2012), and FAM83D was reported to be required for the recruitment of the chromokinesin Kid to the spindle in HeLa cells (Santamaria et al., 2008).

Previously, I identified FAM83D as a CK1α-specific interactor, although the relative amounts of CK1α co-precipitating with FAM83D, even at the over-expression level, were always much lower compared to the amounts of CK1α in the immunoprecipitates of the other FAM83 members (Fulcher, Bozatzi et al., 2018). Armed with the knowledge that FAM83D is a spindle-localised protein, I hypothesised that the FAM83D-CK1α interaction might take place in a cell cycle-dependent manner, thereby explaining the low amounts of CK1α in FAM83D immunoprecipitates from asynchronous cell extracts.

In this chapter, I set out to explore the possibility that FAM83D interacts with CK1α in mitosis, and examine whether this interaction is indeed important for correct and efficient spindle positioning.

4.2: Results:

4.2.1: FAM83D interacts with CK1α only in mitosis:

In order to explore the cellular roles of FAM83D at the endogenous level, I generated *FAM83D* knockout and *FAM83D*$^{GFP/GFP}$ knockin human osteosarcoma U2OS

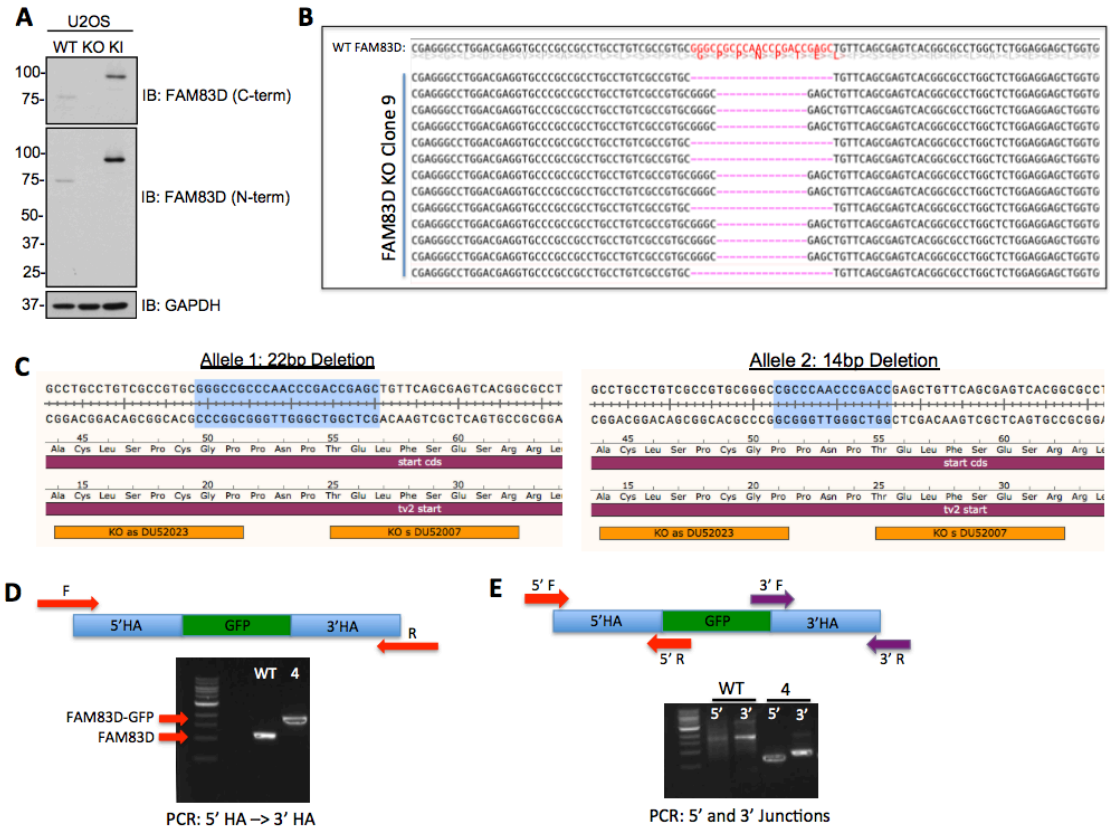

Figure 4-1: Generation of *FAM83D* knockout and *FAM83D*$^{GFP/GFP}$ knockin U2OS cells: A: Immunoblot (IB) confirmation of wild-type (WT), *FAM83D* knockout (KO), and *FAM83D*$^{GFP/GFP}$ knockin (KI) U2OS cell lines. Extracts were probed with antibodies raised against the N- or C-terminus of FAM83D (n=3). **B:** Genomic DNA sequencing analysis of the *FAM83D* KO cell line (clone 9). Pink dashes show the deleted bases, relative to the WT sequence. **C:** The guide RNAs (gRNA), along with their DU numbers (Table 2-8) used to target *FAM83D* are shown in orange. A 22 bp deletion on one allele, and a 14 bp deletion on the other allele was found. as, antisense gRNA; s, sense gRNA. **D:** Amplification of genomic DNA from WT and KI clone 4 cells with PCR, using primers outside the 5' and 3' homology arms (HA), confirmed integration of green fluorescent protein (*GFP*) within the *FAM83D* locus. F, forward primer; R, reverse primer (n=1). **E:** Amplification of genomic DNA from WT and KI clone 4 cells with PCR, using primers within *GFP* and outside the HA, at both the 5' and 3' junctions of the donor cassette, confirmed successful integration of GFP into the C-terminus of *FAM83D*. 5' F, 5' Forward primer; 5' R, 5' Reverse primer; 3' F, 3' Forward primer; 3' R, 3' Reverse primer (n=1).

cell lines using CRISPR/Cas9 gene editing technology (Figure 4-1A). Successful knockout of *FAM83D* was confirmed by immunoblotting (Figure 4-1A) and DNA sequencing (Figure 4-1B). As the CRISPR guide RNAs were designed to target exon 2 of *FAM83D,* and

targeting this region could potentially result in expression of truncated FAM83D N-terminal protein fragments, I checked a full range of molecular weights, and could not detect any N-terminal FAM83D truncated fragments (Figure 4-1A). DNA sequencing revealed a 14 bp deletion on one *FAM83D* allele, and a 22 bp deletion on another allele (Figure 4-1C). Both allelic deletions are predicted to create an out-of-frame shift, resulting in a premature stop codon. Successful knockin of the GFP tag onto the C-terminus of *FAM83D* was confirmed by immunoblotting (Figure 4-1A), and genomic PCR (Figure 4-1D). Amplification of the 5' and 3' junctions between *GFP* and the surrounding *FAM83D* sequences confirmed that the GFP-tag had integrated at the correct position within the *FAM83D* locus (Figure 4-1E).

Having verified the endogenous *FAM83D*$^{GFP/GFP}$ knockin U2OS cell line, whether FAM83D could interact with CK1α in mitosis in these cells was explored. To obtain mitotic cells, cells were treated with nocodazole to arrest them in prometaphase, followed by a brief release into fresh medium to allow them to progress into mitosis. Following treatment, mitotic cells were collected by shake-off. Asynchronous cells were employed as a control. Cells were lysed and subjected to anti-GFP immunoprecipitation, and subsequent immunoblotting. Interestingly, FAM83D exhibited a striking change in electrophoretic mobility in mitotic extracts, compared to asynchronous extracts, indicative of a potential post-translational modification (Figure 4-2A). This is consistent with a previous report suggesting that FAM83D is phosphorylated in mitosis (Santamaria et al., 2008). Probing the eluates with antibodies against CK1α, δ and ε, revealed that the only FAM83-relevent CK1 isoform to co-precipitate with FAM83D was CK1α, and this interaction only took place in mitotic, but not asynchronous, extracts (Figure 4-2A). The known interactions between FAM83D and HMMR or DYNLL1 were not significantly

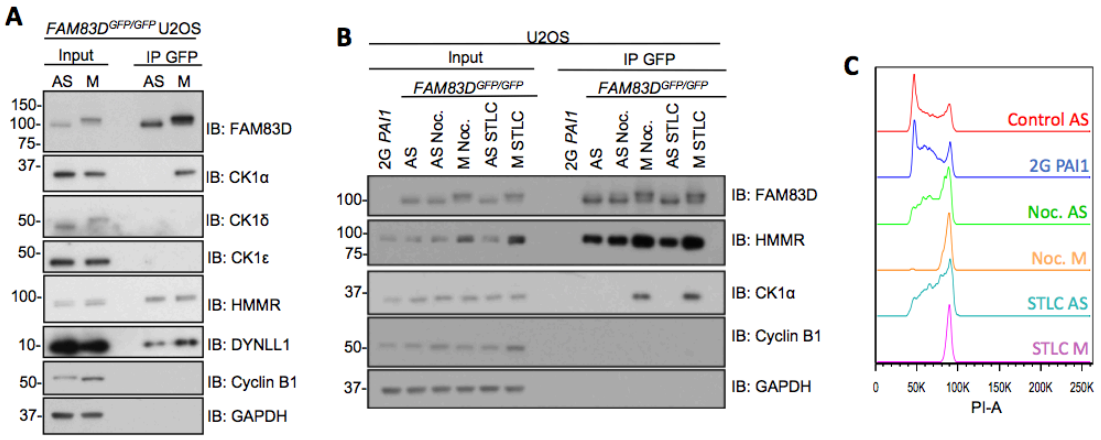

Figure 4-2: FAM83D only interacts with CK1α in mitotic extracts: A: *FAM83D*$^{GFP/GFP}$ knockin U2OS cells were synchronised in mitosis (M) with nocodazole. Untreated, asynchronous (AS) cells were used as a control. Lysed extracts were subjected to anti-GFP immunoprecipitations (IP), and whole cell lysate (Input) and IP samples were analysed by immunoblotting (IB) with the indicated antibodies (n=3). **B:** *FAM83D*$^{GFP/GFP}$ knockin U2OS cells were synchronised in mitosis (M) with either nocodazole (M Noc.) or STLC (M STLC) and collected by shake off. Cells treated were nocodazole or STLC that remained adherent after shake-off (AS Noc.; AS STLC) were used as drug-treated, non-mitotic controls. Asynchronous (AS) cells were used as a control. For a GFP only control, 2G-*PAI1* U2OS cells which express low levels of *GFP* were used. Lysed extracts were subjected to anti-GFP IPs, and Input and IP samples were analysed by IB with the indicated antibodies (n=3). **C:** Propidium iodide staining analyses revealing cell cycle distribution profiles for the samples described in B.

altered between asynchronous and mitotic samples, suggesting that their mode of interaction is more constitutive (Figure 4-2A).

Next, I sought to eliminate the possibility that the FAM83D-CK1α interaction was occurring as an off-target effect of nocodazole treatment. *FAM83D*$^{GFP/GFP}$ cells were treated with either nocodazole, or the Eg5 inhibitor S-Trityl L-Cysteine (STLC) (Skoufias et al., 2006), which also arrests cells in mitosis, but, unlike nocodazole, results in monopolar spindle formation. Nocodazole-treated cells were washed in PBS and re-plated in fresh full media to allow them to progress into mitosis prior to lysis. Mitotic nocodazole- and STLC- treated cells were collected by shake-off. The cells that remained

adherent after shake-off were collected for use as drug-treated, non-mitotic controls. Untreated, asynchronous *FAM83D*$^{GFP/GFP}$ cells were used as a negative control. To make sure that CK1α did not co-precipitate with the GFP tag of FAM83D-GFP, I made use of a *PAI1* transcriptional reporter U2OS cell line (2G *PAI1*), in which low levels of *GFP* are expressed under basal conditions (Rojas-Fernandez, Herhaus et al., 2015). Following lysis, samples were subjected to immunoprecipitation with anti-GFP coupled beads. Consistent with previous observations (Figure 4-2A), FAM83D exhibited a change in electrophoretic mobility and CK1α only co-precipitated with FAM83D in the nocodazole-treated mitotic lysates (Figure 4-2B). Critically, I observed the same result in STLC-treated mitotic extracts, further demonstrating the mitotic nature of the FAM83D-CK1α interaction (Figure 4-2B). Importantly, I observed neither a FAM83D mobility shift, nor any CK1α in FAM83D immunoprecipitates, from non-mitotic nocodazole or STLC-treated extracts, thereby suggesting that the FAM83D-CK1α interaction and FAM83D mitotic mobility shift are not off-target effects resulting from the drug treatments (Figure 4-2B). No CK1α co-precipitated with the free GFP protein in the 2G *PAI1* control extracts (Figure 4-2B), demonstrating that CK1α does not interact with the isolated GFP protein. Staining cells from each of these treatments with propidium iodide, and subjecting them to flow cytometric-based DNA-profiling, confirmed the enriched G2/M cell populations in nocodazole- and STLC-treated mitotic cells (Figure 4-2C), whereas the DNA profiles were spread over G1, S and G2/M phases with the other treatments (Figure 4-2C).

Next, to address whether the GFP-tag knocked in to the *FAM83D* gene was artificially inducing the FAM83D mobility shift or interaction with CK1α in mitotic cells, I performed endogenous FAM83D immunoprecipitations using polyclonal antibodies raised against the C-terminus of FAM83D, in both mitotic and asynchronous extracts.

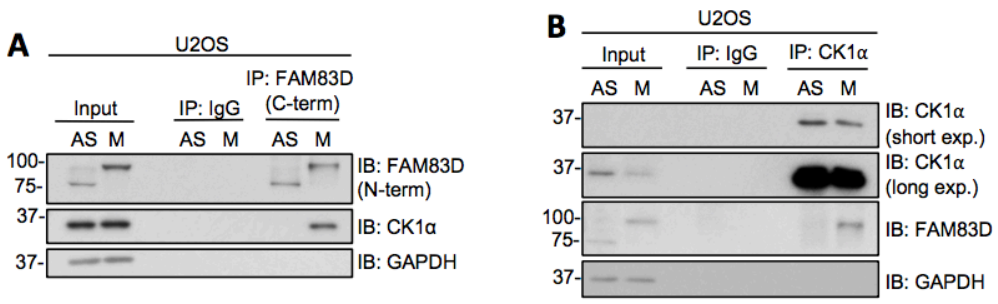

Figure 4-3: Confirming the mitotic FAM83D-CK1α interaction at the endogenous level: **A:** Wild-type U2OS cells were synchronised in mitosis with nocodazole (M). Asynchronous (AS) cells were used as a control. Lysed extracts were subjected to immunoprecipitation (IP) with either control IgG or anti-FAM83D antibody coupled to sepharose beads. Input and IP samples were analysed by immunoblotting (IB) with the indicated antibodies (n=3). **B:** As in A. except that anti-CK1α antibody coupled to sepharose beads were used for the IP (n=3).

Sheep pre-immune IgG immunoprecipitations were performed in parallel as a control. Probing these samples confirmed that the FAM83D-CK1α interaction takes place only in mitotic extracts, and showed that the mitotic mobility shift of FAM83D occurs independently of the GFP fusion tag (Figure 4-3A). No FAM83D or CK1α was observed in the IgG control immunoprecipitates (Figure 4-3A). Analogous results were obtained when endogenous CK1α was immunoprecipitated under the same conditions (Figure 4-3B).

Finally, to decipher exactly when FAM83D associates with CK1α in the cell division cycle, I arrested *FAM83D*$^{GFP/GFP}$ U2OS cells in G2 using the CDK1 inhibitor RO-3306, or in mitosis using STLC. STLC-treated mitotic cells were isolated by shake-off, washed and re-plated into fresh medium, and lysed every 2 h from 0 – 6 h, by which time the cells had entered G1. Asynchronous cells were included as a control. Lysates from these cells were subjected to anti-GFP immunoprecipitations, and evaluated for co-precipitation of CK1α by immunoblotting. FAM83D-GFP displayed a robust mobility

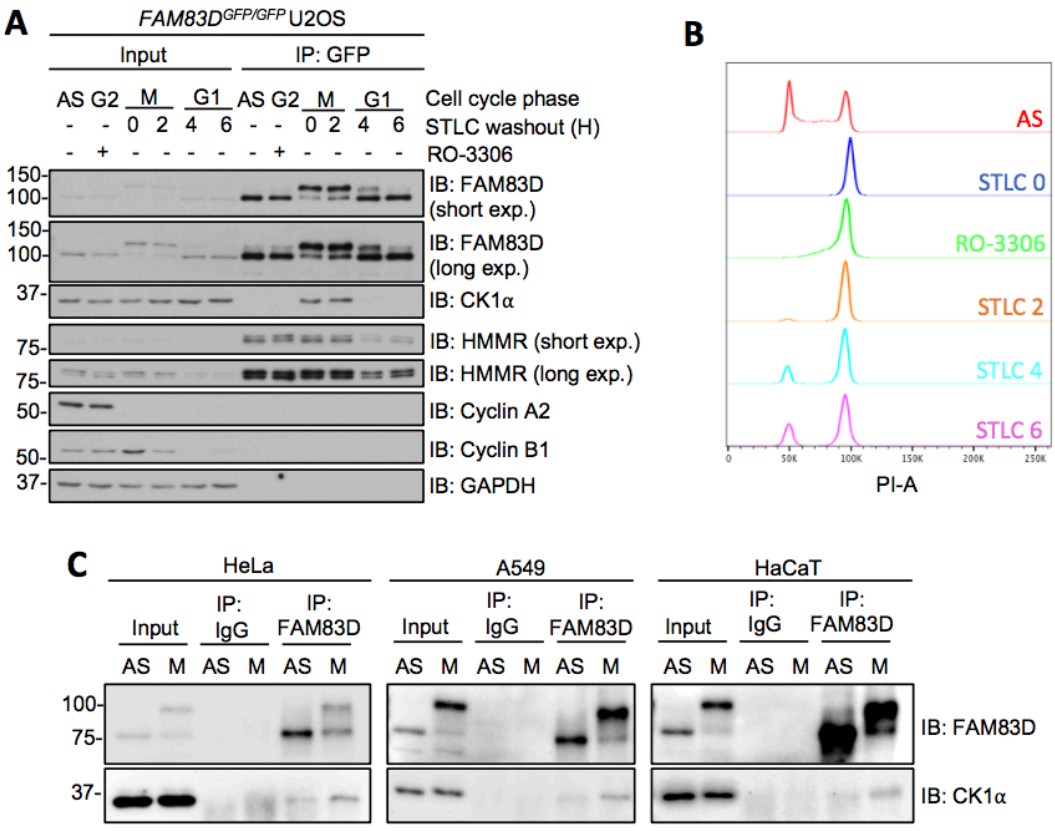

Figure 4-4: The mitotic FAM83D-CK1α interaction is not unique to U2OS cells: A: *FAM83D*$^{GFP/GFP}$ knockin cells were synchronised in G2 with RO-3306 for 20 h, or arrested in mitosis (M) using STLC for 16 h. STLC-treated mitotic cells were isolated by shake-off, washed and re-plated into fresh medium. Cells were lysed at the indicated time points after STLC wash-out, allowing them to pass through mitosis and enter G1. Asynchronous (AS) cells were used as a control. Cell lysates were subjected to anti-GFP immunoprecipitation (IP) and Input and IP extracts were subjected to SDS-PAGE and immunoblotting (IB) with the indicated antibodies (n=3). **B:** Propidium iodide-stained DNA distribution profiles for the samples described in A. **C:** AS or STLC-synchronised (M) wild-type HeLa, A549, or HaCaT cells were subjected to IP with either IgG- or anti-FAM83D-coupled sepharose beads. Input and IP samples were analysed by IB with the indicated antibodies (n=3).

shift only in the mitotic samples (Figure 4-4A). Consistently, CK1α only co-precipitated with FAM83D in mitotic, but not G2-arrested or G1 samples (Figure 4-4A). Successful treatments were confirmed through immunoblotting with antibodies against G2 and M

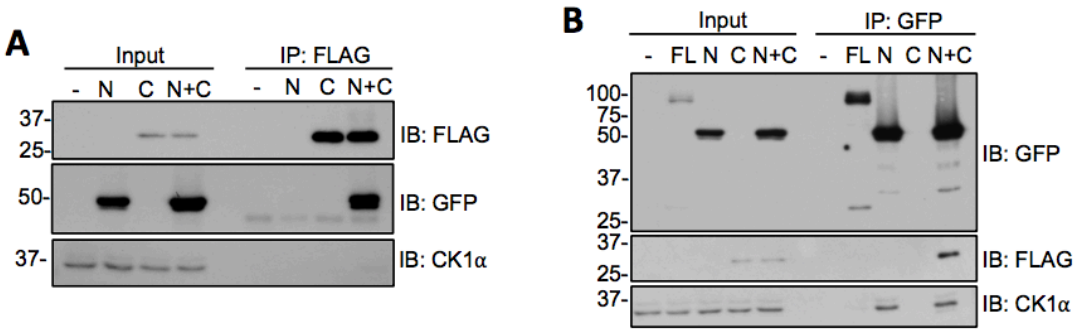

Figure 4-5: The C-terminus of FAM83D is inhibitory towards CK1α binding: A: *FAM83D* knockout U2OS cells were transiently transfected with plasmids encoding GFP-tagged FAM83D N-terminus incorporating the DUF1669 (N), FLAG-tagged FAM83D C-terminus (C) domain lacking the DUF1669, or with both N and C fragments together. Cells were lysed and extracts subjected to anti-FLAG immunoprecipitations (IP). Whole cell extracts (Input) and IP samples were separated by SDS-PAGE, before immunoblotting (IB) with the indicated antibodies (n=2). **B:** As in A. except that a GFP-tagged full-length (FL) plasmid was also included, and GFP IPs were performed instead of FLAG IPs (n=2).

phase specific cyclins (Cyclin A and B respectively) (Figure 4-4A), and with DNA distribution profiling (Figure 4-4B).

To test whether the mitotic FAM83D-CK1α interaction occurs in other mammalian cells, I expanded the interaction analysis to include three additional human cell lines, namely cervical cancer HeLa, lung adenocarcinoma A549, and human keratinocyte HaCaT cell lines. Endogenous FAM83D immunoprecipitated from these cells in STLC-synchronised mitotic extracts, but not from asynchronous extracts, co-precipitated CK1α (Figure 4-4C). As in U2OS cells, FAM83D also displayed a pronounced electrophoretic mobility shift in mitotic extracts from these cell lines (Figure 4-4C).

I next sought to probe the mitosis-dependent nature of the FAM83D-CK1α interaction. Given that the N-terminal DUF1669 of FAM83 proteins mediates CK1 binding (Fulcher et al., 2018), I reasoned that the C-terminus of FAM83D may be acting in an autoinhibitory manner, to prevent CK1α binding until mitosis. In line with this

hypothesis, isolated FAM83D C-terminal fragments lacking the DUF1669 co-precipitated N-terminal FAM83D fragments, yet did not co-precipitate CK1α (Figure 4-5A). In contrast, the N-terminal DUF1669-containing fragment of FAM83D co-precipitated CK1α even under asynchronous conditions (Figure 4-5B). This suggests that the DUF1669 of FAM83D is both necessary and sufficient to interact with CK1α, and that the C-terminus of FAM83D may be having an autoinhibitory effect, to prevent the FAM83D-CK1α interaction until mitosis.

Collectively, these data suggest that FAM83D and CK1α associate robustly only in mitosis, at the endogenous level. This is the first FAM83-CK1 interaction identified which requires a stimulus, and that is dependent on cell cycle stage.

4.2.2: FAM83D recruits CK1α to the spindle apparatus in mitosis:

In the previous chapter, I proposed that FAM83 proteins act as cellular anchoring proteins for CK1 isoforms in cells and, in doing so, recruit CK1 isoforms to distinct cellular compartments to potentially regulate their substrate accessibility and/or availability (Fulcher et al., 2018). If this were the case, one might expect FAM83D to recruit CK1α to the spindle apparatus in mitosis. To address this, I subjected the *FAM83D*$^{GFP/GFP}$ knockin, *FAM83D* knockout, and wild-type U2OS cells to immunofluorescence microscopy, after they were synchronised in mitosis with STLC. In *FAM83D*$^{GFP/GFP}$ cells, I observed robust co-localisation between endogenous FAM83D-GFP fluorescence and endogenous CK1α signals on the STLC-induced monopolar spindles (Figure 4-6A). In wild-type cells, which express *FAM83D* without the GFP-tag fusion, I observed CK1α localisation on the mitotic spindle, and did not detect any contaminating fluorescence from the GFP channel (Figure 4-6A). Strikingly, in *FAM83D* knockout cells, I could not detect any CK1α on the spindle apparatus, suggesting that CK1α cannot localise to the

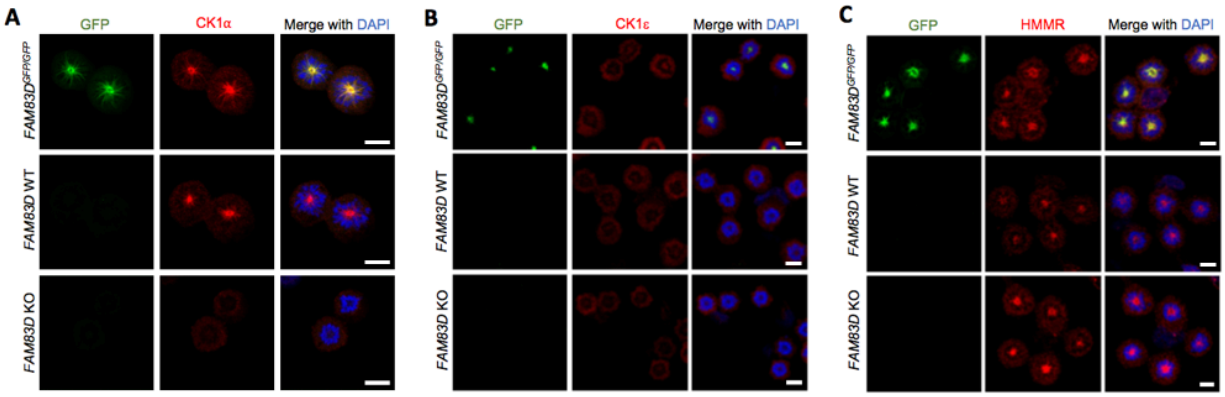

Figure 4-6: FAM83D directs CK1α, but not CK1ε or HMMR, to the mitotic spindle: A: STLC-synchronised mitotic (M) wild-type (WT), *FAM83D* knockout (KO), and *FAM83D*$^{GFP/GFP}$ knockin U2OS cells were subjected to anti-CK1α immunofluorescence and GFP fluorescence microscopy. DNA is stained with DAPI. Representative images representative of 3 independent experiments are included. **B:** As in A. except that cells were subjected to anti-CK1ε immunofluorescence (n=2). **C:** As in A. except that cells were subjected to anti-HMMR immunofluorescence (n=2). Scale bars; 20 µM.

spindle in the absence of FAM83D (Figure 4-6A). To validate the specificity of this assay, I repeated this experiment and instead stained for the CK1ε isoform. In this context, no CK1ε staining was detected at the spindle apparatus in either the wild-type, *FAM83D* knockout or *FAM83D*$^{GFP/GFP}$ cells (Figure 4-6B). Furthermore, the localisation of HMMR to the spindle

was independent of whether FAM83D was present in the cell or not, in line with previous reports suggesting HMMR recruits FAM83D to the spindle in mitosis (Dunsch et al., 2012) (Figure 4-6C).

I previously identified two conserved residues (equivalent to D249 and F283 of FAM83D) that were critical for the FAM83-CK1 interaction (Fulcher et al., 2018) (see section 3.2.1). These phenylalanine and aspartate residues, which reside within the CK1-binding DUF1669 of FAM83 members, abolished the FAM83-CK1 interaction when mutated to alanine in FAM83E-H (Fulcher et al., 2018). Armed with this insight, I first

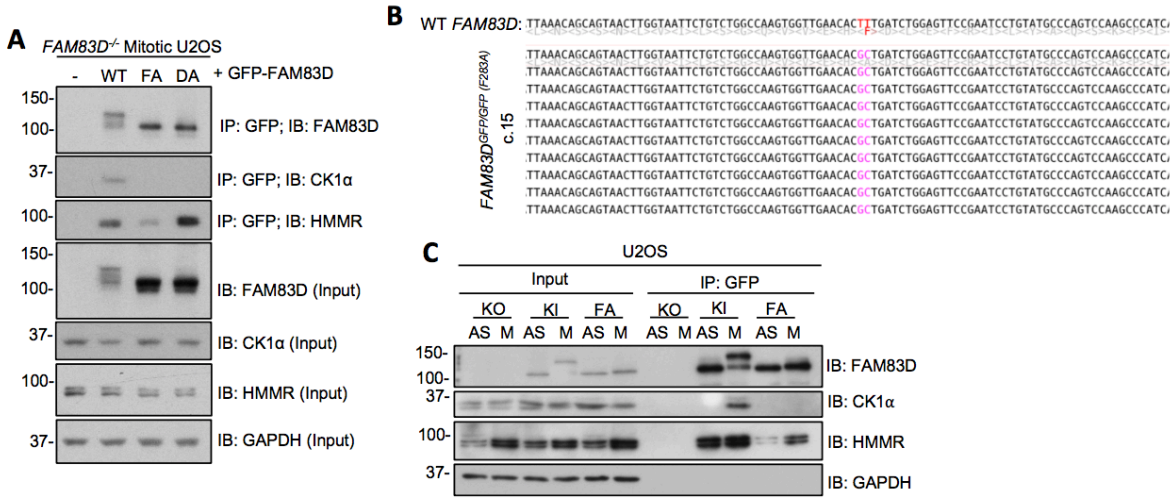

Figure 4-7: Generation of *FAM83D*$^{GFP/GFP\ (F283A)}$ knockin U2OS cells: A: *FAM83D*$^{-/-}$ knockout (KO) U2OS cells were transiently transfected with vectors encoding GFP-FAM83D (WT), GFP-FAM83D(F283A) (FA), or GFP-FAM83D(D249A) (DA). Untransfected cells were included as a control (-). Following transfection, cells were synchronised in mitosis with STLC. Mitotic cells were collected, lysed and subjected to anti-GFP immunoprecipitation (IP) with GFP TRAP beads. Whole cell extracts (Input) and IP samples were immunoblotted (IB) with the indicated antibodies (n=3). **B:** Genomic DNA sequencing analysis confirmed the F283A mutation in the *FAM83D*$^{GFP/GFP\ (F283A)}$ knockin cells (clone 15), relative to the WT sequence. **C:** *FAM83D*$^{-/-}$ KO, *FAM83D*$^{GFP/GFP}$ knockin (KI), and *FAM83D*$^{GFP/GFP\ (F283A)}$ knockin (FA) U2OS cells were STLC-synchronised and mitotic cells (M) isolated by shake off. Asynchronous (AS) cells were included as a control. Cells were lysed and subjected to GFP TRAP IP and subsequent IB with the indicated antibodies (n=3).

confirmed that mutation of these Phe and Asp residues impact the FAM83D-CK1α interaction in mitotic cells, by transiently introducing GFP-tagged wild-type FAM83D, or the GFP-tagged F283A and D249A FAM83D mutants, into *FAM83D* knockout U2OS cells, and synchronising them with STLC. Subjecting lysates from these cells to anti-GFP immunoprecipitation revealed that, whilst wild-type GFP-FAM83D was able to co-precipitate CK1α, both the D249A and F283A GFP-FAM83D mutants could not (Figure 4-7A). Interestingly, the FAM83D mitotic mobility shift was visible for the wild- type GFP-

FAM83D protein, but not for the F283A and D249A GFP-FAM83D mutants (Figure 4-7A), suggesting that this FAM83D mitotic modification might be dependent on CK1α binding.

In an attempt to bypass any potential limitations of over-expression systems, I decided to make a *FAM83D*$^{GFP/GFP\ (F283A)}$ cell line using CRISPR/Cas9, to allow us to evaluate this FAM83D CK1α-binding-deficient mutant at the endogenous level. After confirming successful homozygous knockin of the GFP tag and F283A mutation by DNA sequencing (Figure 4-7B), I synchronised these cells in mitosis using STLC, and subjected extracts from these cells to anti-GFP immunoprecipitations, to test the ability of FAM83D(F283A)-GFP to co-precipitate CK1α. This was performed in parallel with extracts from *FAM83D*$^{GFP/GFP}$ and *FAM83D* knockout cells. Asynchronous cells were used as controls for all the cell lines used. Whilst FAM83D-GFP could robustly co-precipitate endogenous CK1α in mitotic, but not asynchronous extracts, no CK1α was detected in the immunoprecipitates of the FAM83D(F283A)-GFP mutant (Figure 4-7C). Consistent with the over-expression data (Figure 4-7A), no mitotic mobility shift of the FAM83D(F283A)-GFP knockin protein was observed (Figure 4-7C).

To test if the FAM83D(F283A)-GFP mutant still localised to the spindle apparatus, I synchronised *FAM83D* knockout, *FAM83D*$^{GFP/GFP}$, and *FAM83D*$^{GFP/GFP\ (F283A)}$ cells in mitosis using STLC, and subjected these cells to fluorescence microscopy, after co-staining for endogenous CK1α. In *FAM83D*$^{GFP/GFP}$ cells, I observed robust GFP fluorescence from the mitotic spindle, which co-localised with endogenous CK1α (Figure 4-8A). No CK1α was detected on the spindle in *FAM83D* knockout cells (Figure 4-8A), consistent with previous observations (Figure 4-6A). As predicted, I detected no CK1α on the spindle in *FAM83D*$^{GFP/GFP\ (F283A)}$ cells (Figure 4-8A), however, the relative GFP fluorescence on the spindle apparatus was lower in this cell line (Figure 4-8A). Quantification of the CK1α signal on mitotic spindles across these cell lines corroborated

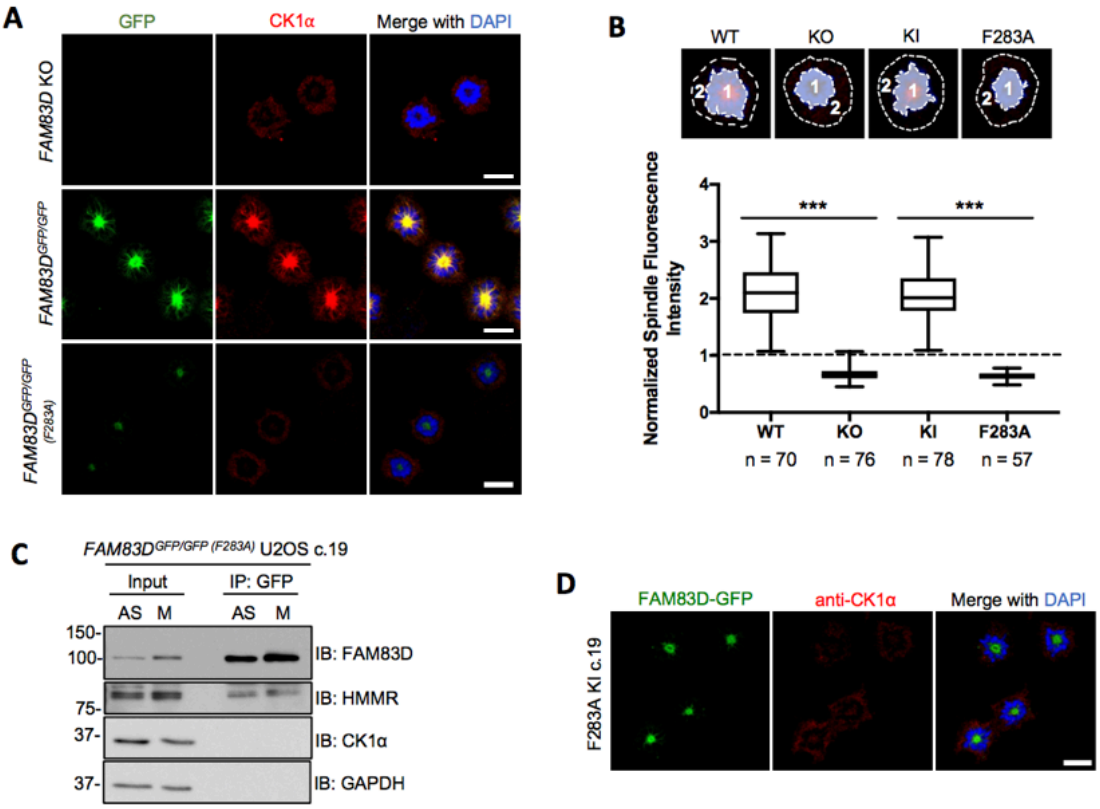

Figure 4-8: *FAM83D*$^{GFP/GFP\ (F283A)}$ cells fail to recruit CK1α to mitotic spindles: A: *FAM83D* knockout (KO), *FAM83D*$^{GFP/GFP}$ knockin (KI), and *FAM83D*$^{GFP/GFP\ (F283A)}$ knockin (F283A) U2OS cells were subjected to anti-CK1α immunofluorescence and GFP fluorescence microscopy. DNA is stained with DAPI. Representative images representative of 2 independent experiments are included. Scale bars; 20 µM. **B:** Quantification of CK1α spindle localisation for the cells described in panel A. and Figure 4-6A. Cell images denote the measured regions used to calculate the ratios on the box plot (1 = spindle roi, 2 = cytoplasm roi). Box plot whiskers denote the minimum and maximum measured values. ***, *P*<0.0001; ANOVA. Analysis was performed on the indicated number of cells, n=2. **C:** *FAM83D*$^{GFP/GFP\ (F283A)}$ knockin U2OS cells (clone 19) were synchronised in mitosis with STLC (M). Asynchronous (AS) cells were included as a control. Cells were lysed and subjected to anti-GFP immunoprecipitation (IP), and whole cell extracts (Input) and IP samples were immunoblotted (IB) with the indicated antibodies (n=2). **D:** The cell line described in C. was subjected to anti-CK1α immunofluorescence and GFP fluorescence microscopy. DNA is stained with DAPI. Representative images representative of 2 independent experiments are included. Scale bars; 20 µM.

these observations (Figure 4-8B).Identical results for both the immunoprecipitation and immunofluorescence data were obtained with an independent CRISPR clone, confirming these results (Figure 4-8C&D).

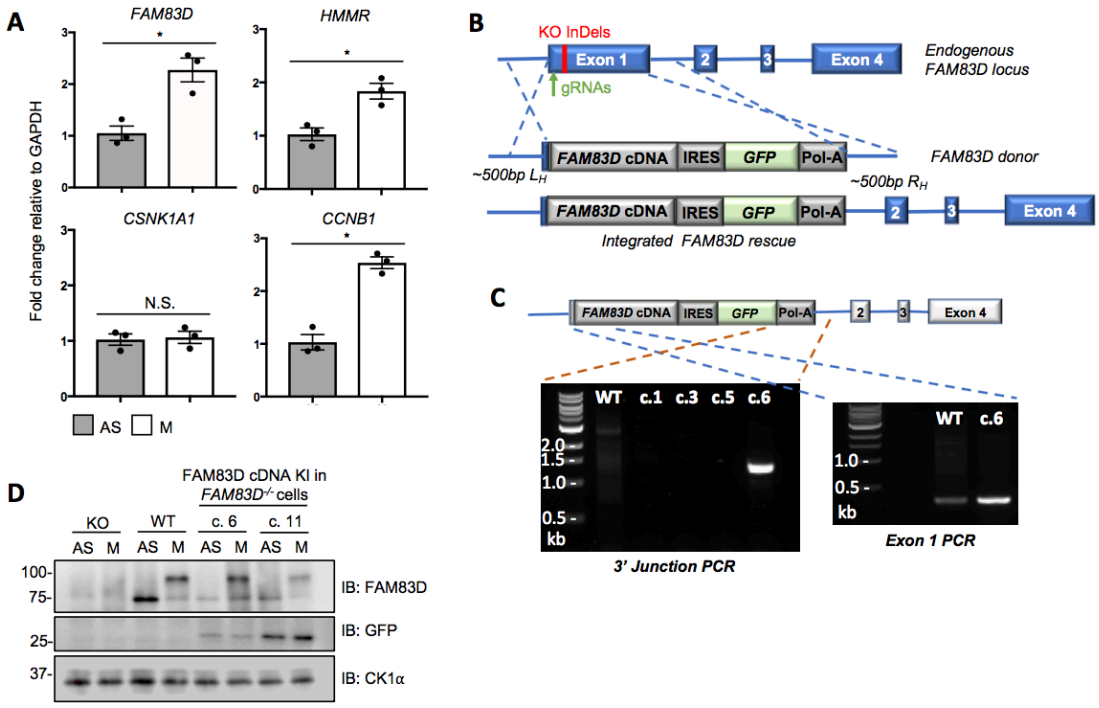

Figure 4-9: Restoring *FAM83D* at the native locus in *FAM83D* knockout U2OS cells: A: STLC-synchronised mitotic wild-type U2OS cells were subjected to qRT-PCR analysis using primers for *FAM83D*, *HMMR*, *CSNK1A1,* and *CCNB1*. AS cells were used as a control. Error bars, SEM; *, *P*<0.01; Student's *T*-test (n=3). **B:** Schematic illustrating the CRISPR-based strategy used to reintroduce FAM83D into the *FAM83D*$^{-/-}$ knockout background. KO InDels, insertion/deletion responsible for the *FAM83D* knockout; IRES, internal ribosome entry site; Pol-A, polyadenosine tail. **C:** Representative strategy for verifying correct integration of the cDNA rescue cassette. Amplification of genomic DNA from wild-type (WT) cells and the indicated putative knockin clones with PCR, using a primer pair recognising sequences within GFP and outside the pol-A tail (3' Junction PCR), or a primer pair recognising sequences within the 5' UTR and exon 1 (Exon 1 PCR), showed correct integration of the polycistronic cassette within the *FAM83D* locus. **D:** *FAM83D*$^{-/-}$ (KO), WT, and two independent clones from the CRISPR/Cas9-mediated knockin rescue of *FAM83D* cDNA into *FAM83D*$^{-/-}$ cells (c. 6 and c. 11), were synchronised in mitosis (M) with STLC. Asynchronous (AS) cells were included as a control. Cells were lysed and subjected to immunoblotting (IB) with the indicated antibodies (n=3).

Having observed such a drastic ablation of spindle-localised CK1α in *FAM83D* knockout cells, I next sought to test whether reintroducing *FAM83D* into the knockout background could rescue this defect. However, transcriptional analysis of *FAM83D* transcripts by qRT-PCR showed a significant two-fold increase in transcript levels in

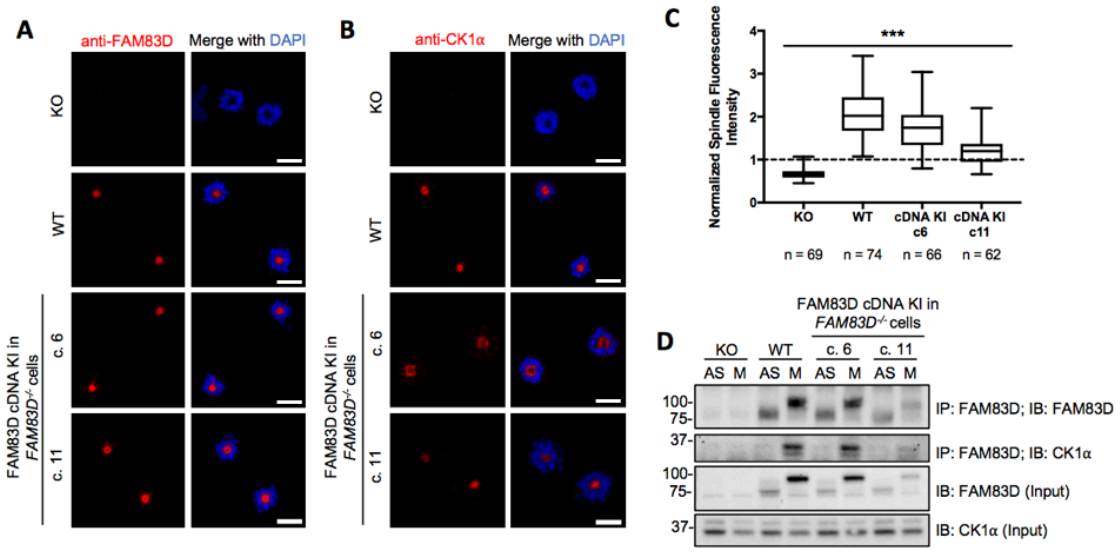

Figure 4-10: Restoring FAM83D at the native locus rescues CK1α spindle localisation: A-B: *FAM83D*$^{-/-}$ (KO), wild-type (WT), and two independent clones of a CRISPR/Cas9-mediated knockin rescue of *FAM83D* cDNA into *FAM83D*$^{-/-}$ cells (c. 6 and c. 11), were STLC-synchronised in mitosis, fixed, and stained with antibodies recognizing FAM83D (A) or CK1α (B). Representative images from 1 independent experiments are included. Scale bars; 20 µM. **C:** Quantification of CK1α spindle localisation for the experiment described in B. using the same strategy employed in Figure 4-8B. ***, *P*<0.0001; ANOVA. Analysis was performed on the indicated number of cells, n=1. **D:** The cell lines described in A. were STLC-synchronised in mitosis (M) or left asynchronous (AS), lysed and subjected to immunoprecipitation (IP) with anti-FAM83D-coupled sepharose beads, before immunoblotting (IB) with the indicated antibodies (n=3).

mitotic, over asynchronous cells (Figure 4-9A), suggesting FAM83D is a cell cycle-regulated gene, similar to *HMMR* and *CCNB1* (Figure 4-9A). In contrast, I did not detect any difference in CK1α transcript levels between asynchronous and mitotic cells (Figure 4-9A). Thus, given the inherent cell cycle-regulated nature of the *FAM83D* promoter, I worried that constitutive over-expression-based rescue experiments may disrupt this endogenous regulation. Therefore, I sought to develop a more elegant rescue method.

To this end, a polycistronic cassette consisting of the wild-type *FAM83D* cDNA, an IRES element, a *GFP* reporter, followed by a polyadenosine tail, was knocked in

directly downstream of the endogenous *FAM83D* promoter (Figure 4-9B). Two homozygous rescue clones, clone 6 and 11, were obtained and verified by PCR (Figure 4-9C) and DNA sequencing. In both clones, the expression of the FAM83D protein, along with its mitotic mobility shift, closely mirrored that seen in wild-type cells, however the expression of *FAM83D* in clone 11 was slightly lower than that observed in clone 6 (Figure 4-9D). In both clones, both FAM83D and CK1α localised to the mitotic spindle (Figure 4-10A-C), and the reinstated FAM83D co-precipitated CK1α only in mitosis (Figure 4-10D).

Collectively, these data suggest that FAM83D recruits CK1α to the spindle apparatus in mitosis, and in the absence of FAM83D, CK1α can no longer be directed to mitotic spindles.

4.2.3: Exploring FAM83D and CK1α localisation in unperturbed cells:

As most of the imaging so far had been performed on STLC-arrested mitotic cells, which present with non-physiological monopolar spindles, I next sought to examine the dynamics of the FAM83D-CK1α interaction in unperturbed cells, in the absence of any drug-induced cell synchronisation. To this end, and to enable imaging of live cells, a mCherry tag was knocked into the N-terminus of the CK1α-encoding *CSNK1A1* gene, in *FAM83D*$^{GFP/GFP}$ U2OS cells. As a control, an mCherry tag was knocked into the N-terminus of *CSNK1E*, the gene encoding CK1ε. First, these cell lines were verified with immunoblotting (Figure 4-11A), and PCR (Figure 4-11B), and successful in-frame homozygous knockin of the mCherry tag confirmed with DNA sequencing. Subjecting STLC-arrested mitotic, or asynchronous, extracts from these cell lines to anti-mCherry immunoprecipitations, confirmed that the FAM83D-GFP knockin protein could still interact with mCherry-CK1α in mitosis (Figure 4-11C). Consistent with previous observations, no FAM83D-GFP was detected in mCherry-CK1ε immunoprecipitates

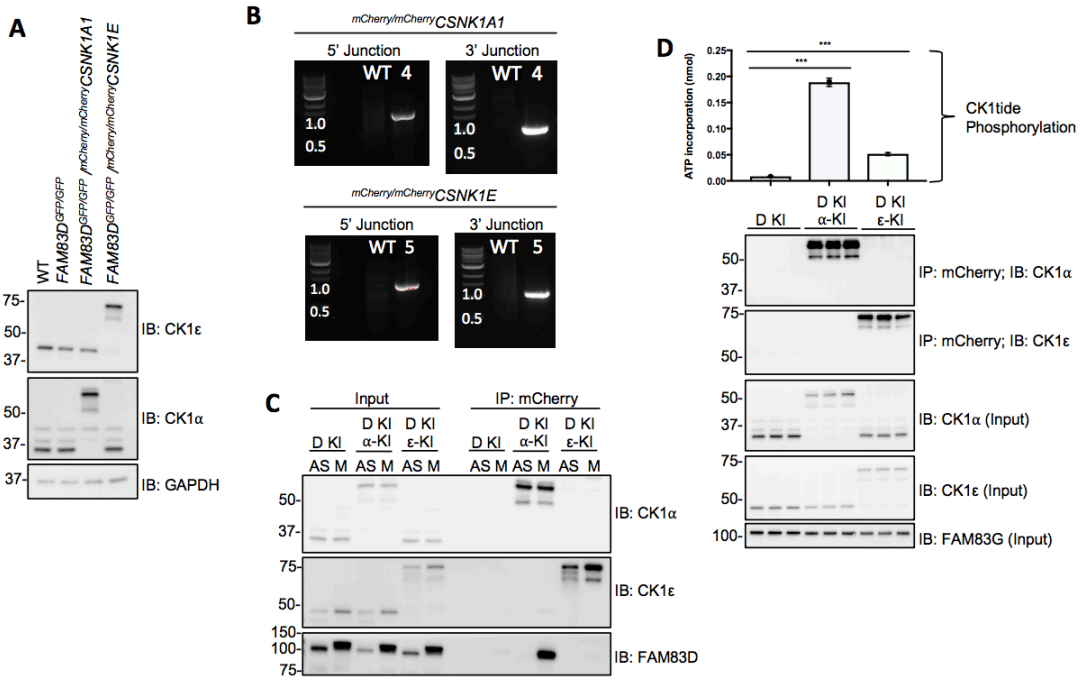

Figure 4-11: Generation of *$^{mCherry/mCherry}$CSNK1* knockin U2OS cell lines: A: Wild-type (WT), *FAM83D$^{GFP/GFP}$* knockin (D-KI), *FAM83D$^{GFP/GFP}$* knockin with *$^{mCherry/mCherry}$CSNK1A1* (D-KI, α-KI), and *FAM83D$^{GFP/GFP}$* knockin with *$^{mCherry/mCherry}$CSNK1E* (D-KI, ε-KI) U2OS cells were lysed, and subjected to immunoblotting (IB) with the indicated antibodies (n=2). **B:** Genomic DNA amplification with PCR using DNA isolated from WT and *FAM83D$^{GFP/GFP}$* knockin with *$^{mCherry/mCherry}$CSNK1A1* clone 4 U2OS cells (upper panel), or from WT and *FAM83D$^{GFP/GFP}$* knockin with *$^{mCherry/mCherry}$CSNK1E* clone 5 U2OS cells (lower panel), using primers recognising sequences between *mCherry* and the 5' UTR (5' Junction), or between *mCherry* and exon 1 (3' Junction), confirmed correct integration of *mCherry* within the *CSNK1A1* and *CSNK1E* loci respectively (n=1). **C:** The cell lines described in A. were synchronised in mitosis with STLC (M) or left asynchronous (AS). Cells were lysed and subjected to immunoprecipitation (IP) with anti-mCherry beads, before IB with the indicated antibodies (n=2). **D:** The cell lines described in A. were lysed and subjected to IP with anti-mCherry beads, and IPs were subjected to an *in vitro* kinase assay using an optimised CK1 substrate peptide (CK1tide) and [γ^{32}P]-ATP. n=3, Error bars, SEM, ***, *P*<0.0001; ANOVA.

(Figure 4-11C). Finally, I confirmed that the addition of an mCherry tag onto either CK1α or ε did not render these kinases inactive, by performing *in vitro* kinase assays against an optimised CK1 substrate peptide (CK1tide) (Figure 4-11D).

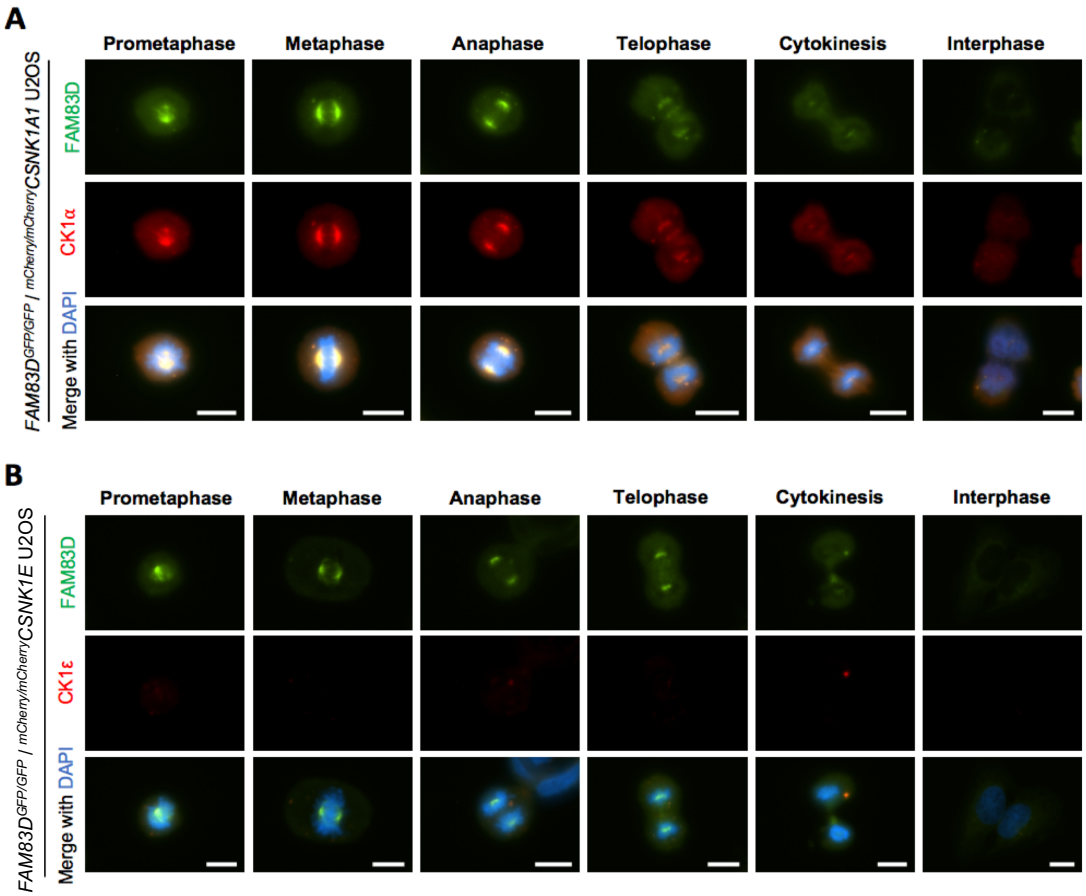

Figure 4-12: Exploring FAM83D-CK1α localisation in unperturbed cells: A: Asynchronous (AS) *FAM83D*$^{GFP/GFP}$/ $^{mCherry/mCherry}$*CSNK1A1* knockin U2OS cells were fixed and imaged. Representative images from the indicated cell cycle stages are included (n=3). Scale bars; 10 µM. **B:** As in A. except that asynchronous *FAM83D*$^{GFP/GFP}$ / $^{mCherry/mCherry}$*CSNK1E* knockin U2OS cells were used.

Having been satisfied that these cell lines did not present with any concerning defects with regard to the FAM83D-CK1α interaction, I subjected these cells to fluorescence microscopy. I observed overlapping centrosomal and spindle fluorescence between FAM83D-GFP and mCherry-CK1α from prometaphase through to anaphase, with less intense co-fluorescence evident in the latter stages of mitosis (Figure 4-12A). In contrast, I did not observe spindle localisation of mCherry-CK1ε, nor co-localisation with FAM83D-GFP, at any stage of mitosis (Figure 4-12B).

Collectively, these data demonstrate that the FAM83D-mediated recruitment of CK1α to the mitotic spindle occurs in unperturbed cells, and is not an indirect effect of either drug-induced synchronisation, or fixation artefacts.

4.2.4: Exploring the regulation of FAM83D during the cell cycle:

Given the prominent mobility shift of the FAM83D protein in mitosis, I decided to investigate this intriguing FAM83D modification further. The mitotic electrophoretic mobility shift collapsed substantially when FAM83D-GFP knockin immunoprecipitates were subjected to λ-phosphatase treatment, suggesting that this mobility shift was due to phosphorylation (Figure 4-13A). Using the mobility shift as a read-out, I examined FAM83D phosphorylation over the course of a cell division through immunoblotting, following release from STLC arrest after synchronisation. The levels of cyclin B1 and phospho-Histone H3 were vastly reduced as cells exited mitosis and entered G1, as expected (Figure 4-13B). Interestingly, under these conditions, I observed concurrent reduction in the levels of both HMMR and phospho-FAM83D as cells exited mitosis, suggesting that the FAM83D-HMMR complex is also regulated in a cell cycle-dependent manner (Figure 4-13B).

Such patterns in the levels of cell cycle-regulated proteins are often associated with their proteolytic degradation following mitotic exit, or during the metaphase-to-anaphase transition (Chang et al., 2003, Koepp, 2014). In contrast, the protein levels of CK1α did not change after the STLC washout (Figure 4-13B). Considering that both FAM83D and CK1α appear to dissociate from mitotic spindles following the metaphase-to-anaphase transition (Figure 4-12A), it seems likely that, following FAM83D

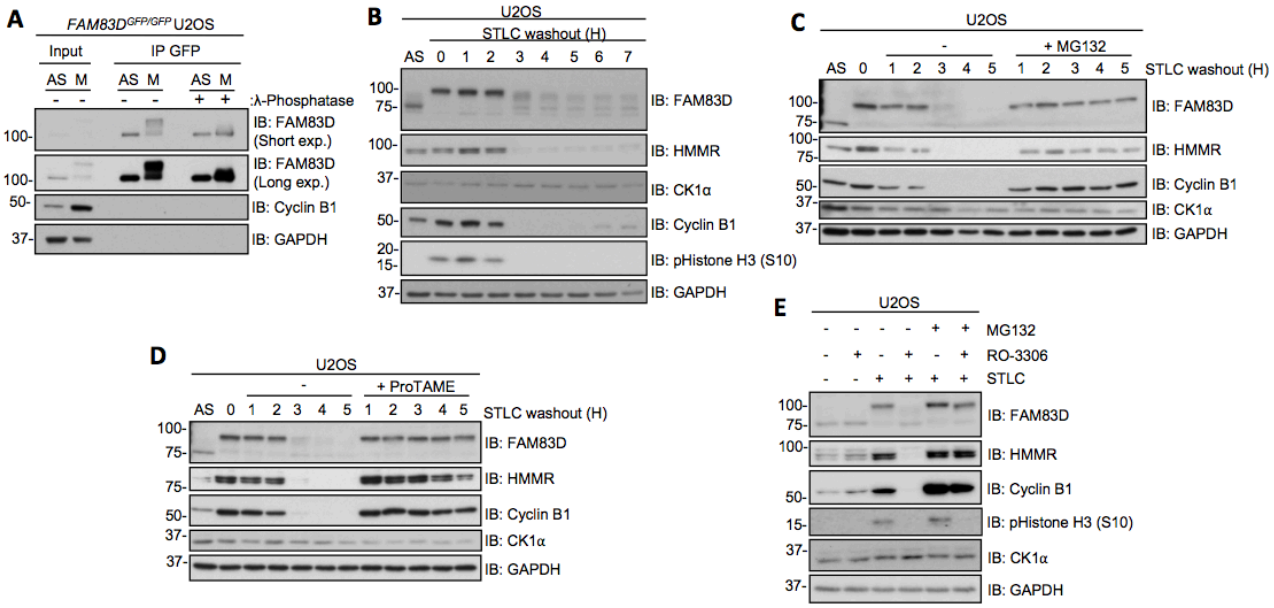

Figure 4-13: FAM83D is phosphorylated in mitosis and is degraded following mitotic exit: A: Nocodazole-synchronised mitotic *FAM83D*$^{GFP/GFP}$ knockin U2OS cells were lysed and subjected to GFP TRAP immunoprecipitation (IP), followed by incubation ± λ-phosphatase. Asynchronous (AS) cells were used as a control. Whole cell extracts (Input) and IP samples were subjected to SDS-PAGE and subsequent immunoblotting (IB) with the indicated antibodies (n=3). **B:** STLC-synchronised mitotic wild-type U2OS cells were lysed at the indicated time points following STLC washout. AS cells were used as a control. Lysed extracts were subjected to IB with the indicated antibodies (n=3). **C:** As in B. except that cells were released into medium ± MG132 (n=3). **D:** As in C. except that ProTAME was used instead of MG132 (n=3). **E:** Wild-type U2OS cells were either left asynchronous (AS), or arrested in mitosis with STLC and collected by shake-off (M). AS and M STLC-arrested cells were incubated in media containing combinations of RO-3306 and MG132 as indicated, prior to lysis. MG132 was applied for 1.5 h, whereas RO-3306 was applied for the last 1 h of incubation prior to lysis. Samples were lysed and extracts were subjected to SDS-PAGE, before IB with the indicated antibodies (n=3).

degradation, CK1α can no longer localise to the spindle and subsequently dissociates into the cytoplasm.

In line with this proteolytic degradation hypothesis, the reduction in FAM83D and HMMR protein levels following STLC washout could be blocked with MG132 (Figure 4-13C), suggesting that both FAM83D and HMMR may indeed undergo proteasomal

degradation following mitotic exit. As expected, Cyclin B1 levels were also rescued by MG132 treatment (Figure 4-13C). As MG132 is also known to inhibit the metaphase-to-anaphase transition through the stabilisation of the anaphase-promoting complex/cyclosome (APC/C) E3 ligase substrate securin (Chang et al., 2003), this transitional delay could also potentially explain the lack of phospho-FAM83D and HMMR degradation in the presence of MG132. Indeed, analogous results on phospho-FAM83D and HMMR stabilisation were observed when STLC-arrested cells were released into medium containing the APC/C inhibitor ProTAME (Zeng, Sigoillot et al., 2010) (Figure 4-13D). The protein levels of CK1α were unaffected by either MG132 or ProTAME treatments (Figure 4-13C&D). In an attempt to confirm that the mitotic post-translational machinery triggers FAM83D and HMMR degradation in cells, I first arrested wild-type U2OS cells in mitosis with STLC, and isolated them by mitotic shake-off. Mitotic cells were released into medium containing either the CDK1 inhibitor RO-3306, or DMSO, in the presence or absence of MG132. CDK1 inhibition during mitosis triggers rapid mitotic exit (Vassilev, 2006, Vassilev, Tovar et al., 2006). Forced mitotic exit under these conditions resulted in robust FAM83D, HMMR and Cyclin B1 degradation, whereas the addition of MG132 blocked their proteolysis (Figure 4-13E). Thus, these data suggest that it is the mitotic post-translational machinery that regulates FAM83D and HMMR stability as cells progress through mitosis.

The constitutive interaction between FAM83D and HMMR, along with their apparent synergistic regulation (Figure 4-13), prompted me to investigate a possible role for HMMR in the regulation of the FAM83D-CK1α complex in mitosis (Figure 4-14A). Indeed, as observed in U2OS cells, a robust FAM83D mitotic phospho-mobility shift was evident in wild-type mouse embryonic fibroblasts (MEFs), but this shift was completely absent in *HMMR* knockout MEFs (Figure 4-14B). These data are consistent with the

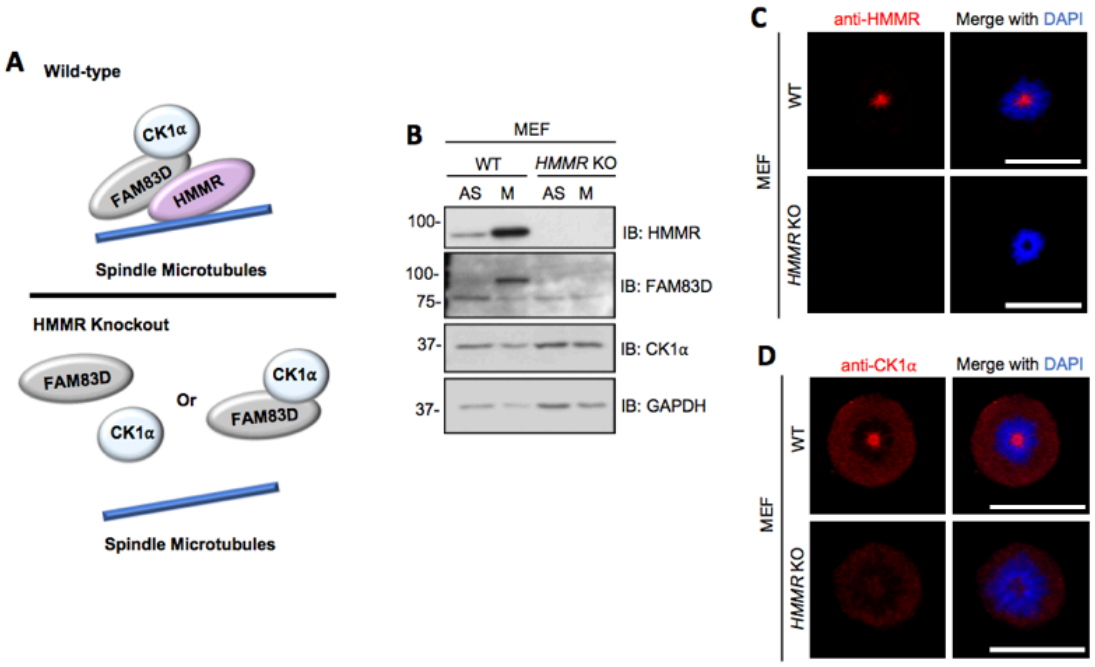

Figure 4-14: The FAM83D-CK1α complex does not localise to the spindle in *HMMR* knockout MEFs: A: Schematic representing the predicted effects of *HMMR* knockout on FAM83D-CK1α delivery to the mitotic spindle. In the absence of HMMR, no FAM83D, and by extension no CK1α, can localise to the spindle. **B:** STLC-synchronised mitotic (M) wild-type (WT) and *HMMR* knockout (KO) mouse embryonic fibroblasts (MEFs) were lysed and subjected to immunoblotting (IB) with the indicated antibodies. Asynchronous (AS) cells were included as a control (n=3). **C-D:** The cells described in B. were STLC-synchronised in mitosis and subjected to immunofluorescence microscopy with an anti-HMMR antibody (C) or an anti-CK1α antibody (D). DNA is stained with DAPI. Scale bars; 20 µM (n=2).

notion that HMMR directs FAM83D to the mitotic spindle, and hence, in the absence of HMMR, FAM83D can no longer localise to the spindle, and is thus not phosphorylated. If this were the case, one would expect that CK1α should not be recruited to mitotic spindles in the absence of HMMR. After first confirming that HMMR localises to the spindle in wild-type, but not *HMMR* knockout MEFs (Figure 4-14C), I examined CK1α localisation within these cells. In line with the working hypothesis, I detected robust

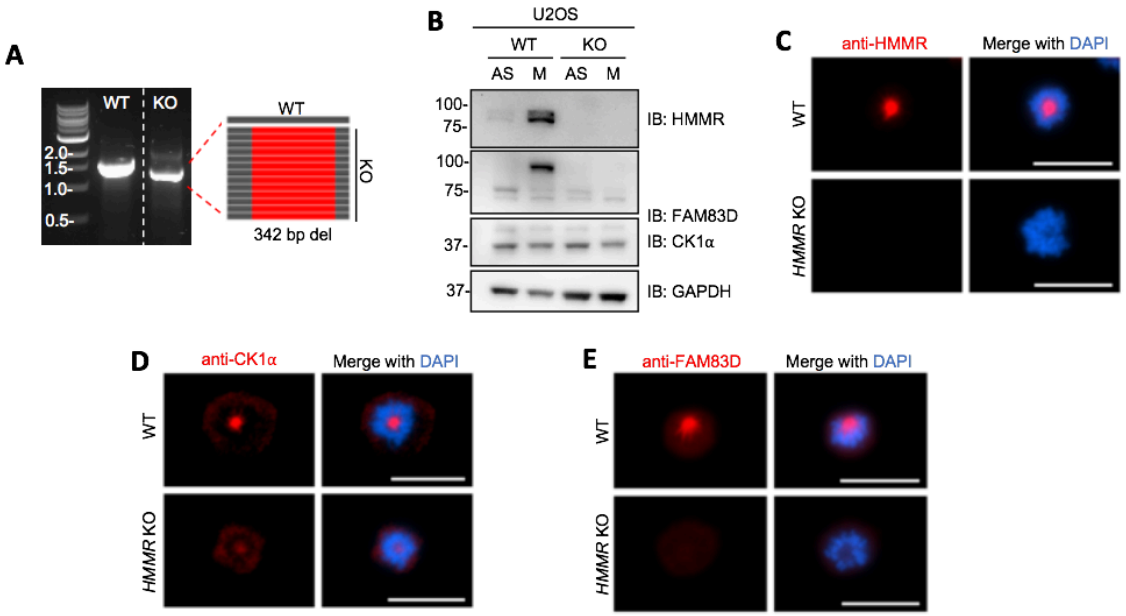

Figure 4-15: Confirming murine observations in *HMMR* knockout U2OS cells: **A:** Amplification of the region spanning the 5'UTR and the intronic region between exons 1 and 2, revealed a deletion in the *HMMR* gene in *HMMR* knockout (KO) cells compared to wild-type (WT) cells, confirmed to be a 342 bp deletion by DNA sequencing. **B**: WT and KO cells were arrested in mitosis (M) with STLC and isolated by shake-off. Asynchronous cells (AS) were included as a control. Samples were lysed and subjected to immunoblotting (IB) with the indicated antibodies (n=3). **C-E**: WT and KO cells were synchronised in mitosis with STLC and stained with antibodies recognising HMMR (C), CK1α (D) and FAM83D (E). DNA is stained with DAPI. Scale bars; 20 µM (n=1).

CK1α staining on mitotic spindles in wild-type MEFs, but not in *HMMR* knockout MEFs (Figure 4-14D).

To confirm that these observations following genetic ablation of *HMMR* were not unique to the mouse, I generated human *HMMR* knockout U2OS cells and confirmed successful knockout of *HMMR* with PCR using genomic DNA as a template (Figure 4-15A), and immunoblotting (Figure 4-15B). DNA sequencing revealed a 342 bp deletion originating within exon 1 of the *HMMR* locus. Consistent with the observations in MEFs,

FAM83D did not undergo mitotic phosphorylation in the absence of HMMR (Figure 4-15B), and both HMMR and CK1α were absent from mitotic spindles (Figure 4-15C-D). While HMMR still localises to the spindle in the absence of *FAM83D* (Figure 4-6C), no FAM83D was detected on spindles in *HMMR* knockout cells (Figure 4-15E).

Collectively, these data add support to the model where HMMR directs FAM83D to the mitotic spindle, and present CK1α as a member of this protein complex. Furthermore, these findings suggest that the mitotic phospho-mobility shift of FAM83D relies on the recruitment of both FAM83D and CK1α to the spindle.

4.2.5: Examining the role of CK1α in FAM83D phosphorylation:

Given the absence of FAM83D(F283A)-GFP mitotic phosphorylation (Figure 4-7C) despite its spindle localisation (Figure 4-8A), I began to wonder whether CK1α may be directly or indirectly involved in FAM83D phosphorylation in mitosis. To test this, I designed an artificial recruitment strategy where CK1α was conjugated to an anti-GFP nanobody (aGFP.16), and examined whether this polypeptide (aGFP.16-CK1α) was capable of recruiting nanobody-bound CK1α to FAM83D(F283A)-GFP in *FAM83D*$^{GFP/GFP\ (F283A)}$ cells, and thereby artificially reconstitute the FAM83D-CK1α complex (Figure 4-16A). Excitingly, expression of aGFP.16-CK1α rescued the phospho-mobility shift of FAM83D(F283A)-GFP, regardless of whether cells were in mitosis or not (Figure 4-16B). I also observed co-precipitation of aGFP.16-CK1α in FAM83D(F283A)-GFP immunoprecipitates (Figure 4-16B). During the course of these experiments, I noticed that this rescued FAM83D(F283A)-GFP mobility shift was slightly smaller than the mitotic mobility shift of FAM83D-GFP (Figure 4.16B). Thus, to confirm that aGFP.16-CK1α was not phosphorylating random residues on FAM83D, I repeated this experiment in wild-type *FAM83D*$^{GFP/GFP}$ U2OS cells. As seen with FAM83D(F283A)-GFP, FAM83D-GFP

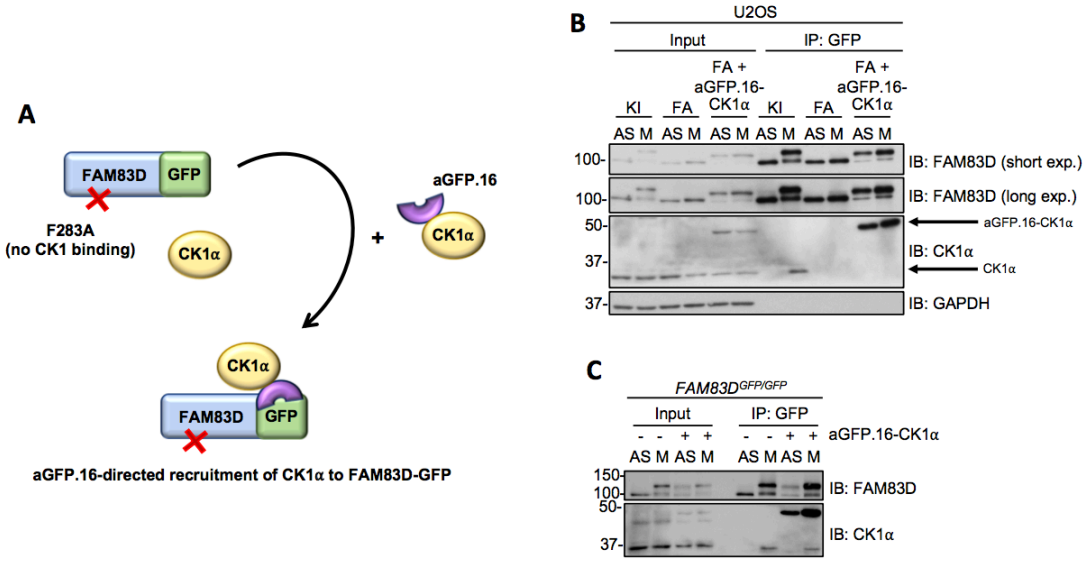

Figure 4-16: Artificial reconstruction of the FAM83D-CK1α interaction in *FAM83D*$^{GFP/GFP\ (F283A)}$ cells restores FAM83D phosphorylation. A: Schematic representation of the anti-GFP nanobody (aGFP.16)-based targeting strategy used to deliver CK1α to the CK1-binding-deficient FAM83D(F283A)-GFP mutant. **B:** STLC-synchronised mitotic *FAM83D*$^{GFP/GFP}$ knockin (KI), *FAM83D*$^{GFP/GFP\ (F283A)}$ (FA), and *FAM83D*$^{GFP/GFP\ (F283A)}$ stably expressing aGFP.16-CK1α (FA + aGFP.16-CK1α) U2OS cells were subjected to anti-GFP immunoprecipitation (IP), followed by immunoblotting (IB) with the indicated antibodies. Asynchronous (AS) cells were used as controls (n=3). **C:** As in B, except that the aGFP.16-CK1α was targeted to wild-type FAM83D-GFP in *FAM83D*$^{GFP/GFP}$ knockin U2OS cells (n=3).

also exhibited a constitutive phospho-mobility shift, regardless of cell cycle stage (Figure 4-16C). Crucially, the aGFP.16-CK1α-induced phospho-shift migrated to the same level as the mitotic FAM83D-GFP in control cells (Figure 4-16C). Thus, as there is no apparent larger mitotic mobility shifts when wild-type FAM83D-GFP is bound to aGFP.16-CK1α, I attribute the slight reduction in mobility seen with the aGFP.16-CK1α-bound FAM83D(F283A)-GFP mutant to potential conformational defects resulting from the F283A mutation, potentially occluding one or more of the phospho-acceptor residues from aGFP.16-CK1α.

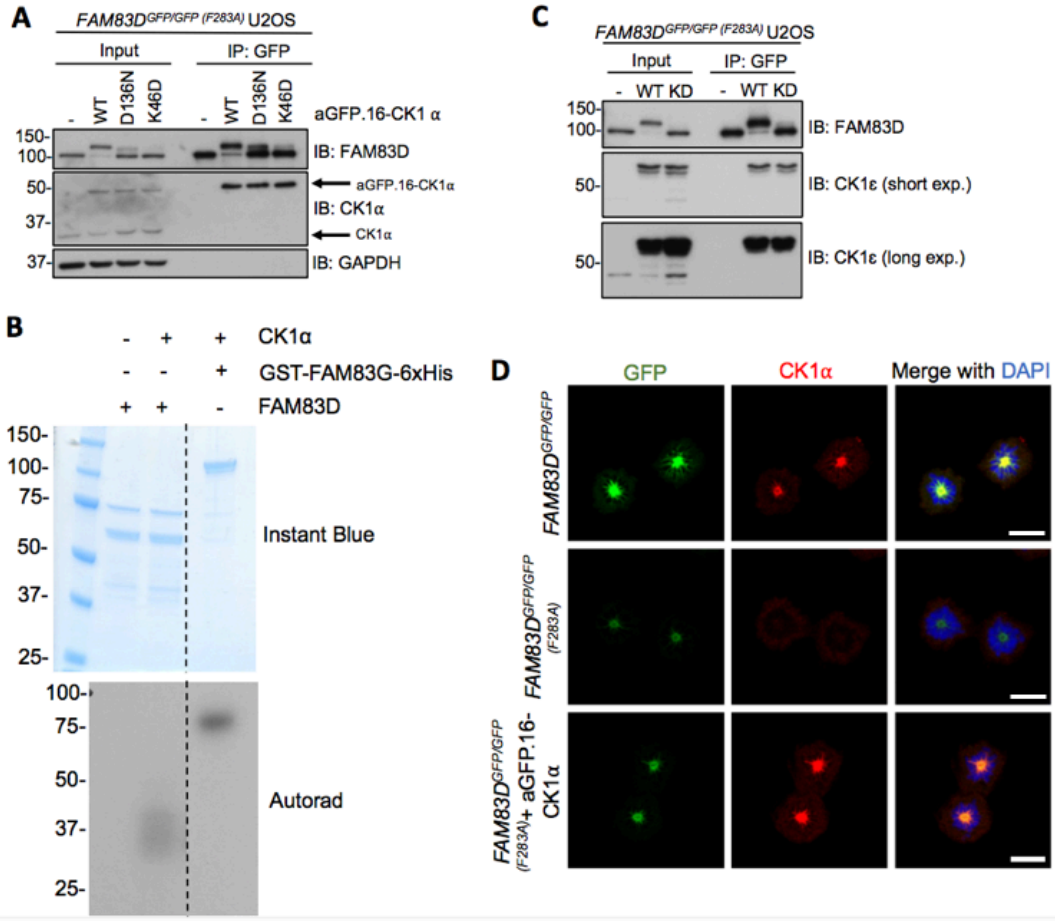

Figure 4-17: CK1 catalytic activity appears to be critical for mitotic FAM83D phosphorylation: A: *FAM83D*$^{GFP/GFP\ (F283A)}$ U2OS cells were infected with retroviruses encoding wild-type aGFP.16-CK1α (WT), or aGFP.16-CK1α with one of two distinct CK1α kinase-inactive mutants (D136N or K46D). Uninfected cells (-) were included as a control. Cells were lysed, subjected to anti-GFP IP and IB with the indicated antibodies (n=3). **B:** An *in vitro* kinase assay was set up using recombinant GST-FAM83D, and GST-CK1α. GST-FAM83D without CK1α is a negative control. Recombinant GST-FAM83G-6xHis serves as a positive control for CK1α activity. Following incubation with [γ^{32}P]-ATP, reactions were stopped and subjected to SDS-PAGE. The gel was stained with InstantBlue and imaged, before being subjected to autoradiography (autorad) (n=3). **C:** *FAM83D*$^{GFP/GFP\ (F283A)}$ cells were infected with retroviruses encoding wild-type aGFP.16-CK1ε (WT), or a kinase-dead aGFP.16-CK1ε (D128N) mutant (KD). Uninfected cells (-) were included as a control. Cells were lysed, subjected to anti-GFP IP and IB with the indicated antibodies (n=3). **D:** STLC-synchronised mitotic *FAM83D*$^{GFP/GFP}$ knockin, *FAM83D*$^{GFP/GFP\ (F283A)}$, and *FAM83D*$^{GFP/GFP\ (F283A)}$ stably expressing aGFP.16-CK1α U2OS cells were fixed and stained using anti-CK1α antibody. DNA is stained with DAPI. Scale bar; 20 µM (n=2).

The phosho-mobility shift of FAM83D(F283A)-GFP restored through the targeted delivery of aGFP.16-CK1α relied on CK1α catalytic activity, as two catalytically inactive

mutants of CK1α (K46D and D136N) failed to fully restore the phospho-mobility shift (Figure 4-17A). Indeed, a smaller, less intense phospho-mobility shift was observed when these aGFP-CK1α mutants were recruited to FAM83D(F283A)-GFP, however, it should be noted that even if these mutations leave CK1α with a small amount of residual catalytic output, that may be sufficient to induce partial phosphorylation when artificially forcing the constitutive interaction between these proteins. Alternatively, the interaction between FAM83D and CK1α may be required to present FAM83D to a priming kinase(s), prior to the final phosphorylation step(s) by CK1α. In agreement with a requirement for a priming kinase, under conditions where recombinant CK1α could phosphorylate purified FAM83G *in vitro*, it failed to phosphorylate recombinant FAM83D (Figure 4-17B). Interestingly, when wild-type CK1ε, which does not interact with FAM83D nor localise to the spindle, was delivered to FAM83D(F283A)-GFP by aGFP.16, it too rescued the FAM83D phospho-mobility shift (Figure 4.17C). Thus, the proximal catalytic activity of CK1 appears sufficient for the FAM83D phospho-shift, and this observation highlights the notion that subcellular localisation and substrate association are important determinants for CK1 targets in cells. Importantly, robust co-localisation between FAM83D(F283A)-GFP and aGFP.16-CK1α on intact mitotic spindles was observed (Figure 4-17D), suggesting that the aGFP.16-CK1α is binding the FAM83D(F283A)-GFP target within cells, and not just in extracts.

Through delivering CK1α to the mitotic spindle, it is likely that FAM83D acts to position CK1α for phosphorylation of mitotic CK1α substrates, including FAM83D itself. However, this hypothesis relies on CK1α being catalytically active when bound to FAM83D in mitosis. To examine the catalytic status of FAM83D-bound CK1α, I employed

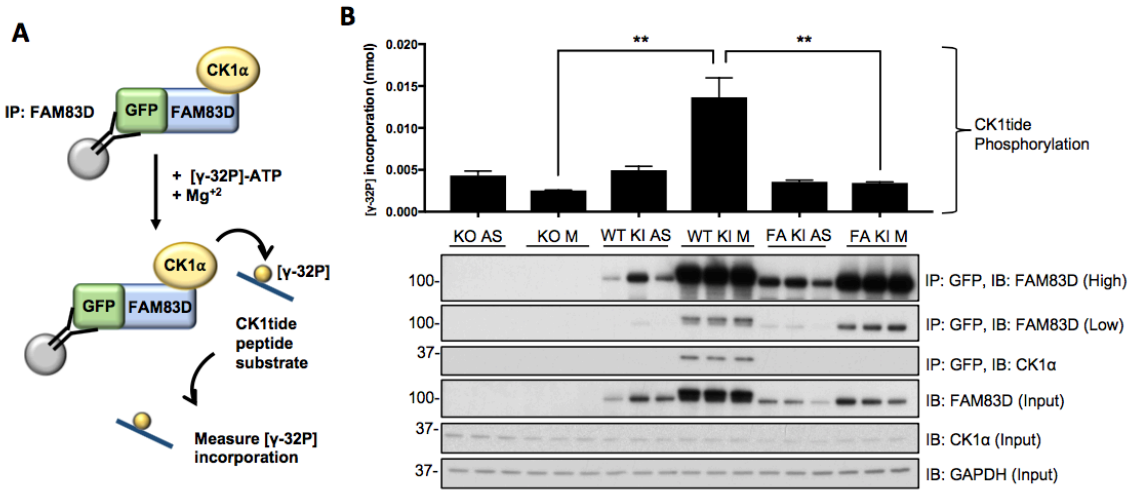

Figure 4-18: FAM83D-bound CK1α is a catalytically-active kinase: A: Schematic depicting the IP kinase assay strategy used to test whether FAM83D-bound CK1α was catalytically active. **B:** *FAM83D* knockout (KO), *FAM83D*$^{GFP/GFP}$ knockin (KI), and *FAM83D*$^{GFP/GFP\ (F283A)}$ knockin (FA) U2OS cells were synchronised in mitosis (M) using STLC. Lysed extracts were subjected to anti-GFP IPs, followed by [γ-32P]-ATP kinase assays, using an optimised CK1 substrate peptide (CK1tide). Asynchronous (AS) cells were used as controls. Error bars, SEM; *P*<0.01; ANOVA (n=3). Input and IP samples were analysed by IB with the indicated antibodies.

an immunoprecipitation-based *in vitro* kinase assay strategy, in order to isolate the FAM83D-CK1α complex, and subsequently measure phosphorylation of an optimised substrate peptide (CK1tide) in the presence of [γ-^{32}P]-ATP (Figure 4-18A). Excitingly, when anti-GFP immunoprecipitates from *FAM83D* knockout, *FAM83D*$^{GFP/GFP}$, and *FAM83D*$^{GFP/GFP\ (F283A)}$ U2OS cells were subjected to these kinase assays, only those from mitotic FAM83D-GFP extracts, which co-precipitated endogenous CK1α, displayed significant kinase activity towards CK1tide (Figure 4-18B), suggesting that FAM83D-bound CK1α functions as an active kinase.

4.2.6: The HMMR-FAM83D-CK1α complex regulates spindle positioning:

Throughout the course of these experiments, I have generated data supporting a model where the HMMR-FAM83D-CK1α complex localises to the mitotic spindle, and in doing so, acts to direct an active kinase to the spindle apparatus for, presumably, phosphorylation-mediated control of mitosis. Thus, I set out to identify where in the cell division pathway this protein complex may act. Separately, FAM83D, and CK1α have been implicated in mitotic resolution, and correct spindle/chromosome alignment (Dunsch et al., 2012, Gross, Simerly et al., 1997, Santamaria et al., 2008, Wang et al., 2013). So, I sought to test whether FAM83D and CK1α act in the same pathway in mitosis. To achieve this, a collaboration was initiated with the Maxwell laboratory (University of British Columbia), who previously identified a role for the FAM83D-interacting protein HMMR in spindle positioning.

Compared to wild-type and *FAM83D*$^{GFP/GFP}$ U2OS cells, there was a significant delay in the metaphase-to-anaphase transition in *FAM83D* knockout and *FAM83D*$^{GFP/GFP\ (F283A)}$ cell lines (Figure 4-19A-C). When spindle orientation was analysed in these cells, spindles orientated at a fixed angle in knockout and *FAM83D*$^{GFP/GFP\ (F283A)}$ cells (Figure 4-19D, yellow lines), consistent with the phenotype described following siRNA-mediated depletion of *FAM83D* (Dunsch et al., 2012). The position of the cell-division axis at anaphase, relative to its expected position aligned with the long cell axis in interphase, deviated significantly in *FAM83D*$^{-/-}$ and *FAM83D*$^{GFP/GFP\ (F283A)}$ cells, compared to wild-type and *FAM83D*$^{GFP/GFP}$ cells (Figure 4-20A&B). Excitingly, this phenotype in *FAM83D*$^{-/-}$ cells was rescued when *FAM83D cDNA* was restored at the endogenous *FAM83D* locus, with full rescue observed when restored FAM83D expression was comparable to that of wild-type cells (rescue clone 6) and a partial rescue observed when restored FAM83D expression was lower than that of wild-type cells (rescue clone 11) (Figure 4-20A&B).

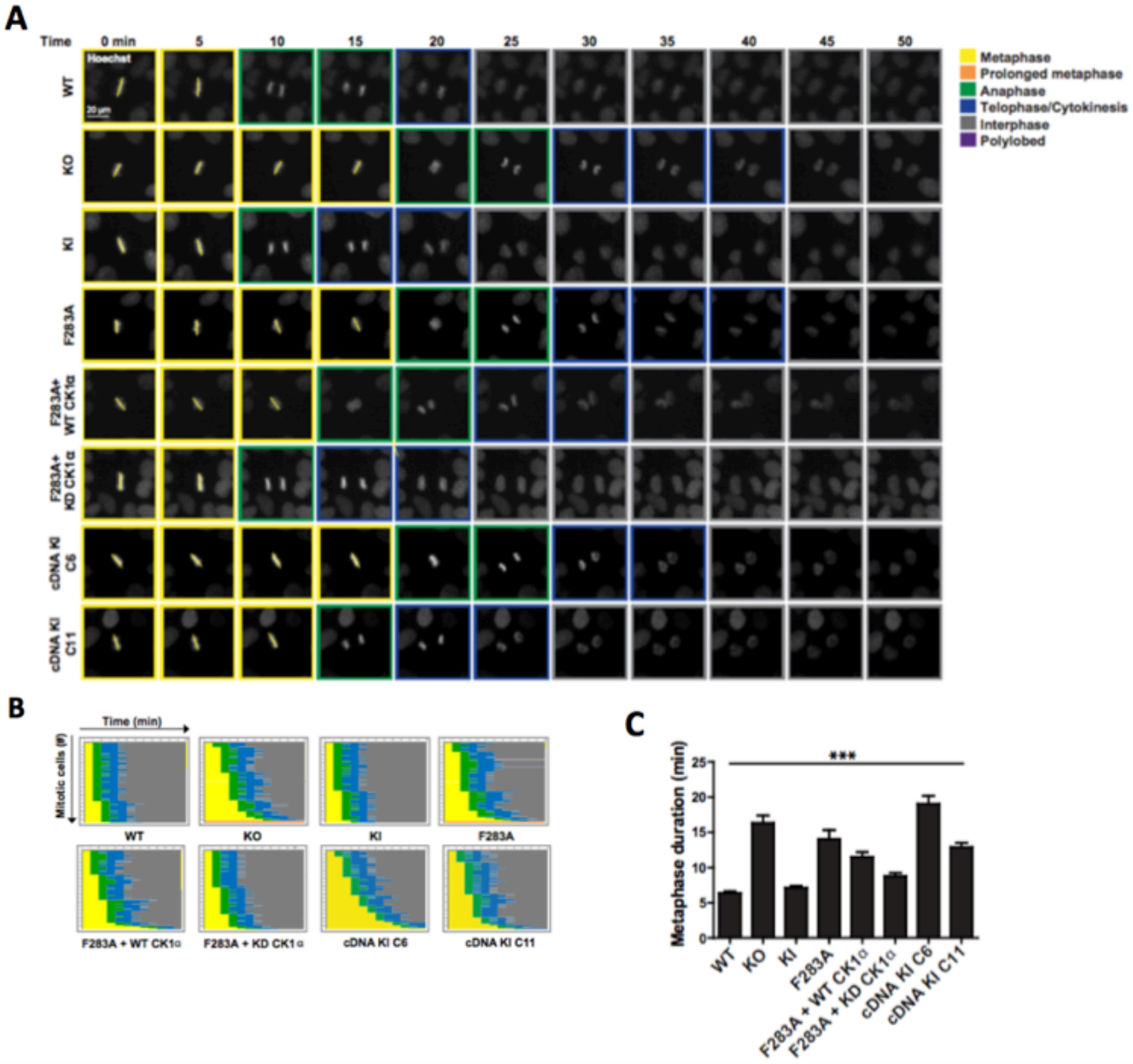

Figure 4-19: The metaphase-to-anaphase transition duration is increased following ablation of CK1α spindle recruitment: A: Representative images initiating at metaphase for the indicated mitotic U2OS cell lines stained with Hoechst, taken every 5 min as they progress through division. Mitotic stage was determined by chromosome condensation and is indicated by the coloured boxes. Scale bar; 20 µm. **B:** Graphical representation for the kinetics of transition from metaphase alignment (yellow) to anaphase (green), and cytokinesis (blue). 100 mitotic cells per genotype are plotted; n=2. **C:** Length of time needed to transition from metaphase to anaphase. Mean of 100 mitotic cells per genotype are plotted; n=2. Error bars, SEM. ***, *P*< 0.0001; ANOVA (*credit: Zhengcheng He*).

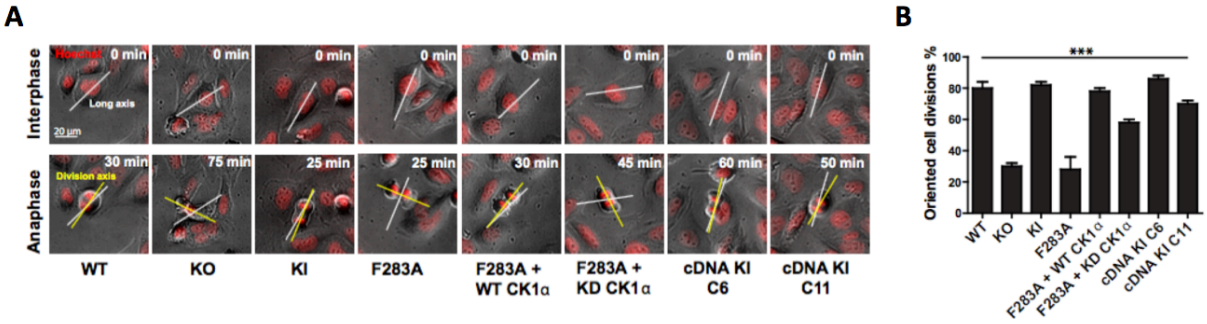

Figure 4-20: Absence of spindle-localised CK1α causes spindle mispositioning: A: Representative bright field images for the mitotic U2OS cell lines, indicating the long axis during interphase (white line) preceding mitosis, and the division axis determined at anaphase (yellow line). DNA is stained with Hoechst. Scale bar; 20 µm. **B**: Percentage of oriented divisions for U2OS cells grown in subconfluent cultures. An oriented division axis was defined as being less than 30° removed from the long axis of the interphase cell. Mean of 50 cells per genotype are plotted, n=2. Error bars, SEM. ***, *P*< 0.0001; ANOVA. (*credit: Zhengcheng He*).

In order to better study the process of spindle orientation in these cell lines, individual *FAM83D*$^{-/-}$, *FAM83D*$^{GFP/GFP}$ or *FAM83D*$^{GFP/GFP\ (F283A)}$ U2OS cells were seeded onto L-shaped fibronectin-coated micropatterns, which cause cells to position their spindle on a defined axis (Thery et al., 2005), and measured the angles of spindle orientation. Whereas wild-type and *FAM83D*$^{GFP/GFP}$ cells orientated their spindles along the defined, predicted axes, significant deviations in the predicted spindle orientation axes were observed in *FAM83D*$^{-/-}$ and *FAM83D*$^{GFP/GFP\ (F283A)}$ cells (Figure 4-21A), with near 80% unable to orientate their spindles correctly (Figure 4-21B). As seen with the previous spindle orientation experiments (Figure 4-20A&B), this phenotype in the *FAM83D*$^{-/-}$ cells was fully rescued in *FAM83D* cDNA knockin rescue clone 6, and partially in clone 11 (Figure 4-21A&B).

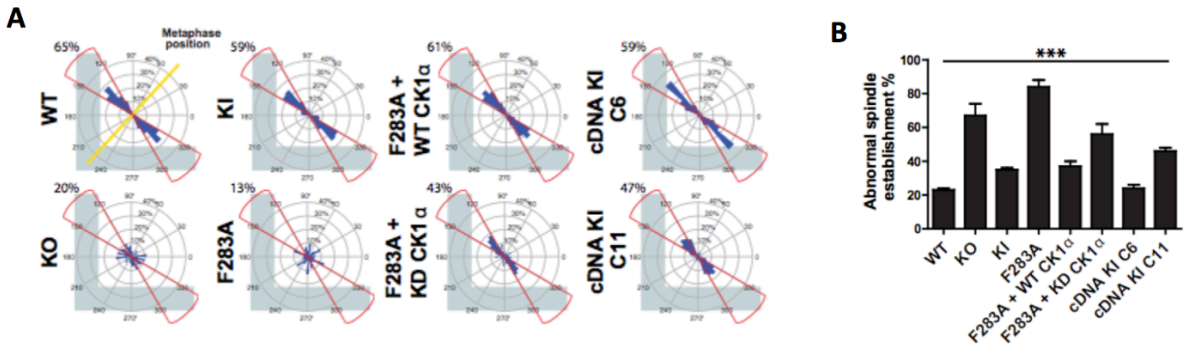

Figure 4-21: Cells devoid of spindle-localised CK1α fail to orientate their spindles on L-shaped micropatterns: A: Circular graphs, superimposed on L-shaped micropatterns, show the distribution of cell division angles measured at anaphase. Angles for 100 U2OS cells are plotted per cell line, n=2. Metaphase plate position is indicated (yellow line) and the percentages of division angles ± 15° from the expected axis (red line) are indicated. **B:** Percentage of metaphase U2OS cells that align chromosomes outside of the expected axis (angles ± 15°). Mean of 100 cells per genotype are plotted, n=2. Error bars, SEM. ***, *P*< 0.0001; ANOVA (*credit: Zhengcheng He*).

During the process of analysing spindle positioning in these cell lines, a random orientation of the initial spindle position was observed, which is normally directed by the position of retraction fibers (Thery et al., 2007) and the assembly of subcortical actin (Fink et al., 2011, Kwon, Bagonis et al., 2015). Thus, actin dynamics were examined in these cells. To monitor actin dynamics during the process of spindle assembly and orientation, cells were transfected with actin-Red Fluorescent Protein (RFP) prior to seeding cells onto L-shaped fibronectin-coated micropatterns (Figure 4-22A). In wild-type cells, subcortical actin was polarised adjacent to the right angle of the L-shape following DNA condensation through to anaphase (Figure 4-22B). However, actin appeared to be randomly organised with respect to the micropattern in *FAM83D*$^{-/-}$ and *FAM83D*$^{GFP/GFP\ (F283A)}$ cells during the spindle-assembly process (Figure 4-22B). This observation in *FAM83D*$^{-/-}$ cells was rescued in *FAM83D* cDNA knockin clone 6, and

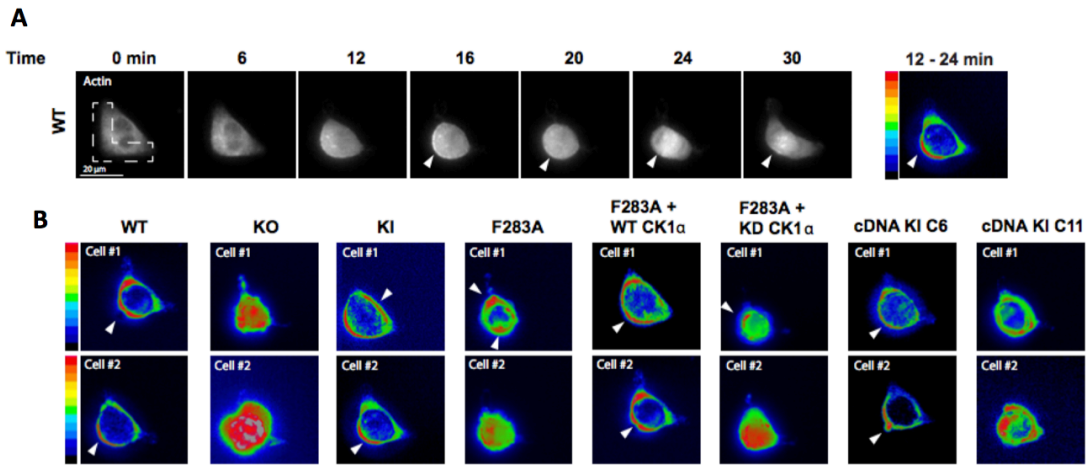

Figure 4-22: Cells devoid of spindle-localised CK1α present with disordered subcortical actin cytoskeletons: A: Representative images of RFP-actin localisation in mitotic U2OS cells grown on fibronectin-coated, L-shaped micropatterns, which is superimposed. Arrowheads indicate polarised cortical actin. Heatmap shows the intensity of RFP-actin localisation (Image J z-projection standard deviation) as the cell progresses from prophase to metaphase (12-24 min). Scale bar; 20 µm. **B:** Heatmap additive intensities of RFP-actin localisation in two representative mitotic U2OS cells for each cell line grown on fibronectin-coated, L-shaped micropatterns. Arrowheads indicate polarised cortical actin (*credit: Zhengcheng He*).

partially in clone 11 (Figure 4-22B). *FAM83D*$^{GFP/GFP}$ cells organised their actin in a manner comparable to that seen in wild-type cells (Figure 4-22B).

The targeted delivery of wild-type or kinase-dead (K46D) CK1α to FAM83D-GFP (F283A) in knockin cells, using the aGFP.16-CK1α strategy (Figure 4-16A), notwithstanding the potential caveats of overexpression, allowed us to explore the role of CK1α catalytic activity in metaphase length and spindle orientation. Delivery of both wild-type and kinase-dead aGFP.16-CK1α resulted in shortening of the metaphase delay observed in *FAM83D*$^{GFP/GFP\ (F283A)}$ cells (Figure 4-19A-C). However, the spindle orientation defect in *FAM83D*$^{GFP/GFP\ (F283A)}$ cells was rescued completely with aGFP.16-CK1α, whereas

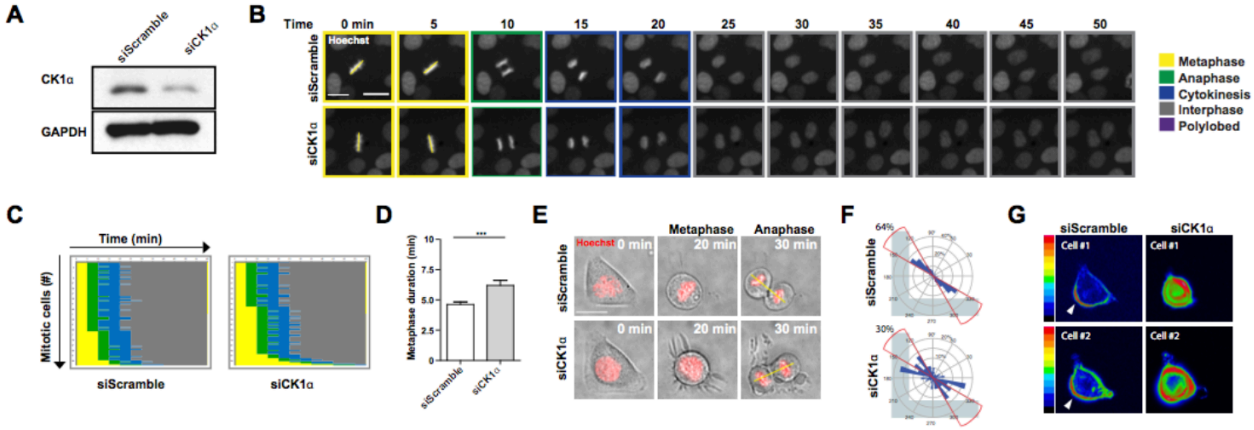

Figure 4-23: siRNA knockdown of CK1α phenocopies the effects of *FAM83D* knockout on spindle positioning: A: Immunoblot analysis of U2OS cell extracts 48 h after treatment with scrambled siRNA (siScramble) controls or siRNA targeting CK1α (siCK1α). **B:** Representative images of mitotic U2OS cells stained with Hoechst, beginning at metaphase and taken every 5 min as they progressed through division. Mitotic stage was determined by chromosome condensation and is indicated by the coloured boxes. Scale bar; 20 µm. **C:** Graphical representation of the kinetics of transition from metaphase alignment (yellow) to anaphase (green), and cytokinesis (blue), determined by the morphology of chromosomes and daughter cells, respectively. The kinetics of 100 mitotic cells per genotype are plotted as measured for 50 cells per experiment from 2 independent experiments. **D:** Length of time needed to transition from metaphase to anaphase. Mean ± SEM is plotted for 2 independent experiments, which each measured 50 mitotic cells per genotype (n = 100 mitotic cells per genotype total). *** p< 0.0001, Student's *T*-test. **E:** Representative images of mitotic U2OS cells stained with Hoechst and grown on L-shaped micropatterns previously coated with fibronectin. The cell division angle at anaphase is indicated (yellow line). Scale bar; 20 µm. **F:** Circular graphs, superimposed on a L-shaped micropattern, show the distribution of cell division angles measured at anaphase. Angles are plotted for 100 U2OS cells per genotype measured from 2 independent experiments. The percentages of division angles ± 15° from the expected axis (red line) are indicated. **G:** Heatmap additive intensities of RFP-actin localisation in two representative mitotic U2OS cells for each genotype grown on fibronectin-coated, L-shaped micropatterns. Arrowheads indicate polarised cortical actin (*credit: Zhengcheng He*).

only partially with the kinase-dead aGFP.16-CK1α, in both sub-confluent cultures (Figure 4-20A&B) and L-shaped micropatterns (Figure 4-21A&B). Actin was correctly polarised

in *FAM83D*$^{GFP/GFP\ (F283A)}$ cells rescued with wild-type, but not with the kinase-dead aGFP.16-CK1α (Figure 4-22B).

Similar spindle mis-positioning and actin cytoskeletal defects were observed when CK1α was knocked down using siRNA oligonucleotides (Figure 4-23), reinforcing the notion that FAM83D and CK1α act together within the same pathway in mitosis.

During the course of performing these phenotypic assays, frequent plasma membrane blebbing on one of the daughter cells in *FAM83D*$^{-/-}$ and *FAM83D*$^{GFP/GFP\ (F283A)}$ cells was also observed, at the latter stages of mitosis. This phenomenon, known as asymmetric membrane elongation (AME), is a compensatory mechanism to ensure equal distribution of cell size following mitosis, when the spindle is misorientated (Kiyomitsu & Cheeseman, 2013). Live cell-microscopy confirmed blebbing in *FAM83D*$^{-/-}$ and *FAM83D*$^{GFP/GFP\ (F283A)}$ cells, but not in wild-type, or *FAM83D*$^{GFP/GFP}$ cells, or in both clones rescued through knockin of *FAM83D* cDNA into the endogenous *FAM83D* locus in the *FAM83D*$^{-/-}$ background (Figure 4-24A-B). Reduction of blebbing in *FAM83D*$^{GFP/GFP\ (F283A)}$ cells to levels seen in wild-type cells was observed when cells were rescued with wild-type aGFP.16-CK1α whereas an intermediate phenotype was observed with the kinase-dead aGFP.16-CK1α rescue (Figure 4-24B).

Importantly, there was no difference in daughter cell size between all cell lines (Figure 4-24C), suggesting that the observed AME compensatory mechanism was functioning correctly.

Taken together, these data indicate the FAM83D-CK1α interaction is critical for timely mitotic progression, including the processes of orienting both the mitotic spindle and the concurrent cell division axis.

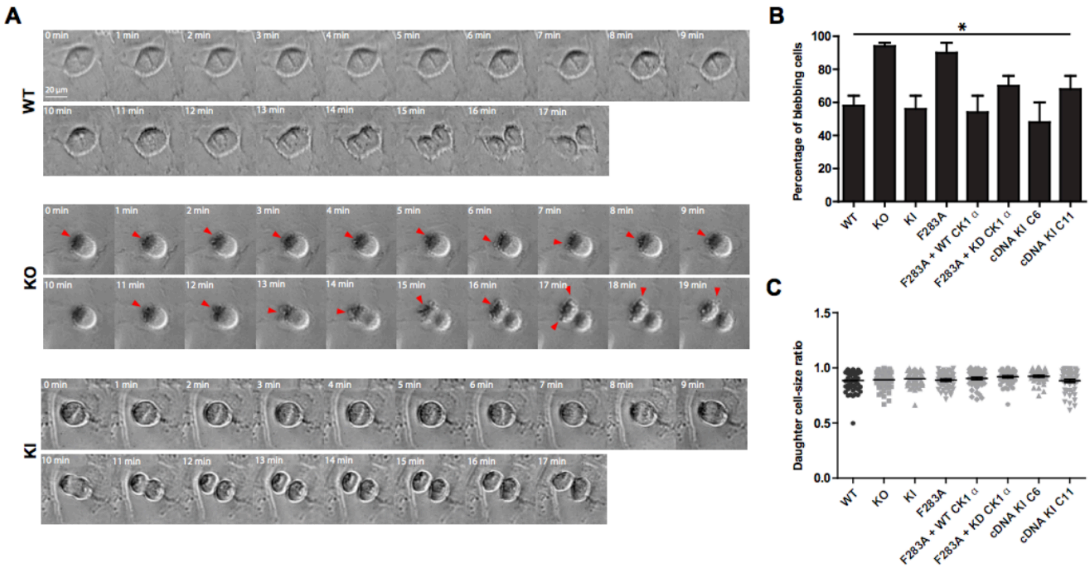

Figure 4-24: Asymmetric membrane elongation is prevalent in cells devoid of spindle-localised CK1α: A: Representative bright field images initiating at metaphase for mitotic U2OS cells taken every 1 min as they progress through division. Asymmetric membrane elongation, or membrane blebbing, is indicated by red arrowheads and only occurred on one daughter cell. Scale bar; 20 µm. **B**: Percentage of mitotic cells that displayed membrane blebbing. Mean of 50 cells per genotype are plotted from 2 independent experiments. Error bars; SEM. * *P*< 0.005, ANOVA. **C**: Daughter cell size ratio following U2OS cell division remains unchanged. Mean of 50 cells per genotype are plotted from 2 independent experiments. Error bars; SEM (*credit: Lin Mei*).

4.3: Conclusions:

Correctly orientated cell division, primarily achieved through the proper positioning of the mitotic spindle, is crucial for both normal development, and maintenance of healthy tissues. (Fleming, Temchin et al., 2009, Kiyomitsu & Cheeseman, 2012, Konno, Shioi et al., 2008, Lu & Johnston, 2013). By conclusively placing CK1α at the mitotic spindle, and demonstrating that spindle-localised CK1α appears to regulate spindle positioning and timely cell division, these data present strong evidence for CK1α as a new player in the phosphorylation-mediated control of mammalian mitosis. Interestingly, the mechanism by which FAM83D acts to bind and direct CK1α to mitotic spindles draws parallels with the way TPX2 recruits and regulates Aurora Kinase A during

mitosis (Bayliss et al., 2003, Chen et al., 2014). While interacting partners of FAM83D, including HMMR and DYNLL1, offer insights into how FAM83D localises to the mitotic spindle to recruit CK1α, the full extent of CK1α substrates that potentially mediate proper spindle positioning, to ensure error-free progression through mitosis, remain to be defined. Furthermore, exactly how the spindle-localised FAM83D-CK1α complex can appear to regulate the spatially-distinct actin network during mitosis remains to be determined. However, phosphorylation of CK1α substrates could trigger their translocation from the spindle to the actin network, or indeed anywhere within the cell, either directly or indirectly. Nonetheless, the findings that the FAM83D-CK1α complex acts at the mitotic spindle add to the evidence for intricate subcellular regulation of CK1 isoforms by FAM83 proteins (Bozatzi et al., 2018, Fulcher et al., 2018, Kuga et al., 2016a, Kuga et al., 2013).

Traditionally, when one thinks of mitotic kinases, CK1 isoforms do not get mentioned, with prominent names such as Cyclin-dependent kinases (CDKs), Aurora kinases, Polo-like kinase (PLKs) and Nima-related kinases (NEKs) stealing the cell division lime light (Nigg, 2001). However, given the reported participation of CK1 isoforms in such diverse biological processes (see section 1.2.4), it is perhaps not surprising that some studies have explored and reported on roles for CK1α in the cell-division cycle. From as early as 1992, CK1α has been reported to localise to the mitotic spindle apparatus (Brockman et al., 1992), and large-scale mitotic spindle proteomic studies have also identified CK1α as a spindle-localised protein (Sauer et al., 2005). More recently, anti-CK1α antibodies injected into the cytosol of developing mouse embryos was shown to result in either complete abolition of, or a significant delay in, progression to the first mitotic cleavage (Gross et al., 1997). Interestingly, CK1α morpholino injection in mouse oocytes resulted in meiotic chromosomal alignment and congression defects

(Wang et al., 2013). However, these studies lacked any mechanistic understanding into how CK1α regulated these processes. Interestingly, CK1 activity in *C. elegans* embryos was shown to regulate spindle positioning through regulating force generation at the cell cortex (Panbianco, Weinkove et al., 2008). However, FAM83D and the other FAM83 proteins are not conserved in invertebrates, thus there will likely be some differences in the way CK1 regulates spindle positioning in this context.

Beyond CK1α, the phosphorylation-mediated control of spindle positioning has been attributed to several other protein kinase families. Of note, the activity of CDKs, PLKs, and Aurora kinases have all been shown to be critically important in regulating spindle orientation (Chen et al., 2014, Connell et al., 2017, Enserink & Kolodner, 2010, Gallini, Carminati et al., 2016, Johnston, Hirono et al., 2009, Kotak, Afshar et al., 2016, Ly, Ahmad et al., 2014, Sana, Keshri et al., 2018, Tame et al., 2016). Both their recruitment to the mitotic spindle, and their activities once they are recruited there are tightly regulated (Bayliss et al., 2003, Chen et al., 2014, Enserink & Kolodner, 2010, Golsteyn et al., 1995). In the case of PLK1, the centrosomal PLK1 pool regulates spindle positioning through the PLK1-dependent spindle positioning pathway, and acts to strip Dynein/NuMA from the cortex when the spindle pole gets too close to the cortex (Kiyomitsu & Cheeseman, 2012). PLK1 itself is regulated downstream of CDK1 and Aurora A, illustrating some of the crosstalk evident between these mitotic kinases (Macurek et al., 2008). Thus, the concerted action of mitotic kinases likely functions within a tightly controlled phosphorylation-network to ensure the correct and efficient orientation of the mitotic spindle. Given the requirement for a priming phosphorylation event for many CK1 substrates, it is highly likely that such cross-talk also extends to mitotic CK1α substrates. Future efforts aimed at elucidating these mitotic CK1α substrates, and examining if they too are subject to co-regulation by other mitotic

kinases, will further decipher the intricate phospho-controlled network evident in the mammalian cell cycle, and help to establish which branches of the pathway would be most suitable to small molecule-based inhibition in disease.

5. An Affinity-directed PROtein Missile (AdPROM) system for targeted degradation of endogenous proteins:

5.1: Background:

Studying protein function at the endogenous level remains the gold standard in biomedical research. However, for many proteins, studying them at the endogenous level is not always feasible, and is dependent on numerous factors. Such factors can include the absence of a robust antibody that recognises the target protein of interest, or lack of detectable catalytic activity to assay. Furthermore, if the protein of interest is required for cell viability, genetic ablation experiments are often very challenging, if not impossible, to accomplish (Wang, Birsoy et al., 2015). As FAM83 proteins are a fairly novel, largely uncharacterised family of proteins, commercially-available tools to study them are somewhat scarce. Thus, in combination with generating specific antibodies for each FAM83 member, I sought to design and implement novel technologies to aid me in the investigation of FAM83 biology, and beyond. Here, I sought to develop a proteolytic methodology, to aid us in studying FAM83 function.

The degradation of many proteins by the ubiquitin-proteasome system (UPS) is crucial for maintenance of cellular homeostasis, and plays a fundamental role in protein turnover (Adams, 2003, Budenholzer, Cheng et al., 2017, Tanaka, 2009). The UPS centres around the sequential action of E1 ubiquitin-activating enzymes, E2 ubiquitin-conjugating enzymes, and E3 ubiquitin ligases which attach the small protein ubiquitin onto target proteins (Adams, 2003, Budenholzer et al., 2017, Nandi, Tahiliani et al., 2006, Tanaka, 2009). Subsequently, additional ubiquitin molecules can be conjugated to the existing ubiquitin on the monoubiquitinated protein, creating a chain of ubiquitins

on the target protein, with distinct chain types being linked to specific biological processes (Akutsu, Dikic et al., 2016, Komander & Rape, 2012, Pickart & Eddins, 2004). For example, and of relevance here, ubiquitins linked in a lysine 48-linked manner mark proteins for degradation via the proteasome (Akutsu et al., 2016, Komander & Rape, 2012, Pickart & Eddins, 2004).

The human genome encodes two E1 enzymes, around 50 E2 enzymes, and over 600 E3 ubiquitin ligases (Li, Bengtson et al., 2008, Wenzel, Stoll et al., 2011, Zhao, Bhuripanyo et al., 2012). The substrate specificity of the UPS is conferred through substrate-recognition elements within the E3 ligase complexes (Bulatov & Ciulli, 2015, Jackson, Eldridge et al., 2000). The Cullin RING (really interesting new gene) E3 ligases (CRLs) constitute the largest family of UPS-contributing E3 ligases. The CRL family is comprised of seven evolutionarily conserved members, designated CUL1, CUL2, CUL3, CUL4A, CUL4B, CUL5 and CUL7 (Bulatov & Ciulli, 2015, Zheng, Schulman et al., 2002). All cullins share similar structural and catalytic features, and are bound in a complex with selective adaptor and substrate-recognition subunits, as well as one RING E3 ligase protein, either RBX1 or RBX2 (Bulatov & Ciulli, 2015, Cardote, Gadd et al., 2017, Zhao & Sun, 2013, Zheng et al., 2002). CRLs are activated through the post-translational process of NEDDylation, which acts to covalently attach the small ubiquitin-like modifier NEDD8 onto lysine residues within the Cullin backbone (Enchev, Schulman et al., 2015). NEDDylation, like ubiquitination, requires its own cognate E1, E2 and E3 enzymes, which sequentially function to activate and ligate the NEDD8 molecule onto the Cullin (Enchev et al., 2015). A selective inhibitor of the NEDD8-activating enzyme, MLN4924, inhibits the activation of CRLs in cells, and thereby blocks the ubiquitination of CRL substrates, thus preventing their degradation (Soucy, Smith et al., 2009). Upon binding to the cognate substrate receptor subunit, the CRL substrate is positioned in close proximity to

the RBX1/2 RING E3 ligase and its associated E2-ubiquitin conjugate. The optimally positioned substrate is then ubiquitinated by RBX1/2, priming it for proteolysis through the proteasome (Bulatov & Ciulli, 2015, Cardote et al., 2017, Duda, Scott et al., 2011, Zheng et al., 2002).

In the case of CUL2, the proteins Elongin B and C serve as adaptor proteins, and the tumor suppressor protein Von Hippel-Lindau (VHL) acts as the substrate receptor (Cardote et al., 2017, Kamura, Maenaka et al., 2004, Yu, White et al., 2001). The best characterised CUL2 substrate is hypoxia-inducible factor 1 alpha (HIF1α). Under normoxic conditions, HIF1α is hydroxylated on proline residues by a class of enzymes termed prolyl hydroxylases. Hydroxyproline-modified HIF1α is recognised and bound by VHL, which subsequently recruits HIF1α to the CUL2-CRL complex for its ubiquitination, marking it for proteolysis (Figure 5-1) (Kamura et al., 2004, Yu et al., 2001). The VHL-BOX domain of VHL, comprised of residues T152-H191 of the human VHL protein, mediates the association between VHL and the elongin B/C adaptor proteins (Kamura et al., 2004). Other CRL complexes function in analogous ways, employing distinct adaptor and substrate receptor proteins for the ubiquitination of their substrates (Bosu & Kipreos, 2008, Bulatov & Ciulli, 2015, Duda et al., 2011, Kamura et al., 2004, Zhao & Sun, 2013, Zheng et al., 2002).

Molecular studies on CRLs have established the key mode of substrate degradation to be proximity-driven ubiquitination (Bosu & Kipreos, 2008, Bulatov & Ciulli, 2015). As such, the CRL-UPS has been successfully exploited, both as a research tool and for the development of therapeutics. For example, PROteolysis TArgeting ChimeraS (PROTACS) are an emerging class of small molecule that harbour a target protein recognition moiety on one end, with an E3 ligase recognition element on the other. In this capacity, upon PROTAC administration, PROTACs act to direct specific

target proteins to E3 ligase complexes to promote their proximity-dependent ubiquitination and subsequent proteolysis (Sakamoto, Kim et al., 2001, Zengerle, Chan et al., 2015). The successful application of some PROTACs, which encompass moieties that bind components of CRL systems such as VHL, demonstrate that CRL systems can be successfully exploited for target protein degradation, provided that the target protein can be effectively recruited to the CRL substrate receptors (Bulatov & Ciulli, 2015, Sakamoto et al., 2001, Zengerle et al., 2015).

Historically, the idea of targeted proteolysis was first demonstrated in 1994, when Dohmen and colleagues fused a temperature-sensitive dihydrofolate reductase enzyme harbouring an N-terminal arginine (Arg-DHFR) to both Ura3 and Cdc28 proteins in *S. cerevisiae* (Dohmen, Wu et al., 1994). Arg-DHFR is long-lived at 23°C, but is quickly degraded at 37°C. Importantly, this temperature-sensitive degron property of Arg-DHFR is conferred to proteins it is tagged to, thus, fusion of Arg-DHFR to Ura3 and Cdc28 triggered their degradation when the yeast cells were cultured at 37°C (Dohmen et al., 1994). As such, this system was named the heat-inducible degron. This system was later adapted in order to improve target protein degradation kinetics (Labib, Tercero et al., 2000), and since then there has been great research interest aimed at generating targeted proteolysis methodologies that are compatible with higher eukaryotes. Most notably was the development of the auxin-inducible degron. Plant cell signalling relies on phytohormones such as auxin (AUX), and upon exposure to hormones of the auxin family such as indole-3-acetic acid (IAA), the AUX/IAA family of transcriptional repressor proteins are rapidly degraded (Nishimura, Fukagawa et al., 2009, Tan, Calderon-Villalobos et al., 2007). Such degradation is achieved through a specific form of the SCF CRL E3 Ligase complex, containing the substrate receptor F-box Transport Inhibitor Response 1 (TIR1). Auxin hormones bind to TIR1, in order to promote the association

between the SCF-CRL complex and AUX/IAA transcriptional repressor proteins, and trigger AUX/IAA ubiquitination, priming them for proteolysis (Nishimura et al., 2009, Tan et al., 2007). Whilst other eukaryotes lack this auxin-inducible response, the SCF degradation pathway is conserved, implying that such auxin-inducible degradation could be transferred to other eukaryotic cells. The Kanemaki lab first demonstrated this possibility in chicken, mouse, yeast and human cells, and showed rapid, reversible degradation of essential POIs in these different cell lines (Nishimura et al., 2009). This was achieved through fusing an IAA17 degron sequence on to the POI, and simultaneously overexpressing TIR1 in the target cells. Rapid protein degradation was observed following IAA treatment (Nishimura et al., 2009). As it is generally believed that the auxin degradation pathway is only active in plants, any off-target effects resulting from auxin treatment are thought to be minimal. That said, IAA oxidation by eukaryotic peroxidases has been reported to be toxic at high doses (Folkes, Dennis et al., 1999), highlighting the need to test auxin sensitivity in the target cell line before using this system. One of the key limitations of the Auxin-inducible system is that it cannot be used to explore the effects of endogenous protein degradation, without first inserting the IAA degron sequence at the POI locus. This has not been such an impediment in yeast (Nishimura et al., 2009), however in higher eukaryotes this has been more challenging, owing to the much less efficient homologous recombination in these cells compared to that seen in yeast.

Recent years have seen the advancement of gene editing technologies, such as CRISPR/Cas9 (Cong et al., 2013, Sander & Joung, 2014). This has made it relatively simple to achieve gene knockouts in somatic cells, provided that the gene of interest is not essential for cell survival or proliferation. It is estimated that there are over 1800 genes that are impossible to knockout with conventional CRISPR/Cas9 methods (Wang et al.,

2015). Similarly, the CRISPR/Cas9 system has been successfully employed to knockin fluorescent reporter tags, such as green fluorescent protein (GFP), onto target genes. However, the success of genetic knockins rely on the knockin tag not impinging on target gene expression and/or function of the protein product. With such advances, the AID degron sequence was also successfully knocked into genes encoding cohesin and dynein in human colorectal cancer HCT116 cells (Natsume, Kiyomitsu et al., 2016). Following TIR1 overexpression, IAA-responsive degradation of cohesin and dynein were observed (Natsume et al., 2016). Whilst this auxin-inducible approach presents a powerful tool to achieve target protein degradation in cells, inserting a non-fluorescent AID degron tag homozygously onto the POI locus remains a challenge. This is not such a problem for fluorescent knockin tags, which allow rapid isolation of fluorescent-positive cell clones through fluorescence-activated cell sorting (FACS) (Rojas-Fernandez et al., 2015). Such fluorescent tags also allow for robust localisation, proteomic and biochemical studies, and additionally, present a tantalising target for the specific proteolysis of tagged proteins of interest.

Concomitantly, recent years have also witnessed the rapid development and use of small, isolated variable domain fragments, derived from single chain antibodies, as seen in species such as camels and sharks (Fridy, Li et al., 2014, Kirchhofer, Helma et al., 2010, Rothbauer, Zolghadr et al., 2008). A key advantage of these small polypeptides (hereafter referred to as nanobodies) is that their coding sequence can be easily packaged into plasmids for expression in multiple cellular systems. Once expressed, nanobodies retain their specificity and affinity for their protein targets. Many nanobodies have been generated against distinct targets, including fluorescent proteins such as GFP (Fridy et al., 2014, Kirchhofer et al., 2010, Rothbauer et al., 2008).

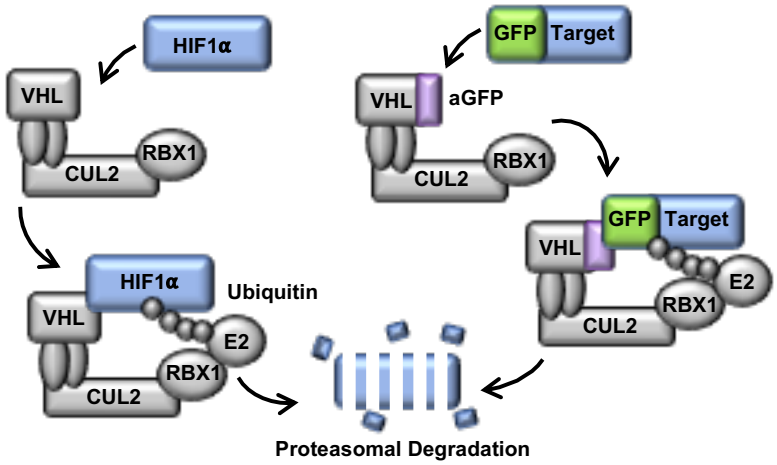

Figure 5-1: Conceptual design of AdPROM: Schematic illustration of the CRL-mediated degradation of HIF1α (left-hand side), and AdPROM-mediated degradation of GFP-tagged targets (right-hand side). VHL; Von Hippel-Lindau protein, CUL2; Cullin 2, RBX1; RING-box protein 1, E2; E2 ubiquitin-conjugating enzyme, aGFP; anti-GFP nanobody.

Here, I sought to combine the nanobody and CRISPR/Cas9 technologies to generate a method to degrade GFP-tagged knockin proteins of interest. An approach where one could express VHL conjugated to an anti-GFP (aGFP) nanobody within cells, and in doing so recruit the GFP-tagged knockin protein to the CUL2-CRL complex for its proteolysis, was envisaged (Figure 5-1). This approach was named the Affinity-directed PROtein Missile (AdPROM) system, and its development and characterisation will be explored in detail within this chapter.

5.2: Results:

5.2.1: AdPROM is effective for degradation of selective GFP-tagged knockin proteins:

In order to test the effectiveness of the conceived AdPROM design, two different GFP knockin cell lines were infected with AdPROM retroviruses encoding either VHL-aGFP, or aGFP-VHL, along with control retroviruses encoding free GFP as an infection

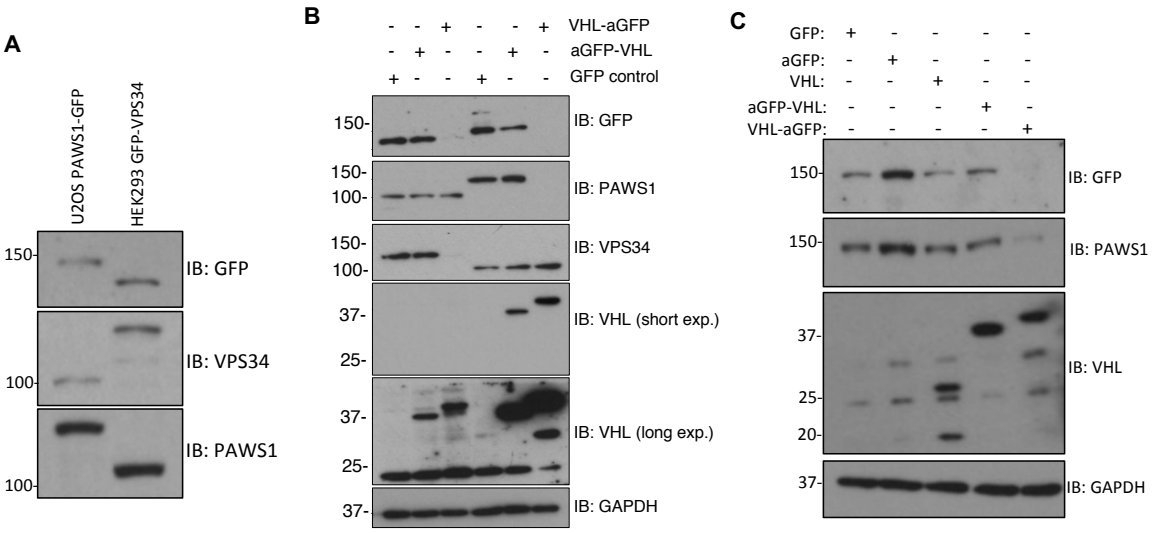

Figure 5-2: AdPROM is effective for degradation of GFP-VPS34 and PAWS1-GFP: A: Western blot analysis of extracts from PAWS1-GFP and GFP-VPS34 knockin U2OS and HEK 293 cells respectively, using the indicated antibodies (n=3). **B:** Cells described in A. were infected with control retroviruses (GFP) or retroviruses encoding aGFP-VHL or VHL-aGFP. Cells were lysed and extracts (20 µg) were separated by SDS–PAGE, prior to immunoblotting (IB) with the indicated antibodies (n=3). **C:** PAWS1-GFP knockin U2OS cells were infected with retroviruses encoding GFP, aGFP, VHL, aGFP-VHL, or VHL-aGFP. Following lysis, extracts were subjected to SDS-PAGE and subsequent IB with the indicated antibodies (n=3).

vector control. For this purpose, GFP-VPS34 HEK 293 and FAM83G-GFP (hereafter referred to as PAWS1-GFP) U2OS knockin cells were used, generated by Annika Hornberger and Polyxeni Bozatzi respectively (Figure 5-2A). Following infection and selection of AdPROM-expressing clones with the antibiotic puromycin, the abundance of GFP-VPS34 and PAWS1-GFP knockin proteins were evaluated by immunoblotting with antibodies against GFP, VPS34 and PAWS1. Whilst in control vector, and aGFP-VHL-expressing cells, where the levels of both GFP-VPS34 and PAWS1-GFP remained unaltered, robust depletion of both GFP knockin proteins in cells expressing VHL-aGFP was observed (Figure 5-2B). Importantly, in HEK 293 cells in which PAWS1 is not

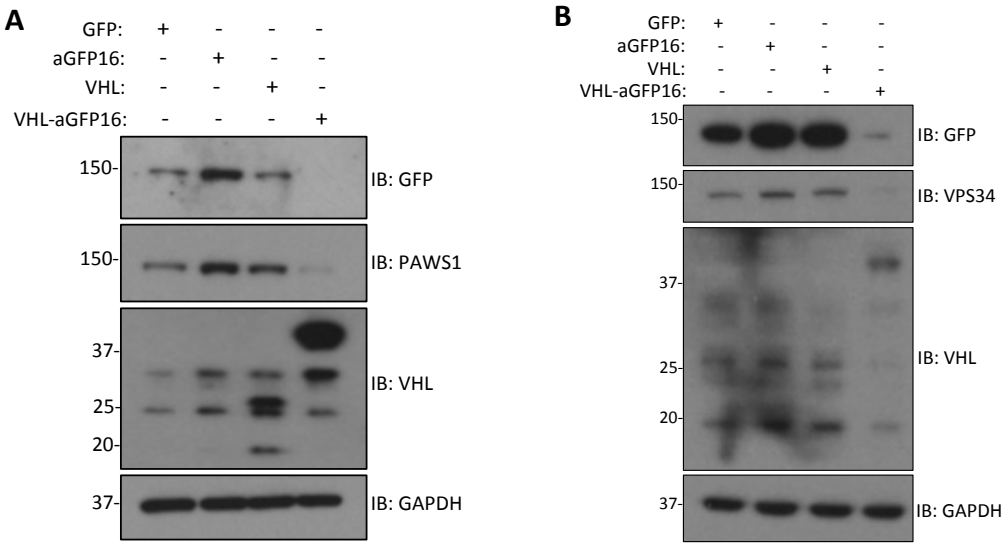

Figure 5-3: Swapping aGFP for a distinct GFP nanobody does not hinder AdPROM-mediated degradation: A: PAWS1-GFP knockin U2OS cells were infected with control retroviruses (GFP) or retroviruses encoding aGFP.16, VHL, or VHL-aGFP.16. Cells were lysed and extracts (20 µg) were separated by SDS–PAGE, prior to immunoblotting (IB) with the indicated antibodies (n=3). **B:** As in A, except that GFP-VPS34 knockin HEK 293 cells were used (n=3).

modified to possess a GFP fusion tag, no PAWS1 depletion was observed, suggesting that VHL-aGFP only targets GFP-tagged proteins for degradation (Figure 5-2B). Similar observations were made in U2OS cells in which the VPS34 gene is not edited to encode a GFP fusion protein (Figure 5-2B). Collectively, these data suggested that the conjugation of aGFP onto the C-terminus, but not the N-terminus, of VHL was essential for proteolysis. Consequently, the VHL-aGFP polypeptide was used as the effective orientation for the AdPROM system in subsequent experiments.

In order to confirm that the individual VHL and aGFP components that constitute the AdPROM system did not drive the degradation of GFP-tagged proteins on their own, PAWS1-GFP knockin U2OS cells were infected with retroviruses encoding untethered

VHL or aGFP. As expected, neither VHL nor aGFP when expressed individually caused a reduction in PAWS1-GFP protein levels (Figure 5-2C).

Furthermore, to circumvent the possibility that VHL-aGFP was causing degradation through non-UPS mechanisms, the aGFP was replaced with an independently-derived, distinct camelid anti-GFP nanobody which recognises a different epitope on GFP (hereafter referred to as aGFP.16). The AdPROM system encompassing VHL-aGFP.16 also drove degradation of GFP-VPS34 and PAWS1-GFP when expressed in cells, whereas individual expression of VHL or aGFP.16 did not (Figure 5-3A&B).

5.2.2: AdPROM exploits the CRL-UPS for targeted degradation of GFP-tagged knockin proteins:

Next, I sought to confirm that the observed degradation of GFP-VPS34 and PAWS1-GFP was indeed being mediated by the predicted CUL2-CRL machinery. To test this, cells were treated with the pan-Cullin NEDDylation inhibitor MLN4924 (Soucy et al., 2009), and the levels of the GFP-tagged knockin proteins were monitored. As expected, treatment of both U2OS and HEK 293 cells with MLN4924 resulted in robust inhibition of CUL2 NEDDylation, and concomitant stabilisation of its endogenous substrate HIF1α (Figure 5-4A). Under these conditions, in cells expressing VHL-aGFP, levels of both GFP-VPS34 and PAWS1-GFP were partially restored with MLN4924 treatment, whereas no changes in their protein levels were detected in control cells (Figure 5-4A). Importantly, the expression of the VHL-aGFP AdPROM did not appear to stabilise HIF1α, suggesting that AdPROM does not interfere with substrate recognition by the endogenous CUL2-CRL complex (Figure 5-4A). To test the involvement of the proteasome in AdPROM-induced protein degradation, PAWS1-GFP knockin U2OS cells were treated with the proteasome inhibitor Bortezomib, and PAWS1-GFP levels were monitored by

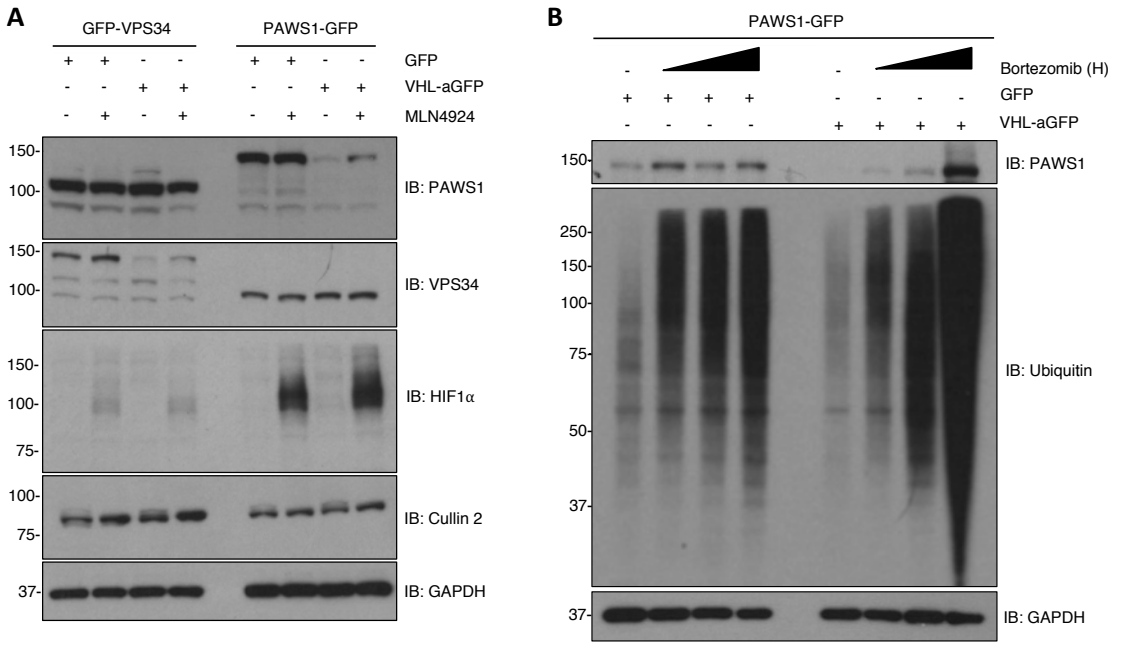

Figure 5-4: AdPROM exploits the CRL-UPS for degradation of target proteins: A: GFP-VPS34 HEK 293 and PAWS1-GFP U2OS knockin cell lines were infected with retroviruses encoding either control (GFP) or VHL-aGFP. Infected cells were then treated with either DMSO or the pan-Cullin NEDDylation inhibitor MLN4924 (1 µM) for 6 h, as indicated. Extracts (20 µg protein) were resolved by SDS–PAGE, and subjected to immunoblotting (IB) with the indicated antibodies (n=3). **B:** Control (GFP) or VHL-aGFP PAWS1-GFP U2OS cells described in A were treated with 10 µM Bortezomib for 0, 4, 10 or 24 h prior to lysis. Extracts (20 µg protein) were resolved by SDS–PAGE, and subjected to IB with the indicated antibodies (n=3).

immunoblotting. Whereas no significant changes in PAWS1-GFP protein levels were detected in control cells treated with Bortezomib, stabilisation of PAWS1-GFP was observed in a time-dependent manner in VHL-aGFP expressing cells, following Bortezomib addition to the culture media (Figure 5-4B). Collectively, these data suggest that the AdPROM-mediated degradation of GFP-tagged knockin protein occurs through the predicted CUL2-UPS machinery.

5.2.3: Adapting the AdPROM system for inducible degradation of GFP-tagged knockin proteins:

Having demonstrated utility of the AdPROM system in the constitutive degradation of GFP-tagged knockin proteins, I next sought to adapt AdPROM into an inducible proteolytic tool. For this purpose, the pRetroX Tet-On retroviral system was employed to clone VHL-aGFP.16, with the hope of achieving tetracycline (Tet)-inducible expression of the VHL-aGFP.16 AdPROM. Using this approach, in cells expressing either an empty vector or VHL-aGFP.16 under the control of the Tet-inducible promoter, no changes in GFP-VPS34 protein levels were observed in the absence of the Tet analogue doxycycline (Figure 5-5A). However, whereas no changes in GFP-VSP34 protein levels were detected in empty vector-expressing cells in response to doxycycline treatment, time-dependent degradation of GFP-VPS34 was observed in the VHL-aGFP.16-expressing cells, following induction with doxycycline (Figure 5-5A). Interestingly, a concomitant reduction in the levels of the VPS34-interacting protein UVRAG was evident, suggesting that AdPROM has the potential to target protein complexes for degradation (Figure 5-5A).

Given the role VPS34 plays in the generation of phosphatidylinositol 3-phosphate (PI3P) on endosomal membranes, in its capacity as a PI3P lipid kinase (Bago, Malik et al., 2014, Gillooly, Morrow et al., 2000), I sought to test if AdPROM-mediated GFP-VPS34 proteolysis would impact endogenous VPS34 biology. Endosomal PI3P acts to recruit proteins containing FYVE and PX domains, in order to mediate downstream signalling (Gillooly et al., 2000). To visualise endosomal PI3P, I made use of a recently-developed AlexaFluor-488-conjugated probe attached to the PX domain of P40phox (Kanai, Liu et al., 2001, Malik, Macartney et al., 2018, Munson, Allen et al., 2015). A PI3P-interaction-deficient PX domain mutant conjugated to AlexaFluor-594 served as a negative control in these assays, and allowed simultaneous visualisation of both the

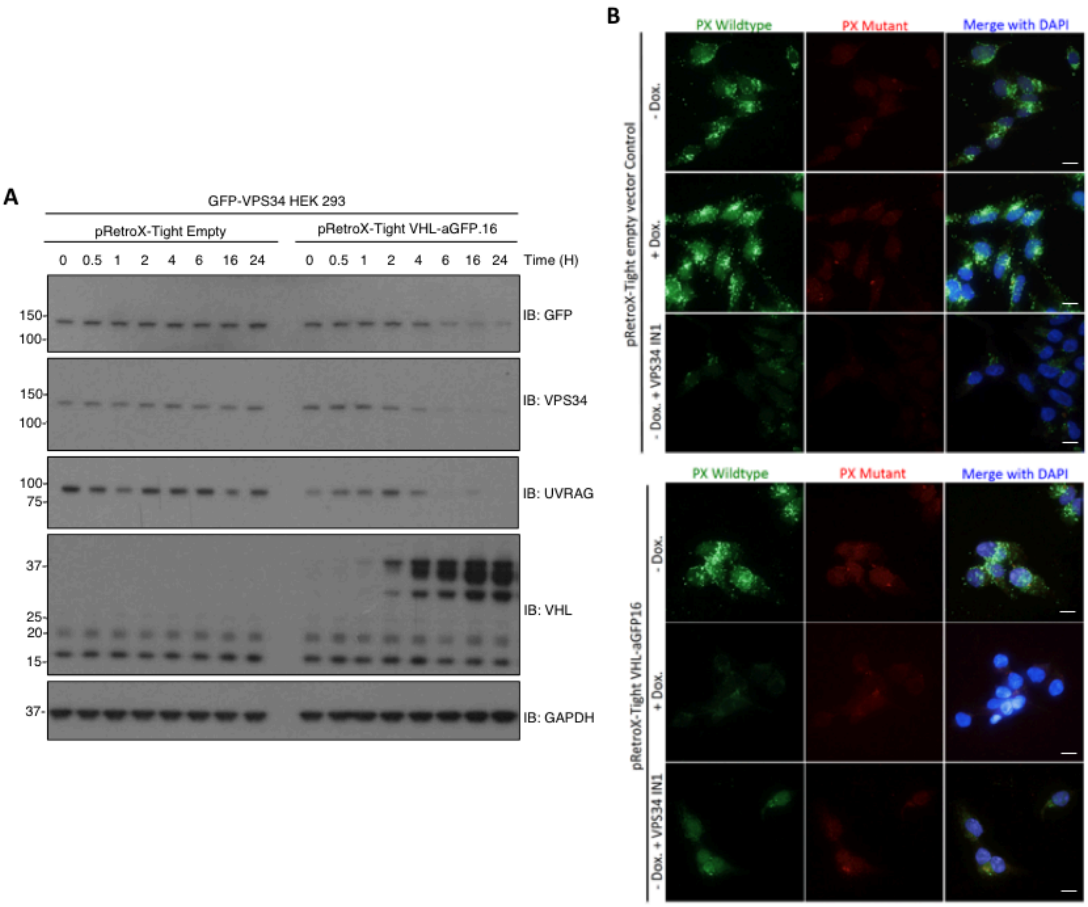

Figure 5-5: Adapting AdPROM for Tet-inducible degradation of target proteins: A: GFP-VPS34 HEK 293 knockin cells were first infected with the pRetroX-Tet-ON advanced vector (Clontech) and selected for the expression of the Tet-transactivator. Cells were then infected with either the pRetroX-Tight empty vector control or the pRetroX-Tight vector encoding VHL-aGFP.16. Cells were then treated with 2 µg/ml doxycycline for the indicated time points prior to lysis. Extracts (20 µg protein) were resolved by SDS–PAGE, and subjected to immunoblotting (IB) with the indicated antibodies (n=3). **B:** GFP-VPS34 HEK 293 knockin cells expressing the pRetroX system described in A. were either left untreated, treated with doxycycline (2 µg/ml; 24 h), or with VPS34-IN1 (2.5 µM, 1 h). Cells were permeabilised in liquid nitrogen, and fixed in 3.7% (w/v) paraformaldehyde before staining with fluorescently-labelled selective PI3P binding (green) and interaction deficient (red) probes as described in the Material and methods section. DNA is stained with DAPI. Representative images from one field of view, representative of 2 independent experiments are included. Scale bars; 20 µM.

the wild-type and mutant PI3P probes in the same samples (Malik et al., 2018). Using these fluorescent probes, endosomal PI3P levels in response to GFP-VPS34 degradation

with the Tet-inducible VHL-aGFP.16 AdPROM were examined. Whereas no difference in cellular PI3P puncta was observed in response to doxycycline in empty vector-expressing cells, there was a substantial reduction in PI3P puncta in VHL-aGFP.16-expressing cells following GFP-VPS34 degradation (Figure 5-5B). This reduction in PI3P puncta was similar to that seen in response to VPS34 inhibition with the VPS34 kinase inhibitor VPS34-IN1 (Bago et al., 2014) (Figure 5-5B). Under identical conditions, no PI3P puncta were detected with the mutant probe, suggesting that the puncta that were assayed were indeed PI3P (Figure 5-5B). Thus, AdPROM-induced degradation of GFP-VPS34 appears to impact the cellular function of VPS34, which is at least comparable to its chemical inhibition using small molecule inhibitors.

5.2.4: Adapting AdPROM for degradation of unmodified target proteins in cells:

As mentioned above, knocking in fluorescent tags onto target proteins can potentially affect their stability and/or cellular function(s). To combat these potential limitations, I sought to expand the AdPROM system and explore whether unmodified, native proteins could be targeted for degradation. To test this, I made use of a nanobody raised against the inflammasome protein ASC (Schmidt, Lu et al., 2016) (Figure 5-6A), and fused it onto the C terminus of VHL. A FLAG tag was introduced at the N-terminus of VHL to facilitate easier visualisation.

Following successful expression of FLAG-VHL-aASC in cells, through retroviral infections, the protein levels of ASC in ASC-expressing K-562 cells were monitored. Control retroviruses encoding unfused FLAG-aASC or VHL were also included. Whereas no detectable decrease in ASC abundance was observed in cells treated with control retroviruses, a substantial reduction in the protein levels of ASC was observed in VHL-aASC-expressing cells (Figure 5-6B). In order to demonstrate the affinity of the aASC

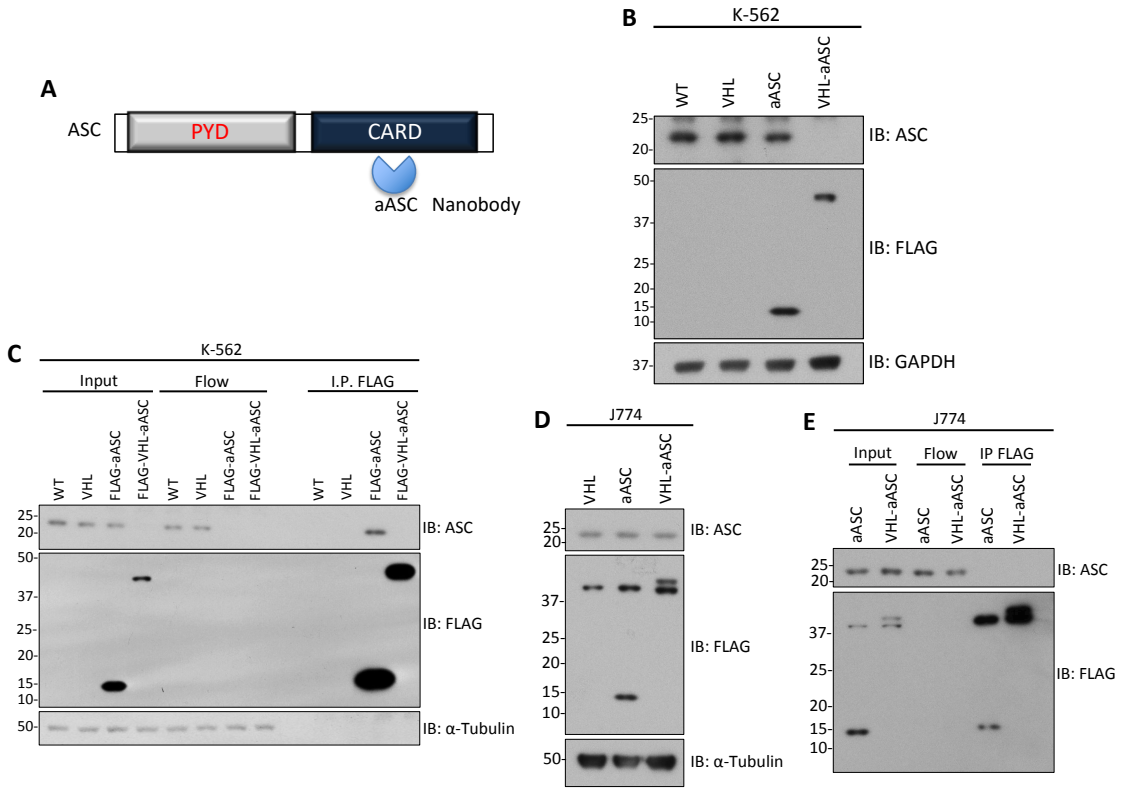

Figure 5-6: The AdPROM system is adaptable for degradation of endogenous ASC: A: Domain structure of ASC with the N-terminal Pyrin domain (PYD) and C-terminal Caspase recruitment domain (CARD) indicated. The aASC nanobody recognises the CARD domain of human ASC. **B:** Uninfected human K-562 cells (WT) or cells infected with retroviruses encoding VHL, FLAG-aASC or FLAG-VHL-aASC were lysed, and extracts (20 µg protein) were resolved by SDS-PAGE. Separated proteins were subjected to immunoblotting (IB) with the indicated antibodies (n=3). **C:** Extracts (1 mg protein) from the cells described in B. were subjected to immunoprecipitation (IP) with anti-FLAG M2 resin. The resulting IP, and Input and flow-through (flow) samples (20 µg protein) were resolved by SDS-PAGE and subjected to IB with the indicated antibodies (n=3). **D**: As in B. except that murine J774 monocyte cells were used (n=3). **E:** As in C. except that murine J774 monocytes from D. were used (n=3).

nanobody for the human ASC protein, anti-FLAG immunoprecipitations were performed. In FLAG-aASC-expressing K-562 cells, ASC was robustly immunoprecipitated and depleted from flow-through extracts (Figure 5-6C). As ASC was degraded by VHL-aASC, immunoprecipitations from FLAG-VHL-aASC-expressing cells did not immunoprecipitate ASC, as expected (Figure 5-6C). As the aASC nanobody was reported to be specific for the human ASC protein (Schmidt et al., 2016), I repeated these

experiments in murine J774 monocytes. Consistently, no degradation of murine ASC was detected in FLAG-VHL-aASC-expressing cells (Figure 5-6D), and FLAG-aASC immunoprecipitations failed to coimmunoprecipitate the murine ASC protein (Figure 5-6E). Collectively, these data highlight the versatility of the AdPROM system, and showcase successful adaptation of AdPROM for degradation of endogenous, unmodified human ASC protein.

Nanobodies are just one class of high-affinity polypeptide binder that have been developed in recent years. Whereas nanobodies rely on immunisation of single chain antibody-producing animals, such as camels, in order to obtain functional high-affinity binders, a number of synthetic approaches have successfully yielded specific polypeptide binders as well. One such method exploits the backbone of the human 10th fibronectin type III domain, where varying combinations of residues within the variable regions are screened for their ability to bind the target antigen (Sha, Gencer et al., 2013). Resulting polypeptide binders are referred to as monobodies, and there have been a few high-affinity monobodies developed for specific targets (Sha et al., 2013, Wojcik, Hantschel et al., 2010, Wojcik, Lamontanara et al., 2016). To examine if monobodies were also compatible with the AdPROM system, I chose two distinct monobodies that recognise the protein tyrosine phosphatase SHP2 (also known as PTPN11). SHP2 possesses two SH2 domains at its N-terminus, termed N-SH2 and C-SH2 respectively, with N-SH2 being slightly more N-terminal than C-SH2 (Sha et al., 2013). The monobodies chosen to test within the AdPROM system bind to either the N-SH2 and C-SH2 domains of SHP2, and are designated aNSa1 and aCS3 respectively (Sha et al., 2013)(Figure 5-7A).

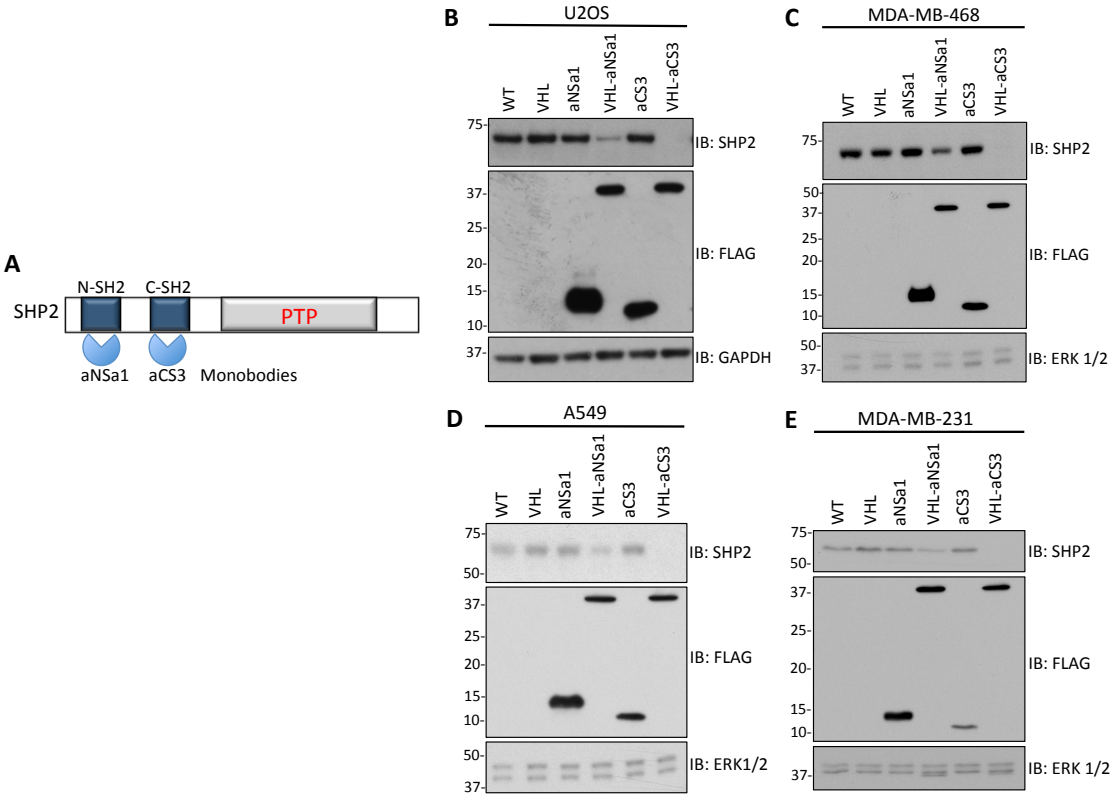

Figure 5-7: AdPROM is adaptable for degradation of endogenous SHP2 using monobodies instead of nanobodies: A: Domain structure of SHP2. N-SH2; N-terminal SH2 domain. C-SH2; C-terminal SH2 domain. PTP; protein tyrosine phosphatase domain. The monobodies aNSa1 and aCS3 recognise the N-SH2 and C-SH2 domains of SHP2 respectively. **B:** U2OS cells were infected with retroviruses encoding VHL, FLAG-NSa1, FLAG-aCS3, FLAG-VHL-aNSa1 or FLAG-VHL-aCS3, or left uninfected (WT). Cell extracts (20 µg protein) were resolved by SDS-PAGE and subjected to immunoblotting (IB) with the indicated antibodies (n=3). **C-E:** as in B. except that MDA-MB-468 mammary gland adenocarcinoma (C), A549 pulmonary adenocarcinoma (D) and MDA-MB-231 breast cancer (E) cells were used (n=3).

FLAG-VHL-aNSa1 and FLAG-VHL-aCS3 were packaged into mammalian-expression pBABED retroviral vectors, and retroviruses were produced. Following successful infection of U2OS osteosarcoma cells, the levels of SHP2 were evaluated by immunoblotting. Control retroviral infections encoding FLAG-aNSa1, FLAG-aCS3, or VHL were performed in parallel. The endogenous SHP2 levels were unaltered and comparable between uninfected cells and cells infected with the VHL, FLAG-aNSa1 or

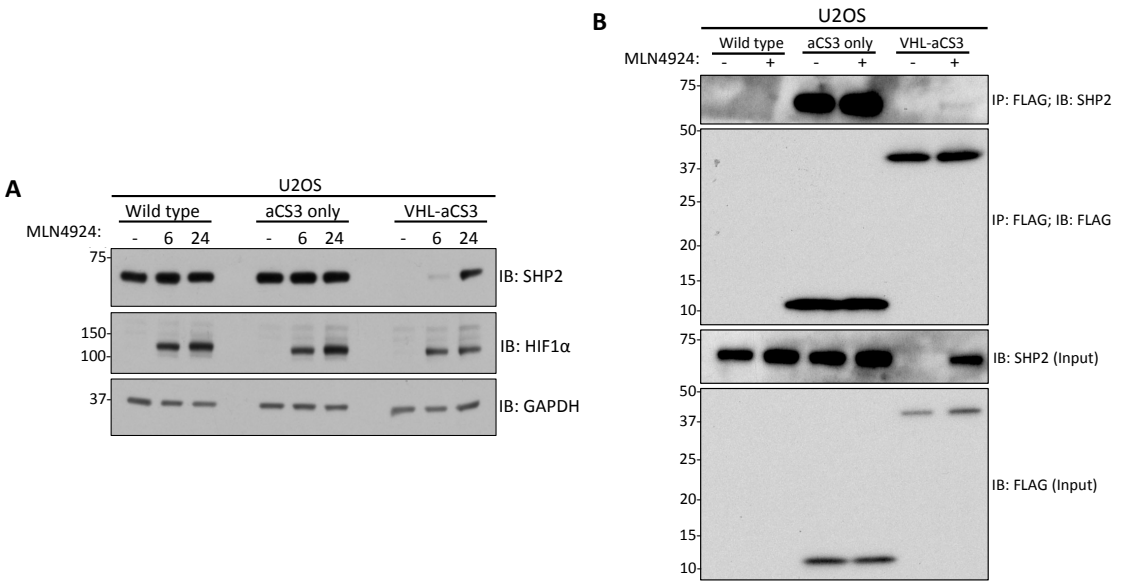

Figure 5-8: AdPROM employs the CRL-UPS for SHP2 degradation: A: Uninfected U2OS cells (wild type) or cells infected with retroviruses encoding FLAG-aCS3 or FLAG-VHL-aCS3 were treated with MLN4924 (1 µM) for 0, 6 or 24 h. Cells were lysed and extracts (20 µg protein) were resolved by SDS-PAGE and subjected to immunoblotting (IB) with the indicated antibodies. HIF1α serves as a positive control for MLN4924 treatment (n=3). **B:** U2OS cells treated with or without MLN4924 (1 µM) for 24 h were lysed and extracts (1 mg protein) were subjected to immunoprecipitation (IP) with anti-FLAG M2 resin. Following elution, both the IPs and Input extracts (20 µg protein) were resolved by SDS-PAGE, and subjected to IB with the indicated antibodies (n=3).

FLAG-aCS3 controls (Figure 5-7B). In contrast, compared to these cells, a substantial reduction in SHP2 protein levels was observed in cells expressing FLAG-VHL-aNSa1, and an even greater reduction in cells expressing FLAG-VHL-aCS3 (Figure 5-7B). Similar results in SHP2 degradation were detected in MDA-MB-468 mammary gland adenocarcinoma (Figure 5-7C), A549 pulmonary adenocarcinoma (Figure 5-7D), and MDA-MB-231 breast cancer cells (Figure 5-7E), suggesting that the observations on SHP2 protein abundance are not due to cell type-specific mechanisms.

Next, in order to confirm that VHL-bound monobodies also mediate degradation through the predicted CUL2-CRL machinery, FLAG-VHL-aCS3-expressing cells were treated with the pan-Cullin NEDDylation inhibitor MLN4924 (Soucy et al., 2009).

Uninfected and control FLAG-aCS3 cells were also treated. In uninfected cells, or in cells expressing FLAG-aCS3, MLN4924 treatment had no effect on SHP2 protein levels (Figure 5-8A). In stark contrast, MLN4924 treatment rescued the degradation of SHP2 in FLAG-VHL-aCS3-expressing cells (Figure 5-8A). Consistent with previous observations, expression of the SHP2 AdPROM system did not appear to stabilise the endogenous VHL substrate HIF1α, suggesting the monobody version of AdPROM does not impact hypoxia signalling either (Figure 5-8A). To demonstrate the affinity of the aCS3 and aNSa1 monobodies for the SHP2 protein, anti-FLAG immunoprecipitations were performed in aCS3 cells, with or without prior treatment with MLN4924 for 24 h. In FLAG-aCS3-expressing cells, SHP2 was robustly immunoprecipitated, irrespective of MLN4924 treatment (Figure 5-8B). As SHP2 was degraded by VHL-aCS3, anti-FLAG immunoprecipitations from FLAG-VHL-aCS3-expressing cells did not co-immunoprecipitate SHP2 in the absence of MLN4924 treatment, whereas some SHP2 could be detected in the eluates following treatment with MLN4924 (Figure 5-8B).

Collectively, these data highlight that both nanobodies and monobodies recognising endogenous target proteins can be successfully employed as effective affinity probes within the AdPROM system, provided they can bind their intended targets within cells. Furthermore, the AdPROM-mediated degradation of endogenous SHP2 appears to be mediated by the intended CUL2-CRL machinery.

5.2.5: Comparing the proteolytic AdPROM with an RNA interference approach, for the depletion of SHP2:

In order to evaluate the degradation rate of AdPROM targets, the VHL-aCS3 sequence was packaged into the Tet-inducible pRetroX Tet-On system described above (see section 5.2.3), and introduced it into MDA-MB-468 cells. An empty vector pRetroX-

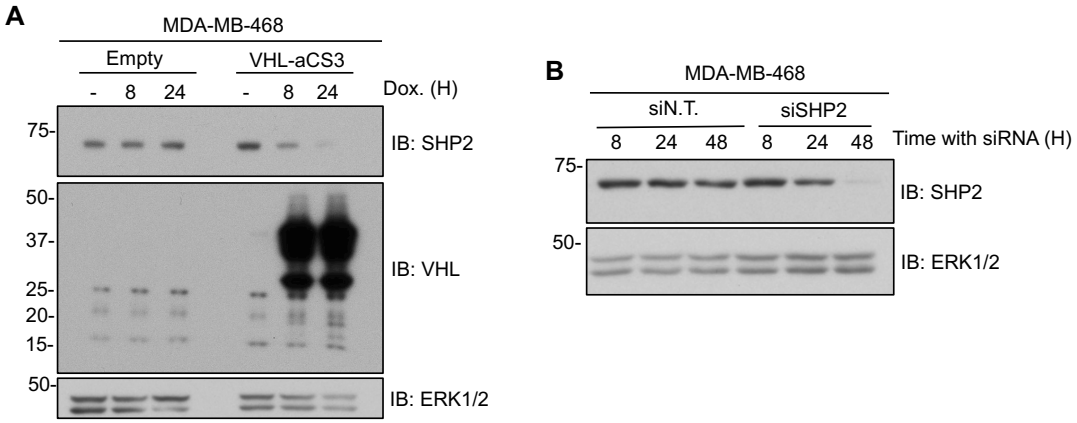

Figure 5-9: Comparing proteolytic AdPROM with siRNA for the depletion of SHP2: A: MDA-MB-468 cells were infected with retroviruses encoding the pRetroX-Tet-On transactivator and either pRetroX-Tight empty vector (empty) or pRetroX-Tight-VHL-aCS3 (VHL-aCS3). Infected cells were treated with doxycycline (2 µg/ml) for the indicated time points prior to lysis. Cell extracts (20 µg protein) were separated by SDS-PAGE, and subjected to immunoblotting (IB) with the indicated antibodies (n=3). **B:** MDA-MB-468 cells were transfected with non-targeting control siRNAs (siN.T.) or siRNAs targeting SHP2 (siSHP2) and lysed at the indicated time points after transfection. Cell extracts (20 µg protein) were separated by SDS-PAGE, and subjected to IB with the indicated antibodies (n=3).

Tight plasmid was introduced as a control. Treatment of VHL-aCS3 cells, but not the empty vector cells, with doxycycline induced a time-dependent reduction in SHP2 protein levels, which coincided with expression of the VHL-aCS3 AdPROM (Figure 5-9A). Under these conditions, SHP2 levels appeared to be substantially reduced after 8 h, and almost completely reduced after 24 h, treatment with doxycycline (Figure 5-9A); suggesting that AdPROM system induces degradation fairly rapidly after its successful expression.

Next, to evaluate how AdPROM-mediated SHP2 proteolysis compares with conventional siRNA-induced depletion, MDA-MB-468 cells were transfected with either control non-targeting siRNAs, or an siRNA pool designed to target SHP2 transcripts. Cells

were lysed 8, 24 and 48 h after transfection. Whereas control siRNAs had no effect on SHP2 protein levels at all time points tested, siRNAs against SHP2 induced SHP2 depletion only at 48 h post-transfection (Figure 5-9B). These results suggest that RNA interference approaches, which rely on native protein turnover rates, are not as efficient at depleting SHP2 compared with the AdPROM system, which degrades proteins independently of their half-life duration.

5.2.6: Leveraging AdPROM technology to study FAM83D:

I previously showed that CK1α fails to localise to the mitotic spindle in *FAM83D* knockout cells. To further ascertain whether CK1α-recruitment to the spindle apparatus was dependent on FAM83D, I sought to use AdPROM to efficiently degrade FAM83D-GFP in *FAM83D*$^{GFP/GFP}$ U2OS cells (Figure 5-10A). Whereas the control VHL, or aGFP.16 retroviruses had no effect on FAM83D-GFP protein levels compared to control uninfected cells (Figure 5-10B), robust FAM83D-GFP degradation was observed in cells expressing VHL-aGFP.16 (Figure 5-10B), suggesting that AdPROM-mediated proteolysis was compatible with FAM83D-GFP.

Next, the spindle localisation of CK1α was examined in these cells. Robust co-fluorescence was observed between FAM83D-GFP and CK1α staining in uninfected, VHL, or aGFP.16-expressing cells (Figure 5-10C). However, when FAM83D-GFP was degraded in VHL-aGFP.16-expressing cells, I observed concurrent absence of CK1α on the spindle apparatus (Figure 5-10C), consistent with the model that FAM83D recruits CK1α to the mitotic spindle.

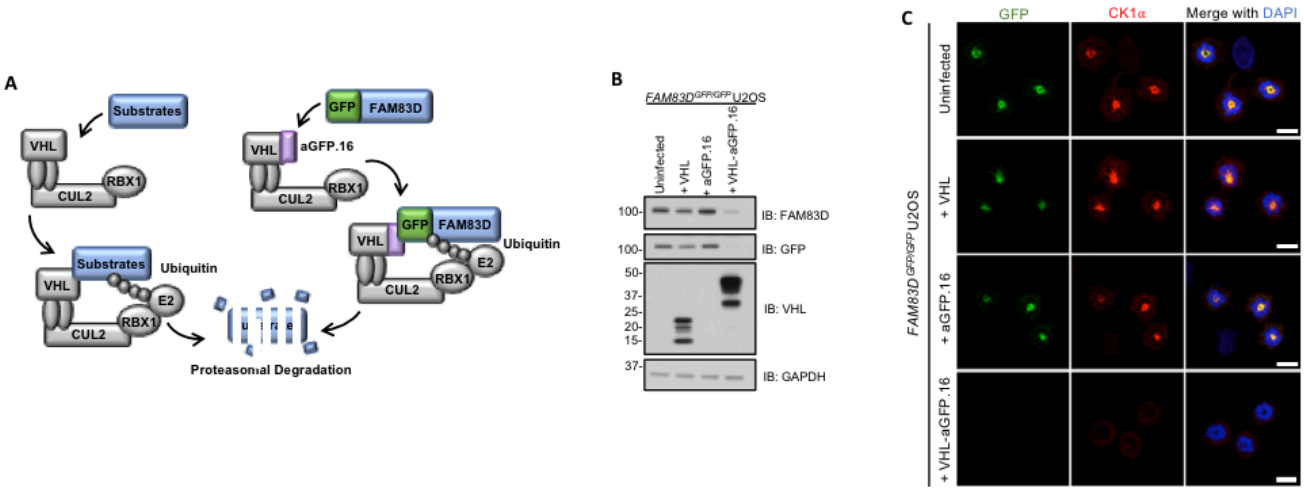

Figure 5-10: AdPROM-mediated degradation of FAM83D-GFP: A: Schematic illustration of the AdPROM-mediated degradation of FAM83D-GFP. VHL; Von Hippel-Lindau protein, CUL2; Cullin 2, RBX1; RING-box protein 1, E2; E2 ubiquitin-conjugating enzyme, aGFP.16; anti-GFP.16 nanobody. **B:** *FAM83D*$^{GFP/GFP}$ knockin U2OS cells were infected with retroviruses encoding either VHL, aGFP.16, or VHL-aGFP.16. Uninfected cells were used as a control. Cells were lysed and subjected to immunoblotting (IB) with the indicated antibodies (n=3). **C:** The cell lines described in B. were subjected to anti-CK1α immunofluorescence and GFP fluorescence microscopy. DNA is stained with DAPI. Scale bars; 20 µM (n=2).

As a proof of principle, I wondered if an anti-mCherry nanobody (LAM2) could also be tethered to VHL, to facilitate degradation of endogenous mCherry-tagged CK1α in *FAM83D*$^{GFP/GFP}$ / $^{mCherry/mCherry}$*CSNK1A1* U2OS cells (Figure 5-11A). The expression of the VHL-LAM2 AdPROM resulted in robust mCherry-CK1α degradation, without affecting FAM83D-GFP levels (Figure 5-11B).

As a whole, as corroborating data can be obtained through both genetic ablation of *FAM83D,* and targeted proteolysis of FAM83D-GFP, these results suggest that AdPROM will be a useful tool for examining the biology of FAM83-CK1 interactions in future research endeavours.

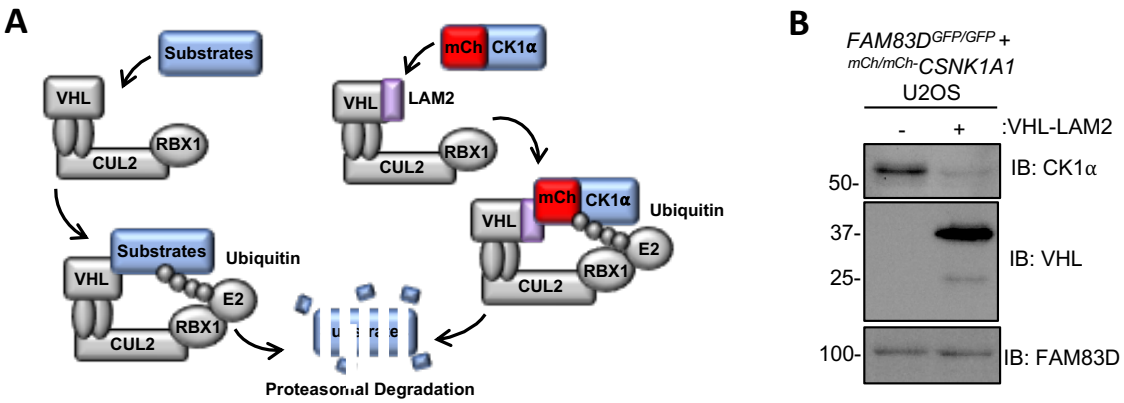

Figure 5-11: AdPROM-mediated degradation of mCherry-CK1α: A: Schematic illustration of the AdPROM-mediated degradation of mCherry-CK1α. VHL; Von Hippel-Lindau protein, CUL2; Cullin 2, RBX1; RING-box protein 1, E2; E2 ubiquitin-conjugating enzyme, LAM2; llama anti-mCherry nanobody 2. **B:** *FAM83D*$^{GFP/GFP}$ / $^{mCherry/mCherry}$*CSNK1A1* knockin U2OS cells were infected with retroviruses encoding VHL-aGFP.16. Uninfected cells were used as a control. Cells were lysed and subjected to immunoblotting (IB) with the indicated antibodies (n=1).

5.3: Conclusions:

Efficient and specific targeted proteolysis of endogenous cellular proteins is desirable in both basic research, and in potential therapeutic approaches. Here I describe an effective proteolytic AdPROM system that recruits target proteins to the CUL2-CRL complex for the subsequent ubiquitination and degradation of the target protein via the proteasome. I showcase that two distinct types of high-affinity binding proteins, namely nanobodies and monobodies, act as effective affinity probes for the AdPROM system. Importantly, the AdPROM system does not appear to impact endogenous hypoxia signalling, which is regulated by the VHL-CUL2 complex.

Whilst the current pool of available nanobodies, monobodies, and similar high-affinity polypeptide binders is limited, the multiple, diverse, potential uses of these molecules will likely see an exponential rise in their development in the following years.

That said, even in the absence of individual protein-targeting binders, binders recognising epitope tags such as the GFP nanobody described here, can be effectively employed, assuming that the fusion of the epitope tag onto the target protein does not impact protein function/stability.

In some cases, VHL may not be the ideal substrate receptor to tether the high-affinity binder to. Indeed, the precise tolerances of the CUL2-CRL complex for VHL-recruited substrates, in terms of their protein mass and composition, have not yet been established. Thus, it is prudent to develop an array of varied E3 ligase components that are compatible with the AdPROM system, that will allow for the targeted proteolysis of target proteins in cases where VHL AdPROMs do not function optimally.

In order to improve the AdPROM system, the ability to control AdPROM expression in an inducible manner is desirable. Whilst we have demonstrated the efficacy of a Tet-inducible AdPROM, such transcriptional inducible systems are not ideal as they require both transcription and translation of the AdPROM polypeptide before target protein degradation is observed, which can take many hours. Thus, the development of a rapid inducible AdPROM system is an important next step, and will facilitate studies into the effects of POI degradation at key, short-lived cellular events. That said, with increasing pharmaceutical interest in PROTACs (Bulatov & Ciulli, 2015, Sakamoto et al., 2001, Zengerle et al., 2015), technologies such as the constitutive AdPROM system should be able to rapidly inform if a putative PROTAC target can be degraded by the intended E3 ligase complex, prior to expensive and laborious investments of time and resources into PROTAC development.

6. Conclusions and Future Perspectives:

The CK1 family of Ser/Thr protein kinases have been implicated in many cellular processes, from Wnt signalling to the DNA damage response (Knippschild et al., 2005a, Schittek & Sinnberg, 2014, Venerando et al., 2014) (see section 1.2.4). Despite such a wide plethora of apparent functions, regulatory mechanisms responsible for coordinating these constitutively-active enzymes remain elusive. Here, the FAM83 family of proteins are presented as interactors of selective CK1 family isoforms, with the data-driven suggestion that FAM83-CK1 interactions act to localise CK1 isoforms to distinct cellular sites. In this capacity, FAM83 members may act to position CK1 isoforms in close proximity to their substrates within the cellular compartments in which each FAM83 protein resides. Alternatively, the FAM83 members may act as signalosome assembly platforms, and act to bridge the gap between CK1 isoforms and their substrates. Indeed, the diverse sets of interactors reported for each FAM83 member would suggest that non-CK1 interacting partners of FAM83 proteins are in abundance (Bozatzi et al., 2018, Cummins et al., 2018, Dunsch et al., 2012, Kuga et al., 2016a, Santamaria et al., 2008, Vogt et al., 2014). In this vein, each FAM83-interacting protein should be considered as a putative CK1 substrate, and be tested experimentally.

An additional regulatory mechanism prevalent for some kinases such as Aurora A and CDKs is direct allosteric activation through binding interacting partners (Bayliss et al., 2003, Ito, 2000). Whilst direct allosteric activation of CK1α by FAM83G *in vitro* was ruled out in this thesis, the potential contribution of allosteric activation will need to be further explored for the other FAM83 members. With the notion that FAM83 proteins can act to streamline CK1 signal transduction by recruiting selective CK1 isoforms to

distinct locations in mind, charting the FAM83-dependent CK1 substrate landscape, through phosphoproteomic approaches, will be an important next step.

In the case of the mitotic FAM83D-CK1α interaction, deciphering the CK1α substrate(s) responsible for coordinating precise spindle positioning will provide mechanistic insights into this regulatory pathway. Research into the phosphorylation-mediated control of spindle positioning has focussed primarily on three main kinase families, namely CDKs, AURKs, and PLKs. However, the extent of phosphorylation reported over a cell division cycle is unlikely to be explained by these kinase families alone, thereby suggesting roles for other kinases in mitosis. Interestingly, a recent phosphoproteomic screen found that near 50% of all cell cycle phosphopeptides conformed to the predicted CK1 consensus motif (Ly et al., 2017). Thus, the influence that CK1α exerts on the regulation of the cell division cycle may be far-reaching. The FAM83D-CK1α interaction is the first FAM83-CK1 interaction identified to be dependent on cell cycle stage, and indeed, to require a stimulus in general. For the less robust FAM83-CK1 interactions, elucidating their biological niche may illuminate further stimuli-dependent FAM83-CK1 associations.

Recently, the FAM83D-interacting protein HMMR, which is responsible for recruiting FAM83D and by extension CK1α to spindle microtubules, was found to regulate the PLK1-dependent spindle positioning pathway (Connell et al., 2017). PLK1 is a Ser/Thr protein kinase that possesses a polo-box domain, thought to be important in mediating PLK1 localisation (Combes, Alharbi et al., 2017, Garcia-Alvarez, de Carcer et al., 2007). The polo-box domain binds to phospho-epitopes on docking proteins, thereby localising PLK1 to spindle poles and kinetochores (Combes et al., 2017, Garcia-Alvarez et al., 2007, Park et al., 2010). Spindle pole-localised PLK1 is thought to regulate the activity of dynein complexes at the cortex, to create a balanced equilibrium of pulling

forces acting to position the spindle (Kiyomitsu & Cheeseman, 2012). In short, when a spindle pole gets too close to the cortex, PLK1 activity acts to strip dynein motor complexes from that near-cortex, resulting in greater pulling forces from the opposite cortex, and reestablishment of a centralised spindle (Kiyomitsu & Cheeseman, 2012). Cells lacking HMMR were found to have reduced PLK1 activity at spindle poles, and could not strip cortical dynein complexes effectively, resulting in aberrant spindle positioning (Connell et al., 2017). Given that cells lacking HMMR also lack FAM83D-CK1α on mitotic spindles, any defects resulting from HMMR depletion could be explained by non-delivery of CK1α to the spindle apparatus. Indeed, *FAM83D* knockout and *FAM83D*$^{GFP/GFP\ (F283A)}$ cells, as well as siCK1α-depleted cells, also present with spindle positioning defects. Thus, future efforts aimed at testing the tantalising hypothesis that CK1α also acts in the PLK1-dependent spindle positioning pathway may provide mechanistic insights into how CK1α regulates spindle orientation at the molecular level.

The HMMR-FAM83D-CK1α complex could be envisaged to regulate PLK1 activity by at least two mechanisms. Firstly, CK1α may act to activate PLK1 in a direct or indirect manner, although the upstream PLK1 kinase is generally believed to be Aurora A (Macurek et al., 2008). Secondly, and more likely, CK1α may act to phosphorylate a docking protein at the spindle pole to generate a phospho-epitope to facilitate polo-box domain binding, and allow PLK1 recruitment. Any FAM83D-centred phosphoproteomic screens should thus be examined for putative spindle-pole (and/or kinetochore) localised proteins, and tested for their ability to bind PLK1 following their phosphorylation by CK1α. However, it should be noted that HMMR is also reported to localise the TPX2-Aurora A complex to mitotic spindles (BlancoKuchenbaecker et al., 2015, Chen et al., 2014), so defects resulting from HMMR depletion are likely more severe than those resulting from FAM83D ablation alone.

Ultimately, cancer cells grown in culture do not care which direction they divide. However, in development, the precise control of spindle orientation is critical for tissue establishment, and for the asymmetric distribution of cell fate determining factors (Bergstralh et al., 2017, Lu & Johnston, 2013, Siller & Doe, 2009). Thus, to truly appreciate the physiological role of the HMMR-FAM83D-CK1α complex, and any accompanying defects following perturbation of this pathway, animal models are a logical next step. Whilst *CSNK1A1* is an essential gene, *FAM83D* and *HMMR* are not (Wang et al., 2015). Indeed, *HMMR* knockout mice present with neurodevelopmental defects, likely arising from spindle misorientation (Connell et al., 2017). Thus, ablation of *FAM83D* and/or *HMMR* in mice, or other animal models, would be predicted to facilitate the evaluation of CK1α in developmental cell divisions, without affecting the essential non-mitotic CK1α functions.

Many CK1 substrates appear to be degraded following their phosphorylation (Del Valle-Perez et al., 2011, Eide, Woolf et al., 2005, Gao et al., 2002, Huart et al., 2009, Xu, Lee et al., 2010). Given the dynamic nature of cell division, the cellular landscape must be quickly changed in order to facilitate mitotic exit and entry into interphase. Central to this notion is the proteolytic degradation of mitotic proteins following completion of their mitotic roles (Ang & Wade Harper, 2005, Chang et al., 2003, Koepp, 2014). Thus, it is feasible that CK1α-mediated phosphorylation of mitotic substrates simply acts to prime them for proteolysis by creating a phospho-degron signal. Indeed, in the case of FAM83D, which exhibits mitotic phosphorylation dependent on its interaction with CK1α, it seems to be the phosho-FAM83D species that is degraded following mitotic exit. Thus, examining any putative mitotic CK1 substrates on the basis that they may be degraded following their phosphorylation might be insightful. This will be particularly important when designing phosphoproteomic experiments, as

proteasomal inhibition may need to be employed in order to efficiently capture CK1-dependent phosphopeptides. Perhaps comparison of the proteomes and phosphoproteomes between wild-type and *FAM83D* knockout or *FAM83D*$^{GFP/GFP\ (F283A)}$ cells would address this question. Comparing the proteomes/phosphoproteomes between *FAM83D* knockout and *FAM83D*$^{GFP/GFP\ (F283A)}$ cells would additionally allow distinction between general FAM83D-dependent events (knockout cells) and FAM83D-dependent CK1α events (F283A cells).

The contribution of FAM83D to disease, if any, remains poorly defined. That said, FAM83D has been reported to promote the progression of certain cancers, namely those of ovarian, gastric, breast, colorectal, lung and hepatocellular origin (Huang et al., 2017, Liao, Liu et al., 2015, Lin, Chen et al., 2016, Perez-Pena et al., 2017, Shi et al., 2016, Wang, Han et al., 2015a, Yan, Yao et al., 2017, Zhang, Yu et al., 2019, Zhu, Diao et al., 2019). Whether this is merely an association, or if FAM83D truly is a driver of proliferation in these cancers, needs to be further investigated. Furthermore, whether this putative carcinogenic role requires the association of FAM83D with CK1α needs to be explored. Interestingly, lenalidomide-induced degradation of CK1α was recently shown to be effective in the treatment of pre-leukemic human myelodysplastic syndrome (MDS) (Stahl & Zeidan, 2017). In contrast, other studies have demonstrated that CK1 inhibitors stabilise β-Catenin and activate Wnt signalling, which promotes cell proliferation (MacDonald et al., 2009, Schittek & Sinnberg, 2014, Teo & Kahn, 2010). The findings presented here would suggest that the anti-proliferative effects of CK1α inhibitors might be occurring, at least in part, through the inhibition of the mitotic FAM83D-CK1α pool.

Given the participation of CK1 family kinases in such diverse signalling pathways, and the seemingly antagonistic roles within the same signalling pathway at different

stages of signal transduction (Del Valle-Perez et al., 2011, Knippschild et al., 2005a, Schittek & Sinnberg, 2014) (see section 1.2.4), pan-cellular inhibition of CK1 isoforms is likely not going to be effective, from both basic research and therapeutic perspectives. Teasing out specific CK1 functions using inhibitors will thus be very challenging, as would untangling CK1 processes following their knockdown with RNA interference approaches. A more attractive means of facilitating functional characterisation of CK1 isoforms may be to disrupt their interaction with FAM83 proteins, or other regulatory binding partners. In the case of CK1α in mitosis, both the ablation of FAM83D and the disruption of the FAM83D-CK1α interaction removed CK1α from mitotic spindles, yet presumably did not disrupt the other, non-mitotic roles of CK1α. Furthermore, knockout of *FAM83G* resulted in disruption of canonical Wnt signalling (Bozatzi et al., 2018), but, again, presumably did not impact the non-Wnt functions of CK1α. Whilst this model needs to be tested more comprehensively, abolition of FAM83-CK1 interactions may provide a novel means to study the biology of specific CK1 isoforms.

The identification of the biological niche(s) of the other FAM83-CK1 interactions is an important next step, in order to further test the working hypothesis that FAM83 proteins serve to direct CK1 isoforms to distinct cellular sites. Perhaps through creating a screen containing many different stimuli, involving growth factors and cellular stresses, the affinities of the other FAM83-CK1 interactions can be assessed in order to probe the biological pathways they might participate in. Indeed, as CK1 kinases have been extensively linked to DNA damage responses, the identification of a FAM83-CK1 pair involved in DNA damage signalling would be an interesting finding. Furthermore, many of the reported signalling pathways regulated by CK1 are principally important during development. Thus, in order to decipher any FAM83-CK1 pairs contributing to

these processes, such as the Hippo and Hedgehog pathways, a more physiological developmental model may need to be employed.

From a therapeutic standpoint, CK1 kinases have long been deemed undruggable. This is largely due to the vast array of cellular processes they seem to control. Furthermore, due to the highly homologous kinase domains between isoforms (Knippschild et al., 2005a, Schittek & Sinnberg, 2014) (Figure 1-2), off-target effects pertaining to related CK1 members and additional protein kinases have been a strong cause for concern. Perhaps targeted proteolysis of FAM83 members, using PROTAC technology for example, would be a viable strategy to shut down specific CK1 functions in disease. In line with this idea, AdPROM-mediated proteolytic degradation of FAM83D also removed CK1α from mitotic spindles, suggesting such proteolytic approaches would be effective.

In summary, the identification that FAM83 proteins act as regulatory subunits of CK1 isoforms adds to the evidence for the intricate control of CK1 kinases in cells. Using the FAM83D-CK1α interaction as an example, the model whereby FAM83 proteins act to recruit CK1 isoforms to distinct cellular sites so that they can elicit their functions was tested. Future efforts aimed at elucidating FAM83-dependent CK1 substrates is an important next step and, in combination with delineating the biology of the other non-characterised FAM83-CK1 interactions, will hopefully provide deeper insights into whether CK1 kinases will indeed be viable therapeutic targets.

References:

Adams J (2003) The proteasome: structure, function, and role in the cell. *Cancer Treat Rev* 29 Suppl 1: 3-9

Agostinis P, Pinna LA, Meggio F, Marin O, Goris J, Vandenheede JR, Merlevede W (1989) A synthetic peptide substrate specific for casein kinase I. *FEBS Lett* 259: 75-8

Akashi M, Tsuchiya Y, Yoshino T, Nishida E (2002) Control of intracellular dynamics of mammalian period proteins by casein kinase I epsilon (CKIepsilon) and CKIdelta in cultured cells. *Mol Cell Biol* 22: 1693-703

Akutsu M, Dikic I, Bremm A (2016) Ubiquitin chain diversity at a glance. *J Cell Sci* 129: 875-80

Allan C, Burel JM, Moore J, Blackburn C, Linkert M, Loynton S, Macdonald D, Moore WJ, Neves C, Patterson A, Porter M, Tarkowska A, Loranger B, Avondo J, Lagerstedt I, Lianas L, Leo S, Hands K, Hay RT, Patwardhan A et al. (2012) OMERO: flexible, model-driven data management for experimental biology. *Nat Methods* 9: 245-53

Amit S, Hatzubai A, Birman Y, Andersen JS, Ben-Shushan E, Mann M, Ben-Neriah Y, Alkalay I (2002) Axin-mediated CKI phosphorylation of beta-catenin at Ser 45: a molecular switch for the Wnt pathway. *Genes Dev* 16: 1066-76

An J, Ponthier CM, Sack R, Seebacher J, Stadler MB, Donovan KA, Fischer ES (2017) pSILAC mass spectrometry reveals ZFP91 as IMiD-dependent substrate of the CRL4(CRBN) ubiquitin ligase. *Nat Commun* 8: 15398

Ang XL, Wade Harper J (2005) SCF-mediated protein degradation and cell cycle control. *Oncogene* 24: 2860-70

Arnaud L, Pines J, Nigg EA (1998) GFP tagging reveals human Polo-like kinase 1 at the kinetochore/centromere region of mitotic chromosomes. *Chromosoma* 107: 424-9

Badura L, Swanson T, Adamowicz W, Adams J, Cianfrogna J, Fisher K, Holland J, Kleiman R, Nelson F, Reynolds L, St Germain K, Schaeffer E, Tate B, Sprouse J (2007) An inhibitor of casein kinase I epsilon induces phase delays in circadian rhythms under free-running and entrained conditions. *J Pharmacol Exp Ther* 322: 730-8

Bago R, Malik N, Munson MJ, Prescott AR, Davies P, Sommer E, Shpiro N, Ward R, Cross D, Ganley IG, Alessi DR (2014) Characterization of VPS34-IN1, a selective inhibitor of Vps34, reveals that the phosphatidylinositol 3-phosphate-binding SGK3 protein kinase is a downstream target of class III phosphoinositide 3-kinase. *Biochem J* 463: 413-27

Bain J, Plater L, Elliott M, Shpiro N, Hastie CJ, McLauchlan H, Klevernic I, Arthur JS, Alessi DR, Cohen P (2007) The selectivity of protein kinase inhibitors: a further update. *Biochem J* 408: 297-315

Barr FA, Sillje HH, Nigg EA (2004) Polo-like kinases and the orchestration of cell division. *Nat Rev Mol Cell Biol* 5: 429-40

Bartel CA, Parameswaran N, Cipriano R, Jackson MW (2016) FAM83 proteins: Fostering new interactions to drive oncogenic signaling and therapeutic resistance. *Oncotarget* 7: 52597-52612

Bayliss R, Sardon T, Vernos I, Conti E (2003) Structural basis of Aurora-A activation by TPX2 at the mitotic spindle. *Mol Cell* 12: 851-62

Beachy PA, Karhadkar SS, Berman DM (2004) Tissue repair and stem cell renewal in carcinogenesis. *Nature* 432: 324-31

Behrend L, Milne DM, Stoter M, Deppert W, Campbell LE, Meek DW, Knippschild U (2000) IC261, a specific inhibitor of the protein kinases casein kinase 1-delta and -epsilon, triggers the mitotic checkpoint and induces p53-dependent postmitotic effects. *Oncogene* 19: 5303-13

Bergstralh DT, Dawney NS, St Johnston D (2017) Spindle orientation: a question of complex positioning. *Development* 144: 1137-1145

Bernard P, Hardwick K, Javerzat JP (1998) Fission yeast bub1 is a mitotic centromere protein essential for the spindle checkpoint and the preservation of correct ploidy through mitosis. *J Cell Biol* 143: 1775-87

Bettayeb K, Oumata N, Echalier A, Ferandin Y, Endicott JA, Galons H, Meijer L (2008) CR8, a potent and selective, roscovitine-derived inhibitor of cyclin-dependent kinases. *Oncogene* 27: 5797-807

Beyaert R, Vanhaesebroeck B, Declercq W, Van Lint J, Vandenabele P, Agostinis P, Vandenheede JR, Fiers W (1995) Casein kinase-1 phosphorylates the p75 tumor necrosis factor receptor and negatively regulates tumor necrosis factor signaling for apoptosis. *J Biol Chem* 270: 23293-9

Bibian M, Rahaim RJ, Choi JY, Noguchi Y, Schurer S, Chen W, Nakanishi S, Licht K, Rosenberg LH, Li L, Feng Y, Cameron MD, Duckett DR, Cleveland JL, Roush WR (2013) Development of highly selective casein kinase 1delta/1epsilon (CK1delta/epsilon) inhibitors with potent antiproliferative properties. *Bioorg Med Chem Lett* 23: 4374-80

Bieging KT, Mello SS, Attardi LD (2014) Unravelling mechanisms of p53-mediated tumour suppression. *Nat Rev Cancer* 14: 359-70

Bischof J, Leban J, Zaja M, Grothey A, Radunsky B, Othersen O, Strobl S, Vitt D, Knippschild U (2012) 2-Benzamido-N-(1H-benzo[d]imidazol-2-yl)thiazole-4-carboxamide derivatives as potent inhibitors of CK1delta/epsilon. *Amino Acids* 43: 1577-91

Bischoff JR, Plowman GD (1999) The Aurora/Ipl1p kinase family: regulators of chromosome segregation and cytokinesis. *Trends Cell Biol* 9: 454-9

Blanco I, Kuchenbaecker K, Cuadras D, Wang X, Barrowdale D, de Garibay GR, Librado P, Sanchez-Gracia A, Rozas J, Bonifaci N, McGuffog L, Pankratz VS, Islam A, Mateo F, Berenguer A, Petit A, Catala I, Brunet J, Feliubadalo L, Tornero E et al. (2015) Assessing associations between the AURKA-HMMR-TPX2-TUBG1 functional module and breast cancer risk in BRCA1/2 mutation carriers. *PLoS One* 10: e0120020

Blanco MA, Sanchez-Diaz A, de Prada JM, Moreno S (2000) APC(ste9/srw1) promotes degradation of mitotic cyclins in G(1) and is inhibited by cdc2 phosphorylation. *EMBO J* 19: 3945-55

Bolanos-Garcia VM (2005) Aurora kinases. *Int J Biochem Cell Biol* 37: 1572-7

Bosu DR, Kipreos ET (2008) Cullin-RING ubiquitin ligases: global regulation and activation cycles. *Cell Div* 3: 7

Bozatzi P, Dingwell KS, Wu KZ, Cooper F, Cummins TD, Hutchinson LD, Vogt J, Wood NT, Macartney TJ, Varghese J, Gourlay R, Campbell DG, Smith JC, Sapkota GP (2018) PAWS1 controls Wnt signalling through association with casein kinase 1alpha. *EMBO Rep* 19

Bozatzi P, Sapkota GP (2018) The FAM83 family of proteins: from pseudo-PLDs to anchors for CK1 isoforms. *Biochem Soc Trans* 46: 761-771

Bradford MM (1976) A rapid and sensitive method for the quantitation of microgram quantities of protein utilizing the principle of protein-dye binding. *Anal Biochem* 72: 248-54

Brockman JL, Gross SD, Sussman MR, Anderson RA (1992) Cell cycle-dependent localization of casein kinase I to mitotic spindles. *Proc Natl Acad Sci U S A* 89: 9454-8

Brockschmidt C, Hirner H, Huber N, Eismann T, Hillenbrand A, Giamas G, Radunsky B, Ammerpohl O, Bohm B, Henne-Bruns D, Kalthoff H, Leithauser F, Trauzold A, Knippschild U (2008) Anti-apoptotic and growth-stimulatory functions of CK1 delta and epsilon in ductal adenocarcinoma of the pancreas are inhibited by IC261 in vitro and in vivo. *Gut* 57: 799-806

Brown NG, VanderLinden R, Watson ER, Qiao R, Grace CR, Yamaguchi M, Weissmann F, Frye JJ, Dube P, Ei Cho S, Actis ML, Rodrigues P, Fujii N, Peters JM, Stark H, Schulman BA (2015) RING E3 mechanism for ubiquitin ligation to a disordered substrate visualized for human anaphase-promoting complex. *Proc Natl Acad Sci U S A* 112: 5272-9

Bryja V, Schulte G, Rawal N, Grahn A, Arenas E (2007) Wnt-5a induces Dishevelled phosphorylation and dopaminergic differentiation via a CK1-dependent mechanism. *J Cell Sci* 120: 586-95

Budenholzer L, Cheng CL, Li Y, Hochstrasser M (2017) Proteasome Structure and Assembly. *J Mol Biol* 429: 3500-3524

Bulatov E, Ciulli A (2015) Targeting Cullin-RING E3 ubiquitin ligases for drug discovery: structure, assembly and small-molecule modulation. *Biochem J* 467: 365-86

Cardote TAF, Gadd MS, Ciulli A (2017) Crystal Structure of the Cul2-Rbx1-EloBC-VHL Ubiquitin Ligase Complex. *Structure* 25: 901-911 e3

Carmel G, Leichus B, Cheng X, Patterson SD, Mirza U, Chait BT, Kuret J (1994) Expression, purification, crystallization, and preliminary x-ray analysis of casein kinase-1 from Schizosaccharomyces pombe. *J Biol Chem* 269: 7304-9

Carmena M, Ruchaud S, Earnshaw WC (2009) Making the Auroras glow: regulation of Aurora A and B kinase function by interacting proteins. *Curr Opin Cell Biol* 21: 796-805

Cegielska A, Gietzen KF, Rivers A, Virshup DM (1998) Autoinhibition of casein kinase I epsilon (CKI epsilon) is relieved by protein phosphatases and limited proteolysis. *J Biol Chem* 273: 1357-64

Chang CH, Kuo CJ, Ito T, Su YY, Jiang ST, Chiu MH, Lin YH, Nist A, Mernberger M, Stiewe T, Ito S, Wakamatsu K, Hsueh YA, Shieh SY, Snir-Alkalay I, Ben-Neriah Y (2017) CK1alpha ablation in keratinocytes induces p53-dependent, sunburn-protective skin hyperpigmentation. *Proc Natl Acad Sci U S A* 114: E8035-E8044

Chang DC, Xu N, Luo KQ (2003) Degradation of cyclin B is required for the onset of anaphase in Mammalian cells. *J Biol Chem* 278: 37865-73

Chang LF, Zhang Z, Yang J, McLaughlin SH, Barford D (2014) Molecular architecture and mechanism of the anaphase-promoting complex. *Nature* 513: 388-393

Chen H, Connell M, Mei L, Reid GSD, Maxwell CA (2018) The non-motor adaptor HMMR dampens Eg5-mediated forces to preserve the kinetics and integrity of chromosome segregation. *Mol Biol Cell*

Chen H, Mohan P, Jiang J, Nemirovsky O, He D, Fleisch MC, Niederacher D, Pilarski LM, Lim CJ, Maxwell CA (2014) Spatial regulation of Aurora A activity during mitotic spindle assembly requires RHAMM to correctly localize TPX2. *Cell Cycle* 13: 2248-61

Chen Y, Sasai N, Ma G, Yue T, Jia J, Briscoe J, Jiang J (2011) Sonic Hedgehog dependent phosphorylation by CK1alpha and GRK2 is required for ciliary accumulation and activation of smoothened. *PLoS Biol* 9: e1001083

Cheng KY, Lowe ED, Sinclair J, Nigg EA, Johnson LN (2003) The crystal structure of the human polo-like kinase-1 polo box domain and its phospho-peptide complex. *EMBO J* 22: 5757-68

Cheong JK, Virshup DM (2011) Casein kinase 1: Complexity in the family. *Int J Biochem Cell Biol* 43: 465-9

Chijiwa T, Hagiwara M, Hidaka H (1989) A newly synthesized selective casein kinase I inhibitor, N-(2-aminoethyl)-5-chloroisoquinoline-8-sulfonamide, and affinity purification of casein kinase I from bovine testis. *J Biol Chem* 264: 4924-7

Choi SY, Huang P, Jenkins GM, Chan DC, Schiller J, Frohman MA (2006) A common lipid links Mfn-mediated mitochondrial fusion and SNARE-regulated exocytosis. *Nat Cell Biol* 8: 1255-62

Cipriano R, Bryson BL, Miskimen KL, Bartel CA, Hernandez-Sanchez W, Bruntz RC, Scott SA, Lindsley CW, Brown HA, Jackson MW (2014a) Hyperactivation of EGFR and downstream effector phospholipase D1 by oncogenic FAM83B. *Oncogene* 33: 3298-306

Cipriano R, Graham J, Miskimen KL, Bryson BL, Bruntz RC, Scott SA, Brown HA, Stark GR, Jackson MW (2012) FAM83B mediates EGFR- and RAS-driven oncogenic transformation. *J Clin Invest* 122: 3197-210

Cipriano R, Miskimen KL, Bryson BL, Foy CR, Bartel CA, Jackson MW (2013) FAM83B-mediated activation of PI3K/AKT and MAPK signaling cooperates to promote epithelial cell transformation and resistance to targeted therapies. *Oncotarget* 4: 729-38

Cipriano R, Miskimen KL, Bryson BL, Foy CR, Bartel CA, Jackson MW (2014b) Conserved oncogenic behavior of the FAM83 family regulates MAPK signaling in human cancer. *Mol Cancer Res* 12: 1156-65

Cohen P (1999) The development and therapeutic potential of protein kinase inhibitors. *Curr Opin Chem Biol* 3: 459-65

Cohen P (2002a) The origins of protein phosphorylation. *Nat Cell Biol* 4: E127-30

Cohen P (2002b) Protein kinases--the major drug targets of the twenty-first century? *Nat Rev Drug Discov* 1: 309-15

Cohen P (2009) Targeting protein kinases for the development of anti-inflammatory drugs. *Curr Opin Cell Biol* 21: 317-24

Combes G, Alharbi I, Braga LG, Elowe S (2017) Playing polo during mitosis: PLK1 takes the lead. *Oncogene* 36: 4819-4827

Cong L, Ran FA, Cox D, Lin S, Barretto R, Habib N, Hsu PD, Wu X, Jiang W, Marraffini LA, Zhang F (2013) Multiplex genome engineering using CRISPR/Cas systems. *Science* 339: 819-23

Connell M, Chen H, Jiang J, Kuan CW, Fotovati A, Chu TL, He Z, Lengyell TC, Li H, Kroll T, Li AM, Goldowitz D, Frappart L, Ploubidou A, Patel MS, Pilarski LM, Simpson EM, Lange PF, Allan DW, Maxwell CA (2017) HMMR acts in the PLK1-dependent spindle positioning pathway and supports neural development. *Elife* 6

Cozza G, Gianoncelli A, Montopoli M, Caparrotta L, Venerando A, Meggio F, Pinna LA, Zagotto G, Moro S (2008) Identification of novel protein kinase CK1 delta (CK1delta) inhibitors through structure-based virtual screening. *Bioorg Med Chem Lett* 18: 5672-5

Cruciat CM (2014) Casein kinase 1 and Wnt/beta-catenin signaling. *Curr Opin Cell Biol* 31: 46-55

Cruciat CM, Dolde C, de Groot RE, Ohkawara B, Reinhard C, Korswagen HC, Niehrs C (2013) RNA helicase DDX3 is a regulatory subunit of casein kinase 1 in Wnt-beta-catenin signaling. *Science* 339: 1436-41

Cummins TD, Wu KZL, Bozatzi P, Dingwell KS, Macartney TJ, Wood NT, Varghese J, Gourlay R, Campbell DG, Prescott A, Griffis E, Smith JC, Sapkota GP (2018) PAWS1 controls cytoskeletal dynamics and cell migration through association with the SH3 adaptor CD2AP. *J Cell Sci* 131

Dawson IA, Roth S, Akam M, Artavanis-Tsakonas S (1993) Mutations of the fizzy locus cause metaphase arrest in Drosophila melanogaster embryos. *Development* 117: 359-76

Dawson IA, Roth S, Artavanis-Tsakonas S (1995) The Drosophila cell cycle gene fizzy is required for normal degradation of cyclins A and B during mitosis and has homology to the CDC20 gene of Saccharomyces cerevisiae. *J Cell Biol* 129: 725-37

Del Valle-Perez B, Arques O, Vinyoles M, de Herreros AG, Dunach M (2011) Coordinated action of CK1 isoforms in canonical Wnt signaling. *Mol Cell Biol* 31: 2877-88

Delehouze C, Godl K, Loaec N, Bruyere C, Desban N, Oumata N, Galons H, Roumeliotis TI, Giannopoulou EG, Grenet J, Twitchell D, Lahti J, Mouchet N, Galibert MD, Garbis SD, Meijer L (2014) CDK/CK1 inhibitors roscovitine and CR8 downregulate amplified MYCN in neuroblastoma cells. *Oncogene* 33: 5675-87

DeMaggio AJ, Lindberg RA, Hunter T, Hoekstra MF (1992) The budding yeast HRR25 gene product is a casein kinase I isoform. *Proc Natl Acad Sci U S A* 89: 7008-12

Denef N, Neubuser D, Perez L, Cohen SM (2000) Hedgehog induces opposite changes in turnover and subcellular localization of patched and smoothened. *Cell* 102: 521-31

Dephoure N, Zhou C, Villen J, Beausoleil SA, Bakalarski CE, Elledge SJ, Gygi SP (2008) A quantitative atlas of mitotic phosphorylation. *Proc Natl Acad Sci U S A* 105: 10762-7

Deshaies RJ (1999) SCF and Cullin/Ring H2-based ubiquitin ligases. *Annu Rev Cell Dev Biol* 15: 435-67

Dohmen RJ, Wu P, Varshavsky A (1994) Heat-inducible degron: a method for constructing temperature-sensitive mutants. *Science* 263: 1273-6

Drogemuller M, Jagannathan V, Becker D, Drogemuller C, Schelling C, Plassais J, Kaerle C, Dufaure de Citres C, Thomas A, Muller EJ, Welle MM, Roosje P, Leeb T (2014) A mutation in the FAM83G gene in dogs with hereditary footpad hyperkeratosis (HFH). *PLoS Genet* 10: e1004370

Dube P, Herzog F, Gieffers C, Sander B, Riedel D, Muller SA, Engel A, Peters JM, Stark H (2005) Localization of the coactivator Cdh1 and the cullin subunit Apc2 in a cryo-electron microscopy model of vertebrate APC/C. *Mol Cell* 20: 867-79

Duda DM, Scott DC, Calabrese MF, Zimmerman ES, Zheng N, Schulman BA (2011) Structural regulation of cullin-RING ubiquitin ligase complexes. *Curr Opin Struct Biol* 21: 257-64

Dumaz N, Milne DM, Meek DW (1999) Protein kinase CK1 is a p53-threonine 18 kinase which requires prior phosphorylation of serine 15. *FEBS Lett* 463: 312-6

Dunsch AK, Hammond D, Lloyd J, Schermelleh L, Gruneberg U, Barr FA (2012) Dynein light chain 1 and a spindle-associated adaptor promote dynein asymmetry and spindle orientation. *J Cell Biol* 198: 1039-54

Echalier A, Endicott JA, Noble ME (2010) Recent developments in cyclin-dependent kinase biochemical and structural studies. *Biochim Biophys Acta* 1804: 511-9

Eide EJ, Vielhaber EL, Hinz WA, Virshup DM (2002) The circadian regulatory proteins BMAL1 and cryptochromes are substrates of casein kinase Iepsilon. *J Biol Chem* 277: 17248-54

Eide EJ, Woolf MF, Kang H, Woolf P, Hurst W, Camacho F, Vielhaber EL, Giovanni A, Virshup DM (2005) Control of mammalian circadian rhythm by CKIepsilon-regulated proteasome-mediated PER2 degradation. *Mol Cell Biol* 25: 2795-807

Elia AE, Cantley LC, Yaffe MB (2003) Proteomic screen finds pSer/pThr-binding domain localizing Plk1 to mitotic substrates. *Science* 299: 1228-31

Elia AE, Rellos P, Haire LF, Chao JW, Ivins FJ, Hoepker K, Mohammad D, Cantley LC, Smerdon SJ, Yaffe MB (2003) The molecular basis for phosphodependent substrate targeting and regulation of Plks by the Polo-box domain. *Cell* 115: 83-95

Elledge SJ, Spottswood MR (1991) A new human p34 protein kinase, CDK2, identified by complementation of a cdc28 mutation in Saccharomyces cerevisiae, is a homolog of Xenopus Eg1. *EMBO J* 10: 2653-9

Elmore S (2007) Apoptosis: a review of programmed cell death. *Toxicol Pathol* 35: 495-516

Elyada E, Pribluda A, Goldstein RE, Morgenstern Y, Brachya G, Cojocaru G, Snir-Alkalay I, Burstain I, Haffner-Krausz R, Jung S, Wiener Z, Alitalo K, Oren M, Pikarsky E, Ben-Neriah Y (2011) CKIalpha ablation highlights a critical role for p53 in invasiveness control. *Nature* 470: 409-13

Enchev RI, Schulman BA, Peter M (2015) Protein neddylation: beyond cullin-RING ligases. *Nat Rev Mol Cell Biol* 16: 30-44

Enserink JM, Kolodner RD (2010) An overview of Cdk1-controlled targets and processes. *Cell Div* 5: 11

Etchegaray JP, Machida KK, Noton E, Constance CM, Dallmann R, Di Napoli MN, DeBruyne JP, Lambert CM, Yu EA, Reppert SM, Weaver DR (2009) Casein kinase 1 delta regulates the pace of the mammalian circadian clock. *Mol Cell Biol* 29: 3853-66

Evans T, Rosenthal ET, Youngblom J, Distel D, Hunt T (1983) Cyclin: a protein specified by maternal mRNA in sea urchin eggs that is destroyed at each cleavage division. *Cell* 33: 389-96

Eyers PA, Murphy JM (2013) Dawn of the dead: protein pseudokinases signal new adventures in cell biology. *Biochem Soc Trans* 41: 969-74

Fang G, Yu H, Kirschner MW (1998) Direct binding of CDC20 protein family members activates the anaphase-promoting complex in mitosis and G1. *Mol Cell* 2: 163-71

Fink J, Carpi N, Betz T, Betard A, Chebah M, Azioune A, Bornens M, Sykes C, Fetler L, Cuvelier D, Piel M (2011) External forces control mitotic spindle positioning. *Nat Cell Biol* 13: 771-8

Fish KJ, Cegielska A, Getman ME, Landes GM, Virshup DM (1995) Isolation and characterization of human casein kinase I epsilon (CKI), a novel member of the CKI gene family. *J Biol Chem* 270: 14875-83

Flajolet M, He G, Heiman M, Lin A, Nairn AC, Greengard P (2007) Regulation of Alzheimer's disease amyloid-beta formation by casein kinase I. *Proc Natl Acad Sci U S A* 104: 4159-64

Fleming ES, Temchin M, Wu Q, Maggio-Price L, Tirnauer JS (2009) Spindle misorientation in tumors from APC(min/+) mice. *Mol Carcinog* 48: 592-8

Flotow H, Graves PR, Wang AQ, Fiol CJ, Roeske RW, Roach PJ (1990) Phosphate groups as substrate determinants for casein kinase I action. *J Biol Chem* 265: 14264-9

Flotow H, Roach PJ (1991) Role of acidic residues as substrate determinants for casein kinase I. *J Biol Chem* 266: 3724-7

Foldynova-Trantirkova S, Sekyrova P, Tmejova K, Brumovska E, Bernatik O, Blankenfeldt W, Krejci P, Kozubik A, Dolezal T, Trantirek L, Bryja V (2010) Breast cancer-specific mutations in CK1epsilon inhibit Wnt/beta-catenin and activate the Wnt/Rac1/JNK and NFAT pathways to decrease cell adhesion and promote cell migration. *Breast Cancer Res* 12: R30

Folkes LK, Dennis MF, Stratford MR, Candeias LP, Wardman P (1999) Peroxidase-catalyzed effects of indole-3-acetic acid and analogues on lipid membranes, DNA, and mammalian cells in vitro. *Biochem Pharmacol* 57: 375-82

Fridy PC, Li Y, Keegan S, Thompson MK, Nudelman I, Scheid JF, Oeffinger M, Nussenzweig MC, Fenyo D, Chait BT, Rout MP (2014) A robust pipeline for rapid production of versatile nanobody repertoires. *Nat Methods* 11: 1253-60

Fry AM, Bayliss R, Roig J (2017) Mitotic Regulation by NEK Kinase Networks. *Front Cell Dev Biol* 5: 102

Fu J, Bian M, Liu J, Jiang Q, Zhang C (2009) A single amino acid change converts Aurora-A into Aurora-B-like kinase in terms of partner specificity and cellular function. *Proc Natl Acad Sci U S A* 106: 6939-44

Fulcher LJ, Bozatzi P, Tachie-Menson T, Wu KZL, Cummins TD, Bufton JC, Pinkas DM, Dunbar K, Shrestha S, Wood NT, Weidlich S, Macartney TJ, Varghese J, Gourlay R, Campbell DG, Dingwell KS, Smith JC, Bullock AN, Sapkota GP (2018) The DUF1669 domain of FAM83 family proteins anchor casein kinase 1 isoforms. *Sci Signal* 11

Fuziwara CS, Saito KC, Leoni SG, Waitzberg AFL, Kimura ET (2019) The Highly Expressed FAM83F Protein in Papillary Thyroid Cancer Exerts a Pro-Oncogenic Role in Thyroid Follicular Cells. *Front Endocrinol (Lausanne)* 10: 134

Gallini S, Carminati M, De Mattia F, Pirovano L, Martini E, Oldani A, Asteriti IA, Guarguaglini G, Mapelli M (2016) NuMA Phosphorylation by Aurora-A Orchestrates Spindle Orientation. *Curr Biol* 26: 458-69

Gao C, Chen YG (2010) Dishevelled: The hub of Wnt signaling. *Cell Signal* 22: 717-27

Gao ZH, Seeling JM, Hill V, Yochum A, Virshup DM (2002) Casein kinase I phosphorylates and destabilizes the beta-catenin degradation complex. *Proc Natl Acad Sci U S A* 99: 1182-7

Garcia-Alvarez B, de Carcer G, Ibanez S, Bragado-Nilsson E, Montoya G (2007) Molecular and structural basis of polo-like kinase 1 substrate recognition: Implications in centrosomal localization. *Proc Natl Acad Sci U S A* 104: 3107-12

Ghoshal N, Smiley JF, DeMaggio AJ, Hoekstra MF, Cochran EJ, Binder LI, Kuret J (1999) A new molecular link between the fibrillar and granulovacuolar lesions of Alzheimer's disease. *Am J Pathol* 155: 1163-72

Giet R, Prigent C (1999) Aurora/Ipl1p-related kinases, a new oncogenic family of mitotic serine-threonine kinases. *J Cell Sci* 112 (Pt 21): 3591-601

Gietzen KF, Virshup DM (1999) Identification of inhibitory autophosphorylation sites in casein kinase I epsilon. *J Biol Chem* 274: 32063-70

Gillooly DJ, Morrow IC, Lindsay M, Gould R, Bryant NJ, Gaullier JM, Parton RG, Stenmark H (2000) Localization of phosphatidylinositol 3-phosphate in yeast and mammalian cells. *EMBO J* 19: 4577-88

Glover CV, 3rd (1998) On the physiological role of casein kinase II in Saccharomyces cerevisiae. *Prog Nucleic Acid Res Mol Biol* 59: 95-133

Glover DM (1989) Mitosis in Drosophila. *J Cell Sci* 92 (Pt 2): 137-46

Glover DM (1991) Mitosis in the Drosophila embryo--in and out of control. *Trends Genet* 7: 125-32

Glover DM, Leibowitz MH, McLean DA, Parry H (1995) Mutations in aurora prevent centrosome separation leading to the formation of monopolar spindles. *Cell* 81: 95-105

Gmachl M, Gieffers C, Podtelejnikov AV, Mann M, Peters JM (2000) The RING-H2 finger protein APC11 and the E2 enzyme UBC4 are sufficient to ubiquitinate substrates of the anaphase-promoting complex. *Proc Natl Acad Sci U S A* 97: 8973-8

Golan A, Yudkovsky Y, Hershko A (2002) The cyclin-ubiquitin ligase activity of cyclosome/APC is jointly activated by protein kinases Cdk1-cyclin B and Plk. *J Biol Chem* 277: 15552-7

Golsteyn RM, Mundt KE, Fry AM, Nigg EA (1995) Cell cycle regulation of the activity and subcellular localization of Plk1, a human protein kinase implicated in mitotic spindle function. *J Cell Biol* 129: 1617-28

Gonczy P (2008) Mechanisms of asymmetric cell division: flies and worms pave the way. *Nat Rev Mol Cell Biol* 9: 355-66

Good MC, Zalatan JG, Lim WA (2011) Scaffold proteins: hubs for controlling the flow of cellular information. *Science* 332: 680-6

Gotta M, Dong Y, Peterson YK, Lanier SM, Ahringer J (2003) Asymmetrically distributed C. elegans homologs of AGS3/PINS control spindle position in the early embryo. *Curr Biol* 13: 1029-37

Graves PR, Haas DW, Hagedorn CH, DePaoli-Roach AA, Roach PJ (1993) Molecular cloning, expression, and characterization of a 49-kilodalton casein kinase I isoform from rat testis. *J Biol Chem* 268: 6394-401

Grill SW, Howard J, Schaffer E, Stelzer EH, Hyman AA (2003) The distribution of active force generators controls mitotic spindle position. *Science* 301: 518-21

Grill SW, Hyman AA (2005) Spindle positioning by cortical pulling forces. *Dev Cell* 8: 461-5

Gross SD, Anderson RA (1998) Casein kinase I: spatial organization and positioning of a multifunctional protein kinase family. *Cell Signal* 10: 699-711

Gross SD, Simerly C, Schatten G, Anderson RA (1997) A casein kinase I isoform is required for proper cell cycle progression in the fertilized mouse oocyte. *J Cell Sci* 110 (Pt 24): 3083-90

Gu GM, Zhan YY, Abuduwaili K, Wang XL, Li XQ, Zhu HG, Liu CL (2018) MiR-940 inhibits the progression of NSCLC by targeting FAM83F. *Eur Rev Med Pharmacol Sci* 22: 5964-5971

Halekotte J, Witt L, Ianes C, Kruger M, Buhrmann M, Rauh D, Pichlo C, Brunstein E, Luxenburger A, Baumann U, Knippschild U, Bischof J, Peifer C (2017) Optimized 4,5-Diarylimidazoles as Potent/Selective Inhibitors of Protein Kinase CK1delta and Their Structural Relation to p38alpha MAPK. *Molecules* 22

Hans F, Skoufias DA, Dimitrov S, Margolis RL (2009) Molecular distinctions between Aurora A and B: a single residue change transforms Aurora A into correctly localized and functional Aurora B. *Mol Biol Cell* 20: 3491-502

Hartwell LH (1974) Saccharomyces cerevisiae cell cycle. *Bacteriol Rev* 38: 164-98

Hartwell LH, Mortimer RK, Culotti J, Culotti M (1973) Genetic Control of the Cell Division Cycle in Yeast: V. Genetic Analysis of cdc Mutants. *Genetics* 74: 267-86

Hastie CJ, McLauchlan HJ, Cohen P (2006) Assay of protein kinases using radiolabeled ATP: a protocol. *Nat Protoc* 1: 968-71

Hesse J, Ebbesen P, Kristensen G (1978) Correlation between polyion effect on cell susceptibility to in vitro infection with murine C-type viruses and polyion effect on some membrane-related functions. *Intervirology* 9: 173-83

Hoekstra MF, DeMaggio AJ, Dhillon N (1991) Genetically identified protein kinases in yeast. II: DNA metabolism and meiosis. *Trends Genet* 7: 293-7

Hoekstra MF, Liskay RM, Ou AC, DeMaggio AJ, Burbee DG, Heffron F (1991) HRR25, a putative protein kinase from budding yeast: association with repair of damaged DNA. *Science* 253: 1031-4

Hoshi N, Langeberg LK, Scott JD (2005) Distinct enzyme combinations in AKAP signalling complexes permit functional diversity. *Nat Cell Biol* 7: 1066-73

Hua Z, Huang X, Bregman H, Chakka N, DiMauro EF, Doherty EM, Goldstein J, Gunaydin H, Huang H, Mercede S, Newcomb J, Patel VF, Turci SM, Yan J, Wilson C, Martin MW (2012) 2-Phenylamino-6-cyano-1H-benzimidazole-based isoform selective casein kinase 1 gamma (CK1gamma) inhibitors. *Bioorg Med Chem Lett* 22: 5392-5

Huang M, Ma X, Shi H, Hu L, Fan Z, Pang L, Zhu F, Yang X, Xu W, Liu B, Zhu Z, Li C (2017) FAM83D, a microtubule-associated protein, promotes tumor growth and progression of human gastric cancer. *Oncotarget* 8: 74479-74493

Huart AS, MacLaine NJ, Meek DW, Hupp TR (2009) CK1alpha plays a central role in mediating MDM2 control of p53 and E2F-1 protein stability. *J Biol Chem* 284: 32384-94

Huart AS, MacLaine NJ, Narayan V, Hupp TR (2012) Exploiting the MDM2-CK1alpha protein-protein interface to develop novel biologics that induce UBL-kinase-modification and inhibit cell growth. *PLoS One* 7: e43391

Hutterer A, Berdnik D, Wirtz-Peitz F, Zigman M, Schleiffer A, Knoblich JA (2006) Mitotic activation of the kinase Aurora-A requires its binding partner Bora. *Dev Cell* 11: 147-57

Ikezu S, Ikezu T (2014) Tau-tubulin kinase. *Front Mol Neurosci* 7: 33
Ingham PW, McMahon AP (2001) Hedgehog signaling in animal development: paradigms and principles. *Genes Dev* 15: 3059-87

Ishikawa HO, Xu A, Ogura E, Manning G, Irvine KD (2012) The Raine syndrome protein FAM20C is a Golgi kinase that phosphorylates bio-mineralization proteins. *PLoS One* 7: e42988

Ito M (2000) Factors controlling cyclin B expression. *Plant Mol Biol* 43: 677-90

Izeradjene K, Douglas L, Delaney AB, Houghton JA (2004) Casein kinase I attenuates tumor necrosis factor-related apoptosis-inducing ligand-induced apoptosis by regulating the recruitment of fas-associated death domain and procaspase-8 to the death-inducing signaling complex. *Cancer Res* 64: 8036-44

Jackson PK, Eldridge AG, Freed E, Furstenthal L, Hsu JY, Kaiser BK, Reimann JD (2000) The lore of the RINGs: substrate recognition and catalysis by ubiquitin ligases. *Trends Cell Biol* 10: 429-39

Jang YJ, Lin CY, Ma S, Erikson RL (2002) Functional studies on the role of the C-terminal domain of mammalian polo-like kinase. *Proc Natl Acad Sci U S A* 99: 1984-9

Jang YJ, Ma S, Terada Y, Erikson RL (2002) Phosphorylation of threonine 210 and the role of serine 137 in the regulation of mammalian polo-like kinase. *J Biol Chem* 277: 44115-20

Jaras M, Miller PG, Chu LP, Puram RV, Fink EC, Schneider RK, Al-Shahrour F, Pena P, Breyfogle LJ, Hartwell KA, McConkey ME, Cowley GS, Root DE, Kharas MG, Mullally A, Ebert BL (2014) Csnk1a1 inhibition has p53-dependent therapeutic efficacy in acute myeloid leukemia. *J Exp Med* 211: 605-12

Jenkins GM, Frohman MA (2005) Phospholipase D: a lipid centric review. *Cell Mol Life Sci* 62: 2305-16

Ji JH, Hwang HI, Lee HJ, Hyun SY, Kang HJ, Jang YJ (2010) Purification and proteomic identification of putative upstream regulators of polo-like kinase-1 from mitotic cell extracts. *FEBS Lett* 584: 4299-305

Johnston CA, Hirono K, Prehoda KE, Doe CQ (2009) Identification of an Aurora-A/PinsLINKER/Dlg spindle orientation pathway using induced cell polarity in S2 cells. *Cell* 138: 1150-63

Kalab P, Heald R (2008) The RanGTP gradient - a GPS for the mitotic spindle. *J Cell Sci* 121: 1577-86

Kam Y, Exton JH (2002) Dimerization of phospholipase d isozymes. *Biochem Biophys Res Commun* 290: 375-80

Kamura T, Maenaka K, Kotoshiba S, Matsumoto M, Kohda D, Conaway RC, Conaway JW, Nakayama KI (2004) VHL-box and SOCS-box domains determine binding specificity for Cul2-Rbx1 and Cul5-Rbx2 modules of ubiquitin ligases. *Genes Dev* 18: 3055-65

Kanai F, Liu H, Field SJ, Akbary H, Matsuo T, Brown GE, Cantley LC, Yaffe MB (2001) The PX domains of p47phox and p40phox bind to lipid products of PI(3)K. *Nat Cell Biol* 3: 675-8

Kang J, Chen Y, Zhao Y, Yu H (2007) Autophosphorylation-dependent activation of human Mps1 is required for the spindle checkpoint. *Proc Natl Acad Sci U S A* 104: 20232-7

Ke YW, Dou Z, Zhang J, Yao XB (2003) Function and regulation of Aurora/Ipl1p kinase family in cell division. *Cell Res* 13: 69-81

Kelly AE, Sampath SC, Maniar TA, Woo EM, Chait BT, Funabiki H (2007) Chromosomal enrichment and activation of the aurora B pathway are coupled to spatially regulate spindle assembly. *Dev Cell* 12: 31-43

Kemmler S, Stach M, Knapp M, Ortiz J, Pfannstiel J, Ruppert T, Lechner J (2009) Mimicking Ndc80 phosphorylation triggers spindle assembly checkpoint signalling. *EMBO J* 28: 1099-110

Kim JW, Lee SK, Lee ZH, Park JC, Lee KE, Lee MH, Park JT, Seo BM, Hu JC, Simmer JP (2008) FAM83H mutations in families with autosomal-dominant hypocalcified amelogenesis imperfecta. *Am J Hum Genet* 82: 489-94

King DP, Takahashi JS (2000) Molecular genetics of circadian rhythms in mammals. *Annu Rev Neurosci* 23: 713-42

King RW, Deshaies RJ, Peters JM, Kirschner MW (1996) How proteolysis drives the cell cycle. *Science* 274: 1652-9

Kirchhofer A, Helma J, Schmidthals K, Frauer C, Cui S, Karcher A, Pellis M, Muyldermans S, Casas-Delucchi CS, Cardoso MC, Leonhardt H, Hopfner KP, Rothbauer U (2010) Modulation of protein properties in living cells using nanobodies. *Nat Struct Mol Biol* 17: 133-8

Kiyomitsu T, Cheeseman IM (2012) Chromosome- and spindle-pole-derived signals generate an intrinsic code for spindle position and orientation. *Nat Cell Biol* 14: 311-7

Kiyomitsu T, Cheeseman IM (2013) Cortical dynein and asymmetric membrane elongation coordinately position the spindle in anaphase. *Cell* 154: 391-402

Klebe C, Prinz H, Wittinghofer A, Goody RS (1995) The kinetic mechanism of Ran--nucleotide exchange catalyzed by RCC1. *Biochemistry* 34: 12543-52

Klebig C, Korinth D, Meraldi P (2009) Bub1 regulates chromosome segregation in a kinetochore-independent manner. *J Cell Biol* 185: 841-58

Kloss B, Price JL, Saez L, Blau J, Rothenfluh A, Wesley CS, Young MW (1998) The Drosophila clock gene double-time encodes a protein closely related to human casein kinase Iepsilon. *Cell* 94: 97-107

Knippschild U, Gocht A, Wolff S, Huber N, Lohler J, Stoter M (2005a) The casein kinase 1 family: participation in multiple cellular processes in eukaryotes. *Cell Signal* 17: 675-89

Knippschild U, Kruger M, Richter J, Xu P, Garcia-Reyes B, Peifer C, Halekotte J, Bakulev V, Bischof J (2014) The CK1 Family: Contribution to Cellular Stress Response and Its Role in Carcinogenesis. *Front Oncol* 4: 96

Knippschild U, Milne DM, Campbell LE, DeMaggio AJ, Christenson E, Hoekstra MF, Meek DW (1997) p53 is phosphorylated in vitro and in vivo by the delta and epsilon isoforms of casein kinase 1 and enhances the level of casein kinase 1 delta in response to topoisomerase-directed drugs. *Oncogene* 15: 1727-36

Knippschild U, Wolff S, Giamas G, Brockschmidt C, Wittau M, Wurl PU, Eismann T, Stoter M (2005b) The role of the casein kinase 1 (CK1) family in different signaling pathways linked to cancer development. *Onkologie* 28: 508-14

Koepp DM (2014) Cell cycle regulation by protein degradation. *Methods Mol Biol* 1170: 61-73

Komander D, Rape M (2012) The ubiquitin code. *Annu Rev Biochem* 81: 203-29

Konno D, Shioi G, Shitamukai A, Mori A, Kiyonari H, Miyata T, Matsuzaki F (2008) Neuroepithelial progenitors undergo LGN-dependent planar divisions to maintain self-renewability during mammalian neurogenesis. *Nat Cell Biol* 10: 93-101

Kotak S, Afshar K, Busso C, Gonczy P (2016) Aurora A kinase regulates proper spindle positioning in C. elegans and in human cells. *J Cell Sci* 129: 3015-25

Kotak S, Busso C, Gonczy P (2012) Cortical dynein is critical for proper spindle positioning in human cells. *J Cell Biol* 199: 97-110

Kotak S, Busso C, Gonczy P (2013) NuMA phosphorylation by CDK1 couples mitotic progression with cortical dynein function. *EMBO J* 32: 2517-29

Kotak S, Busso C, Gonczy P (2014) NuMA interacts with phosphoinositides and links the mitotic spindle with the plasma membrane. *EMBO J* 33: 1815-30

Kraft C, Herzog F, Gieffers C, Mechtler K, Hagting A, Pines J, Peters JM (2003) Mitotic regulation of the human anaphase-promoting complex by phosphorylation. *EMBO J* 22: 6598-609

Kramer ER, Gieffers C, Holzl G, Hengstschlager M, Peters JM (1998) Activation of the human anaphase-promoting complex by proteins of the CDC20/Fizzy family. *Curr Biol* 8: 1207-10

Kramer ER, Scheuringer N, Podtelejnikov AV, Mann M, Peters JM (2000) Mitotic regulation of the APC activator proteins CDC20 and CDH1. *Mol Biol Cell* 11: 1555-69

Kronja I, Orr-Weaver TL (2011) Translational regulation of the cell cycle: when, where, how and why? *Philos Trans R Soc Lond B Biol Sci* 366: 3638-52

Kucherenko Y, Zelenak C, Eberhard M, Qadri SM, Lang F (2012) Effect of casein kinase 1alpha activator pyrvinium pamoate on erythrocyte ion channels. *Cell Physiol Biochem* 30: 407-17

Kufer TA, Sillje HH, Korner R, Gruss OJ, Meraldi P, Nigg EA (2002) Human TPX2 is required for targeting Aurora-A kinase to the spindle. *J Cell Biol* 158: 617-23

Kuga T, Kume H, Adachi J, Kawasaki N, Shimizu M, Hoshino I, Matsubara H, Saito Y, Nakayama Y, Tomonaga T (2016a) Casein kinase 1 is recruited to nuclear speckles by FAM83H and SON. *Sci Rep* 6: 34472

Kuga T, Kume H, Kawasaki N, Sato M, Adachi J, Shiromizu T, Hoshino I, Nishimori T, Matsubara H, Tomonaga T (2013) A novel mechanism of keratin cytoskeleton organization through casein kinase Ialpha and FAM83H in colorectal cancer. *J Cell Sci* 126: 4721-31

Kuga T, Sasaki M, Mikami T, Miake Y, Adachi J, Shimizu M, Saito Y, Koura M, Takeda Y, Matsuda J, Tomonaga T, Nakayama Y (2016b) FAM83H and casein kinase I regulate the organization of the keratin cytoskeleton and formation of desmosomes. *Sci Rep* 6: 26557
Kumar R, Tao M (1975) Multiple forms of casein kinase from rabbit erythrocytes. *Biochim Biophys Acta* 410: 87-98

Kwon M, Bagonis M, Danuser G, Pellman D (2015) Direct Microtubule-Binding by Myosin-10 Orients Centrosomes toward Retraction Fibers and Subcortical Actin Clouds. *Dev Cell* 34: 323-37

Labib K, Tercero JA, Diffley JF (2000) Uninterrupted MCM2-7 function required for DNA replication fork progression. *Science* 288: 1643-7

Lahav-Baratz S, Sudakin V, Ruderman JV, Hershko A (1995) Reversible phosphorylation controls the activity of cyclosome-associated cyclin-ubiquitin ligase. *Proc Natl Acad Sci U S A* 92: 9303-7

Lee KS, Erikson RL (1997) Plk is a functional homolog of Saccharomyces cerevisiae Cdc5, and elevated Plk activity induces multiple septation structures. *Mol Cell Biol* 17: 3408-17

Lee KS, Grenfell TZ, Yarm FR, Erikson RL (1998) Mutation of the polo-box disrupts localization and mitotic functions of the mammalian polo kinase Plk. *Proc Natl Acad Sci U S A* 95: 9301-6

Lee KS, Yuan YL, Kuriyama R, Erikson RL (1995) Plk is an M-phase-specific protein kinase and interacts with a kinesin-like protein, CHO1/MKLP-1. *Mol Cell Biol* 15: 7143-51

Lee MG, Nurse P (1987) Complementation used to clone a human homologue of the fission yeast cell cycle control gene cdc2. *Nature* 327: 31-5

Lee SK, Lee KE, Jeong TS, Hwang YH, Kim S, Hu JC, Simmer JP, Kim JW (2011) FAM83H mutations cause ADHCAI and alter intracellular protein localization. *J Dent Res* 90: 377-81

Lee SY, Meier R, Furuta S, Lenburg ME, Kenny PA, Xu R, Bissell MJ (2012) FAM83A confers EGFR-TKI resistance in breast cancer cells and in mice. *J Clin Invest* 122: 3211-20

Li G, Yin H, Kuret J (2004) Casein kinase 1 delta phosphorylates tau and disrupts its binding to microtubules. *J Biol Chem* 279: 15938-45

Li W, Bengtson MH, Ulbrich A, Matsuda A, Reddy VA, Orth A, Chanda SK, Batalov S, Joazeiro CA (2008) Genome-wide and functional annotation of human E3 ubiquitin ligases identifies MULAN, a mitochondrial E3 that regulates the organelle's dynamics and signaling. *PLoS One* 3: e1487

Liao W, Liu W, Liu X, Yuan Q, Ou Y, Qi Y, Huang W, Wang Y, Huang J (2015) Upregulation of FAM83D affects the proliferation and invasion of hepatocellular carcinoma. *Oncotarget* 6: 24132-47

Lin B, Chen T, Zhang Q, Lu X, Zheng Z, Ding J, Liu J, Yang Z, Geng L, Wu L, Zhou L, Zheng S (2016) FAM83D associates with high tumor recurrence after liver transplantation involving expansion of CD44+ carcinoma stem cells. *Oncotarget* 7: 77495-77507

Litchfield DW, Luscher B (1993) Casein kinase II in signal transduction and cell cycle regulation. *Mol Cell Biochem* 127-128: 187-99

Liu C, Li Y, Semenov M, Han C, Baeg GH, Tan Y, Zhang Z, Lin X, He X (2002) Control of beta-catenin phosphorylation/degradation by a dual-kinase mechanism. *Cell* 108: 837-47

Liu CY, Zha ZY, Zhou X, Zhang H, Huang W, Zhao D, Li T, Chan SW, Lim CJ, Hong W, Zhao S, Xiong Y, Lei QY, Guan KL (2010) The hippo tumor pathway promotes TAZ degradation by phosphorylating a phosphodegron and recruiting the SCF{beta}-TrCP E3 ligase. *J Biol Chem* 285: 37159-69

Livak KJ, Schmittgen TD (2001) Analysis of relative gene expression data using real-time quantitative PCR and the 2(-Delta Delta C(T)) Method. *Methods* 25: 402-8

Llamazares S, Moreira A, Tavares A, Girdham C, Spruce BA, Gonzalez C, Karess RE, Glover DM, Sunkel CE (1991) polo encodes a protein kinase homolog required for mitosis in Drosophila. *Genes Dev* 5: 2153-65

Lohka MJ, Hayes MK, Maller JL (1988) Purification of maturation-promoting factor, an intracellular regulator of early mitotic events. *Proc Natl Acad Sci U S A* 85: 3009-13

London N, Biggins S (2014) Signalling dynamics in the spindle checkpoint response. *Nat Rev Mol Cell Biol* 15: 736-47

Lorenz P, Pepperkok R, Ansorge W, Pyerin W (1993) Cell biological studies with monoclonal and polyclonal antibodies against human casein kinase II subunit beta demonstrate participation of the kinase in mitogenic signaling. *J Biol Chem* 268: 2733-9

Lu MS, Johnston CA (2013) Molecular pathways regulating mitotic spindle orientation in animal cells. *Development* 140: 1843-56

Ly T, Ahmad Y, Shlien A, Soroka D, Mills A, Emanuele MJ, Stratton MR, Lamond AI (2014) A proteomic chronology of gene expression through the cell cycle in human myeloid leukemia cells. *Elife* 3: e01630

Ly T, Whigham A, Clarke R, Brenes-Murillo AJ, Estes B, Madhessian D, Lundberg E, Wadsworth P, Lamond AI (2017) Proteomic analysis of cell cycle progression in asynchronous cultures, including mitotic subphases, using PRIMMUS. *Elife* 6

MacDonald BT, Tamai K, He X (2009) Wnt/beta-catenin signaling: components, mechanisms, and diseases. *Dev Cell* 17: 9-26

Machicoane M, de Frutos CA, Fink J, Rocancourt M, Lombardi Y, Garel S, Piel M, Echard A (2014) SLK-dependent activation of ERMs controls LGN-NuMA localization and spindle orientation. *J Cell Biol* 205: 791-9

Macurek L, Lindqvist A, Lim D, Lampson MA, Klompmaker R, Freire R, Clouin C, Taylor SS, Yaffe MB, Medema RH (2008) Polo-like kinase-1 is activated by aurora A to promote checkpoint recovery. *Nature* 455: 119-23

Malik N, Macartney T, Hornberger A, Anderson KE, Tovell H, Prescott AR, Alessi DR (2018) Mechanism of activation of SGK3 by growth factors via the Class 1 and Class 3 PI3Ks. *Biochem J* 475: 117-135

Malik R, Lenobel R, Santamaria A, Ries A, Nigg EA, Korner R (2009) Quantitative analysis of the human spindle phosphoproteome at distinct mitotic stages. *J Proteome Res* 8: 4553-63

Malik R, Nigg EA, Korner R (2008) Comparative conservation analysis of the human mitotic phosphoproteome. *Bioinformatics* 24: 1426-32

Malumbres M, Barbacid M (2005) Mammalian cyclin-dependent kinases. *Trends Biochem Sci* 30: 630-41

Malumbres M, Harlow E, Hunt T, Hunter T, Lahti JM, Manning G, Morgan DO, Tsai LH, Wolgemuth DJ (2009) Cyclin-dependent kinases: a family portrait. *Nat Cell Biol* 11: 1275-6

Manning G, Whyte DB, Martinez R, Hunter T, Sudarsanam S (2002) The protein kinase complement of the human genome. *Science* 298: 1912-34

Mao Y, Liu J, Zhang D, Li B (2016) miR-143 inhibits tumor progression by targeting FAM83F in esophageal squamous cell carcinoma. *Tumour Biol*

Marin O, Bustos VH, Cesaro L, Meggio F, Pagano MA, Antonelli M, Allende CC, Pinna LA, Allende JE (2003) A noncanonical sequence phosphorylated by casein kinase 1 in beta-catenin may play a role in casein kinase 1 targeting of important signaling proteins. *Proc Natl Acad Sci U S A* 100: 10193-200

Marin O, Meggio F, Sarno S, Andretta M, Pinna LA (1994) Phosphorylation of synthetic fragments of inhibitor-2 of protein phosphatase-1 by casein kinase-1 and -2. Evidence that phosphorylated residues are not strictly required for efficient targeting by casein kinase-1. *Eur J Biochem* 223: 647-53

Maritzen T, Lohler J, Deppert W, Knippschild U (2003) Casein kinase I delta (CKIdelta) is involved in lymphocyte physiology. *Eur J Cell Biol* 82: 369-78

Marshall CJ (1994) Signal transduction. Hot lips and phosphorylation of protein kinases. *Nature* 367: 686

Martini S, Soliman T, Gobbi G, Mirandola P, Carubbi C, Masselli E, Pozzi G, Parker PJ, Vitale M (2018) PKCepsilon Controls Mitotic Progression by Regulating Centrosome Migration and Mitotic Spindle Assembly. *Mol Cancer Res* 16: 3-15

Maruthappu T, McGinty LA, Blaydon DC, Fell B, Maatta A, Duit R, Hawkins T, Braun KM, Simpson MA, O'Toole EA, Kelsell DP (2018) Recessive Mutation in FAM83G Associated with Palmoplantar Keratoderma and Exuberant Scalp Hair. *J Invest Dermatol* 138: 984-987

Mashhoon N, DeMaggio AJ, Tereshko V, Bergmeier SC, Egli M, Hoekstra MF, Kuret J (2000) Crystal structure of a conformation-selective casein kinase-1 inhibitor. *J Biol Chem* 275: 20052-60

Massague J (2004) G1 cell-cycle control and cancer. *Nature* 432: 298-306

Masui Y, Markert CL (1971) Cytoplasmic control of nuclear behavior during meiotic maturation of frog oocytes. *J Exp Zool* 177: 129-45

Matsushime H, Ewen ME, Strom DK, Kato JY, Hanks SK, Roussel MF, Sherr CJ (1992) Identification and properties of an atypical catalytic subunit (p34PSK-J3/cdk4) for mammalian D type G1 cyclins. *Cell* 71: 323-34

McNally FJ (2013) Mechanisms of spindle positioning. *J Cell Biol* 200: 131-40

Meggio F, Perich JW, Marin O, Pinna LA (1992) The comparative efficiencies of the Ser(P)-, Thr(P)- and Tyr(P)-residues as specificity determinants for casein kinase-1. *Biochem Biophys Res Commun* 182: 1460-5

Meggio F, Perich JW, Reynolds EC, Pinna LA (1991) A synthetic beta-casein phosphopeptide and analogues as model substrates for casein kinase-1, a ubiquitous, phosphate directed protein kinase. *FEBS Lett* 283: 303-6

Meng QJ, Logunova L, Maywood ES, Gallego M, Lebiecki J, Brown TM, Sladek M, Semikhodskii AS, Glossop NRJ, Piggins HD, Chesham JE, Bechtold DA, Yoo SH, Takahashi JS, Virshup DM, Boot-Handford RP, Hastings MH, Loudon ASI (2008) Setting clock speed in mammals: the CK1 epsilon tau mutation in mice accelerates circadian pacemakers by selectively destabilizing PERIOD proteins. *Neuron* 58: 78-88

Meyerson M, Enders GH, Wu CL, Su LK, Gorka C, Nelson C, Harlow E, Tsai LH (1992) A family of human cdc2-related protein kinases. *EMBO J* 11: 2909-17

Milne DM, Palmer RH, Campbell DG, Meek DW (1992) Phosphorylation of the p53 tumour-suppressor protein at three N-terminal sites by a novel casein kinase I-like enzyme. *Oncogene* 7: 1361-9

Morris NR (1975) Mitotic mutants of Aspergillus nidulans. *Genet Res* 26: 237-54

Munson MJ, Allen GF, Toth R, Campbell DG, Lucocq JM, Ganley IG (2015) mTOR activates the VPS34-UVRAG complex to regulate autolysosomal tubulation and cell survival. *EMBO J* 34: 2272-90

Munson MJ, Ganley IG (2016) Determination of Cellular Phosphatidylinositol-3-phosphate (PI3P) Levels Using a Fluorescently Labelled Selective PI3P Binding Domain (PX). *Bio Protoc* 6

Murphy JM, Farhan H, Eyers PA (2017a) Bio-Zombie: the rise of pseudoenzymes in biology. *Biochem Soc Trans* 45: 537-544

Murphy JM, Mace PD, Eyers PA (2017b) Live and let die: insights into pseudoenzyme mechanisms from structure. *Curr Opin Struct Biol* 47: 95-104

Murray AW (2011) A brief history of error. *Nat Cell Biol* 13: 1178-82

Musacchio A (2015) The Molecular Biology of Spindle Assembly Checkpoint Signaling Dynamics. *Curr Biol* 25: R1002-18

Nandi D, Tahiliani P, Kumar A, Chandu D (2006) The ubiquitin-proteasome system. *J Biosci* 31: 137-55

Natsume T, Kiyomitsu T, Saga Y, Kanemaki MT (2016) Rapid Protein Depletion in Human Cells by Auxin-Inducible Degron Tagging with Short Homology Donors. *Cell Rep* 15: 210-218

Neef R, Preisinger C, Sutcliffe J, Kopajtich R, Nigg EA, Mayer TU, Barr FA (2003) Phosphorylation of mitotic kinesin-like protein 2 by polo-like kinase 1 is required for cytokinesis. *J Cell Biol* 162: 863-75

Nelson RK, Frohman MA (2015) Physiological and pathophysiological roles for phospholipase D. *J Lipid Res* 56: 2229-37

Nguyen-Ngoc T, Afshar K, Gonczy P (2007) Coupling of cortical dynein and G alpha proteins mediates spindle positioning in Caenorhabditis elegans. *Nat Cell Biol* 9: 1294-302

Nigg EA (2001) Mitotic kinases as regulators of cell division and its checkpoints. *Nat Rev Mol Cell Biol* 2: 21-32

Nijenhuis W, von Castelmur E, Littler D, De Marco V, Tromer E, Vleugel M, van Osch MH, Snel B, Perrakis A, Kops GJ (2013) A TPR domain-containing N-terminal module of MPS1 is required for its kinetochore localization by Aurora B. *J Cell Biol* 201: 217-31

Nishimura K, Fukagawa T, Takisawa H, Kakimoto T, Kanemaki M (2009) An auxin-based degron system for the rapid depletion of proteins in nonplant cells. *Nat Methods* 6: 917-22

Nousiainen M, Sillje HH, Sauer G, Nigg EA, Korner R (2006) Phosphoproteome analysis of the human mitotic spindle. *Proc Natl Acad Sci U S A* 103: 5391-6

Nurse P (1990) Universal control mechanism regulating onset of M-phase. *Nature* 344: 503-8

O'Regan L, Blot J, Fry AM (2007) Mitotic regulation by NIMA-related kinases. *Cell Div* 2: 25

Oakley BR, Morris NR (1983) A mutation in Aspergillus nidulans that blocks the transition from interphase to prophase. *J Cell Biol* 96: 1155-8

Okamura H, Garcia-Rodriguez C, Martinson H, Qin J, Virshup DM, Rao A (2004) A conserved docking motif for CK1 binding controls the nuclear localization of NFAT1. *Mol Cell Biol* 24: 4184-95

Okumura M, Natsume T, Kanemaki MT, Kiyomitsu T (2018) Dynein-Dynactin-NuMA clusters generate cortical spindle-pulling forces as a multi-arm ensemble. *Elife* 7

Osmani AH, McGuire SL, Osmani SA (1991) Parallel activation of the NIMA and p34cdc2 cell cycle-regulated protein kinases is required to initiate mitosis in A. nidulans. *Cell* 67: 283-91

Osmani SA, May GS, Morris NR (1987) Regulation of the mRNA levels of nimA, a gene required for the G2-M transition in Aspergillus nidulans. *J Cell Biol* 104: 1495-504

Oumata N, Bettayeb K, Ferandin Y, Demange L, Lopez-Giral A, Goddard ML, Myrianthopoulos V, Mikros E, Flajolet M, Greengard P, Meijer L, Galons H (2008) Roscovitine-derived, dual-specificity inhibitors of cyclin-dependent kinases and casein kinases 1. *J Med Chem* 51: 5229-42

Panbianco C, Weinkove D, Zanin E, Jones D, Divecha N, Gotta M, Ahringer J (2008) A casein kinase 1 and PAR proteins regulate asymmetry of a PIP(2) synthesis enzyme for asymmetric spindle positioning. *Dev Cell* 15: 198-208

Park DH, Rose LS (2008) Dynamic localization of LIN-5 and GPR-1/2 to cortical force generation domains during spindle positioning. *Dev Biol* 315: 42-54

Park JE, Soung NK, Johmura Y, Kang YH, Liao C, Lee KH, Park CH, Nicklaus MC, Lee KS (2010) Polo-box domain: a versatile mediator of polo-like kinase function. *Cell Mol Life Sci* 67: 1957-70

Pawson T, Scott JD (2005) Protein phosphorylation in signaling--50 years and counting. *Trends Biochem Sci* 30: 286-90

Pepperkok R, Lorenz P, Ansorge W, Pyerin W (1994) Casein kinase II is required for transition of G0/G1, early G1, and G1/S phases of the cell cycle. *J Biol Chem* 269: 6986-91

Pepperkok R, Lorenz P, Jakobi R, Ansorge W, Pyerin W (1991) Cell growth stimulation by EGF: inhibition through antisense-oligodeoxynucleotides demonstrates important role of casein kinase II. *Exp Cell Res* 197: 245-53

Perez-Pena J, Alcaraz-Sanabria A, Nieto-Jimenez C, Paez R, Corrales-Sanchez V, Serrano-Oviedo L, Wali VB, Patwardhan GA, Amir E, Gyorffy B, Pandiella A, Ocana A (2017) Mitotic read-out genes confer poor outcome in luminal A breast cancer tumors. *Oncotarget* 8: 21733-21740

Peters JM (1998) SCF and APC: the Yin and Yang of cell cycle regulated proteolysis. *Curr Opin Cell Biol* 10: 759-68

Pickart CM, Eddins MJ (2004) Ubiquitin: structures, functions, mechanisms. *Biochim Biophys Acta* 1695: 55-72

Pines J (2011) Cubism and the cell cycle: the many faces of the APC/C. *Nat Rev Mol Cell Biol* 12: 427-38

Pintard L, Willems A, Peter M (2004) Cullin-based ubiquitin ligases: Cul3-BTB complexes join the family. *EMBO J* 23: 1681-7

Ponting CP, Russell RR (2002) The natural history of protein domains. *Annu Rev Biophys Biomol Struct* 31: 45-71

Pourhashemi SJ, Ghandehari Motlagh M, Meighani G, Ebrahimi Takaloo A, Mansouri M, Mohandes F, Mirzaii M, Khoshzaban A, Moshtaghi F, Abedkhojasteh H, Heidari M (2014) Missense Mutation in Fam83H Gene in Iranian Patients with Amelogenesis Imperfecta. *Iran J Public Health* 43: 1680-7

Primorac I, Musacchio A (2013) Panta rhei: the APC/C at steady state. *J Cell Biol* 201: 177-89

Pulgar V, Marin O, Meggio F, Allende CC, Allende JE, Pinna LA (1999) Optimal sequences for non-phosphate-directed phosphorylation by protein kinase CK1 (casein kinase-1)--a re-evaluation. *Eur J Biochem* 260: 520-6

Qian YW, Erikson E, Maller JL (1999) Mitotic effects of a constitutively active mutant of the Xenopus polo-like kinase Plx1. *Mol Cell Biol* 19: 8625-32

Radden LA, 2nd, Child KM, Adkins EB, Spacek DV, Feliciano AM, King TR (2013) The wooly mutation (wly) on mouse chromosome 11 is associated with a genetic defect in Fam83g. *BMC Res Notes* 6: 189

Rao PN, Johnson RT (1970) Mammalian cell fusion: studies on the regulation of DNA synthesis and mitosis. *Nature* 225: 159-64

Rashid MS, Mazur T, Ji W, Liu ST, Taylor WR (2018) Analysis of the role of GSK3 in the mitotic checkpoint. *Sci Rep* 8: 14259

Reddy SK, Rape M, Margansky WA, Kirschner MW (2007) Ubiquitination by the anaphase-promoting complex drives spindle checkpoint inactivation. *Nature* 446: 921-5
Rena G, Bain J, Elliott M, Cohen P (2004) D4476, a cell-permeant inhibitor of CK1, suppresses the site-specific phosphorylation and nuclear exclusion of FOXO1a. *EMBO Rep* 5: 60-5

Reppert SM, Weaver DR (2002) Coordination of circadian timing in mammals. *Nature* 418: 935-41

Reynolds N, Ohkura H (2003) Polo boxes form a single functional domain that mediates interactions with multiple proteins in fission yeast polo kinase. *J Cell Sci* 116: 1377-87

Richter J, Bischof J, Zaja M, Kohlhof H, Othersen O, Vitt D, Alscher V, Pospiech I, Garcia-Reyes B, Berg S, Leban J, Knippschild U (2014) Difluoro-dioxolo-benzoimidazol-benzamides as potent inhibitors of CK1delta and epsilon with nanomolar inhibitory activity on cancer cell proliferation. *J Med Chem* 57: 7933-46

Robbins JA, Cross FR (2010) Regulated degradation of the APC coactivator Cdc20. *Cell Div* 5: 23

Rodriguez N, Yang J, Hasselblatt K, Liu S, Zhou Y, Rauh-Hain JA, Ng SK, Choi PW, Fong WP, Agar NY, Welch WR, Berkowitz RS, Ng SW (2012) Casein kinase I epsilon interacts with mitochondrial proteins for the growth and survival of human ovarian cancer cells. *EMBO Mol Med* 4: 952-63

Roffey J, Rosse C, Linch M, Hibbert A, McDonald NQ, Parker PJ (2009) Protein kinase C intervention: the state of play. *Curr Opin Cell Biol* 21: 268-79

Rojas-Fernandez A, Herhaus L, Macartney T, Lachaud C, Hay RT, Sapkota GP (2015) Rapid generation of endogenously driven transcriptional reporters in cells through CRISPR/Cas9. *Sci Rep* 5: 9811

Rothbauer U, Zolghadr K, Muyldermans S, Schepers A, Cardoso MC, Leonhardt H (2008) A versatile nanotrap for biochemical and functional studies with fluorescent fusion proteins. *Mol Cell Proteomics* 7: 282-9

Russell P, Nurse P (1986) Schizosaccharomyces pombe and Saccharomyces cerevisiae: a look at yeasts divided. *Cell* 45: 781-2

Sacristan C, Kops GJ (2015) Joined at the hip: kinetochores, microtubules, and spindle assembly checkpoint signaling. *Trends Cell Biol* 25: 21-8

Sakamoto KM, Kim KB, Kumagai A, Mercurio F, Crews CM, Deshaies RJ (2001) Protacs: chimeric molecules that target proteins to the Skp1-Cullin-F box complex for ubiquitination and degradation. *Proc Natl Acad Sci U S A* 98: 8554-9

Salama M, Benitez-Riquelme D, Elabd S, Munoz L, Zhang P, Glanemann M, Mione MC, Goldin R, Soussi T, Davidson G, Blattner C (2019) Fam83F induces p53 stabilisation and promotes its activity. *Cell Death Differ*

Sana S, Keshri R, Rajeevan A, Kapoor S, Kotak S (2018) Plk1 regulates spindle orientation by phosphorylating NuMA in human cells. *Life Sci Alliance* 1: e201800223

Sander JD, Joung JK (2014) CRISPR-Cas systems for editing, regulating and targeting genomes. *Nat Biotechnol* 32: 347-55

Santaguida S, Vernieri C, Villa F, Ciliberto A, Musacchio A (2011) Evidence that Aurora B is implicated in spindle checkpoint signalling independently of error correction. *EMBO J* 30: 1508-19

Santamaria A, Nagel S, Sillje HH, Nigg EA (2008) The spindle protein CHICA mediates localization of the chromokinesin Kid to the mitotic spindle. *Curr Biol* 18: 723-9

Santamaria A, Wang B, Elowe S, Malik R, Zhang F, Bauer M, Schmidt A, Sillje HH, Korner R, Nigg EA (2011) The Plk1-dependent phosphoproteome of the early mitotic spindle. *Mol Cell Proteomics* 10: M110 004457

Sarasqueta AF, Forte G, Corver WE, de Miranda NF, Ruano D, van Eijk R, Oosting J, Tollenaar RA, van Wezel T, Morreau H (2013) Integral analysis of p53 and its value as prognostic factor in sporadic colon cancer. *BMC Cancer* 13: 277

Sauer G, Korner R, Hanisch A, Ries A, Nigg EA, Sillje HH (2005) Proteome analysis of the human mitotic spindle. *Mol Cell Proteomics* 4: 35-43

Saurin AT, Durgan J, Cameron AJ, Faisal A, Marber MS, Parker PJ (2008) The regulated assembly of a PKCepsilon complex controls the completion of cytokinesis. *Nat Cell Biol* 10: 891-901

Saurin AT, van der Waal MS, Medema RH, Lens SM, Kops GJ (2011) Aurora B potentiates Mps1 activation to ensure rapid checkpoint establishment at the onset of mitosis. *Nat Commun* 2: 316

Sayyab S, Viluma A, Bergvall K, Brunberg E, Jagannathan V, Leeb T, Andersson G, Bergstrom TF (2016) Whole-Genome Sequencing of a Canine Family Trio Reveals a FAM83G Variant Associated with Hereditary Footpad Hyperkeratosis. *G3 (Bethesda)* 6: 521-7

Schittek B, Sinnberg T (2014) Biological functions of casein kinase 1 isoforms and putative roles in tumorigenesis. *Mol Cancer* 13: 231

Schmidt FI, Lu A, Chen JW, Ruan J, Tang C, Wu H, Ploegh HL (2016) A single domain antibody fragment that recognizes the adaptor ASC defines the role of ASC domains in inflammasome assembly. *J Exp Med* 213: 771-90

Selvy PE, Lavieri RR, Lindsley CW, Brown HA (2011) Phospholipase D: enzymology, functionality, and chemical modulation. *Chem Rev* 111: 6064-119

Seong YS, Kamijo K, Lee JS, Fernandez E, Kuriyama R, Miki T, Lee KS (2002) A spindle checkpoint arrest and a cytokinesis failure by the dominant-negative polo-box domain of Plk1 in U-2 OS cells. *J Biol Chem* 277: 32282-93

Sha F, Gencer EB, Georgeon S, Koide A, Yasui N, Koide S, Hantschel O (2013) Dissection of the BCR-ABL signaling network using highly specific monobody inhibitors to the SHP2 SH2 domains. *Proc Natl Acad Sci U S A* 110: 14924-9

Sharp LW (1934) *Introduction to cytology*. McGraw-Hill book company, inc., New York and London,

Shi R, Sun J, Sun Q, Zhang Q, Xia W, Dong G, Wang A, Jiang F, Xu L (2016) Upregulation of FAM83D promotes malignant phenotypes of lung adenocarcinoma by regulating cell cycle. *Am J Cancer Res* 6: 2587-2598

Sigrist SJ, Lehner CF (1997) Drosophila fizzy-related down-regulates mitotic cyclins and is required for cell proliferation arrest and entry into endocycles. *Cell* 90: 671-81

Siller KH, Doe CQ (2009) Spindle orientation during asymmetric cell division. *Nat Cell Biol* 11: 365-74

Sillibourne JE, Milne DM, Takahashi M, Ono Y, Meek DW (2002) Centrosomal anchoring of the protein kinase CK1delta mediated by attachment to the large, coiled-coil scaffolding protein CG-NAP/AKAP450. *J Mol Biol* 322: 785-97

Skoufias DA, DeBonis S, Saoudi Y, Lebeau L, Crevel I, Cross R, Wade RH, Hackney D, Kozielski F (2006) S-trityl-L-cysteine is a reversible, tight binding inhibitor of the human kinesin Eg5 that specifically blocks mitotic progression. *J Biol Chem* 281: 17559-69

Song S, Grenfell TZ, Garfield S, Erikson RL, Lee KS (2000) Essential function of the polo box of Cdc5 in subcellular localization and induction of cytokinetic structures. *Mol Cell Biol* 20: 286-98

Soucy TA, Smith PG, Milhollen MA, Berger AJ, Gavin JM, Adhikari S, Brownell JE, Burke KE, Cardin DP, Critchley S, Cullis CA, Doucette A, Garnsey JJ, Gaulin JL, Gershman RE, Lublinsky AR, McDonald A, Mizutani H, Narayanan U, Olhava EJ et al. (2009) An inhibitor of NEDD8-activating enzyme as a new approach to treat cancer. *Nature* 458: 732-6

St-Denis NA, Bailey ML, Parker EL, Vilk G, Litchfield DW (2011) Localization of phosphorylated CK2alpha to the mitotic spindle requires the peptidyl-prolyl isomerase Pin1. *J Cell Sci* 124: 2341-8

Stahl M, Zeidan AM (2017) Lenalidomide use in myelodysplastic syndromes: Insights into the biologic mechanisms and clinical applications. *Cancer* 123: 1703-1713

Stamos JL, Weis WI (2013) The beta-catenin destruction complex. *Cold Spring Harb Perspect Biol* 5: a007898

Stoter M, Bamberger AM, Aslan B, Kurth M, Speidel D, Loning T, Frank HG, Kaufmann P, Lohler J, Henne-Bruns D, Deppert W, Knippschild U (2005) Inhibition of casein kinase I delta alters mitotic spindle formation and induces apoptosis in trophoblast cells. *Oncogene* 24: 7964-75

Stuckey JA, Dixon JE (1999) Crystal structure of a phospholipase D family member. *Nat Struct Biol* 6: 278-84

Sung TC, Roper RL, Zhang Y, Rudge SA, Temel R, Hammond SM, Morris AJ, Moss B, Engebrecht J, Frohman MA (1997) Mutagenesis of phospholipase D defines a superfamily including a trans-Golgi viral protein required for poxvirus pathogenicity. *EMBO J* 16: 4519-30

Sunkel CE, Glover DM (1988) polo, a mitotic mutant of Drosophila displaying abnormal spindle poles. *J Cell Sci* 89 (Pt 1): 25-38

Swenson KI, Farrell KM, Ruderman JV (1986) The clam embryo protein cyclin A induces entry into M phase and the resumption of meiosis in Xenopus oocytes. *Cell* 47: 861-70

Taipale J, Cooper MK, Maiti T, Beachy PA (2002) Patched acts catalytically to suppress the activity of Smoothened. *Nature* 418: 892-7

Takahashi JS (2017) Transcriptional architecture of the mammalian circadian clock. *Nat Rev Genet* 18: 164-179

Takano A, Uchiyama M, Kajimura N, Mishima K, Inoue Y, Kamei Y, Kitajima T, Shibui K, Katoh M, Watanabe T, Hashimotodani Y, Nakajima T, Ozeki Y, Hori T, Yamada N, Toyoshima R, Ozaki N, Okawa M, Nagai K, Takahashi K et al. (2004) A missense variation in human casein kinase I epsilon gene that induces functional alteration and shows an inverse association with circadian rhythm sleep disorders. *Neuropsychopharmacology* 29: 1901-9

Takemoto A, Kimura K, Yanagisawa J, Yokoyama S, Hanaoka F (2006) Negative regulation of condensin I by CK2-mediated phosphorylation. *EMBO J* 25: 5339-48

Tame MA, Raaijmakers JA, Afanasyev P, Medema RH (2016) Chromosome misalignments induce spindle-positioning defects. *EMBO Rep* 17: 317-25

Tan X, Calderon-Villalobos LI, Sharon M, Zheng C, Robinson CV, Estelle M, Zheng N (2007) Mechanism of auxin perception by the TIR1 ubiquitin ligase. *Nature* 446: 640-5

Tanaka K (2009) The proteasome: overview of structure and functions. *Proc Jpn Acad Ser B Phys Biol Sci* 85: 12-36

Tang Z, Shu H, Oncel D, Chen S, Yu H (2004) Phosphorylation of Cdc20 by Bub1 provides a catalytic mechanism for APC/C inhibition by the spindle checkpoint. *Mol Cell* 16: 387-97

Teo JL, Kahn M (2010) The Wnt signaling pathway in cellular proliferation and differentiation: A tale of two coactivators. *Adv Drug Deliv Rev* 62: 1149-55

Thery M, Jimenez-Dalmaroni A, Racine V, Bornens M, Julicher F (2007) Experimental and theoretical study of mitotic spindle orientation. *Nature* 447: 493-6

Thery M, Racine V, Pepin A, Piel M, Chen Y, Sibarita JB, Bornens M (2005) The extracellular matrix guides the orientation of the cell division axis. *Nat Cell Biol* 7: 947-53

Tuazon PT, Traugh JA (1991) Casein kinase I and II--multipotential serine protein kinases: structure, function, and regulation. *Adv Second Messenger Phosphoprotein Res* 23: 123-64

Urzua B, Martinez C, Ortega-Pinto A, Adorno D, Morales-Bozo I, Riadi G, Jara L, Plaza A, Lefimil C, Lozano C, Reyes M (2015) Novel missense mutation of the FAM83H gene causes retention of amelogenin and a mild clinical phenotype of hypocalcified enamel. *Arch Oral Biol* 60: 1356-67

Vader G, Kauw JJ, Medema RH, Lens SM (2006a) Survivin mediates targeting of the chromosomal passenger complex to the centromere and midbody. *EMBO Rep* 7: 85-92
Vader G, Medema RH, Lens SM (2006b) The chromosomal passenger complex: guiding Aurora-B through mitosis. *J Cell Biol* 173: 833-7

Varjosalo M, Taipale J (2008) Hedgehog: functions and mechanisms. *Genes Dev* 22: 2454-72

Vassilev LT (2006) Cell cycle synchronization at the G2/M phase border by reversible inhibition of CDK1. *Cell Cycle* 5: 2555-6

Vassilev LT, Tovar C, Chen S, Knezevic D, Zhao X, Sun H, Heimbrook DC, Chen L (2006) Selective small-molecule inhibitor reveals critical mitotic functions of human CDK1. *Proc Natl Acad Sci U S A* 103: 10660-5

Venerando A, Girardi C, Ruzzene M, Pinna LA (2013) Pyrvinium pamoate does not activate protein kinase CK1, but promotes Akt/PKB down-regulation and GSK3 activation. *Biochem J* 452: 131-7

Venerando A, Ruzzene M, Pinna LA (2014) Casein kinase: the triple meaning of a misnomer. *Biochem J* 460: 141-56

Vielhaber E, Eide E, Rivers A, Gao ZH, Virshup DM (2000) Nuclear entry of the circadian regulator mPER1 is controlled by mammalian casein kinase I epsilon. *Mol Cell Biol* 20: 4888-99

Visintin R, Prinz S, Amon A (1997) CDC20 and CDH1: a family of substrate-specific activators of APC-dependent proteolysis. *Science* 278: 460-3

Vleugel M, Hoogendoorn E, Snel B, Kops GJ (2012) Evolution and function of the mitotic checkpoint. *Dev Cell* 23: 239-50

Vogt J, Dingwell KS, Herhaus L, Gourlay R, Macartney T, Campbell D, Smith JC, Sapkota GP (2014) Protein associated with SMAD1 (PAWS1/FAM83G) is a substrate for type I bone morphogenetic protein receptors and modulates bone morphogenetic protein signalling. *Open Biol* 4: 130210

Wakefield JG, Stephens DJ, Tavare JM (2003) A role for glycogen synthase kinase-3 in mitotic spindle dynamics and chromosome alignment. *J Cell Sci* 116: 637-46

Walian PJ, Hang B, Mao JH (2016) Prognostic significance of FAM83D gene expression across human cancer types. *Oncotarget* 7: 3332-40

Walton KM, Fisher K, Rubitski D, Marconi M, Meng QJ, Sladek M, Adams J, Bass M, Chandrasekaran R, Butler T, Griffor M, Rajamohan F, Serpa M, Chen Y, Claffey M, Hastings M, Loudon A, Maywood E, Ohren J, Doran A et al. (2009) Selective inhibition of casein kinase 1 epsilon minimally alters circadian clock period. *J Pharmacol Exp Ther* 330: 430-9

Wang D, Han S, Peng R, Wang X, Yang XX, Yang RJ, Jiao CY, Ding D, Ji GW, Li XC (2015a) FAM83D activates the MEK/ERK signaling pathway and promotes cell proliferation in hepatocellular carcinoma. *Biochem Biophys Res Commun* 458: 313-20

Wang G, Jiang Q, Zhang C (2014) The role of mitotic kinases in coupling the centrosome cycle with the assembly of the mitotic spindle. *J Cell Sci* 127: 4111-22

Wang L, Lu A, Zhou HX, Sun R, Zhao J, Zhou CJ, Shen JP, Wu SN, Liang CG (2013) Casein kinase 1 alpha regulates chromosome congression and separation during mouse oocyte meiotic maturation and early embryo development. *PLoS One* 8: e63173

Wang PC, Vancura A, Mitcheson TG, Kuret J (1992) Two genes in Saccharomyces cerevisiae encode a membrane-bound form of casein kinase-1. *Mol Biol Cell* 3: 275-86

Wang SK, Hu Y, Yang J, Smith CE, Richardson AS, Yamakoshi Y, Lee YL, Seymen F, Koruyucu M, Gencay K, Lee M, Choi M, Kim JW, Hu JC, Simmer JP (2016) Fam83h null mice support a neomorphic mechanism for human ADHCAI. *Mol Genet Genomic Med* 4: 46-67

Wang T, Birsoy K, Hughes NW, Krupczak KM, Post Y, Wei JJ, Lander ES, Sabatini DM (2015b) Identification and characterization of essential genes in the human genome. *Science* 350: 1096-101

Warren CD, Brady DM, Johnston RC, Hanna JS, Hardwick KG, Spencer FA (2002) Distinct chromosome segregation roles for spindle checkpoint proteins. *Mol Biol Cell* 13: 3029-41

Wenzel DM, Stoll KE, Klevit RE (2011) E2s: structurally economical and functionally replete. *Biochem J* 433: 31-42

Wicking C, Smyth I, Bale A (1999) The hedgehog signalling pathway in tumorigenesis and development. *Oncogene* 18: 7844-51

Williams GH, Stoeber K (2012) The cell cycle and cancer. *J Pathol* 226: 352-64

Winter M, Milne D, Dias S, Kulikov R, Knippschild U, Blattner C, Meek D (2004) Protein kinase CK1delta phosphorylates key sites in the acidic domain of murine double-minute clone 2 protein (MDM2) that regulate p53 turnover. *Biochemistry* 43: 16356-64

Wojcik J, Hantschel O, Grebien F, Kaupe I, Bennett KL, Barkinge J, Jones RB, Koide A, Superti-Furga G, Koide S (2010) A potent and highly specific FN3 monobody inhibitor of the Abl SH2 domain. *Nat Struct Mol Biol* 17: 519-27

Wojcik J, Lamontanara AJ, Grabe G, Koide A, Akin L, Gerig B, Hantschel O, Koide S (2016) Allosteric Inhibition of Bcr-Abl Kinase by High Affinity Monobody Inhibitors Directed to the Src Homology 2 (SH2)-Kinase Interface. *J Biol Chem* 291: 8836-47

Wu KZ, Jones RA, Tachie-Menson T, Macartney TJ, Wood NT, Varghese J, Gourlay R, Soares RF, Smith JC, Sapkota GP (2019) Pathogenic FAM83G palmoplantar keratoderma mutations inhibit the PAWS1:CK1α association and attenuate Wnt signalling. *Wellcome Open Research* 4

Wu S, Chen L, Becker A, Schonbrunn E, Chen J (2012) Casein kinase 1alpha regulates an MDMX intramolecular interaction to stimulate p53 binding. *Mol Cell Biol* 32: 4821-32

Xiong Y, Beach D (1991) Population explosion in the cyclin family. *Curr Biol* 1: 362-4

Xiong Y, Zhang H, Beach D (1992) D type cyclins associate with multiple protein kinases and the DNA replication and repair factor PCNA. *Cell* 71: 505-14

Xu F, Wang YL, Chang JJ, Du SC, Diao L, Jiang N, Wang HJ, Ma D, Zhang J (2014) Mammalian sterile 20-like kinase 1/2 inhibits the Wnt/beta-catenin signalling pathway by directly binding casein kinase 1epsilon. *Biochem J* 458: 159-69

Xu Y, Lee SH, Kim HS, Kim NH, Piao S, Park SH, Jung YS, Yook JI, Park BJ, Ha NC (2010) Role of CK1 in GSK3beta-mediated phosphorylation and degradation of snail. *Oncogene* 29: 3124-33

Yan L, Yao J, Qiu J (2017) miRNA-495 suppresses proliferation and migration of colorectal cancer cells by targeting FAM83D. *Biomed Pharmacother* 96: 974-981

Yang H, Wei YN, Zhou J, Hao TT, Liu XL (2017) MiR-455-3p acts as a prognostic marker and inhibits the proliferation and invasion of esophageal squamous cell carcinoma by targeting FAM83F. *Eur Rev Med Pharmacol Sci* 21: 3200-3206

Yang WS, Stockwell BR (2008) Inhibition of casein kinase 1-epsilon induces cancer-cell-selective, PERIOD2-dependent growth arrest. *Genome Biol* 9: R92

Ye J, Coulouris G, Zaretskaya I, Cutcutache I, Rozen S, Madden TL (2012) Primer-BLAST: a tool to design target-specific primers for polymerase chain reaction. *BMC Bioinformatics* 13: 134

Yost C, Torres M, Miller JR, Huang E, Kimelman D, Moon RT (1996) The axis-inducing activity, stability, and subcellular distribution of beta-catenin is regulated in Xenopus embryos by glycogen synthase kinase 3. *Genes Dev* 10: 1443-54

Yu F, White SB, Zhao Q, Lee FS (2001) HIF-1alpha binding to VHL is regulated by stimulus-sensitive proline hydroxylation. *Proc Natl Acad Sci U S A* 98: 9630-5

Yu H, Peters JM, King RW, Page AM, Hieter P, Kirschner MW (1998) Identification of a cullin homology region in a subunit of the anaphase-promoting complex. *Science* 279: 1219-22

Zachariae W, Schwab M, Nasmyth K, Seufert W (1998) Control of cyclin ubiquitination by CDK-regulated binding of Hct1 to the anaphase promoting complex. *Science* 282: 1721-4

Zeng X, Sigoillot F, Gaur S, Choi S, Pfaff KL, Oh DC, Hathaway N, Dimova N, Cuny GD, King RW (2010) Pharmacologic inhibition of the anaphase-promoting complex induces a spindle checkpoint-dependent mitotic arrest in the absence of spindle damage. *Cancer Cell* 18: 382-95

Zengerle M, Chan KH, Ciulli A (2015) Selective Small Molecule Induced Degradation of the BET Bromodomain Protein BRD4. *ACS Chem Biol* 10: 1770-7

Zhang Q, Yu S, Lok SIS, Wong AST, Jiao Y, Lee LTO (2019) FAM83D promotes ovarian cancer progression and its potential application in diagnosis of invasive ovarian cancer. *J Cell Mol Med*

Zhao B, Bhuripanyo K, Schneider J, Zhang K, Schindelin H, Boone D, Yin J (2012) Specificity of the E1-E2-E3 enzymatic cascade for ubiquitin C-terminal sequences identified by phage display. *ACS Chem Biol* 7: 2027-35

Zhao B, Li L, Tumaneng K, Wang CY, Guan KL (2010) A coordinated phosphorylation by Lats and CK1 regulates YAP stability through SCF(beta-TRCP). *Genes Dev* 24: 72-85

Zhao Y, Sun Y (2013) Cullin-RING Ligases as attractive anti-cancer targets. *Curr Pharm Des* 19: 3215-25

Zheng N, Schulman BA, Song L, Miller JJ, Jeffrey PD, Wang P, Chu C, Koepp DM, Elledge SJ, Pagano M, Conaway RC, Conaway JW, Harper JW, Pavletich NP (2002) Structure of the Cul1-Rbx1-Skp1-F boxSkp2 SCF ubiquitin ligase complex. *Nature* 416: 703-9

Zhu H, Diao S, Lim V, Hu L, Hu J (2019) FAM83D inhibits autophagy and promotes proliferation and invasion of ovarian cancer cells via PI3K/AKT/mTOR pathway. *Acta Biochim Biophys Sin (Shanghai)*

Appendix:

The following ImageJ macro was developed by Graeme Ball in order to measure mean CK1α staining intensity on mitotic spindles.

```
// Spindle stain quantification macro
// - measure stain in spindle region bounded by DAPI ring exterior
// - measure stain outside DAPI ring region to estimate background
// - for each nucleus identified, report ratio spindle/background
//
// for Luke Fulcher, 2018
//
// Copyright Graeme Ball 2018, Dundee Imaging Facility
// License: Creative Commons CC-BY-NC-SA
//
// parameters
chDAPI = 3;  // channel number for DAPI
chCK1a = 1;  // channel for CK1alpha stain
minSizeSpindle = 8000;  // minimum number of pixels in a spindle region
Dialog.create("Measure_spindle_ratio");
Dialog.addNumber("DAPI channel", chDAPI);
Dialog.addNumber("CK1a channel", chCK1a);
Dialog.show();
chDAPI = Dialog.getNumber();
chCK1a = Dialog.getNumber();
roiManager("reset");
roiManager("UseNames", "true");
roiManager("Show All with labels");
run("Set Measurements...", "area mean standard min integrated display redirect=None decimal=3");
setOption("BlackBackground", true);
```

```
// find spindle regions
Stack.setDisplayMode("grayscale");
Stack.setChannel(chDAPI);
run("Duplicate...", " ");
run("Convert to Mask", "method=Otsu background=Dark calculate black");
run("Fill Holes");
run("Analyze Particles...", "size=" + minSizeSpindle + "-Infinity exclude add");
close();
// create CK1a whole-cell mask with separated cells
Stack.setChannel(chCK1a);
run("Duplicate...", " ");
setAutoThreshold("Triangle dark");
run("Convert to Mask");
run("Fill Holes");
run("Median...", "radius=15");  // clean up rough edges
run("Make Binary");
run("Watershed");
// for each spindle ROI, attempt to find containing cell ROI and create cytoplasm ring ROI
nNuclei = roiManager("count");
setThreshold(1, 255);
for (i = 0; i < nNuclei; i++) {
        roiManager("select", i);
        roiManager("rename", "spindle" + i);
        getSelectionBounds(x, y, w, h);
        x = round(x + w/2);
        y = round(y + h/2);
        doWand(x, y);
        roiManager("add");  // cytoplasm region centred on this spindle
        newCellIndex = roiManager("count") - 1;
        indices = newArray(i, newCellIndex);
```

```
		roiManager("select", indices);
		roiManager("XOR");
		roiManager("add");
		newCytoIndex = roiManager("count") - 1;
		roiManager("select", newCytoIndex);
		roiManager("rename", "cytoplasm" + i);
		roiManager("select", newCellIndex);
		roiManager("delete");
}
close(); // close CK1a whole-cell mask
// make measurements using paired ROIs and write to Results table
run("Clear Results");
Stack.setChannel(chCK1a);
for (i = 0; i < nNuclei; i++) {
		row = nResults;
		setResult("cellID", row, i);
		roiManager("select", i);
		getRawStatistics(nPixels, spMean, min, max, std);
		setResult("spindleMean", row, spMean);
		setResult("spindleTotal", row, (spMean * nPixels));
		roiManager("select", i + nNuclei);  // corresponding cytoplasm ROI
		getRawStatistics(nPixels, cyMean, min, max, std);
		setResult("cytoMean", row, cyMean);
		setResult("ratioS/C", row, (spMean/cyMean));
}
//run("From ROI Manager");
```